GLOBAL PLATE RECONSTRUCTIONS, THE AREA-AGE RELATIONSHIP, AND GLOBAL CHANGES IN SEA LEVEL

by
José Wilson Corrêa Rosa
B.S., Universidade de Brasília, Brasília, Brazil
(1983)

Submitted to the Department of
Earth, Atmospheric, and Planetary Sciences
in Partial Fulfillment of the
Requirements of the Degree of

DOCTOR OF PHILOSOPHY

at the

MASSACHUSETTS INSTITUTE OF TECHNOLOGY

09 November 1989

Signature of Author_____
Department of Earth, Atmospheric, and Planetary Sciences
09 November 1989

Certified by_____
Peter Molnar
Thesis Supervisor

Accepted by_____
Thomas H. Jordan
Chairman, Departmental Committee on Graduate Students

GLOBAL PLATE RECONSTRUCTIONS, THE AREA-AGE RELATIONSHIP, AND GLOBAL CHANGES IN SEA LEVEL

by
José Wilson Corrêa Rosa

Submitted to the Department of Earth, Atmospheric, and Planetary Sciences on 09 November 1989, in partial fulfillment of the requirements for the degree of Doctor of Philosophy

Abstract

For the first time, a study of past changes in the sea level based on changes in the area-age distribution of the oceans is done with the systematic estimation of the associated uncertainties. The differences in the total volume of the ocean basins due to differences in the distribution of area with age of the ocean floor, but assuming a constant area of the ocean basins and a constant volume of ocean water, should have caused a decrease in the sea level of 30 ± 10 meters since anomaly 13 time (35.58 Ma) and a decrease of 97 ± 10 meters since anomaly 25 time (58.94 Ma). To deduce this, we analyzed the available datasets of magnetic anomaly and fracture zone crossings and of the resulting rotation parameters describing finite reconstructions of the major plates. We improved this dataset with the digitization of new data and with the calculation of new and consistent rotation parameters. We built isochron maps for the present time and for reconstructions at the times of anomalies 13 and 25 (35.58 Ma and 58.94 Ma). The northwards movement of India since its collision with Eurasia is another major factor in changes in the sea level since about 50 Ma, the approximate time of the collision.

For the anomaly 13 reconstruction, the change in the volume of the ocean basins due to the northern motion of India yields a decrease in sea level of about 42 meters $\pm$ 16 meters and for the anomaly 25 reconstruction, we have a decrease of about 76 meters $\pm$ 46 meters.

The combination of changes in the sea level due to differences in the area-age distribution, and sea-level changes caused by the penetration of India into Eurasia yield a decrease in the sea level of 72 ± 19 meters since the time of anomaly 13 (35.58 Ma) and a decrease in the sea level of 173 ± 47 meters since anomaly 25 time (58.94 Ma).

The combination of the changes in sea level due to the previous factors and the assumption that most of the ice in Antarctica was formed in the past 30 m. y. gives us predicted decreases in sea level of 143 ± 25 meters since the time of

anomaly 13 (35.58 Ma) and of 244 ± 53 meters since the time of anomaly 25 (58.94 Ma).
Thesis Supervisor: Peter Molnar
Title: Senior Research Associate in Geophysics

Acknowledgements

This thesis brings my name on the front page but it represents the work, confidence, and friendship of several people. I want to say thanks to all of them.

First, I want to thank my advisor, Peter Molnar, for his friendship, patience, and guidance. I thank him for offering me this thesis project, always showing confidence in my work and giving me a lot of freedom in my research.

I want to thank Gene Simmons, my academic advisor at MIT. Special thanks to him for giving me the opportunity to come to MIT. I learned a lot about gravity and consulting with him.

I am very grateful of having been able to meet and work with Joann Stock. I will never stop saying thanks to her for all the friendship, advices and help she always offered me. I am very happy for the privilege of meeting such a intelligent friend, and I hope I will continue working with her.

When I came to MIT, I was impressed with the speed that I made friends here. Thomas Wissler, with his wife Sim, were always ready to help me. I learned a lot about computers, research and bikes with Tom. I certainly enjoyed to learn about chimichangas and chocolate chip cookies with Sim. I will never forget the Black Table Restaurant. Jeff Mann taught me and helped me in my collection of gravity measurements in New Hampshire. I enjoyed the moments that I spent with him and his wife Mary. Lou Caruso was always with a big smile waiting for anybody that would show up in the lab. I hope I can show him and his wife, Debbie, the beauty of the Amazon. Scott Phillips taught me, together with Dave Olgaard, how to pitch softball. Scott, introduced me to Fenway Park, the Boston Red Sox and the Boston Celtics. I will never forget my games for the soccer team. The first season was special for me. Kiyoshi Yomogida, Steve Roecker, and Jeff Mann made that team a competitive and fun one. I would like to say thanks to all the graduate and undergraduate students that I met at MIT.

I want to thank all the researchers that provided me with advice and data, specially John Sclater, Steven Cande, Tanya Atwater, Jeff Severinghaus, Kim Klitgord, and Hans Schouten.

This thesis is dedicated to my father, Wilson Pagel da Rosa, my mother, Maria de Lourdes Corrêa Rosa, my brother, João Willy Corrêa Rosa, my sisters, Solange and Simone Corrêa Rosa; and to my friend, Jessica Tornell. They helped me with their love, support and encouragement.

This research was supported by a fellowship from the Brazilian Antarctic Project (PROANTAR), through the Brazilian Research Council (CNPq), and

by research assistantship of the Massachusetts Institute of Technology.

Contents

Chapter 1

Introduction

Stratigraphic studies show that many transgressions and regressions identified along different continental margins are nearly simultaneous and similar in magnitude, indicating global changes in sea level. Because global changes in sea level reflect changes in tectonic, glacial, and other large scale processes (i.e. the change in the total volume of sea water), sea-level changes indicate the times of major events.

A eustatic sea-level change on a global scale may be caused by a change in the total volume of water in the oceans, by a change in the volume of the ocean basins, or by a combination of both. The change in the volume of water may be due to glaciation and deglaciation, or to the production of juvenile water from magmatic sources or hot springs. Tectonic processes or the filling of the basins by sediments may cause a change in the volume of the ocean basins.

Among these, only tectonic processes seem to be capable of causing long-period sea-level changes (Vail *et al.*, 1977). Pitman (1978) considered that glacial changes and processes such as dessication and flooding of small ocean basins cause rapid changes in sea level of tens of meters, but variation in the volume of midocean ridges, related to changes in the rate of seafloor spreading,

is the mechanism most likely to cause larger and longer lasting changes in sea level.

Pitman [1978] showed that transgressions and regressions that are synchronous worldwide may be caused by changes in the rates of sea-level rise or fall. He indicated that the subsidence rate at the seaward edge of a passive margin platform, due to cooling of the lithosphere, is comparable with the rate at which sea level rises or falls. So, if there is a fall in the sea level, the shoreline will stabilize at that point on a margin where the rate of sea-level fall equals the difference between the rate of subsidence and the rate of sediment infill. If the rate of sea-level fall decreases, a transgression will occur, and if the rate of sea-level fall increases, a regression will occur. If there is a rise in the sea level, the shoreline can stabilize at that point on a margin where the rate of sea-level rise equals the difference between the sedimentation rate and the rate of subsidence. Under these conditions, if the *rate* of sea-level rise increases, a transgression will happen, and if the *rate* of sea-level rise decreases, a regression will occur. Pitman [1978] developed a quantitative relation between the position of the shoreline and the rates of subsidence, of sea-level change, and of sedimentation. He constructed a sea-level curve, where sea level is shown to fall steadily but at varying rates since Late Cretaceous time, due to a decrease in the volume of ocean ridges, resulting from a decrease in the rates of seafloor spreading.

The study of global changes in sea level has major applications that are very important to the oil industry. It is used to improve stratigraphic and structural analysis incorporating the effects of sea-level changes, in the estimation of geologic age before the drilling of a site, and in the development of a global geochronology system.

In regional stratigraphic studies, comparisons of regional sea level curves, based on the analysis of seismic sequences and regional sea-level changes, with

global sea-level curves can suggest age of sequences with poor control and can fill gaps in regional sea-level curves. Such comparisons also help in the prediction of depositional facies and distribution of sequences. In areas with sparse or no well control, the sea-level curves can be used to estimate the geologic age of strata before drilling. In the areas with good subsurface control and well defined biostratigraphic zones, the seismic sequences can be correlated for accurate age control. If the subsurface control is poor within the grid, geologic ages can be inferred by the comparison of a regional chart of relative sea-level changes built from seismic data, with a global sea-level curve.

A major potential application of a global sea-level curve is in the study of geochronology (Vail *et al.*, 1977) since global cycles are defined just by the global change in the relative position of sea level through time. The construction of accurate regional sea-level charts can be used to improve the global chart.

Finally, differences between the regional sea-level curve and the global curve may suggest anomalous regional processes such as tectonic subsidence or uplift (Vail *et al.*, 1977).

The study of sea-level changes is important not only to the petroleum stratigraphy but also to the studies of the heat budget of the earth, the force system on the surface plates, and paleoclimate.

A large portion of the heat loss occurs in young sea floor. Using a thermal model and subsidence of oceanic ridges, the ridge volume can be related to the ridge heat flow (Turcotte and Burke, 1978; Parsons, 1982).

Since orogenic events are mainly associated with plate consumption, past changes in sea level can be indicators of the episodicity of orogeny (Turcotte and Burke, 1978). Turcotte and Burke [1978] associated high global sea levels with cycles of high ridge heat flow. This implies a high rate of plate production and, consequently, a high rate of simultaneous plate consumption.

Parsons [1982] discussed further applications of the study of the area-age

distribution to the study of changes in the force system acting on the plates. A change in this force system would change the magnitudes and directions of plate velocities and hence the rate of plate generation and the distribution of consumption with age. Furthermore, the resultant changes in the area-age distribution would lead to new changes in the force system.

Changes in sea level are correlated with changes in the total surface of continental land and hence have important consequences on paleoclimates. The total continental land area affects total weathering systems, the CO_2 level of the atmosphere and the heat budget of the earth. Berner *et al.*[1983] determined that the CO_2 content of the atmosphere is highly sensitive to changes in the seafloor spreading rates and total continental land area. They determined a much higher CO_2 level for the Cretaceous atmosphere, based on the study of seafloor spreading rates. Assuming that CO_2 level and surface air temperature are correlated with an atmospheric greenhouse model, they predicted paleotemperatures for the Cretaceous. Berner *et al.*[1983] concluded that the predominant factor affecting atmospheric CO_2 and climate over the past 100 Ma., is worldwide tectonic activity.

In addition, the change in the total water and ice coverage can be linked to the absorption of heat from the sun and hence contributes to the total heat budget of the earth.

The ultimate objective of this thesis is to analyze the relationship between the distribution of area with age of the oceans and global changes in sea level. In order to accomplish this objective, we first had to organize a global dataset of magnetic anomalies and fracture zones, and a global dataset of rotation parameters. Then, we had to analyze the magnetic and bathymetric data in order to test the rotation parameters. We improved both of these datasets by digitizing and including more recently published data and by calculating new rotation parameters in order to minimize the uncertainties in the area-age distribution

of the oceans. We used these data to construct a reliable map of the age of the ocean basins for the present time and for 35.58 Ma and 58.94 Ma. We developed a method to measure the areas of a particular age span of the oceans. We used this method to measure the distribution of area with age of the oceans at the present time and at the two particular times chosen for the reconstructions (35.58 Ma and 58.94 Ma). Finally, we analyzed the implications of the resulting area-age distribution for global changes in sea level.

The first goal of the work presented here was to organize a set of magnetic anomalies, fracture zones and plate boundaries that included all the data collected and presented until now in the geophysical literature. We also collected published sets of rotation parameters. These first two steps involved a detailed search in the literature followed by the digitization of all the data that were not included in an earlier database, previously organized by other MIT researchers (Molnar *et al.*, 1975; Molnar *et al.*, 1988; Pardo-Casas and Molnar, 1987; Rosa and Molnar, 1988; Stock and Molnar, 1982, 1987; Suárez and Molnar, 1980) with contributions from Kim Klitgord, Hans Schouten, Tanya Atwater, Steve Cande, and John Sclater. We compiled isochrons for the times of magnetic anomalies 5 (10.59 Ma), 6 (19.90 Ma), 13 (35.58 Ma), 18 (42.01 Ma), 21 (49.55 Ma), 25 (58.94 Ma), 30-31 (68.47 Ma), 34 (84.00 Ma), M0 (118.35 Ma), M4 (125.91 Ma), M11 (132.78 Ma), M16 (141.52 Ma), M21 (149.65 Ma), and M25 (156.42 Ma).

The second task in this thesis was the analysis of the magnetic and bathymetric data in order to test the rotation parameters. This resulted in the refinement and modification of the rotation parameters and of the uncertainties associated with them to build a consistent set of parameters with calculated uncertainties that would work with all the plate boundaries.

We then constructed an internally consistent, reliable map of the age of the ocean basins for the present time and for two particular times in the past (35.58

Ma and 58.94 Ma). These are times of reliable reconstructions, when sea level was different, and when the plate configurations differed from the present plate configuration. This involved the definition of the isochrons for the present time and the later reconstructions of these isochrons to the past ages, as well as the extrapolation of the isochrons to certain areas of the ocean floor which were present in the past but were subducted later and are now not present on the existing ocean floor. The definition of the isochrons involved the analysis of the magnetic and bathymetric data, the digitization of the isochrons, together with the analysis and calculation of the rotation parameters.

The final goal was to analyze the area-age distribution for the present time and for the reconstructions at the times of anomalies 13 and 25 (35.58 Ma and 58.94 Ma respectively), and to associate the changes in these area-age distributions with sea-level changes.

1.1 Overview of Contents

In Chapter 2, we summarize our studies on the rigidity of the Pacific plate during late Cretaceous and Tertiary time, with the analyses of magnetic anomaly and fracture zone crossings, due to Pacific-Farallon-Vancouver-Kula-Nazca spreading, together with the calculation of rotation parameters and associated uncertainties. This portion of our work was already published by Rosa and Molnar [1986, 1988]. These results contributed to an improved tectonic history of the Pacific Ocean with implications for the geologic setting of western North America (see Stock and Molnar, 1988).

Tertiary plate motions in the southeastern Pacific were studied in detail in Chapter 3. This chapter presents an analysis of the data of Cande *et al.* [1982] with the calculation of rotation parameters and associated uncertainties, a stage which was not performed by those workers. The southeastern Pacific region has

undergone a complex tectonic history with spreading between several pairs of plates. Our analysis agrees with the evolution of this region originally proposed by Weissel *et al.* [1977] and supported by Cande *et al.* [1982], involving a major reorganization of plate boundaries between anomaly 26 time and anomaly 18 time.

In Chapter 4 we show the results of our analysis of global magnetic anomaly and fracture zone data, and of published rotation parameters, which were used to build a consistent set of global rotation parameters with calculated uncertainties. These were used together with digitized plate boundaries to define isochrons for the present time and for reconstructions at anomaly 13 time (35.58 Ma) and at anomaly 25 time (58.94 Ma).

In Chapter 5 we present the method used to calculate areas on the surface of the earth. We also discuss the errors associated with the method. This reliable and innovative method is used in Chapter 6 to determine the area-age distribution for the present time and for the reconstructions at the times of anomalies 13 and 25 (35.58 Ma and 58.94 Ma respectively). Finally, we interpret the changes in the area-age distribution in terms of changes in sea level.

Chapter 7 summarizes the results of each of the previous chapters, and presents further conclusions regarding the analysis of these results.

Figure Captions

Figure 1.1. Late Cretaceous to present sea-level curves (adapted from Kominz, 1984). The heavy dashed curve is from Haq *et al.*(1987). Kominz (1984) curve with error range, includes a 48 meters ice-volume correction.

It is a ridge-volume sea-level curve and assumes that the age-depth relationship of Parsons and Sclater (1977) and the magnetic anomaly time scale of Larson *et al.*(1982) are correct. The Pitman (1978) curve is also a ridge-volume derived sea-level curve with a 48 meters ice-volume correction. The Watts and Steckler (1979) sea-level curve is derived from Atlantic continental margin subsidence data. The dashed and dash-dot curves are derived from Paris basin subsidence data. The high (dashed) curve is that of Brunet and Le Pichon (1982) by assuming post-Cretaceous tectonic uplift. The hachured area is a water depth uncertainty. The Bond (1979) sea-level estimates are derived from a combination of stratigraphic data and continental hypsometry.

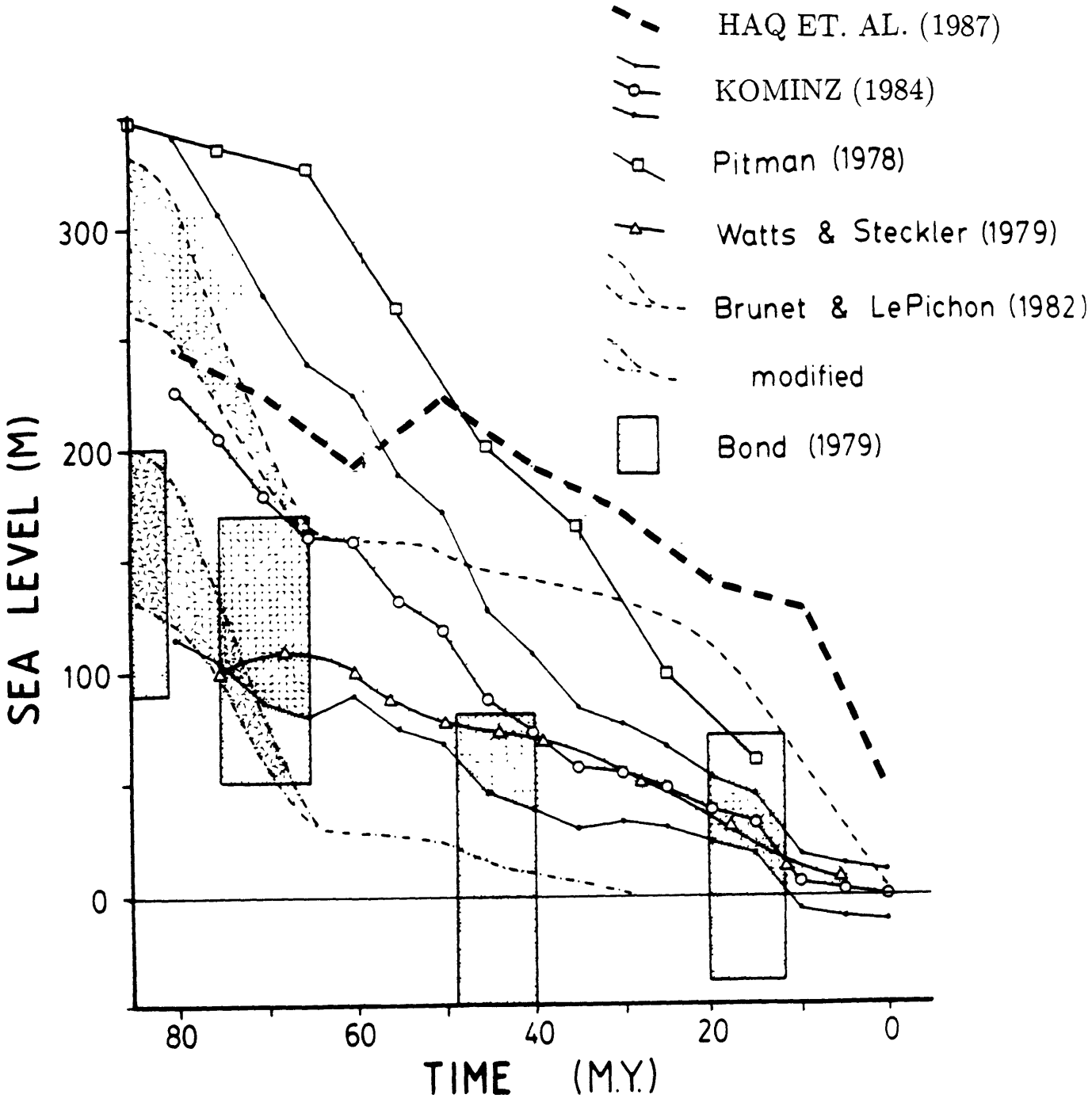
HAQ ET. AL. (1987)
KOMINZ (1984)
Pitman (1978)
Watts & Steckler (1979)
Brunet & LePichon (1982)
modified
Bond (1979)
SEA LEVEL (M)
300
200
100
0
80
60
40
20
0
TIME (M.Y.)

FIGURE 1.1

Chapter 2

Uncertainties in Reconstructions of the Pacific, Farallon, Vancouver, and Kula Plates and Constraints on the Rigidity of the Pacific and Farallon (and Vancouver) Plates between 72 and 35 Mega annum

2.1 Introduction

Since the first efforts to make global reconstructions of the major plates, it has been evident that there must have been an additional plate boundary in the sequence of finite rotations needed to reconstruct the Pacific plate, and hence

the Farallon plate, to other plates. The need for such a boundary is most clearly revealed by a comparison of the reconstructed positions of early Tertiary paleomagnetic poles from the major continents both with those of the Pacific plate and with inferred loci of the spin axis from sediment facies on the Pacific plate [*Gordon and Cox*, 1980; *Suárez and Molnar*, 1980]. Whereas most of the paleomagnetic poles from the continents agree within the uncertainties of one another, they disagree by more than 1000 km with those of the Pacific plate. Consequently, *Gordon and Cox* [1980] and *Suárez and Molnar* [1980] concluded that the additional plate boundary must lie somewhere between the equatorial Pacific and east Antarctica.

Determination of the reconstructed positions of the Farallon and North American plates is further complicated by the possibility of deformation of the Farallon plate during their history of convergence. *Menard* [1978] suggested that around 55 Ma, the Farallon plate split and that the area north of the Murray fracture zone moved as a separate plate, the Vancouver plate, from the remainder of the Farallon plate south of that fracture zone. Because at 55 Ma the Murray fracture zone could have lain 1000 km or more south of its present position, if Menard's [1978] contention were correct, it would not have been the Farallon plate that was subducted beneath most of North America during the Eocene and Oligocene epochs, but rather the Vancouver plate.

Unaware of Menard's [1978] suggestion of a Vancouver plate, the initial purpose of our study was to examine whether an important early Tertiary plate boundary could have lain north of the Eltanin fracture zone system, north of about 45°S in the South Pacific, within what is now the Pacific plate. While this study was in progress, *Engebretson et al.* [1984] presented results similar in many ways to some of those that we present here and showed that a plate boundary probably did not lie north of the Eltanin fracture zone. Shortly afterward, *Stock and Molnar* [1987] found the missing plate boundary within what

is now the Antarctic plate north of west Antarctica. Nevertheless since some aspects of our approach and some details of our results differ from those of *Engebretson et al.* [1984], we also present evidence similar to theirs for the rigidity of the Pacific plate. In addition, we found *Menard* [1978] to have been correct in that the Vancouver plate existed and moved separately from the Farallon plate since the time of anomaly 21.

2.2 Data

The first step was to reexamine all published profiles of magnetic anomalies that we could find from the Pacific plate: *Atwater* [1970] (her unpublished chart), *Bassinger et al.* [1969], *Elvers et al.* [1972, 1973], *Grim and Erickson* [1969], *Handschumacher et al.* [1975], *Hayes and Heirtzler* [1968], *Malahoff and Handschumacher* [1971], *Mason and Raff* [1961], *Molnar et al.* [1975], *Peter* [1966], *Peter et al.* [1970], *Pitman and Hayes* [1968], *Raff* [1966], *Raff and Mason* [1961], *Shih and Molnar* [1975], *Vacquier* [1965], and *Vacquier et al.* [1961]. From them we picked the locations of anomalies 13, 18, 21, 25, the negative anomaly between 30 and 31, and the positive anomaly on the young side of 32, according to the numbering system of *Pitman et al.* [1968] (Figure 2.1). To define fracture zones, we used the contour maps of *Chase et al.* [1970] in the North Pacific and crossings of the Agassiz fracture zone on Mammerickx's map of the South Pacific in the work by *Molnar et al.* [1975]. Unlike *Engebretson et al.* [1984], we did not consider the seafloor formed in the Early Cretaceous and Jurassic periods. Uncertainties were assigned to the location of individual crossings of magnetic anomalies according to the resemblance of the magnetic anomalies to those observed on other profiles and to whether or not satellite navigation was used. For fracture zones, we arbitrarily assigned an uncertainty of 20 km because of the difficulty of defining where within the complicated

topography the plate boundary lay.

All reconstructions are given for particular pairs of magnetic anomalies, not for uniformly spaced intervals of time, because of the uncertainties in the geomagnetic time scale.

For Cenozoic magnetic anomalies we used ages given by *Berggren et al.* [1985], and for Mesozoic anomalies, those of *Kent and Gradstein* [1985]. Values for the anomalies that we used are given in Table 2.1, together with those of *Harland et al.* [1982], which were used by *Engebretson et al.* [1984].

2.3 Search for the Poles of Rotations

In the reconstruction of the history of the Pacific-Farallon-Vancouver-Kula system, only one side remains of the seafloor originally formed at the Pacific-Farallon, Pacific-Vancouver, and Pacific-Kula ridges. The other sides have been consumed in subduction zones. Nevertheless, we can still determine most of the history based only on the magnetic anomalies and fracture zones present today on the Pacific plate. Insofar as the plates were rigid, the magnetic anomalies and the fracture zones represent the locations in the past of the ridges and transform faults. Thus to describe a reconstruction, we calculated the position of the pole of rotation and the angle that brought into accord the two sets of magnetic anomalies of different ages and the corresponding segments of the fracture zones that then were transform faults.

The "best" pole positions and angles for each interval of time between consecutive magnetic anomalies were first calculated using Hellinger's [1979] method and then improved by qualitative analyses of the resulting fits of the data. Hellinger's method [*Hellinger*, 1979; *Stock and Molnar*, 1982] begins with a primary search to find the angle of rotation, for a given pole position, that minimizes the misfit of corresponding segments of magnetic anomalies and fracture

zones. A second iterative search within a particular region is then made for the location of the pole with the minimum misfit. Since we have data from only one plate, points representing a magnetic anomaly of one age were rotated about a given pole to overlie points of an older magnetic anomaly.

Because Hellinger's method uses a least squares analysis of errors, it is sensitive to data that do not follow the assumptions of the method [*Hellinger*, 1979]. A lack of sufficient data to define a trend in a plate boundary, as is the case for some anomalies in the South Pacific, makes Hellinger's method insensitive to these data. Significant differences in trend between corresponding segments of the boundary, caused for instance by changes in direction of spreading or by disruption by propagating ridges and transform faults, can make the distribution of misfits not Gaussian at all [*Hellinger*, 1979]. Although we tried to avoid such situations, one check suggested that we were not entirely successful. The calculated rotations should agree among themselves. For example, if we combine the rotation necessary to rotate anomalies 13 over anomalies 18 with the rotation of anomalies 18 to anomalies 21, we should obtain the rotation for the 13-21 rotation. In practice, however, when rotations such as these three were calculated independently, they were not consistent. "Best" fits obtained by Hellinger's [1981] method were routinely examined visually, and we made qualitative choices of the best fitting reconstructions (Tables 2.2, 2.3, and 2.4). In all cases, however, the reconstructions obtained from Hellinger's method lay well within the uncertainties in the reconstructions that we present.

2.4 Calculations of Uncertainties

Because of the differences in the distribution of magnetic anomalies and fracture zones of different ages, two variations on the procedure outlined by *Stock and Molnar* [1983] were used to describe uncertainties in the rotations. With either

variation we avoid the unwieldy description of the uncertainties in both the position of the pole and the rotation angle, quantities that are dependent on one another. Instead we cast the uncertainty in terms of small perturbing rotations about three orthogonal axes.

For the Pacific-Farallon rotation of anomaly 30-31 to 32 and for the rotations that describe either Pacific-Kula or Pacific-Vancouver motion, we used the method developed by *Stock and Molnar* [1983] and modified slightly by *Molnar and Stock* [1985] (Figure 2.2a). We found the positions of three axes: one in the center of the set of the older anomalies of the pair, a second 90° from it in the direction of transform faults that were, or would have been, active then, and a third 90° from the first in a direction perpendicular to such transform faults. Small rotations about each of these three axes produce small but allowable misfits: (1) a rotation about the first produces a skewed fit, with underlap of some magnetic anomalies and overlap of others, (2) a rotation about the second axis mismatches fracture zones (transform faults), and (3) a rotation about the third systematically mismatches the magnetic anomalies but not the fracture zones. We tolerated uncertainties in positions and misfits of 20 km. The minimum angle of rotation to give a 20-km skewed mismatch can be approximated by

$$\frac{20(km)}{111.4(\frac{km}{degree})sin\frac{L}{2}}$$

where L is the length, in degrees, of the plate boundary for which there are data [*Stock and Molnar*, 1983]. The angle of rotation that gives a 20-km mismatch of the fracture zones or magnetic anomalies is 0.18°.

For the Pacific-Farallon rotations that use data south of the Pioneer fracture zone from both the North and South Pacific, we used a different method to obtain the three orthogonal axes (Figure 2.2b). For each rotation, we took the southernmost crossing of the older anomaly north of the Murray fracture zone as a northern axis. Rotation about this axis would cause a large mismatch

of data in the South Pacific without degrading the fit in the North Pacific substantially. Given the limited number of data, we allowed a rotation of 0.36°, corresponding to misfits of as much as 40 km in the South Pacific. Using the azimuth of the Murray fracture zone, we calculated an axis 90° away from this first point; a rotation about this axis would allow mismatches of 20 km of the fracture zones in both the North and South Pacific. As a southern center, we took a point 90° from the other two. Small rotations about this axis cause much larger mismatches of the magnetic anomalies in the North than in the South Pacific. We allowed a 20-km mismatch for these anomalies at the Murray fracture zone, corresponding to an angle of 0.18°. Examples of the calculated uncertainty regions for each rotation were plotted beside the selected anomalies in Figures 2.3–2.6, and the partial uncertainty rotations are listed in Tables 2.5–2.7.

2.5 Results

2.5.1 Pacific-Farallon, south of the Pioneer fracture zone

As we show below, the magnetic anomalies younger than anomaly 21 and corresponding fracture zones north of the Pioneer fracture zone and south of the Murray fracture zone cannot have formed by spreading of the same Farallon plate from the Pacific plate. It appears that the seafloor between the Pioneer and Murray fracture zones formed by separation of the Pacific plate from the Farallon plate, which lay south of the Murray fracture zone, and not from the Vancouver plate [*Menard*, 1978], which lay north of the Pioneer fracture zone. Thus we begin our discussion with results for Farallon-Pacific motion south of the Pioneer fracture zone. The magnetic anomalies, particularly 13, 18, and 21, between the Pioneer and Murray fracture zones played an important role

in this analysis, since this is the area with the best coverage. To illustrate the reconstructions, we show the rotated points representing the crossings of each anomaly to those of the next older anomaly, and the rotated positions of anomaly 13 over all the others (Figures 2.3–2.5).

Just south of the Murray fracture zone (Figure 2.4), however, there is an anomalously large space between anomalies 13 and 21, where a ridge jump must have occurred [*Menard and Atwater*, 1969; *Harrison and Sclater*, 1972]. Thus anomalies 13 from this segment do not help in the reconstruction. A little farther south of the Murray fracture zone, approximately at 26°N, there are two crossings of anomaly 18 (Figure 2.4). If the trend of these anomalies can be extended to the north, the spacing between anomalies 13 and 18 south of the Murray fracture zone is more than twice the spacing between these anomalies north of this fracture zone. In this case, the ridge jump would have occurred sometime after anomaly 18, and the possibility of asymmetrical spreading could be ruled out, since the maximum distance between two anomalies in the case of a totally asymmetrical spreading must be twice the separation of the anomalies in a symmetrical spreading system. On the other hand, if we consider only anomalies 13 and 21, the spacing between these anomalies just south of the Murray fracture zone is less than twice the spacing between these same anomalies between the Pioneer and Murray fracture zones. In this case, a ridge jump could have occurred, but the possibility of asymmetrical spreading during the interval between 35 and 50 Ma cannot be discarded.

Between the Pioneer and the Murray fracture zones, anomalies 13, 18, and 21 show slight departures from their north-south trends (Figure 2.4). These variations in trends gave us some difficulty when we rotated them over one another and over older anomalies. Although *Menard* [1978] explained these departures as a result of a split of the Farallon plate about 37 Ma, we think that they can be explained by a process of ridge jumping, probably by the

propagation of spreading centers and transform faults [*Hey*, 1977; *Shih and Molnar*, 1975]. In any case this difficulty is most serious for reconstructing anomaly 25 and younger anomalies. Only four crossings define the anomaly 25 lineation between the Pioneer and Murray fracture zones, and only one pair of them can be overlapped by rotated anomalies 13, 18, or 21. We chose to overlap the southern two crossings of anomaly 25 because by doing so we also can match anomalies 21 and 25 south of the Murray fracture zone. If we were to match the northern crossings of anomaly 25, we could match neither crossings of anomaly 21 south of the Murray fracture zone nor the trend of the fracture zones.

Crossings of magnetic anomalies in the South Pacific are few, and by themselves they could not define poles and angles well. We, like *Engebretson et al.* [1985] however, found that we could use the same pole positions (Table 2.2) to match the magnetic anomalies and the trend of the Agassiz fracture zone in the South Pacific with the magnetic anomalies and fracture zones in the North Pacific south of the Pioneer fracture zone (Figures 2.4 and 2.5).

To reconstruct anomaly 25 to anomaly 30-31, we found that we could use the trends of the Surveyor and Mendocino fracture zones and the crossings of these anomalies between them (Figure 2.3). The spacing of these anomalies farther north, however, is too large, and some asymmetric accretion of material to the Farallon and Pacific plates must have occurred there (Figure 2.3).

We found no reliable crossings of anomaly 32 in the South Pacific, but from those profiles of anomaly 30-31 near 35°S, 145°W, we are convinced the spreading rate there was relatively slow and that anomaly 32 must lie only about 100 km west of anomaly 30-31. Nevertheless, crossings of anomalies 30-31 and 32 from the Great Magnetic Bight in the North Pacific to those south of the Murray fracture zone can be rotated to one another such that the predicted position of anomaly 32 in the South Pacific lies just west of anomaly 30-31 there (Figure 2.5).

Thus as *Engebretson et al.* [1984] found, magnetic anomalies and fracture zones in the North and South Pacific are sufficiently concordant that we can be confident that, except for local areas such as the disturbed zone south of the Murray fracture zone, the Farallon and Pacific plates behaved rigidly from the time of anomaly 32 to that of anomaly 13.

2.5.2 Pacific-Vancouver, north of the Pioneer and Mendocino fracture zones

To fit magnetic anomalies north of the Pioneer fracture zone and younger than anomaly 21, we found that the parameters used for the region south of it yield unacceptable misfits (Figure 2.7), and rotation parameters different from those used for the area south of the Pioneer fracture zone are necessary. The need for different parameters is particularly clear from the trends of the Surveyor, Mendocino, and Pioneer fracture zones, which differ by about 11° from that of the Murray fracture zone. It was largely because of this difference in trends of fracture zones that Menard inferred that there must have been a Vancouver plate, separate from the Farallon plate beginning some time between the formation of anomalies 25 and 21. Note also, however, that when the magnetic anomalies north of the Pioneer fracture zone are rotated about the poles determined for the Pacific south of the Pioneer fracture zone, some rotated anomalies lie on the south side of the Mendocino, Surveyor, and Pioneer fracture zones and others mismatch their counterparts by as much as 100 km (Figure 2.7).

When we rotate backward the magnetic anomalies 21 and 18 over crossings of magnetic anomaly 13 south of the Pioneer fracture zone about the poles of rotations determined for the Pacific north of this fracture zone (Table 2.3), the rotated anomalies lie on the south side of the Murray fracture zone (Figure 2.8). This implies that the seafloor be a result of spreading between the Pacific and

Farallon plates and not between the Pacific and Vancouver plates. Only if the creation of the disturbed zone were associated with propagating ridges that crossed the Murray fracture zone, could its trend be oblique to transform faults that offset the Pacific-Farallon ridge. We cannot completely eliminate this possibility, but both the parallelism of the Murray and Clipperton fracture zones and the orthogonality of magnetic anomaly lineations to the Murray fracture zone suggest that the Murray fracture zone formed as a transform fault between the Pacific and Farallon plates and does not reflect deformation near the triple junction of the Pacific, Vancouver, and Farallon plates. Thus we think that the Pacific-Farallon-Vancouver triple junction lay on the Pioneer fracture zone, but we cannot eliminate completely the possibility that it lay on the Murray fracture zone or between these two fracture zones.

Engebretson et al. [1984] did not infer that the Vancouver and Farallon plates were distinct. They relied on various published inferences of linear trends of magnetic anomalies and projections of their intersections with fracture zones to constrain the reconstructions. Locations for such projected intersections probably contain larger errors and discrepancies than those of individual crossings of magnetic anomalies. Thus we suspect that their data included sufficient "noise" to make the misfits of the data north and south of the Pioneer fracture zone seem acceptable without revealing the mismatch of some tens of kilometers that we found.

Replacement of the Farallon plate by the Vancouver plate in global plate reconstructions makes small, but in some cases significant, changes in the calculated rates of subduction beneath western North America between 50 and 35 Ma. In the present coordinates and with respect to the Pacific plate at the time of anomaly 13, the calculated position of the pole of rotation describing the convergence between the Vancouver and Farallon plates from the time of anomaly 21 to that of anomaly 13 is 41°N, 108°W. This position is nearly due east of

the east-west trending Mendocino fracture zone. Although the rotation angle of 7.8°, corresponding to an average angular velocity of 0.56°/yr is not small, the proximity of the pole to the Farallon-Vancouver plate boundary, a maximum of 18° from the pole, means that the relative motion across that boundary was small, less than 20 mm/yr. Moreover, at the part of the west coast of North America where the eastern half of the Mendocino fracture zone would have intersected it, the rate of motion of the Farallon and Vancouver plates would have been smaller and virtually negligible. Ignoring the existence of the Vancouver plate, however, is more serious at its northern extremity, which relative to North America lay near the present latitude of Cape Mendocino at the time of anomalies 13 and 18 [*Stock and Molnar*, 1988]. At this position and at the time of anomaly 13, the calculated velocity of the Vancouver plate with respect to the Farallon plate is about 30 mm/yr. Therefore the calculated average relative velocity between the Vancouver and North American plates at this locality also differs by 30 mm/yr from the velocity that would be calculated for the Farallon and North American plates, assuming that there was no separate Vancouver plate. Thus the inclusion of a separate Vancouver plate is probably unimportant for some crude calculations of the subduction history of western North America, but is important for those seeking quantitative relations between plate motions and the geology of the continental interior of western North America.

Finally note that some authors relate the major reorganization in the Pacific-Farallon-Kula relative motions at about 55 Ma to the death of the Pacific-Kula ridge [e.g., *Byrne*, 1979; *Duncan*, 1982]. *Engebretson et al.* [1984], however, believe that the Pacific-Kula spreading continued until about anomaly 18.

2.5.3 Kula plate

Numerous crossings of anomalies 25 and 30-31 and a few of anomaly 32, plus the trend of the Amlia fracture zone, allow us to determine parameters for the

reconstruction of these anomalies (Figure 2.6). Unfortunately, the published profiles east of the Amlia fracture zone (Figure 2.6) clearly show anomalies that are not part of the sequence in the rest of the world [*Peter et al.*, 1970]. Thus a clear ridge jump makes it impossible to match the best sets of anomalies 30-31 and 32. In any case, the same pole position works for both reconstructions, but the uncertainty for the reconstruction of anomaly 30-31 to 32 is clearly the larger.

2.6 Conclusions

Five results can be listed from our analysis in this chapter. (1) Tables 2.2–2.4 list sets of consistent rotations for the Pacific-Farallon, Pacific-Vancouver, and Pacific-Kula plates between the times of anomalies 13 and 32, and Tables 2.5–2.7 give uncertainties. (2) The Pacific and Farallon plates between the Pioneer and Agassiz fracture zones appear to have been rigid, with neither broken into two plates in that interval of time. (3) Therefore the additional Tertiary plate boundary inferred by *Gordon and Cox* [1980] and *Suárez and Molnar* [1980] must have been south of the area studied within the Pacific plate south of the latitude 43°S, or within the Antarctic plate. (4) Spacings of magnetic anomalies 13, 18, and 21 north of the Pioneer fracture zone and the orientations of the Pioneer, Mendocino, and Surveyor fracture zones differ from those south of the Pioneer fracture zone and suggest that between the formation of anomalies 25 and 21, the northern part of the Farallon plate split from the rest of it to form the Vancouver plate, as *Menard* [1978] had inferred. (5) Therefore it has been the Vancouver plate, not the Farallon plate, that was subducted beneath most of western North America from about 55 Ma until the spreading center was

annihilated at the subduction zone.

Figure Captions

Figure 2.1 Locations of magnetic anomalies and fracture zones used in this chapter. Magnetic anomalies are shown as triangles and identified by number. The Amlia fracture zone is shown as A, and the other fracture zones are shown as C. Oblique Mercator projection with a pole at 72.90°N, 90.77°E.

Figure 2.2a Diagram showing locations of centers of rotation used for calculating uncertainties by the method developed by *Stock and Molnar* [1983] and modified slightly by *Molnar and Stock* [1985]. Points A and D represent the locations of the northernmost and southernmost crossings of the set of the older magnetic anomalies of the pair, respectively. Centers for mismatched magnetic anomalies (m. ma.) and for mismatched fracture zones (m. fz.) are indicated.

Figure 2.2b Diagram showing locations of centers of rotation used for calculating uncertainties by a variation of the method outlined by *Stock and Molnar* [1983]. Points A and B represent the locations of the northernmost and southernmost crossings of the set of the older anomalies of the pair, respectively, in the North Pacific. Points C and D represent similar locations in the South Pacific. Centers for mismatched magnetic anomalies (m. ma.) and for mismatched fracture zones (m. fz.) are indicated.

Figure 2.3. Fits and uncertainties in rotations of magnetic anomalies in the North Pacific. The magnetic anomalies are shown as triangles and identified by number. Numbers in parentheses show inferred locations. The Amlia fracture zone is shown as A, and other fracture zones are shown as C. The solid circles represent the rotation of each anomaly over the next older anomaly. The crosses represent the rotation of magnetic anomaly 13 over all others. Oblique Mercator projection with a pole at 72.90°N, 90.77°E.

Figure 2.4. Detailed view of part of Figure 2.3 showing fits and uncertainties in the rotations of magnetic anomalies between 24°N and the Mendocino fracture zone. The magnetic anomalies are shown as triangles and identified by number. Numbers in parentheses show inferred locations. The fracture zones are shown as C. The solid circles represent the rotation of each anomaly over the next older anomaly. The crosses represent the rotation of magnetic anomaly 13 over all others. Oblique Mercator projection with a pole at 72.90°N, 90.77°E.

Figure 2.5. Fits and uncertainties in rotations of magnetic anomalies in the South Pacific. The magnetic anomalies are shown as triangles and identified by number. Numbers in parentheses show inferred locations. The Agassiz fracture zone is shown as C. The dot-dashed lines represent proposed fracture zones. The solid circles represent the rotation of each anomaly over the next older anomaly. The crosses represent the rotation of magnetic anomaly 13 over all others. Oblique Mercator projection with a pole at 72.90°N, 90.77°E.

Figure 2.6. Detailed view showing fits and uncertainties in the Pacific-Kula rotations. The magnetic anomalies are shown as triangles and identified by number. The Amlia fracture zone is shown as A, and other fracture

zones are shown as C. The solid circles represent the rotation of each anomaly over the next older anomaly.

Figure 2.7. Misfits in the rotations of magnetic anomalies north of Pioneer fracture zone and fits in the rotations south of Pioneer fracture zone using the rotation parameters appropriate for the rotations south of Pioneer fracture zone (Table 2.2). The magnetic anomalies are shown as triangles and identified by number. The fracture zones are shown as C. The solid circles represent the rotation of magnetic anomaly 18 over magnetic anomaly 21. The crosses represent the rotation of magnetic anomaly 13 over magnetic anomalies 18 and 21. Oblique Mercator projection with a pole at 78.00°N, 140.00°W.

Figure 2.8. Fits in the rotations of magnetic anomalies north of Pioneer fracture zone and misfits in the rotations south of Pioneer fracture zone using the rotation parameters appropriate for the rotations north of Pioneer fracture zone (Table 2.3). The magnetic anomalies are shown as triangles and identified by number. The symbol (13) shows the inferred location of magnetic anomaly 13 in the disturbed zone. The fracture zones are shown as C. The solid circles represent the rotation of magnetic anomaly 21 over magnetic anomalies 18 and 13, and also the rotation of magnetic anomaly 18 over magnetic anomaly 13. Oblique Mercator projection with a pole at 78.00°N, 140.00°W.

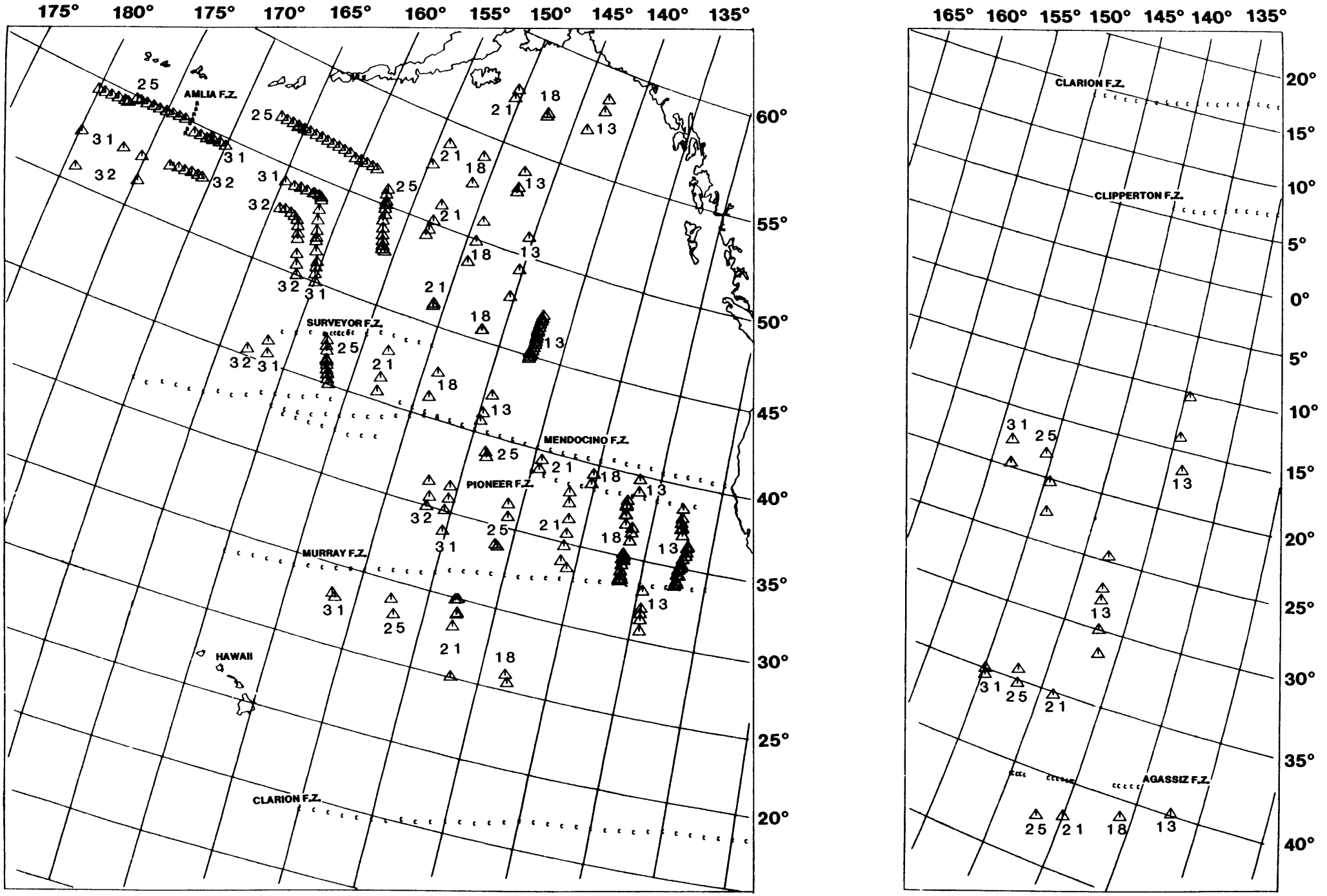
175° 180° 175° 170° 165° 160° 155° 150° 145° 140° 135°
60° 55° 50° 45° 40° 35° 30° 25° 20°
AMLIA F.Z.
SURVEYOR F.Z.
MENDOCINO F.Z.
PIONEER F.Z.
MURRAY F.Z.
HAWAII
CLARION F.Z.
165° 160° 155° 150° 145° 140° 135°
20° 15° 10° 5° 0° 5° 10° 15° 20° 25° 30° 35° 40°
CLARION F.Z.
CLIPPERTON F.Z.
AGASSIZ F.Z.

FIGURE 2.1

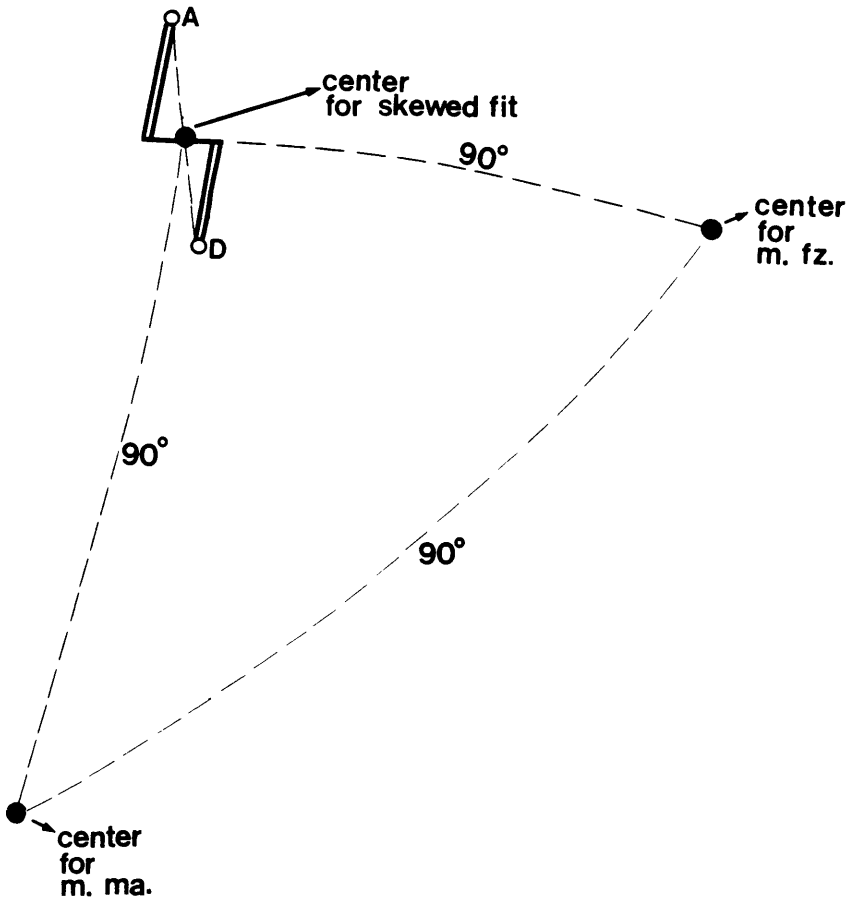
A
center
for skewed fit
90°
D
center
for
m. fz.
90°
90°
center
for
m. ma.

FIGURE 2.2**a**

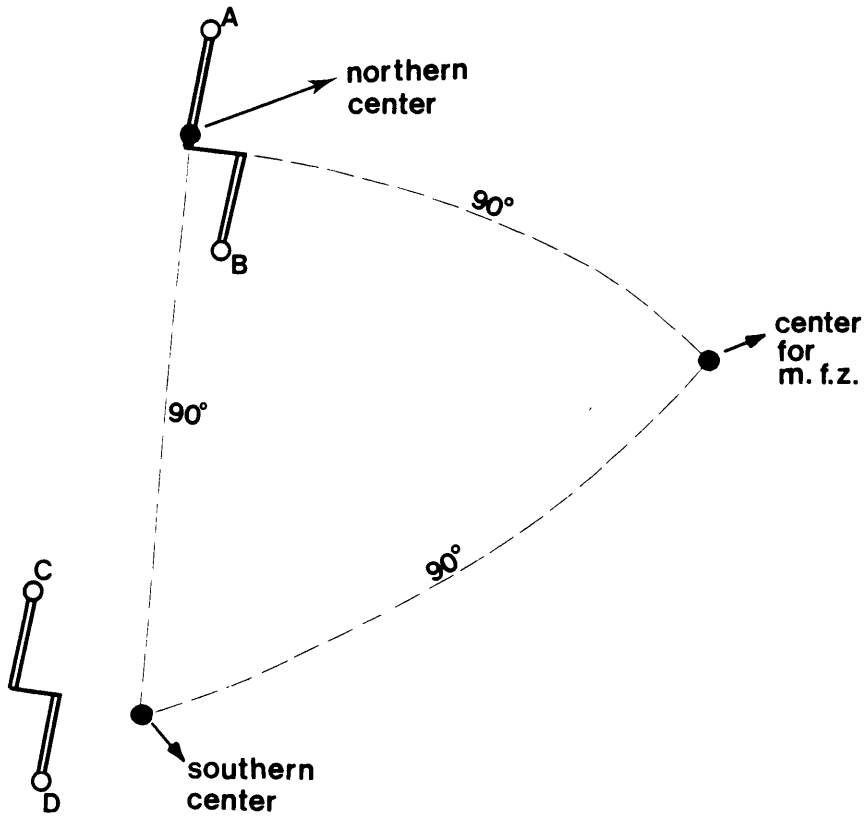
A
northern
center
B
90°
center
for
m. f.z.
90°
90°
C
D
southern
center

FIGURE 2.2**b**

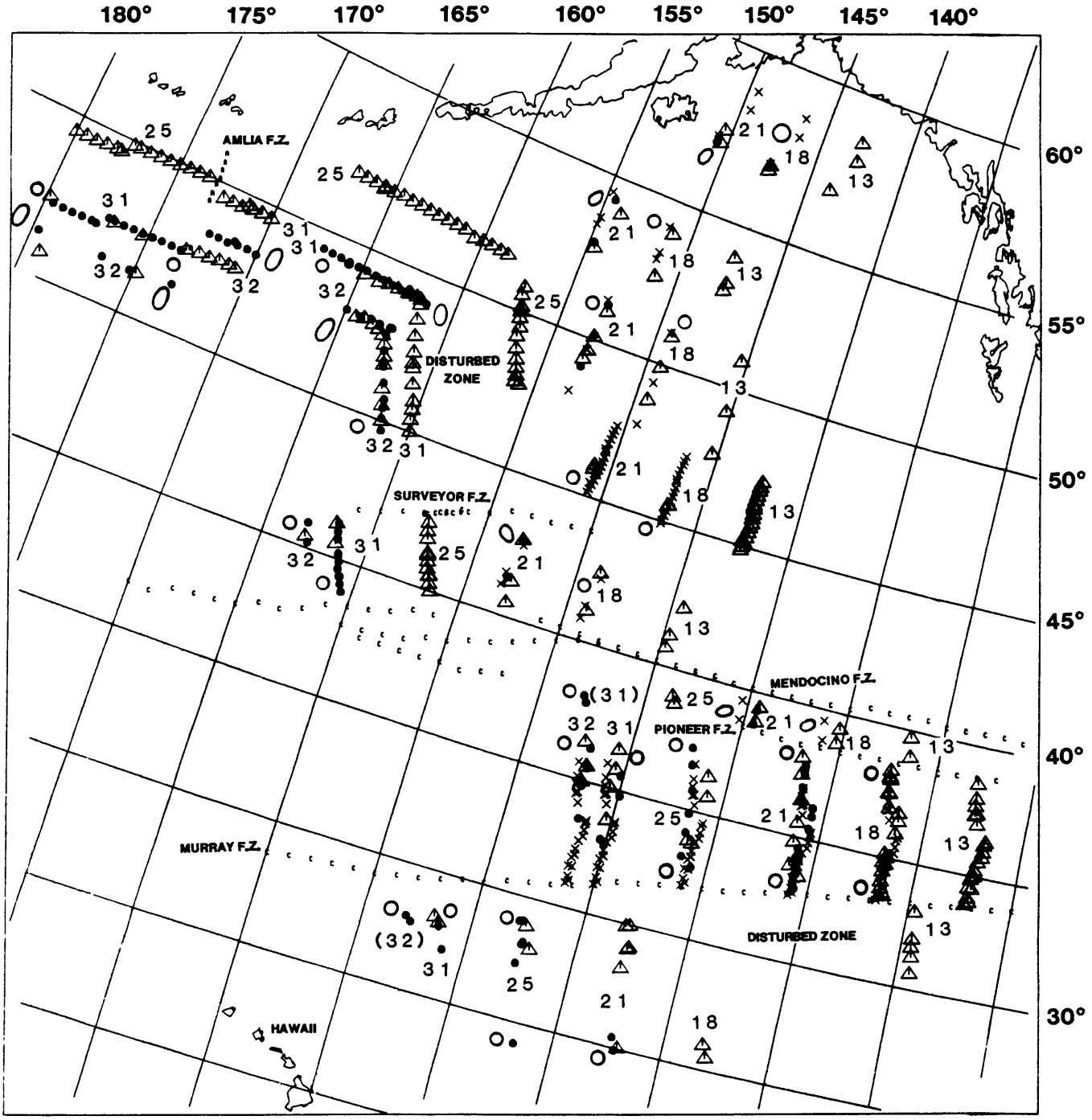
180°
175°
170°
165°
160°
155°
150°
145°
140°
60°
55°
50°
45°
40°
30°
AMLIA F.Z.
DISTURBED ZONE
SURVEYOR F.Z.
MENDOCINO F.Z.
PIONEER F.Z.
MURRAY F.Z.
DISTURBED ZONE
HAWAII

FIGURE 2.3

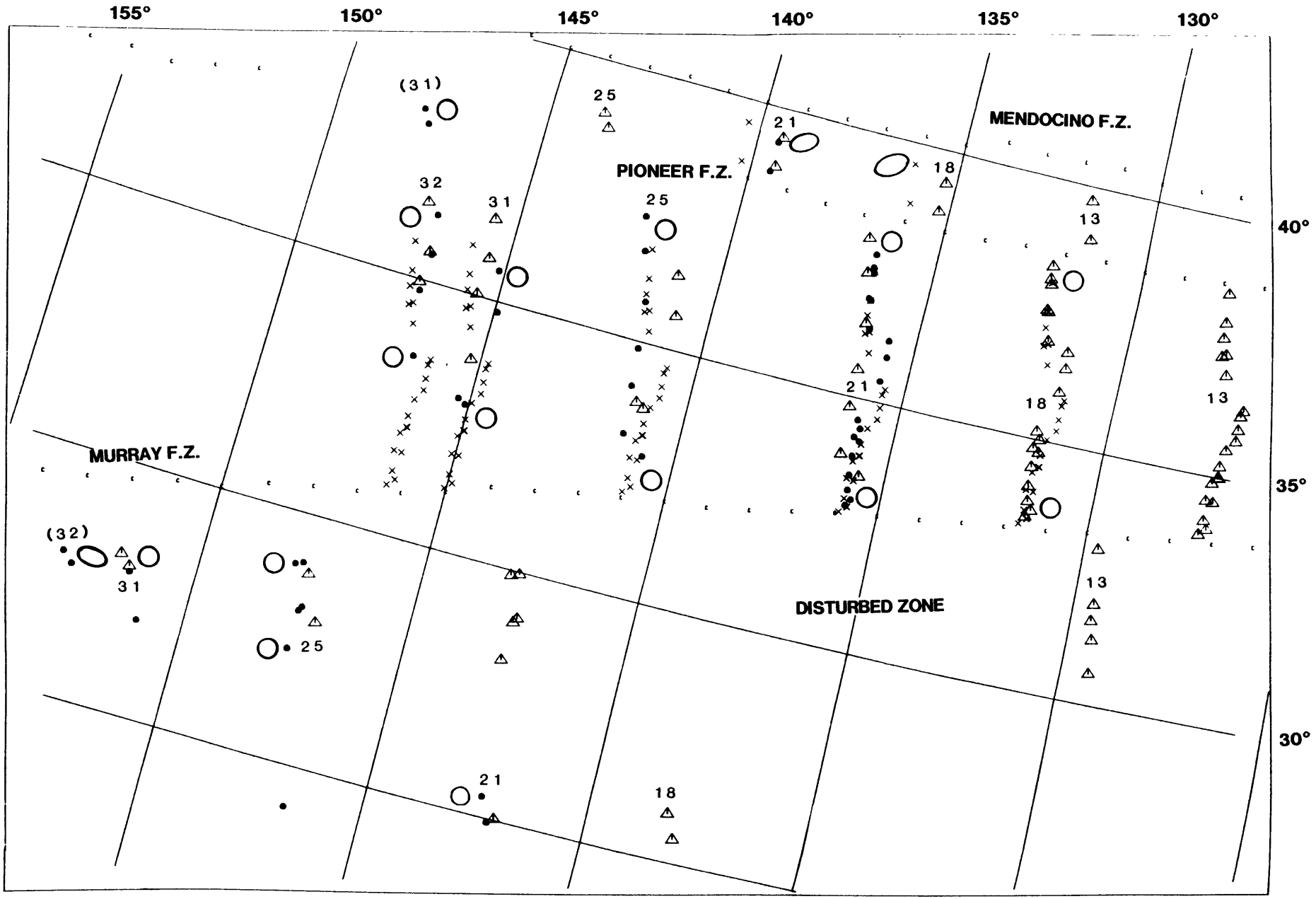
155°
150°
145°
140°
135°
130°
40°
35°
30°
MENDOCINO F.Z.
PIONEER F.Z.
MURRAY F.Z.
DISTURBED ZONE
(31)
25
21
18
32
31
25
13
21
18
13
(32)
31
25
13
21
18

FIGURE 2.4

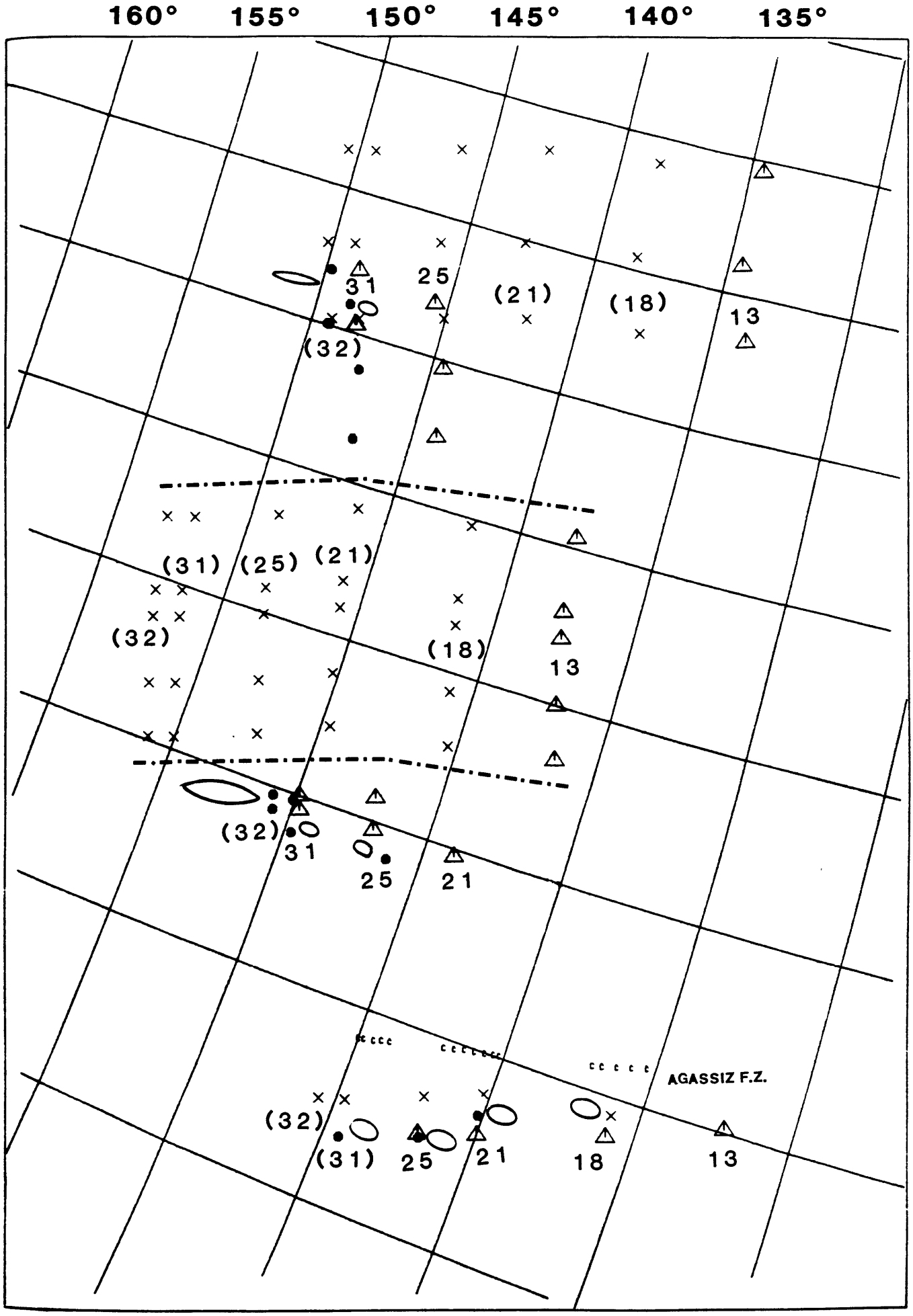
160°
155°
150°
145°
140°
135°
10°
15°
20°
25°
30°
35°
40°
31
25
(21)
(18)
13
(32)
(31)
(25)
(21)
(32)
(18)
13
(32)
31
25
21
AGASSIZ F.Z.
(32)
(31)
25
21
18
13

FIGURE 2.5

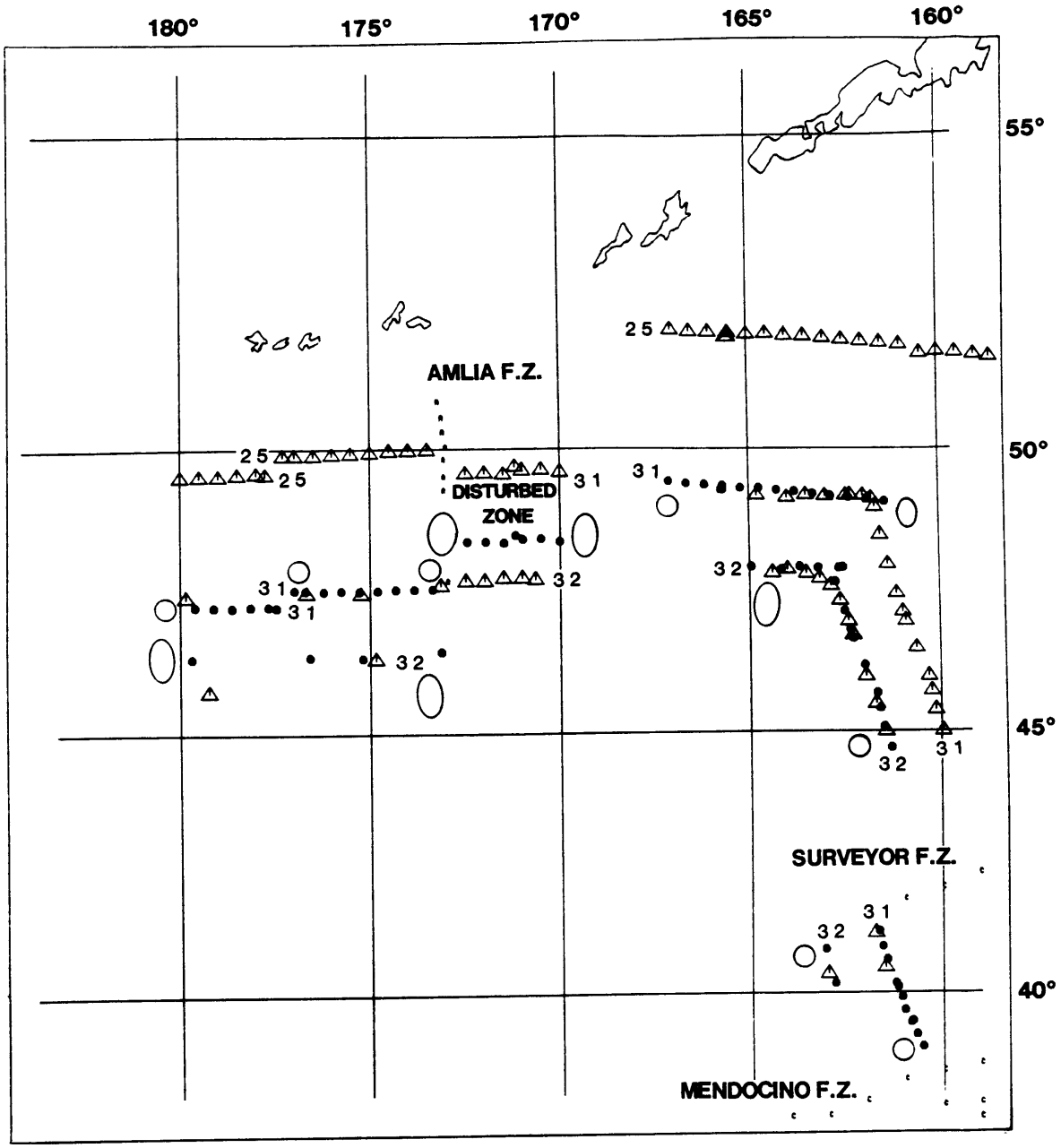
180°
175°
170°
165°
160°
55°
50°
45°
40°
AMLIA F.Z.
DISTURBED ZONE
SURVEYOR F.Z.
MENDOCINO F.Z.
25
31
32

FIGURE 2.6

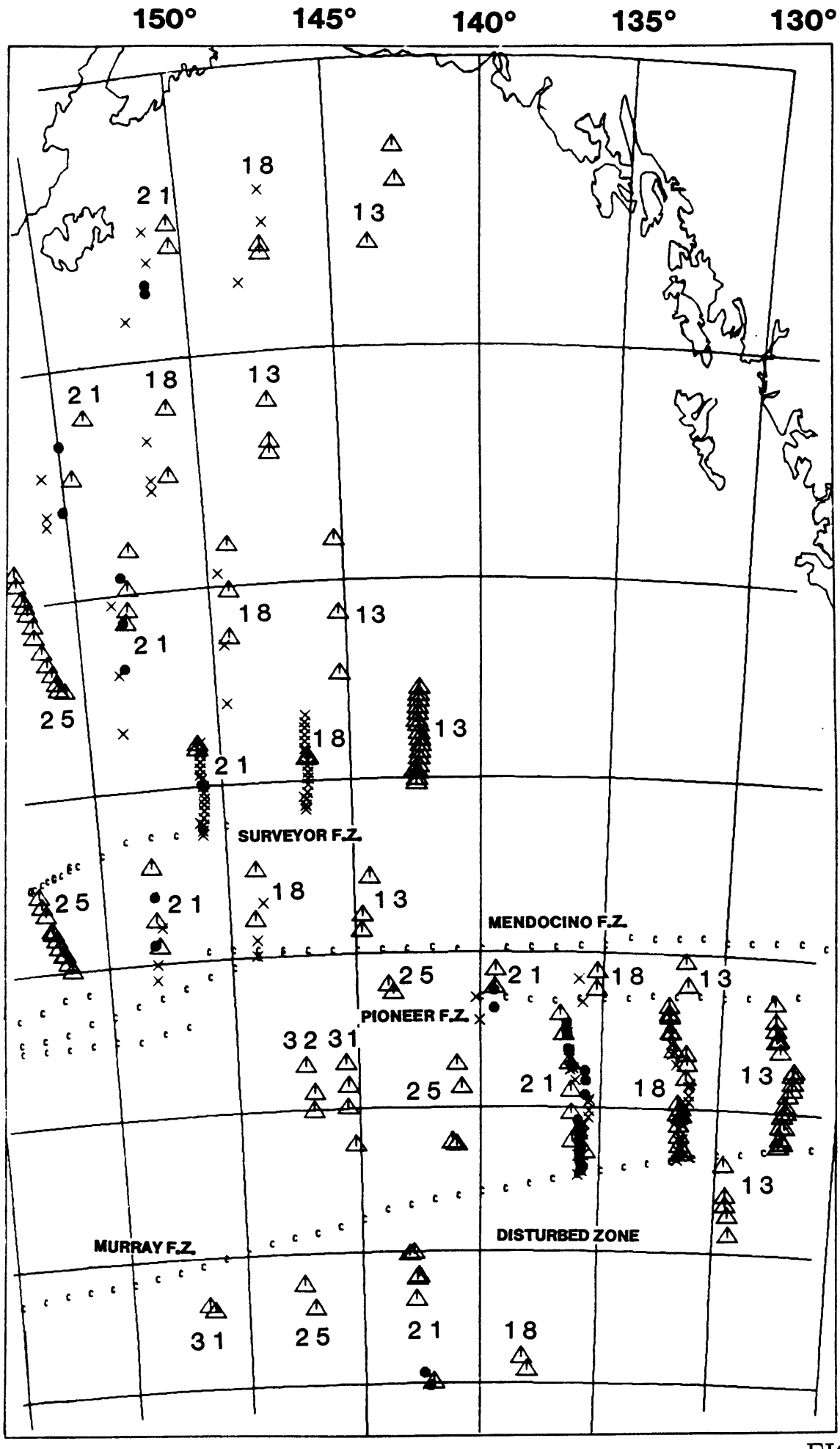
150°
145°
140°
135°
130°
60°
55°
50°
45°
40°
35°
30°
25°
SURVEYOR F.Z.
MENDOCINO F.Z.
PIONEER F.Z.
MURRAY F.Z.
DISTURBED ZONE

FIGURE 2.7

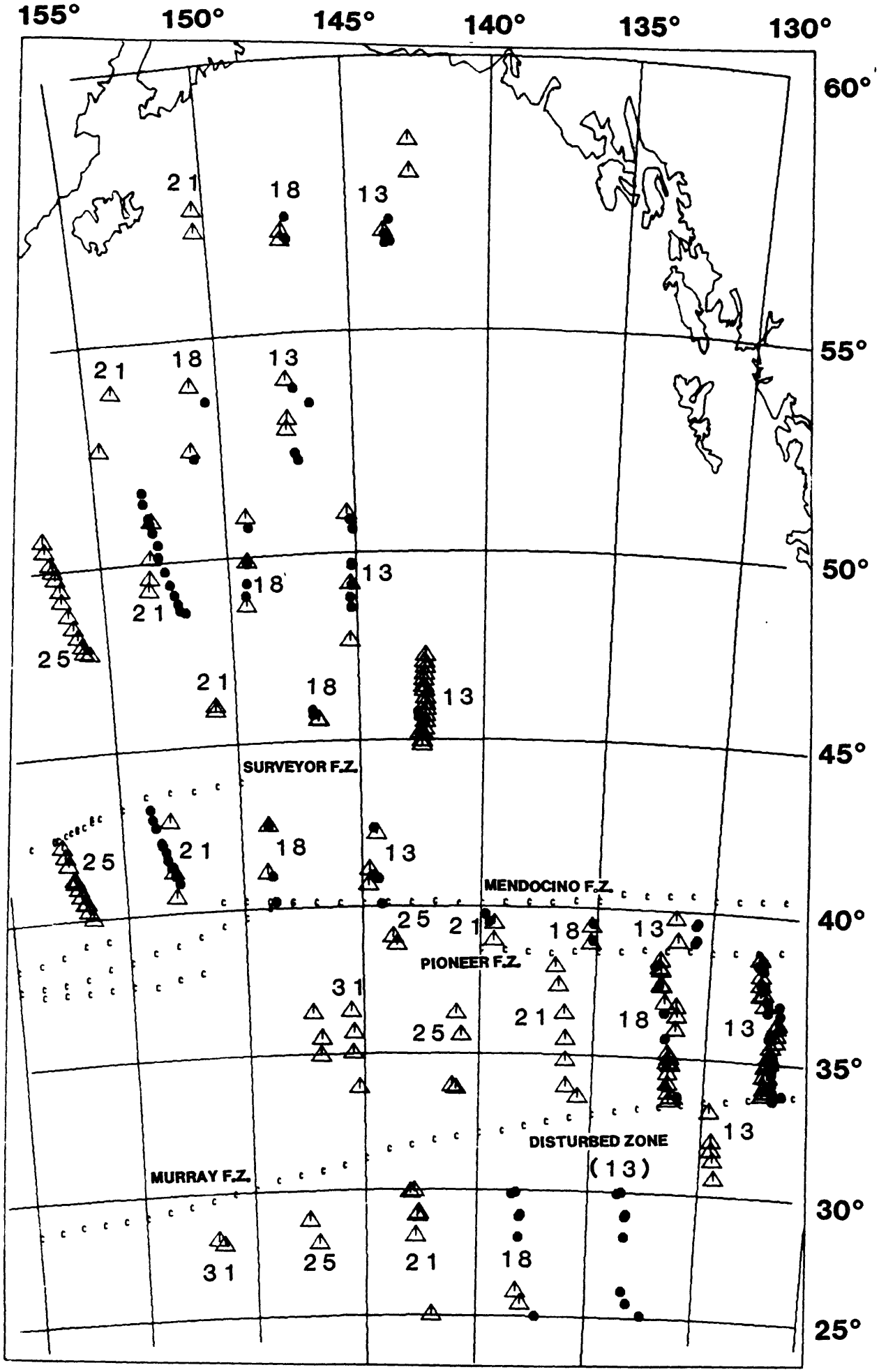
155°
150°
145°
140°
135°
130°
60°
55°
50°
45°
40°
35°
30°
25°
SURVEYOR F.Z.
MENDOCINO F.Z.
PIONEER F.Z.
MURRAY F.Z.
DISTURBED ZONE
(13)

FIGURE 2.8

Chapter 3

Uncertainties in Reconstructions of the Pacific, Antarctica, Farallon, and Aluk Plates during Cenozoic time

3.1 Introduction

Several spreading centers have been active in the southeast Pacific since early Cretaceous time, reflecting spreading among several pairs of plates: Pacific-Antarctica/Bellingshausen, Antarctica/Bellingshausen-Aluk, Pacific-Aluk, Pacific-Farallon, Antarctica/Bellingshausen-Farallon, and Antarctica-Nazca. Our knowledge of the tectonic history of this area was much improved by Cande *et al.*[1982], who, with much new data, identified a major re-organization in plate boundaries between anomaly 26 time and anomaly 18 time. At this time, a large fragment of sea floor was broken off the Pacific plate and joined to the Antarctica plate. This region, east of the Hudson Trough and south of the Hum-

boldt fracture zone (Figure 3.2), had subsequently spread rapidly away from an area in the southwestern Pacific, where a sequence of older anomalies, that were formerly adjacent and part of the same sequence of magnetic anomalies, had been identified by Weissel *et al.*[1977].

Weissel *et al.*[1977] had speculated that the anomalies west of the Henry Trough (Figure 3.2) were formed by Pacific-Aluk spreading. Weissel *et al.*[1977] proposed a model involving a major reorganization of plate boundaries between anomaly 26 time and anomaly 18 time (Figure 3.1). Before anomaly 26 time there was one triple junction involving the Pacific, Aluk and Antarctic plates and one triple junction involving the Pacific, Farallon and Aluk plates (Figure 3.1a). By anomaly 18 time, there was one triple junction involving the Pacific, Antarctic and Farallon plates and one involving the Antarctic, Farallon and Aluk plates (Figure 3.1b). The tectonic history proposed by Cande *et al.*[1982] seems to confirm their speculation. Cande *et al.*[1982] concluded that the reorganization occurred progressively over a 18.5 m.y. interval at about anomaly 21 time (49.55 Ma), and showed how this reorganization happened.

Here we analyze further the data in the southeast Pacific to quantify the reconstructions of the Pacific, Antarctic, Farallon, and Aluk plates at time of selected anomalies. These poles and angles of rotation will be used in later chapters for our global plate reconstructions, which is one of the major objectives of this thesis. In addition, they may be useful in later studies of the history of subduction along the South America and West Antarctica margins.

3.2 Data Analysis

In order to be able to study the region, we digitized the magnetic anomalies, fracture zones and plate boundaries presented by Cande *et al.*[1982] (Figure 3.2, Figure 1 of Cande *et al.*, 1982). These data were separated into groups

according to the spreading centers where the oceanic crust was formed. (Figure 3.3, Figure 2 of Cande *et al.*, 1982).

As described in Chapter 2, we emphasize that all reconstructions here were made for particular pairs of magnetic anomalies, not for uniformly spaced intervals of time, due to the uncertainties in the geomagnetic time scale.

3.3 Search for the Poles of Rotations

With the exception of a small part of seafloor just south of the southernmost point of South America, only one side remains of the seafloor originally formed at the Antarctica-Aluk, Pacific-Aluk, Pacific-Farallon, and Antarctica-Farallon ridges. Therefore, we determined the rotation parameters using only the magnetic anomalies and fracture zones present today on the Pacific and Antarctica plates.

We used the same methodology used in Chapter 2 to define the best-fit pole positions. The "best" pole positions and angles for each interval of time between consecutive magnetic anomalies were first calculated using Hellinger's [1979] method, described in Chapter 2, and then improved by qualitative analyses of the resulting fits of the data. For the southeast Pacific, however, there is much less data than was available for the Pacific-Farallon-Vancouver-Kula system. Thus, we had to make qualitative choices of best fitting reconstructions to define most of the rotation parameters (Tables 3.1 to 3.6).

Sometimes we refer to the Bellingshausen plate, instead of the Antarctica plate, since a reanalysis of early Tertiary magnetic anomalies on the Pacific plate south of the Campbell Plateau by Stock and Molnar [1987] indicated that until a little before anomaly 18 time (42.01 Ma), there was a triple junction of the Pacific, the Antarctic, and a third plate now beneath the Bellingshausen sea, which they named the Bellingshausen plate.

3.4 Calculations of Uncertainties

For the calculation of the uncertainties associated with the rotation parameters (Tables 3.7 to 3.11) we used the method of Stock and Molnar [1983] modified later by Molnar and Stock [1985] and described in the previous chapter (Section 2.4). The calculated partial uncertainty rotations listed In Tables 3.7 to 3.11 can be added to the best-fit rotations to estimate the uncertainty region surrounding the best-fit pole and angle.

Sometimes we could not calculate the uncertainties associated with the rotation parameters due to a lack of data. For example, in those places for which we have just one segment of the isochron with its orientation and size poorly defined by just one magnetic anomaly crossing. If it was impossible to calculate the uncertainties directly from the end points of plate boundaries, we interpolated or extrapolated from the parameters calculated for the adjacent magnetic anomalies.

The uncertainties in the rotation parameters are large because the lengths of plate boundaries are very short. In contrast, in Chapter 2, we studied the Northeast Pacific where the isochrons represent well defined and long plate boundaries, yielding small uncertainties in the rotation parameters.

3.5 Results

The southeast Pacific is a region of complex tectonic history. Calculating the rotation parameters, we noticed several interesting points that we shall discuss now.

Studying the Antarctic-Aluk (Bellingshausen-Aluk) data presented by Cande *et al.*[1982] with their collection of new magnetic anomalies, fracture zones and bathymetric features, we noticed that the data from north and south of one of

the fracture zones, could not be matched with the same rotation parameters, especially sometime before anomaly 10 (Figure 3.2, Figure 1 of Cande *et al.*, 1982). This is the second fracture zone south of the Hero fracture zone and the second fracture zone north of the Tula fracture zone, southeast from the region that is hachured in their figure (Figure 3.2). It is clear that a single reconstruction will not match the magnetic anomaly crossings north and south of this fracture zone for the 13-18 rotation, or for the 18-20 rotation. This fact could be real or it could be a result of poor identifications. A collection of new magnetic anomaly crossings and bathymetric data from this region is necessary to solve this problem.

Another problem that could be solved with the collection of new data is that there are no crossings of magnetic anomalies younger than anomaly 22 south of the Tula fracture zone and there are no crossings of magnetic anomalies older than anomaly 20 north of this fracture zone. We are not sure that the younger data south of the Tula fracture zone would be consistent with the rotation parameters determined for the data just north of this fracture zone.

Another feature noticeable in the Antarctica (Bellingshausen)/Aluk data presented by Cande *et al.*[1982] is that the lineations of magnetic anomalies 25 and 26, south of the Tula fracture zone, have different azimuths from the lineations of magnetic anomalies 23, 24, 27, 28 and 29. This also could be a result of misinterpretation of the magnetic data, sparsity of the magnetic anomaly crossings, unidentified fracture zones with small offset, or poor navigation. We can also notice that there was probably a ridge jump near anomaly 27 time, south of the Heezen fracture zone, where the spacing between the crossings of anomaly 28 and the crossing of anomaly 27 is different from the spacing between these two anomalies just north of this fracture zone. The Antarctica-Aluk reconstructions for anomalies 6 to 13 are the best constrained. There are not enough data to define well the other reconstructions.

In the region corresponding to Antarctica (Bellingshausen)-Farallon spreading, just north of the hachured area in Figure 3.2, there was probably a ridge jump between the times corresponding to magnetic anomalies 13 and 18 at the ridge segment west of the westernmost fracture zone. There was probably another ridge jump between the time of magnetic anomaly 12 and the time of magnetic anomaly 18, along the segment of ridge between the second and the third fracture zones counting from the west to the east.

We calculated the rotation parameters for the Nazca-Antarctic rotations for anomalies 5, 6, and 13, using the Nazca-Pacific and the Pacific-Antarctic poles and angles. If we use the pole and angle for the anomaly 5 rotation to rotate the data from Cande *et al.*[1982], the anomaly 5 crossings rotate parallel to the azimuth of the fracture zones that bound them.

3.6 Conclusions

The southeastern Pacific has been an area of complex tectonic activity with the spreading occurring between at least six different plate boundaries. Cande *et al.*[1982] presented more data and proposed a tectonic history for the area that agrees with that of Weissel *et al.*[1977].

We digitized all the data presented by Cande *et al.*[1982] and calculated rotation parameters with their associated uncertainties. As we expected, the uncertainties are large since we do not have enough data to constrain most of the rotations. However, these data are still useful for determining the age distribution of the ocean floor in this region. The rotation parameters can be used for calculating subduction rates from global plate circuits. Although the lengths of the spreading centers in this region are not large, a reanalysis of the original magnetic profiles and future collection of new magnetic and bathymetric data may reduce the uncertainties and further improve the details of the tectonic

history proposed by Weissel *et al.*[1977] and Cande *et al.*[1982].

Figure Captions

Figure 3.1. Orientations of plate boundaries in the southeast Pacific at different times (from Weissel *et al.*, 1977). Note the change in the plates involved in the two triple junctions at each of the two reconstructions (Figure adapted from Cande *et al.*, 1982).

Figure 3.2. Magnetic anomalies and fracture zones in the southeast Pacific Ocean after Cande *et al.*[1982]. The hachured seafloor was identified by Cande *et al.*[1982] as being formed by Pacific-Aluk spreading (from Cande *et al.*, 1982).

Figure 3.3. Separation of the Antarctica (Bellingshausen) plate into regions according to the spreading ridges at which the crust was formed (from Cande *et al.*, 1982).

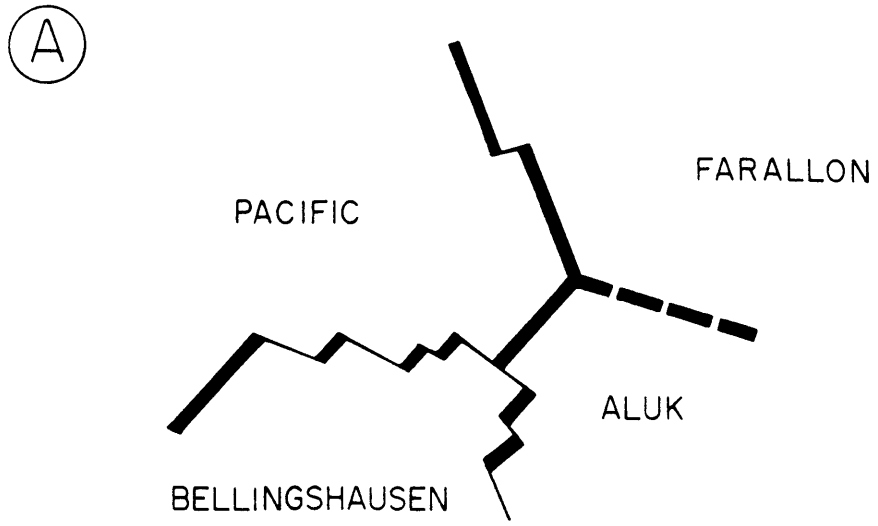
A
PACIFIC
FARALLON
ALUK
BELLINGSHAUSEN
Anomaly 26 Time
(60.48 Ma)
B
PACIFIC
FARALLON
ANTARCTIC
ALUK
Anomaly 18 Time
(42.01 Ma)

FIGURE 3.1

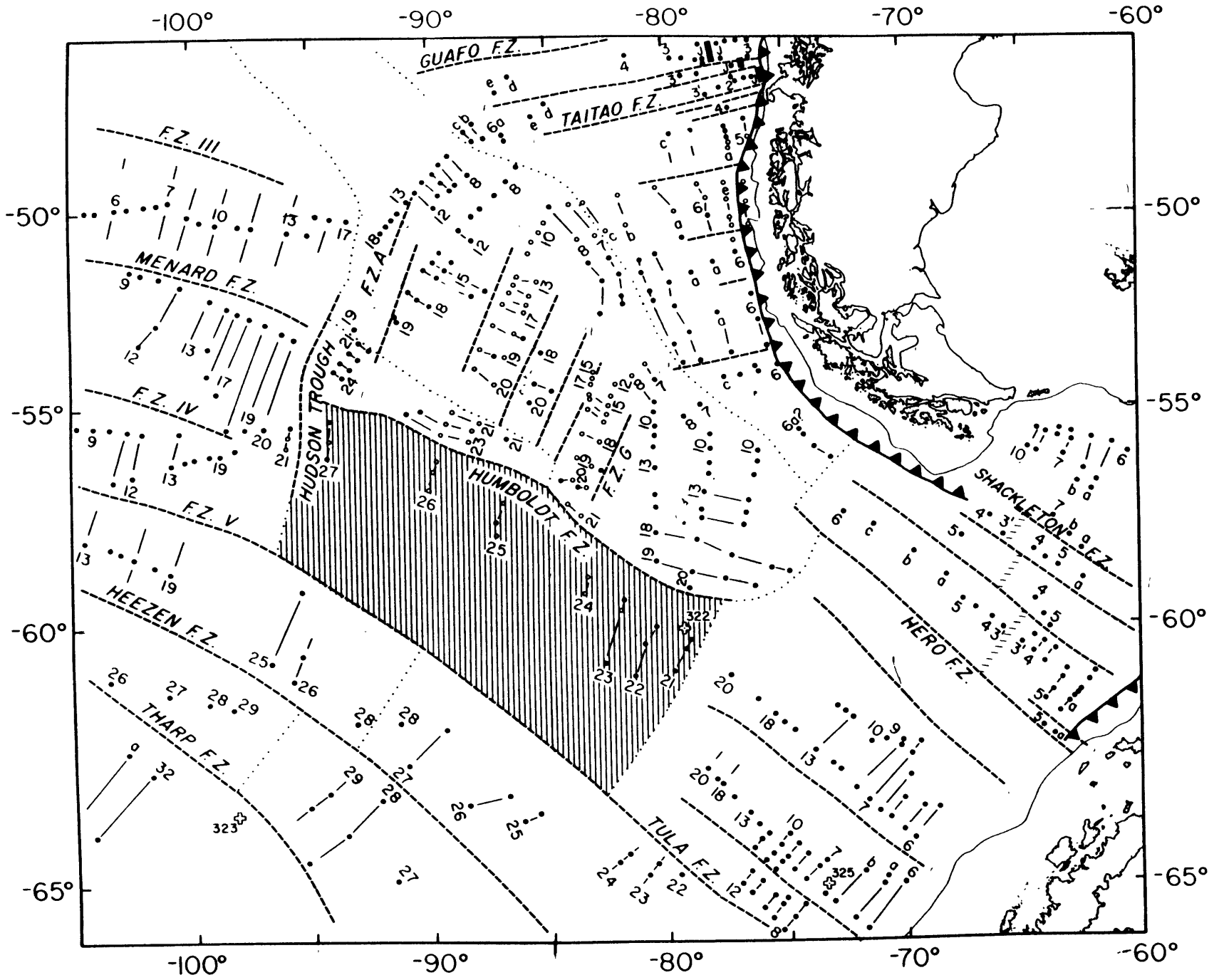

FIGURE 3.2

Fig. 1. Magnetic lineations and tectonic trends in the southeast Pacific. Open circles show new anomaly identifications. Open crosses show DSDP sites. Hachures indicate previously unsurveyed region that is the focus of this study. Anomaly identifications (closed

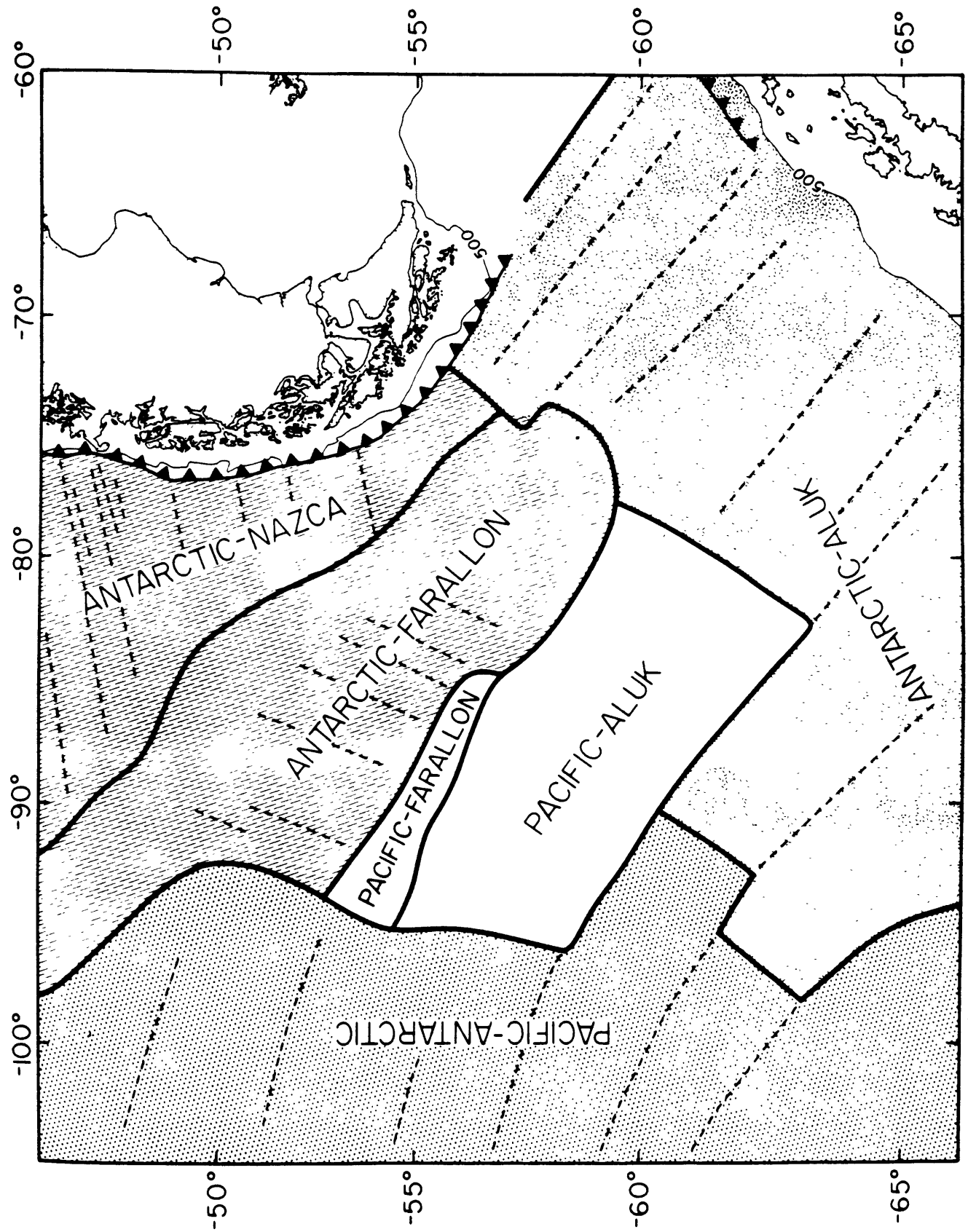
-50°
-55°
-60°
-65°
-60°
-70°
-80°
-90°
-100°
500
ANTARCTIC-NAZCA
ANTARCTIC-FARALLON
PACIFIC-FARALLON
PACIFIC-ALUK
ANTARCTIC-ALUK
PACIFIC-ANTARCTIC

FIGURE 3.3

Chapter 4

Data and Rotation Parameters used in Global Reconstructions

4.1 Introduction

In order to obtain a reliable area-age relationship for the times of the various reconstructions, we assembled rotation parameters from various authors and used our dataset of magnetic anomaly and fracture zone crossings to check them. We also calculated rotation parameters and augmented our dataset of magnetic anomaly and fracture zone crossings whenever necessary or when new data became available. By doing this, we hoped to minimize uncertainties in the reconstructions and, consequently, in the calculations of sea-level changes correlated with the area-age relationship.

We will first describe our collection of magnetic anomalies, fracture zones and other data. We will then discuss the rotation parameters used in the reconstructions. Finally, we will describe how we treated these data to get the isochron map for the present time and the reconstructed isochron maps at particular ages (35.58 Ma and 58.94 Ma).

4.2 Data

4.2.1 Present Plates and Plate Boundaries

We digitized all the ridges, transform faults, and trenches bounding each present tectonic plate from the GEBCO charts (General Bathymetric Charts of the Oceans; Canadian Hydrographic Office, Ottawa). The ridges and transform faults were digitized at the points where a spreading center intersects a transform fault and vice-versa. This dataset, formed by geographic coordinates of the present ridges and transform faults, was the basis for the calculation of many of the younger isochrons, as we will explain later in this chapter (Section 4.4). All the digitizing was done using a 9000 series CALCOMP digitizing table, which can read the coordinates of a point indicated by a cross-hair cursor with an accuracy of 0.001 inch.

The program used to digitize and to invert the digitized coordinates for geographical coordinates was DIGIMAP. We used a newer version of the original DIGMAP software developed by Bortoluzzi and Ligi [1986], modified and adapted to work with the APOLLO and CALCOMP hardware and software. It is a versatile computer program for acquisition of geographical coordinates from maps in widely used cylindric and conic conformal projections: Direct Mercator, Lambert conformal, UTM, and Polar Stereographic. Various reference ellipsoids and datum shift procedures are provided by this program. It also has statistical tests of accuracy. Bortoluzzi and Ligi [1986] indicate that the uncertainty of determining geographical coordinates is, in general, twice the graphic precision of 0.2 mm at any map scale and projection. Accuracy is increased by using good quality maps. In the case of the GEBCO maps, our performance tests indicated a radius of uncertainty of capture of coordinates usually less than the graphic precision, which was around 2005 m.

4.2.2 Magnetic Anomalies and Fracture Zones

The magnetic anomalies and fracture zones were collected and analyzed from several published maps and datasets. For the Pacific plate the data were obtained from the following references: Atwater [1970] (her unpublished chart), Bassinger *et al.*[1969], Cande *et al.*[1982], Cande *et al.*[1989], Christoffel and Falconer [1972], Elvers *et al.*[1972, 1973], Grim and Erickson [1969], Handschumacher *et al.*[1975], Hayes and Heirtzler [1968], Hilde *et al.*[1976], Larson [1976], Larson *et al.*[1972], Malahoff and Handschumacher [1971], Mason and Raff [1961], Molnar *et al.*[1975], Peter [1966], Peter *et al.*[1970], Pitman and Hayes [1968], Raff [1966], Raff and Mason [1961], Shih and Molnar [1975], Stock and Molnar [1987], Vacquier [1965], and Vacquier *et al.*[1961].

For the Indian Ocean, we used the following source of information: Bergh [1977], Bergh and Barrett [1980], Bergh and Norton [1976], Cande and Mutter [1982], Cande *et al.*[1989], Fisher and Sclater [1983], Fullerton *et al.*[1989], Larson [1975, 1977], Liu *et al.*[1983], Markl [1974], Martin *et al.*[1982], Molnar *et al.*[1988], Norton and Sclater [1979], Schlich [1982], Sclater and Fisher [1974], Sclater *et al.*[1976, 1981], Ségoufin [1978], Ségoufin and Patriat [1980, 1981], Weissel and Hayes [1972].

For the Atlantic Ocean, data were available from: Cande and Kristoffersen [1977], Cande *et al.*[1989], Klitgord and Schouten [1986], Kristoffersen and Talwani [1977], Pitman III and Talwani [1972], Rabinowitz and LaBrecque [1979], Srivastava and Tapscott [1986], Vogt and Avery [1974], Vogt *et al.*[1971, 1980, 1981, 1982].

For the Coral Sea, we used the results of Weissel and Watts [1979], while for the Tasman Sea we used the data of Hayes and Ringis [1973] and the data of Weissel and Hayes [1977].

Most of the data were digitized in the form described in the previous section. The locations of anomalies were picked according to the numbering system of

Pitman *et al.*[1968] and are listed in Table 4.1. Whenever possible, we assigned uncertainties to the locations of individual crossings of magnetic anomalies according to the resemblance of the magnetic anomalies to those observed on other profiles and to whether or not satellite navigation was used. For fracture zones, we arbitrarily assigned an uncertainty of 20 km because of the difficulty in defining where within the complicated topography the plate boundary lay.

For Cenozoic magnetic anomalies we used ages given by Berggren *et al.*[1985], and for Mesozoic anomalies, those of Kent and Gradstein [1985].

4.3 Rotation Parameters and Uncertainties in Reconstructions

4.3.1 Rotation Parameters

The most important dataset for our reconstructions are the pole positions and angles of rotations (Tables 4.2 to 4.27). Some of the reconstruction parameters were taken from the literature, while others were calculated here, and some others were interpolated or extrapolated. Some rotations that were calculated by combining rotations listed in the tables are not listed here.

Tables 4.2 to 4.7 give the poles and angles of rotation calculated and described in Chapter 3. They are used in the reconstructions of the southeast Pacific and were calculated using the data digitized from Cande *et al.*[1982].

Table 4.8 gives the East Antarctica-Africa poles and angles of rotations. Parameters for the Cenozoic and late Cretaceous times were taken from Molnar *et al.*[1988]. The anomaly M0 reconstruction parameters were interpolated using Molnar *et al.*'s [1988] anomaly 34 parameters and Norton and Sclater's [1979] anomaly M1 parameters. The parameters for the anomalies M4 and M11 time were interpolated using Ségoufin and Patriat's [1980] parameters for anomalies

M2 and M15. The anomalies M16 and M21 poles and angles were interpolated using Ségoufin and Patriat's [1980] anomaly M15 parameters and Norton and Sclater's [1979] anomaly M22 parameters. The closure pole and angle, at anomaly M22 time (152.11 Ma) (Lawver *et al.*, 1985), were given by Norton and Sclater [1979].

Table 4.9 lists the parameters for East Antarctica-India. Those for Cenozoic and late Cretaceous times were taken from Molnar *et al.*[1988]. The earlier Mesozoic poles were calculated through the plate circuit. The closure pole, at Jurassic time, was taken from Smith and Hallam [1970] and is the same closure pole used by Norton and Sclater [1979] in their study of the Indian Ocean.

Table 4.10 contains parameters for India-Africa rotations. We took those for Cenozoic and late Cretaceous times from Molnar *et al.*[1988]. The earlier Mesozoic parameters were calculated through the plate circuit using the India-Madagascar closure pole calculated from the India-Africa and Africa-Madagascar closure poles from Norton and Sclater [1979]. We used the same Jurassic closure rotation parameters given by Norton and Sclater [1979].

Table 4.26 lists the rotation parameters for the India-Australia spreading. The parameters were taken from Royer and Sandwell [1989]. Since 42.7 Ma, there has been essentially no motion between India and Australia (Royer and Sandwell, 1989).

The Madagascar-Africa rotation parameters are given in Table 4.27. Madagascar has been fixed to Africa since 112.5 Ma (Cochran, 1988). We calculated the Mesozoic parameters from Ségoufin and Patriat's [1980] anomalies M2, M15, and M21 poles and angles based on the measured distances between anomalies. Cochran [1988] reinterpreted the data used by Rabinowitz *et al.*[1983] and concluded that his new interpretation essentially agrees with that of Ségoufin and Patriat [1980] in both anomaly identification and spreading rates. Cochran [1988] supports our use of Ségoufin and Patriat's [1980] poles and angles to

calculate the parameters for the magnetic anomaly times.

In Table 4.11, we list the East Antarctica-Australia rotation parameters. Most of the Cenozoic parameters were calculated by Stock and Molnar [1982, 1988]. The anomaly 21 pole was extrapolated from those for anomalies 25 and 30-31. The spreading changed from a very slow spreading to a fast spreading at about anomaly 19 time (Cande and Mutter, 1982). The late Cretaceous pole and angle for anomaly 34 time (84.00 Ma) were taken from Royer and Sandwell [1989]. Separation between Australia and East Antarctica began at about 96 Ma and both the rotation parameters and the age of closure were taken from Royer and Sandwell [1989].

For the Pacific-West Antarctica rotations (Table 4.12), we used the Cenozoic parameters calculated by Stock and Molnar [1982, 1987, 1988]. We calculated those for the anomalies 25 and 30-31 using the parameters given by Stock and Molnar [1987, 1988]. The anomaly 21 parameters were interpolated by Stock (personal communication, 1989) using those for anomalies 18 and 25. Separation began at anomaly 34 time (84.00 Ma), when the Campbell Plateau broke away from Antarctica (Christoffel and Falconer, 1972). We assign this age to the closure parameters extrapolated by distance from Stock and Molnar [1988].

Stock and Molnar's [1982] work is the basis for Table 4.13, with the parameters for Pacific-Bellingshausen spreading. They calculated the poles and angles for anomalies 25 and 30-31, although at that time they assigned them to Pacific-West Antarctica spreading. The parameters for anomalies younger than anomaly 18 are the same as those for Pacific-West Antarctica spreading (Table 4.12). The anomaly 21 rotation parameters were interpolated in our work using the anomaly 18 parameters for Pacific-Bellingshausen spreading and the anomaly 25 parameters for Pacific-West Antarctica spreading. We assume the existence of a separate Bellingshausen plate prior to anomaly 30-31 time. The anomaly 34 rotation parameters were calculated by Molnar *et al.*[1975], and

were also originally assigned to Pacific-West Antarctica spreading.

The rotation parameters for Greenland-Europe spreading are given in Table 4.14. They result from unpublished work by Klitgord and Schouten (Klitgord, personal communication, 1986). The anomaly 18 parameters were obtained by interpolation between the anomalies 13 and 20 parameters of Klitgord and Schouten (1986, personal communication). We calculated the anomaly 21 parameters in this work. The closure is dated a little before anomaly 24 time, at about 56 Ma. (Kristoffersen and Talwani, 1977).

Rotation parameters for Greenland-North America are listed in Table 4.15. This table is based on the work of Klitgord and Schouten (personal communication, 1986), Srivastava and Tapscott [1986] and on our analysis of the magnetic anomalies and fracture zones. Since about 45 Ma, there has been no motion in the Labrador Sea (Laughton, 1972). We calculated the rotation parameters for anomalies 21, 30-31 and 34 based on our analysis of the parameters for Greenland-North America spreading, [Greenland + North America]-Europe spreading and on our analysis of magnetic anomalies and fracture zones. The initial opening of the Labrador Sea was approximately at 95 Ma (Srivastava and Tapscott, 1986).

Table 4.16 is based mostly on the work of Klitgord and Schouten [1986]. The reconstruction parameters for anomaly 5 were later recalculated by Klitgord and Schouten using an unpublished dataset (Klitgord, personal communication, 1988). We calculated parameters for anomalies 30-31 and 34 based on our reconstructions using magnetic anomalies and fracture zones. The closure pole and angle are given by Srivastava and Tapscott [1986].

Table 4.17 contains parameters for Iberia-North America rotations. We calculated the parameters for anomalies 30-31 and 34. We obtained the parameters for the anomalies M0 and M4 by adding the respective stage poles for Africa-North America spreading to the anomaly 34 rotation parameters for Iberia-

North America spreading. Our analysis agrees with the assumption that Iberia has been fixed to Europe since about anomaly 29 time (65.8 Ma) (Laughton *et al.*, 1972; Sclater *et al.*, 1977).

The Africa-North America rotation parameters, listed in Table 4.18, were also taken from Klitgord and Schouten [1986]. For the anomaly 5 (10.59 Ma) reconstruction, we use the pole interpolated from their results by Stock and Molnar [1988]. We interpolated the anomaly M11 pole and angle from Klitgord and Schouten's [1986] M10N and M16 parameters. Klitgord and Schouten [1986] give rotation parameters for minimum closure and others for maximum closure. We list both in Table 4.18 but we use the maximum closure pole and angle in our reconstructions.

The rotation parameters for the South Atlantic (Africa-South America spreading) are given in Table 4.19. Those for Cenozoic and late Cretaceous times were calculated by Cande *et al.*[1988], and by Pardo-Casas and Molnar [1987]. The parameters for the M0 and M4 anomalies were taken from Martin *et al.*[1982]. The closure parameters, at anomaly M11 time (132.78 Ma) were also taken from Martin *et al.*[1982].

Table 4.20 lists the South America-East Antarctica rotation parameters. All the rotation parameters were calculated through the plate circuit by rotating South America to Africa to East Antarctica.

Table 4.21 gives the Nazca-Pacific rotation parameters. Most of the parameters originated from the work summarized in Chapter 2 (Rosa and Molnar, 1988). Pardo-Casas and Molnar [1987] calculated the parameters for the most recent anomalies. They used Rosa and Molnar's [1988] parameters for displacements during successive intervals to calculate total rotations of the Nazca and Pacific plates. We identified a misprint in the angle for their anomaly 21 time (49.55 Ma) rotation: their rotation parameters, $74.76°N, 122.36°W, -69.98°$, should be replaced by $74.76°N, 122.36°W, -64.98°$. We adjusted some of the

parameters to correspond to 42.01 Ma, the center of the broad normal epoch of anomaly 18 (Berggren *et al.*, 1985). The parameters calculated by Rosa and Molnar [1988] and given by Pardo-Casas and Molnar [1987] correspond to a time of 42.26 Ma, (Berggren *et al.*, 1985) the center of the earliest minor reversal within anomaly 18. We calculated the anomaly 34 parameters using the Nazca-Pacific anomaly 30-31 parameters and the Pacific-Farallon anomaly 30-31 to anomaly 34 reconstruction.

The early Tertiary and late Cretaceous parameters for the spreading between Australia and Lord Howe Rise (Table 4.22) were taken from the studies of Stock and Molnar [1982, 1988]. We extrapolated the anomaly 34 rotation using the parameters for anomalies 30-31 and 32 given by Stock and Molnar [1982, 1988]. The closure parameters, corresponding to an age of about 90.00 Ma, were given by Weissel *et al.*[1977].

Table 4.23 lists the rotation parameters for anomalies on the Pacific plate formed by Pacific-Farallon spreading. All the parameters describe the rotation of the younger anomaly with respect to the fixed older anomaly. The Cenozoic parameters were calculated in Chapter 2 (see also Rosa and Molnar, 1988). We first calculated the 13–18 and 18–21 rotations (Rosa and Molnar, 1988) corresponding to the age of the center of the earliest minor reversal within anomaly 18 (42.26 Ma, Berggren *et al.*, 1985). Stock and Molnar [1988] later used these results to interpolate the 13–18 and 18–21 rotations corresponding to the age of the center of the broad normal epoch of anomaly 18 (42.01 Ma, Berggren *et al.*, 1985). We interpolated the 30-31–34 rotation parameters from the 25–30-31 reconstructions given by Rosa and Molnar [1988] and the 25–34 parameters from Engebretson *et al.*[1984]. The Mesozoic poles and angles come from the work by Engebretson *et al.*[1984].

The poles of rotation for anomalies on the Pacific plate formed by the Pacific-Vancouver spreading (Rosa and Molnar, 1988; Wilson, 1988) are given in Table

4.24. Most of them come from Rosa and Molnar [1988] and from Wilson [1988]. All the poles and angles describe the rotation of the younger anomaly over the fixed older anomaly. We calculated the 0–5, 5–6, and 6–13 parameters using the stage reconstructions of Wilson [1988]. The 21-25, 25–30-31 and 30-31–34 parameters are the same as for Pacific-Farallon spreading, given in Table 4.23.

Table 4.25 gives the rotation parameters for anomalies on the Pacific plate formed by Pacific-Kula spreading. All the parameters describe the rotation of the younger anomaly over the fixed older anomaly. The Cenozoic poles and angles of rotations were basically taken from Chapter 2 (Rosa and Molnar, 1988). The Mesozoic reconstructions were taken from the Pacific-Izanagi-1 parameters of Engebretson *et al.*[1984]. The 22–25 rotation parameters were extrapolated from the 25–30-31 rotation of Rosa and Molnar [1988]. We also extrapolated the 30-31–34 rotation parameters from those given by Engebretson *et al.*[1984] for the 31–34 rotation.

4.3.2 Uncertainties in Reconstructions

To calculate the uncertainties for most of the rotation parameters listed in Tables 4.28 through 4.51, we used the procedure outlined by Stock and Molnar [1983] and modified slightly by Molnar and Stock [1985] (See Chapter 2 (Section 2.4), and Figure 2.2a). This geometrical method yields uncertainties in reconstructions, based on positions of magnetic anomalies and fracture zones with finite uncertainties. Using this method, we describe the uncertainty in the reconstruction in terms of small perturbing rotations about three orthogonal axes (partial uncertainty poles). A rotation about the center of the data region will skew the two plates slightly and a rotation about one the two other axes will cause a mismatch of the magnetic anomalies or a mismatch of the fracture zones.

In our study of the Pacific, Farallon, Vancouver and Kula plates (Chapter 2),

we tolerated uncertainties in positions and misfits of 20 km. In this chapter, we allow different uncertainties in positions and misfits, depending on the quality of our data, which depends on the navigational method, density of bathymetric coverage, and quality of magnetic and topographic signatures. The angle of rotation that gives a x-km skewed mismatch can be approximated by

$$\frac{x(km)}{111.4(\frac{km}{degree})sin\frac{L}{2}}$$

where L is the length (in degrees) of the plate boundary for which there are data [*Stock and Molnar*, 1983]. The angle of rotation that gives a 20-km mismatch of the fracture zones or magnetic anomalies, for a partial uncertainty rotation pole ninety degrees away from the dataset, is 0.18°.

Whenever it was not possible to calculate the uncertainties directly from the geometry of the data distribution (end points of plate boundaries and azimuths of transform faults), we interpolated, extrapolated or used a method analogous to that of Chang *et al.*(submitted for publication, 1989) to combine uncertainties from two pairs of plates to get the uncertainties for a third pair of plates. This method calculates covariance matrices that are summed to yield a covariance matrix for the combined reconstruction. The eigenvalues and eigenvectors of this covariance matrix are analogous to the angles and partial uncertainty poles of partial uncertainty rotations for the combined reconstruction. Therefore, for each reconstruction, we could construct a "pseudo-covariance" matrix with eigenvalues equal to the partial uncertainty rotation angles, and eigenvectors parallel to the partial uncertainty rotation axes. These matrices could then be summed and solved to yield partial uncertainty rotation axes and angles for combined reconstructions.

In tables 4.28 through 4.51, we list the partial uncertainty rotations associated with the rotation parameters listed in tables 4.2 through 4.27. They can be added to the best-fit rotation to represent in latitude-longitude-angle space

the uncertainty associated with the best-fit pole and angle.

4.4 Determination of Isochrons

We are interested in determining the geographic distribution of the isochrons for the times of magnetic anomalies 5, 6, 13, 18, 21, 25, 30-31, 34, M0, M4, M11, M16, M21, and M25. To get the isochrons at these specific times, we rotated the magnetic anomaly crossings on both sides of the ridge by the respective half-angles about the pole of rotation for each anomaly, so that the crossings of the magnetic anomalies would incide at a paleo-ridge axis. We then modified the paleo-ridge axis to best fit the positions of the rotated magnetic anomalies and moved the "modified ridge" back to the position of the original data, by rotating it by the respective half-angles about the pole of rotation for the chosen anomaly. The resulting two lines constitute the isochrons. Figures 4.1 and 4.2 illustrate the procedure.

We will use the calculations for South Atlantic ocean as an example: To define the anomaly 5 time isochrons, we took the magnetic anomaly 5 crossings on both sides of the mid-Atlantic ridge and rotated them about the South America-Africa anomaly 5 pole of rotation by the respective half-angles to the ridge crest (see Table 4.19). We then modified the shape of the plate boundary at the ridge axis using both the present plate boundary and the rotated data, which in many cases is inadequate to define the plate boundary at the time of anomaly 5. We digitized the "modified ridge" and rotated this feature about the same pole of rotation back the present positions of anomaly 5. The resultant lineations constitute the anomaly 5 isochrons in the South Atlantic ocean. These isochrons are constrained by crossings of anomaly 5 where such data exist, and are defined by the shape of the present (younger) ridge crest where such data do not exist.

To get the isochrons for anomaly 6 time, we changed the "modified anomaly 5 ridge" by rotating the crossings of anomaly 6 on both sides of this ridge about the South America-Africa anomaly 6 pole of rotation (Table 4.19) by the respective half-angles. We then digitized the "modified anomaly 6 ridge" and rotated it back about the same pole of rotation so that the resultant lineations constitute the anomaly 6 isochrons on the South Atlantic. Isochrons for anomaly 6 and older are defined by crossings of such anomalies where they exist, and by the isochrons for younger anomalies where data are insufficient.

We were careful to use all sets of data available. Although we were interested in just the isochrons for the times of magnetic anomalies 5, 6, 13, 18, 21, 25, 30-31, 34, M0, M4, M11, M16, M21, and M25, we modified these isochrons whenever we had magnetic anomaly crossings and poles of rotations. Using the South Atlantic again as an example, we digitized "modified ridges" for the times of the Tertiary and Late Cenozoic anomalies 5, 6, 13, 18, 20, 31, 32, 33, and 34. To define the anomaly 21 time isochrons, we used the "modified anomaly 20 ridge", rotated about the South America-Africa anomaly 21 pole of rotation (Table 4.19) by the respective half-angles.

We followed this procedure for all the oceans to obtain the isochrons at the selected times of magnetic anomalies 5, 6, 13, 18, 21, 25, 30-31, 34, M0, M4, M11, M16, M21, and M25. We then had to review each region and connect the isochrons, especially at the triple junctions where the lengths of isochrons change progressively with time; near the trenches, where older seafloor has been subducted, and the shape of the isochrons differ at each time; and in the regions where there is a lack of data.

4.5 Reconstructions for the times of anomalies 13 and 25 (35.58 Ma and 58.94 Ma)

To get the reconstructions for the time of anomaly 13 (35.58 Ma) and for the time of anomaly 25 (58.94 Ma), we rotated all the continents and isochrons with respect to a fixed Africa.

The Caribbean region was rotated with North America. With the rotation of India to its original southern position at anomalies 13 and 25 times, we have an opening between India and Southern Tibet. We traced the coastline of Asia from Sumatra to Southern Iran across this region following the shape of the Himalayas.

We needed to assign an age to the regions of oceanic crust that were subducted later than the times of the reconstructions and are not present today. We show on our reconstructions one possible configuration for each of these areas. In some regions of the earth, where we have isochrons on one side of the plate pair at the present time, we reflected these isochrons onto the other plate. In some of these regions, however, no isochrons were available from the corresponding plate. This is the case for the northwestern Pacific region, where we have the Pacific-Kula and Pacific-Phoenix Mesozoic lineations present today. We assumed that in the past, these isochrons continued to the west to the trenches on the east side of Asia or until they reached the Mesozoic lineations present today on northwestern Australia.

In the gap opened between India and Southern Tibet, we assumed the age of the sea floor to be of Jurassic age. We will make further discussions on the age of this region in Chapter 6 when we use the area-age distribution to calculate changes in sea level.

4.6 Conclusions

We assembled a collection of rotation parameters from various authors. We used our dataset of plate boundaries, magnetic anomaly crossings, and fracture zone crossings to check these rotation parameters. We enlarged this dataset and calculated new rotation parameters several times until we had a group of rotation parameters and a dataset of plate boundaries, magnetic anomaly and fracture zone crossings that were internally consistent. From these, we prepared a map of the age of the ocean floor for the present time.

We discussed in detail our rotation parameters and calculated the uncertainties associated with these parameters. It is the first time that a global analysis of rotation parameters and their uncertainties has been made, resulting in a consistent world map of the age of the oceans.

We also made two reconstructions for the times of anomalies 13 (35.58 Ma) and 25 (58.94 Ma). The resultant global maps show that our rotation parameters are consistent by connecting the rotated isochrons in the triple junctions.

The analyses of the resultant area-age distributions for the present time and for the times of anomalies 13 and 25 are presented later in Chapter 6, when we calculate the sea-level changes associated with each area-age distribution. All the work in the present Chapter was done in order to minimize, and then accurately represent, the uncertainties in the reconstructions and, consequently, in the calculations of sea-level changes.

Figure Captions

Figure 4.1. Schematic diagram of the steps used in the determination of the isochrons. To get a specific isochron, we rotated the magnetic anomaly crossings on both sides of the ridge by the respective half-angles about the pole of rotation for each anomaly, so that the crossings of the magnetic anomalies would incide at the ridge axis. We then modified the ridge axis according to the positions of the rotated magnetic anomalies and rotated the "modified ridge" by the respective half-angles about the pole of rotation for the chosen anomaly. The resulting two lines would constitute the isochrons.

Figure 4.2. Ilustration of the procedure described on Figure 4.1. First, we have the present ridge and magnetic anomaly 5 crossings (Figure 4.2a). We rotate the magnetic anomaly crossings on both sides of the ridge by the respective half-angles about the pole of rotation for anomaly 5 (Figure 4.2b) so that the rotated magnetic anomaly 5 crossings incide at the present ridge (Figure 4.2c). We modify the present ridge based on the rotated crossings of magnetic anomaly 5 (Figure 4.2d). Finally, we rotate the "modified ridge at anomaly 5 time" by the respective half-angles about the pole of rotation for anomaly 5 to get the isochrons for anomaly 5 (Figure 4.2e). To get the isochrons for anomaly 6, we repeat this procedure starting with the "modified ridge at anomaly 5 time" instead of the present ridge.

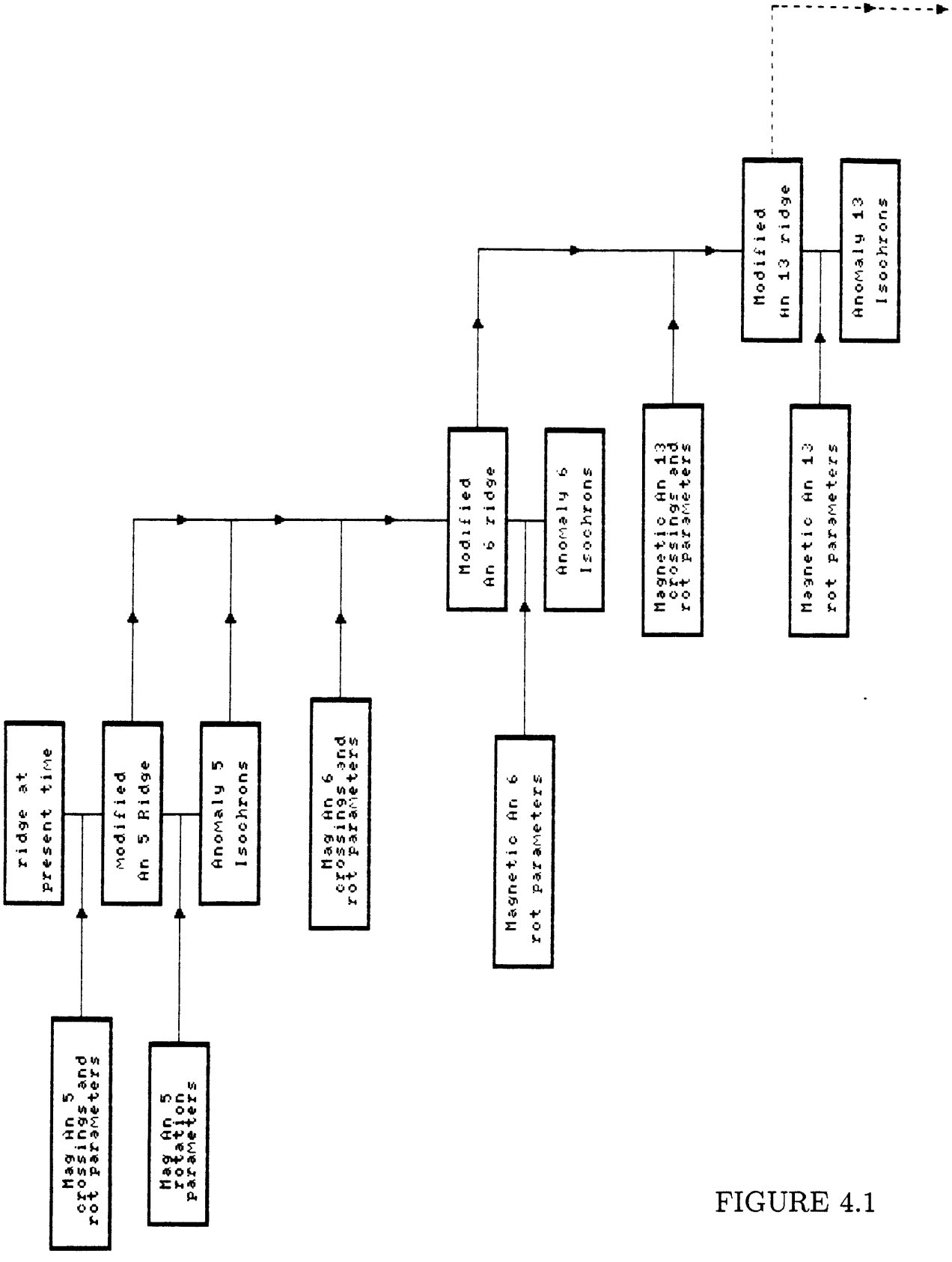
ridge at present time
Modified An 5 Ridge
Anomaly 5 Isochrons
Mag An 5 crossings and rot parameters
Mag An 5 rotation parameters
Mag An 6 crossings and rot parameters
Modified An 6 ridge
Anomaly 6 Isochrons
Magnetic An 6 rot parameters
Magnetic An 13 crossings and rot parameters
Modified An 13 ridge
Anomaly 13 Isochrons
Magnetic An 13 rot parameters

FIGURE 4.1

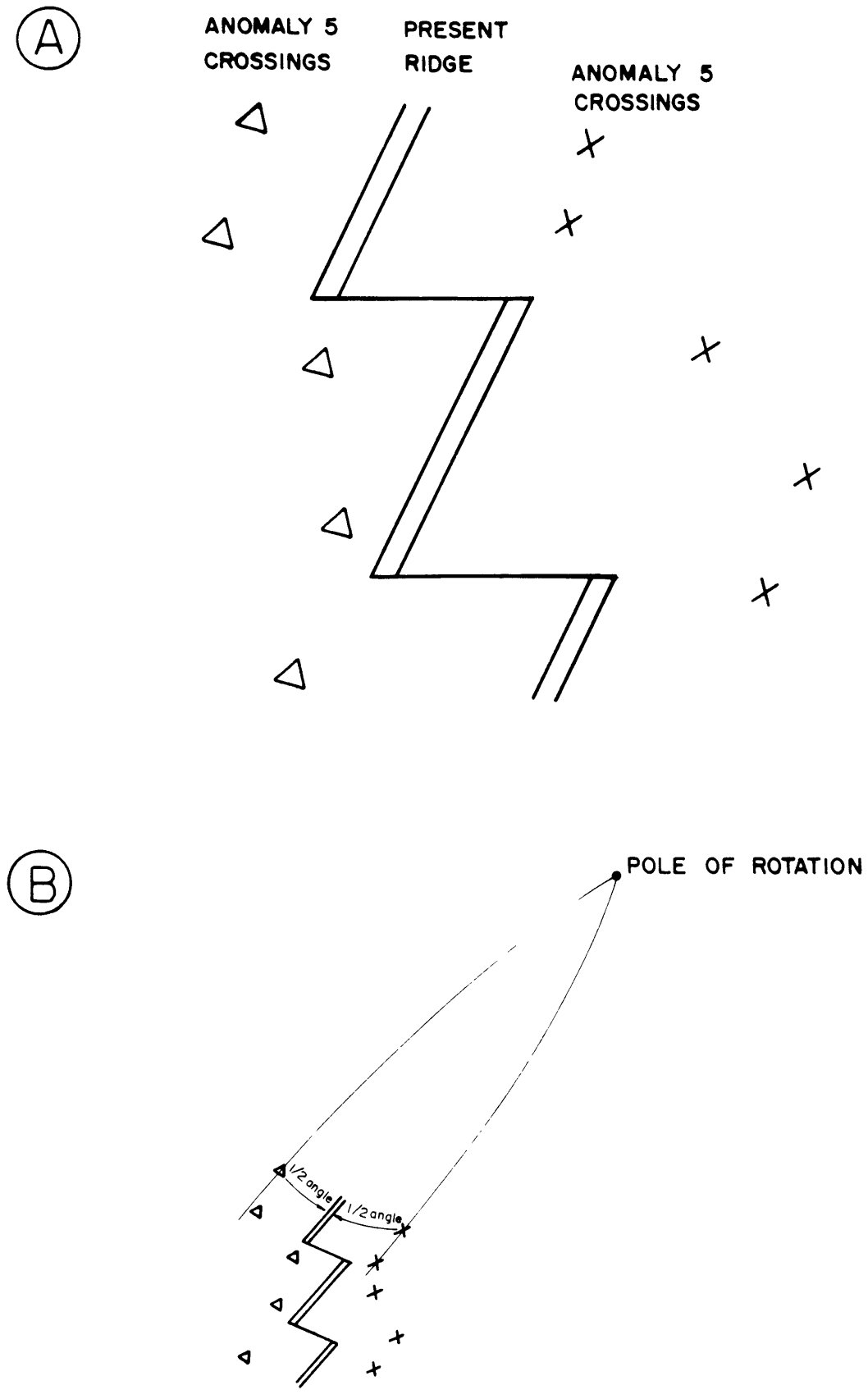
A
ANOMALY 5
CROSSINGS
PRESENT
RIDGE
ANOMALY 5
CROSSINGS
B
POLE OF ROTATION
1/2 angle
1/2 angle

FIGURE 4.2

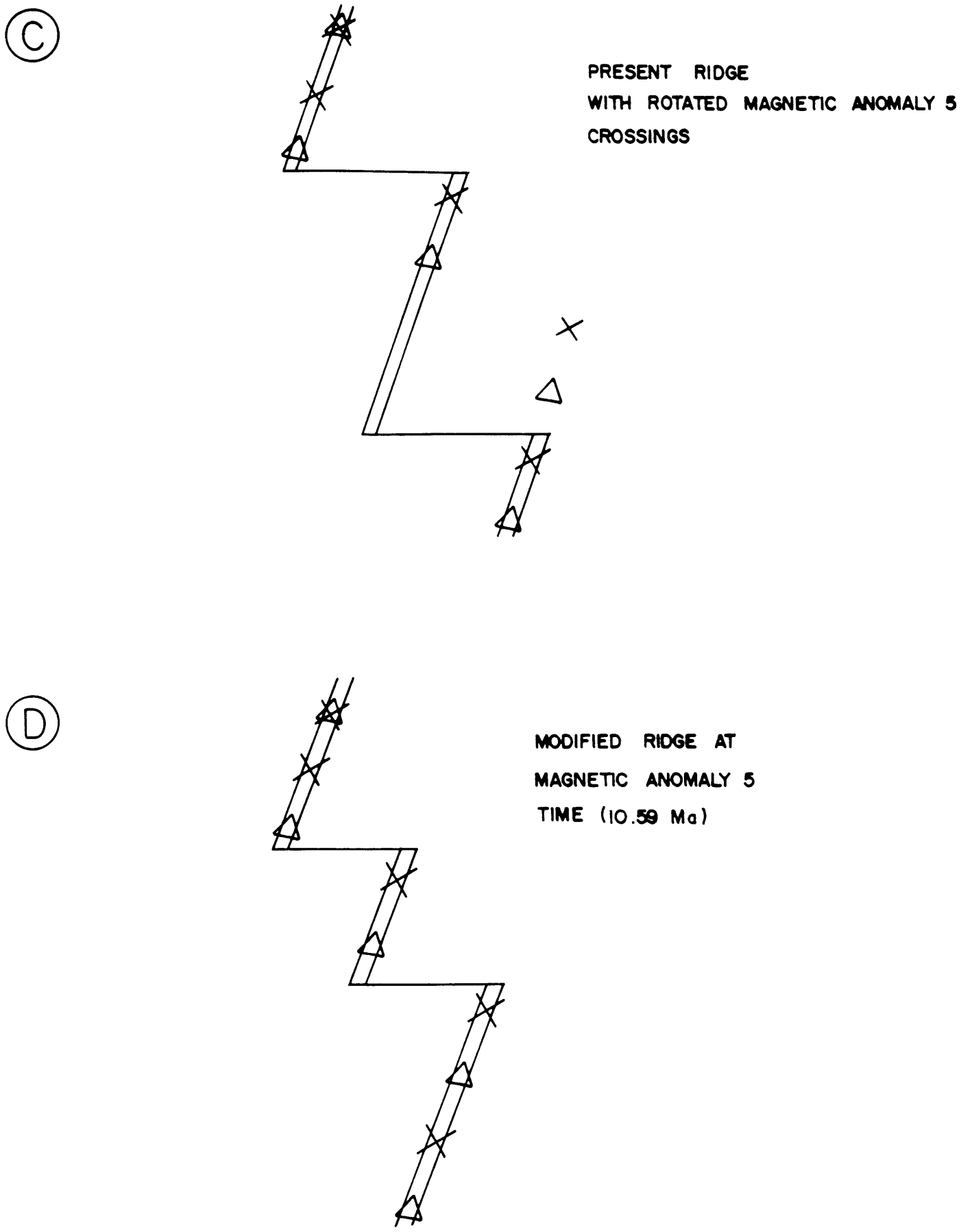
C
PRESENT RIDGE
WITH ROTATED MAGNETIC ANOMALY 5
CROSSINGS
D
MODIFIED RIDGE AT
MAGNETIC ANOMALY 5
TIME (10.59 Ma)

FIGURE 4.3

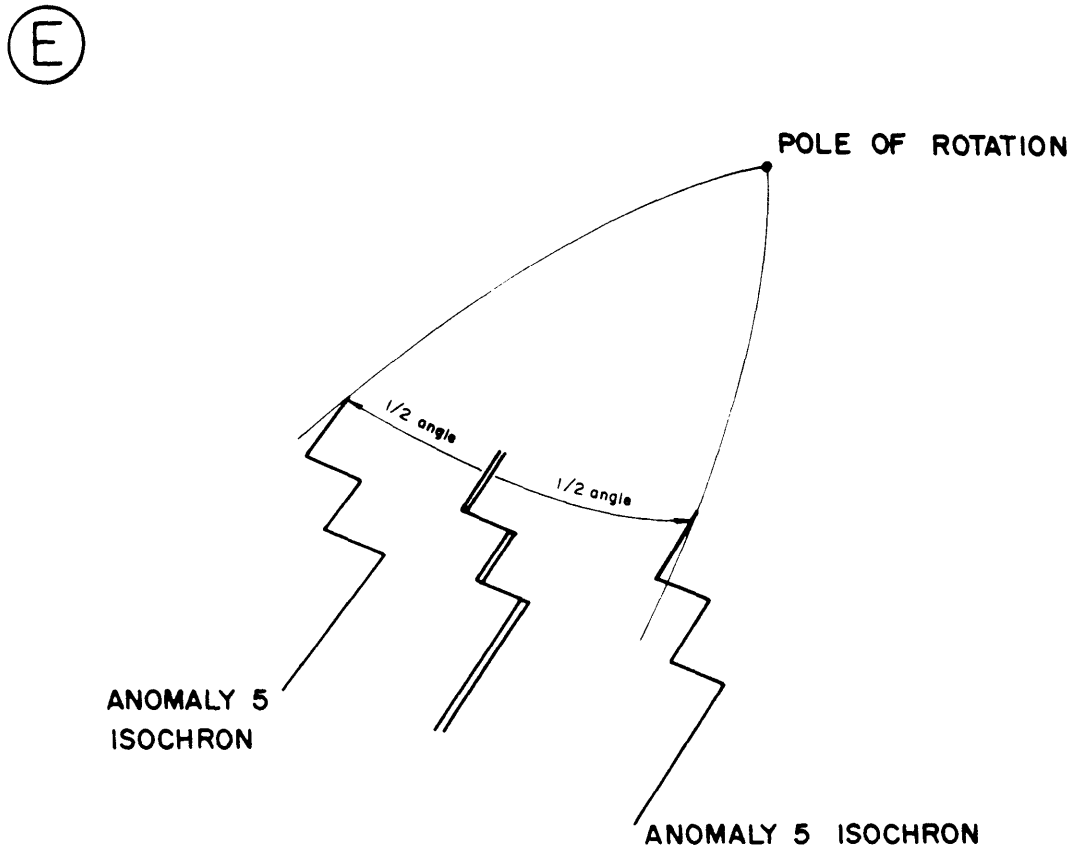
E
POLE OF ROTATION
1/2 angle
1/2 angle
ANOMALY 5
ISOCHRON
ANOMALY 5 ISOCHRON

FIGURE 4.4

Chapter 5

Numerical Determination of the Area-Age Distribution of the Ocean Floor

5.1 Introduction

The global plate reconstructions summarized in Chapter 4, achieved using the rotation parameters compiled from the geophysical literature and those obtained here (Chapters 2, 3 and 4) enable us to view the geographic distribution of the age of the ocean floor at several stages of the geologic time scale.

We should consider now the importance of the area-age relationship obtained for the present-day age zones by Berger and Winterer [1974] and Sclater *et al.*[1980], which was shown by Parsons [1982] to be useful in the determination of the sea level changes, to obtain the hypsometric distribution, and to constrain temporal variations in the heat loss from the ocean floor. Parsons' [1982] work encouraged us to use our global plate reconstruction results in order to perform similar studies for other geologic ages. This chapter summarizes the

mathematical setup of our problem, which is centered on the determination of these area-age distributions. We also show here the results of some tests performed to check the validity of the numerical method, used to compute areas and describe the sources of uncertainties in the results.

5.2 Numerical determination of the area on the surface of a sphere using Stokes Theorem

If we consider the present-day distribution of the ocean floor age zones, we notice that we may have the following types of boundaries for these age zones: magnetic anomalies, fracture zones, ridges, trenches, and the continent-ocean boundary at passive margins (Figure 5.1). The geographical position of each of these features will determine the limits of each age zone. This means that we need to know the geographical coordinates (we will use the colatitude θ and longitude φ) of each point forming these tectonic features at each geologic age considered. This can be obtained by digitizing the present-day tectonic maps of the oceans, including all available data for the magnetic anomalies, and by rotating these points by means of the parameters collected in the previous Chapters (i.e. by using the global plate reconstruction models).

We then use Stokes' Theorem, in order to avoid the calculation of a surface area integral by substituting an equivalent line integral (Figure 5.2):

$$\int\int_A (\vec{\nabla} \times \vec{F}) \cdot \hat{n} dA = \oint_C \vec{F} \cdot d\vec{r} \qquad (5.1)$$

Notice (Figure 5.2) that we have assumed that the unit vector $\hat{n}$ points upwards, perpendicular to the surface A, which implies that we follow the path C in the counterclockwise sense (Hildebrand, 1976).

The only requirement implied by the definition above is that the area A should be contained in a simple region, where the vector $\vec{F}$ is continuously differentiable. A region R is defined as a simple region if any arbitrary closed curve lying in R can be shrunk continuously to a point in R without passing outside R (Hildebrand, 1976).

If we consider the case where the area A is on the surface of a unit sphere (which is the case if we are considering only areas on the surface of a spherical earth model), we have that the unit vector $\hat{n}$ is always coincident with the radial direction of this sphere: $\hat{n} = \hat{r}$ (Figure 5.3). We can then write (5.1) as:

$$\int\int_A (\vec{\nabla} \times \vec{F})_r dA = \oint_C \vec{F} \cdot d\vec{r} \qquad (5.2)$$

Since we want to obtain the area A, we can constrain

$$(\vec{\nabla} \times \vec{F})_r = 1 \qquad (5.3)$$

so that we have only left the right hand side of equation (5.2),

$$A = \oint_C \vec{F} \cdot d\vec{r} \qquad (5.4)$$

We now proceed to determine the vector $\vec{F}$ along the limiting path C.

Because we are using spherical coordinates (r, θ, φ) in the parameterization of our problem, and because on the surface of the earth $r = R$, we can use the definition of curl to rewrite the constraint $(\vec{\nabla} \times \vec{F})_r = 1$ as

$$(\vec{\nabla} \times \vec{F})_r = \frac{1}{Rsin\theta}\left[\frac{\partial}{\partial\theta}(sin\theta F_\varphi) - \frac{\partial F_\theta}{\partial\varphi}\right] = 1 \qquad (5.5)$$

In general $\vec{F}$ is not uniquely specified and we can use two particular solutions to the differential equation in (5.5), in order to obtain the expression for $\vec{F} \cdot d\vec{r}$ in equation (5.4). We first consider the solution for which $F_\theta = 0$.

In this case, equation (5.5) becomes

$$\frac{\partial}{\partial\theta}(sin\theta \cdot F_\varphi) = Rsin\theta$$

which leads us to

$$F_\varphi = -Rcot\theta + \frac{g(\varphi)}{sin\theta} = F_\varphi(\theta,\varphi) \qquad (5.6)$$

where $g(\varphi)$ is a function which is independent of the variable θ resulting from the integration.

This way,

$$\vec{F} = (F_\theta, F_\varphi) = [-Rcot\theta + \frac{g(\varphi)}{sin\theta}](0,1) \qquad (5.7)$$

The path C is composed of points $\hat{r} = (R\theta, (Rsin\theta)\varphi)$ due to the parameterization in spherical coordinates (Figure 5.3). So,

$$\vec{r} = R(\theta(s), [sin\theta(s)]\varphi(s)) \qquad (5.8)$$

where s is the index of each point in the limiting curve C for the area. If we apply the chain rule, $d\vec{r} = \frac{d\vec{r}}{ds}ds$, we get

$$dr_\varphi = R\frac{d}{ds}[sin\theta(s)\varphi(s)]\,ds \qquad (5.9)$$

But, since $F_\theta = 0$ for this particular solution,

$$\vec{F} \cdot d\vec{r} = (F_\theta, F_\varphi) \cdot (dr_\theta, dr_\varphi) = F_\varphi dr_\varphi \qquad (5.10)$$

Then, using Equations (5.4), (5.6), (5.9) and (5.10), we obtain:

$$A = \oint_C \vec{F} \cdot d\vec{r} = A_0 + R\oint_C \frac{g(\varphi(s))}{sin\theta(s)}\frac{d}{ds}[sin\theta(s) \cdot \varphi(s)]\,ds \qquad (5.11)$$

where

$$A_0 = -R^2 \oint_C cot\theta(s) \cdot \frac{d}{ds}[sin\theta(s) \cdot \varphi(s)]\,ds \qquad (5.12)$$

which is the expression for the calculation of the area for the particular case $F_\theta = 0$. This line integral is not easy to solve or implement numerically. So, we should try to find a better equation for $\vec{F}$ different than the equation (5.7).

We now show the case for which the solution of equation (5.5) employs $F_\varphi = 0$.

In this case, equation (5.5) becomes

$$-\frac{\partial F_\theta}{\partial \varphi} = Rsin\theta$$

This leads us to

$$F_\theta = -Rsin\theta \cdot \varphi + g(\theta) \qquad (5.13)$$

(we then have $F_\theta = F_\theta(\theta, \varphi)$).

So,

$$\vec{F} = (F_\theta, F_\varphi) = (-Rsin\theta \cdot \varphi + g(\theta))(1, 0) \qquad (5.14)$$

Using the parameterization in spherical coordinates of each point in the path C ($\hat{r} = (R\theta, Rsin\theta \cdot \varphi)$),

$$\hat{r} = R(\theta(s), sin\theta(s) \cdot \varphi(s))$$

and the chain rule, $d\vec{r} = \frac{d\vec{r}}{ds}ds$, we get

$$dr_\theta = R\frac{d}{ds}[\theta(s)]ds \qquad (5.15)$$

But,

$$\vec{F} \cdot d\vec{r} = (F_\theta, F_\varphi) \cdot (dr_\theta, dr_\varphi) = F_\theta dr_\theta \qquad (5.16)$$

(since $F_\varphi = 0$ for this particular solution).

Then, using equations (5.4), (5.13), (5.15) and (5.16), we obtain

$$A = \oint_C \vec{F} \cdot d\vec{r} = A_0 + R \oint_C g(\theta(s)) \frac{d}{ds}[\theta(s)]ds \qquad (5.17)$$

where

$$A_0 = -R^2 \oint_C sin\theta(s) \cdot \varphi(s) \cdot \frac{d}{ds}[\theta(s)]ds \qquad (5.18)$$

If we compare equations (5.17) and (5.18) with the corresponding equations for the first solution, (5.11) and (5.12), we notice that since we will be using $0 \leq \theta \leq \pi$ and $0 \leq \varphi \leq 2\pi$, the sign change in the $cot\theta(s)$ term in the first solution (equations 5.11 and 5.12) will be more critical than in the second solution (equations 5.17 and 5.18). This is due to the discontinuity we will have in this term due to a singularity which is not present in this second solution. Most important though is the fact that equation (5.17) is easier to solve and to implement numerically than equation (5.12). Thus, we will use (5.17) to calculate the surface areas, but we still must evaluate the function $g(\theta(s))$. This can be achieved by examining the boundary conditions of this particular problem.

Since $\vec{F}$ is an arbitrary vector, we may impose the condition $F_\theta(\theta, \varphi = \varphi_0) = 0$. This will allow us to evaluate the function $g(\theta(s))$:

$$F_\theta(\theta, \varphi = \varphi_0) = -Rsin\theta(s)\varphi_0(s) + g(\theta(s)) = 0$$

then,

$$g(\theta(s)) = \varphi_0(s)Rsin\theta(s)$$

and

$$F_\theta(\theta(s), \varphi(s)) = -Rsin\theta(s)[\varphi(s) - \varphi_0(s)] \qquad (5.19)$$

Finally, equations (5.17) and (5.18) can be written as

$$A = -R^2 \oint_C sin\theta(s)[\varphi(s) - \varphi_0(s)]\frac{d}{ds}[\theta(s)]ds \qquad (5.20)$$

which can be evaluated numerically as

$$A \cong -R^2 \sum_{k=1}^{N} sin\theta_k(\varphi_k - \varphi_0)[\theta_{k+1} - \theta_k] \qquad (5.21)$$

where φ_0 is the longitude of the westernmost point of the boundary C, which was parameterized into N points.

5.3 Application of the numerical method to the original digitized data

The method described in the previous section was applied to the digitized data set. As we recall, the data set consists of geographic coordinates (θ, φ) of a series of tectonic features, which bound each of the age zones considered here. These coordinate pairs (θ, φ) result then from the rotation of the original coordinates of points which were unevenly digitized from present-day tectonic maps of the oceans (Chapter 4). In order to have all points in a given path C (which bounds an area A) at a fixed distance from each other, we decided to perform linear interpolation between each two digitized points in our reconstructed earth models. This is a reasonable approach, since most magnetic anomalies, fracture zones and ridges are nearly linear features, and considering that we have digitized with high density of points the other two types of features (namely, the continental boundaries and trenches). After this interpolation process was used, all consecutive points forming a boundary had the same distance measured from each other. The interpolation process was also very useful in the reconstruction process, since it is easier to identify the point of intersection of two linking features when we are dealing with a larger amount of points in each one of these.

We shall now describe how the linear interpolation was performed to determine the coordinates of the points forming each boundary of an arbitrary area A (Figure 5.1). This method has been widely used in seismology to determine the coordinates of points forming the great circle paths along which seismic surface waves travelled between any two points on the surface of the earth (see Rosa, 1986 for a recent application). In this case, we assume a spherical earth model for simplicity, and consider the system of Cartesian coordinates shown in Figure 5.3. The Cartesian coordinates of the two points (1 and 2) which will be the extremities of the great circle we want to interpolate, are given by:

$$\begin{cases} x_i = R sin\theta_i cos\varphi_i \\ y_i = R sin\theta_i sin\varphi_i \\ z_i = R cos\theta_i \end{cases} \quad , i = 1,2 \qquad (5.22)$$

We then define another system of Cartesian coordinates (x', y', z') such that the x' and y' axes lie in the plane containing the great circle path between the two points (Figure 5.4). We proceed by setting the intersection of the x' axis with the surface of the sphere at one of the points at the end of the great circle [*Rosa*, 1986].

Using this new system of coordinates, we can define the coordinates of equally spaced points located at a distance d from each other along this great circle:

$$\begin{cases} x'_i = R cos\varphi'_i \\ y'_i = R sin\varphi'_i \\ z'_i = 0 \end{cases}$$

$\varphi'_i = i \cdot d$ (i = 1, 2, ...).

To calculate the corresponding coordinates (x_i, y_i, z_i) of these interpolated points, we apply the following rotation operator to these points:

$$\begin{bmatrix} x_i \\ y_i \\ z_i \end{bmatrix} = \begin{bmatrix} a_{11} & a_{12} & a_{13} \\ a_{21} & a_{22} & a_{23} \\ a_{31} & a_{32} & a_{33} \end{bmatrix} \begin{bmatrix} x'_i \\ y'_i \\ z'_i \end{bmatrix} \tag{5.24}$$

for which the elements a_{ij} are obtained by constraining that this operator should perform the following rotations: $(1,0,0)$ to (x_1, y_1, z_1); $(0,0,1)$ to $(x_1, y_1, z_1) \times (x_2, y_2, z_2)$ and $(0,1,0)$ to $[(x_1, y_1, z_1) \times (x_2, y_2, z_2)] \times (x_1, y_1, z_1)$.

Finally, the spherical coordinates of the interpolated points are given by

$$\begin{cases} \theta_i = \frac{\pi}{2} - tan^{-1}\left[\frac{y_i}{x_i}\right] \\ \varphi_i = tan^{-1}\left[\frac{z_i}{\sqrt{x_i^2+y_i^2}}\right] \end{cases} \tag{5.25}$$

We can then obtain the total area bounded by a set of tectonic features by applying equation (5.21) to all interpolated points with coordinates (θ_i, φ_i) given by equation (5.25) above.

5.4 Numerical Methods

The application to our reconstructed (originally digitized) data set requires that we have an idea of the uncertainties of these data. In this section, we try to make an estimate of the uncertainties related to the area calculation process. Other sources of errors, related to the uncertainties envolved in our data set, and in our reconstructed earth models, were discussed in Chapters 2, 3 and 4.

The basic idea behind the tests whose results are presented here is the evaluation of the amount of error which we may have in the calculation of areas using the Stokes Theorem method introduced in section 5.2.

In order to evaluate these errors, we have chosen to digitize a present geographic feature, with well known area, obtain the geographic coordinates of each point bounding this feature, and finally apply our method to calculate the area

of this region. We chose to digitize the border line of three different Brazilian states: Minas Gerais (with a listed area of $587,172 km^2$), Sergipe (with a listed area of $21,994 km^2$), and the Federal District, where Brasília is located (with an area of $5,814 km^2$).

Minas Gerais and the Federal District were digitized from a 1:3,000,000 scale geographic map (Figure 5.5), while the state of Sergipe was digitized from a 1:4,000,000 map (Figure 5.6). We have followed the same area calculation process described in the sections above, and used the same software as was used for the area calculations discussed in Chapter 6. Using an increment distance of 0.001 degrees in equation (5.23), we obtained the following results: $575,382 km^2$ area for the Minas Gerais state (a 2% error if we consider the area listed above), $21,973 km^2$ for the Sergipe state (a 0.1% error), and $5,453 km^2$ for the Federal District (a 6% error from the real value). These results were all obtained using an interpolation distance of 0.01°. We believe that the larger error involved in the last case is due to the inappropriate map used to study the area of the Federal District, which has a small area compared to the other two features, and so should have been obtained from a larger scale map. For the other two states, we considered the error level acceptable since it is less than the errors usually involved in the digitization process. This method should be suitable for the application to our reconstructed tectonic maps of the earth, since most areas considered here are larger than those considered in these tests.

In order to test even further our method and the computer programs written to implement it, we applied an additional test. This time we used a larger area which is known exactly, thereby eliminating doubts on the mapping precision such as those encountered above. We chose a 60° wide segment of a hemisphere of the earth. This segment, bounded by the 30°E and 90°E longitude lines and by the geographic equator, has a total area given by:

$$\frac{1}{12}\left(4\pi R^2\right) = 42,505,372.67$$

where R is the earth's radius (R = 6371 km). To start the area calculation, we generated the points forming the area boundaries at each 1° increment along the two longitudinal lines (30°E and 90°E) and along the equator between 30°E and 90°E. Using interpolation distance values of 0.1°, 0.01° and 0.001°, we obtained the following results for the area of this region: $34,648,274.74km^2$, $41,722,504.09km^2$, and $42,386,233.27km^2$. These correspond to the error values of 18%, 1.8% and 0.28%, respectively, from the above exact value. This shows that our method is also suitable for application in cases where large areas are considered. It is also clear that the use of a small interpolation distance implies smaller errors in our results.

In the case of areas bounded by actual tectonic features (present-day case), the uncertainties are mostly due to possible errors in the location of these features. If we consider the case of areas bounded by reconstructed (rotated) tectonic features, we have additional uncertainties due to uncertainties in the rotation parameters. Such uncertainties can become smaller with the collection of more magnetic anomaly and bathymetric data, better tectonic evolution models for the ocean basins and better definition of their boundaries.

5.5 Conclusions

We defined a method for the calculation of the areas of ocean floor created during a certain period of time by using the Stokes theorem to transform an area integral into a line integral. The method proved to work properly. The errors in the areas calculated by the method are less than 2% of the correct area when the boundaries of the area are digitized from a map with a proper scale

and when an interpolation factor of 0.01° is used in the method. To assure well defined boundaries requires then that the digitization of the boundaries be done carefully using maps with appropriate scales (e.g. 1:3,000,000 would be suitable for a $30,000 km^2$ area) and the digitized points are not very far apart from each other (e.g. not farther away from 1° if we are using an interpolation distance of 0.01°).

The errors in the calculated areas are small compared to the uncertainties in the areas due to the uncertainties in the rotation parameters.

The method developed here will be used to calculate the area of ocean floor created during certain periods of times, and the area of ocean floor in various tectonic reconstructions at specific times. The results of the area calculations and the analysis of these results in terms of sea-level changes are listed and discussed in Chapter 6.

Figure Captions

Figure 5.1 Schematic representation of a particular case where two different areas (bounded by different tectonic features) need to be determined from the geographic coordinates of each point forming these area boundaries.

Figure 5.2 Graphic representation of the unit vector $\hat{n}$, perpendicular to the area A, which is bounded by the line C. The line C is followed in the counter-clockwise sense in the application of Stokes theorem, if the vector $\hat{n}$ points out of the surface where A is located.

Figure 5.3 Spherical coordinate system used in the application of Stokes theorem method for area calculation: each point P is determined by the co-latitude and longitude (θ, φ) pair. The distance $R\theta$ from the north pole, and the distance from the zero meridian to the meridian containing P, $(Rsin\theta)\varphi$, can also be used as a mean of fixing the position of the point.

Figure 5.4 Graphic representation of the linear interpolation method used to determine the geographic coordinates of each point between two any points (labeled 1 and 2) on the surface of a sphere. (x', y', z') represent the rotated reference axes, where Δ is the distance between points 1 and 2, and d is the interpolation distance.

Figure 5.5 Map of the Brazilian state of Minas Gerais and Federal District, reduced from a 1:3,000,000 scale geographic map which was used to digitize the boundaries of these features for the calculation of their areas with the method developed in this Chapter.

Figure 5.6 Map of the Brazilian state of Sergipe, reduced from a 1:4,000,000 map which was used to digitize the boundaries of this state for the calculation of its area, using the method developed in this Chapter.

FIGURE 5.1

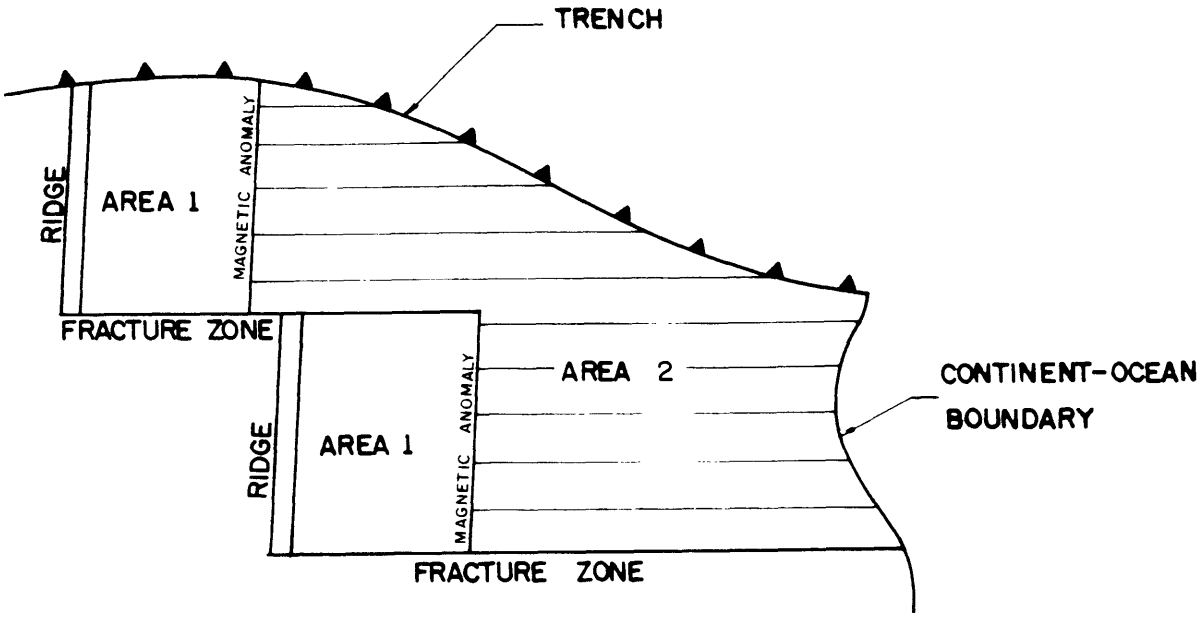
TRENCH
RIDGE
AREA 1
MAGNETIC ANOMALY
FRACTURE ZONE
AREA 2
CONTINENT-OCEAN
BOUNDARY
RIDGE
AREA 1
MAGNETIC ANOMALY
FRACTURE ZONE

FIGURE 5.2

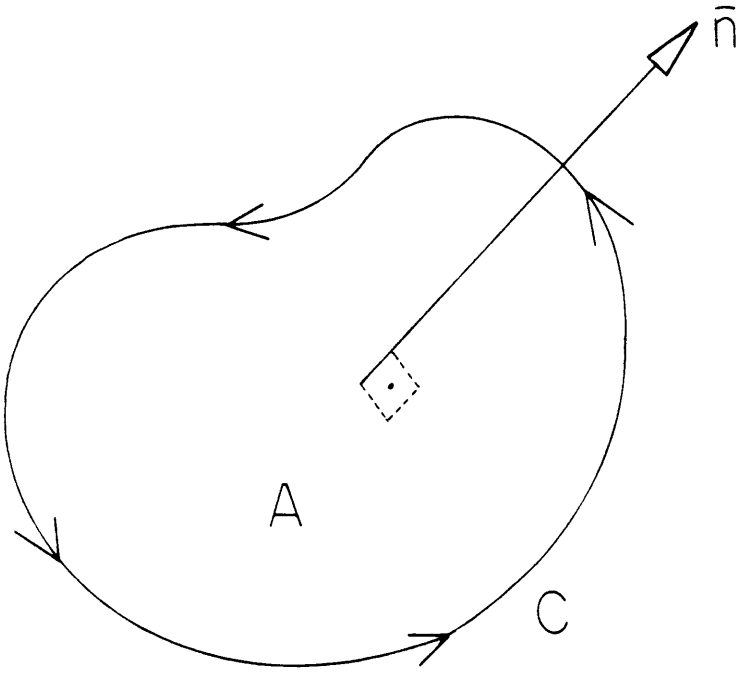

FIGURE 5.3

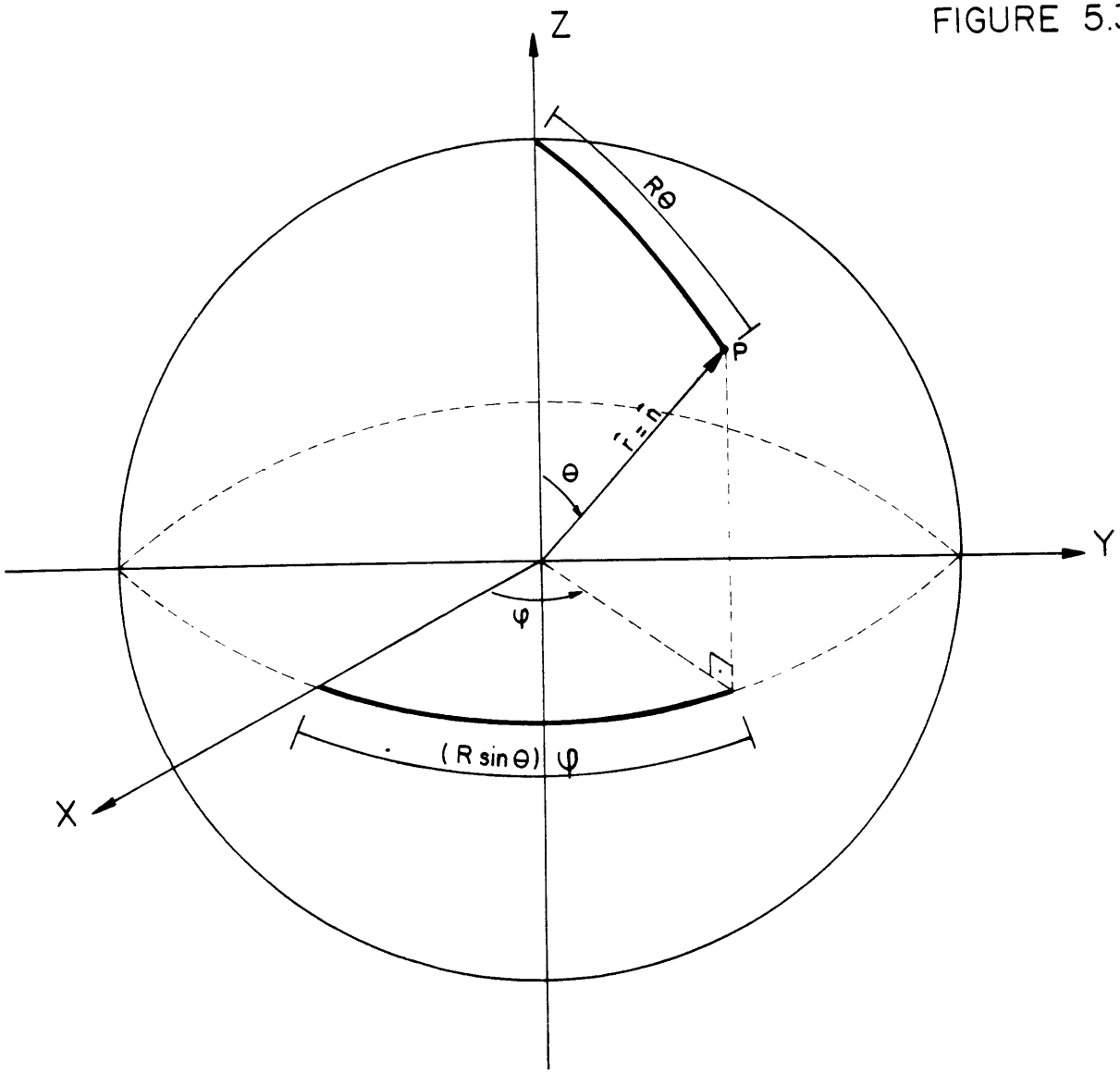

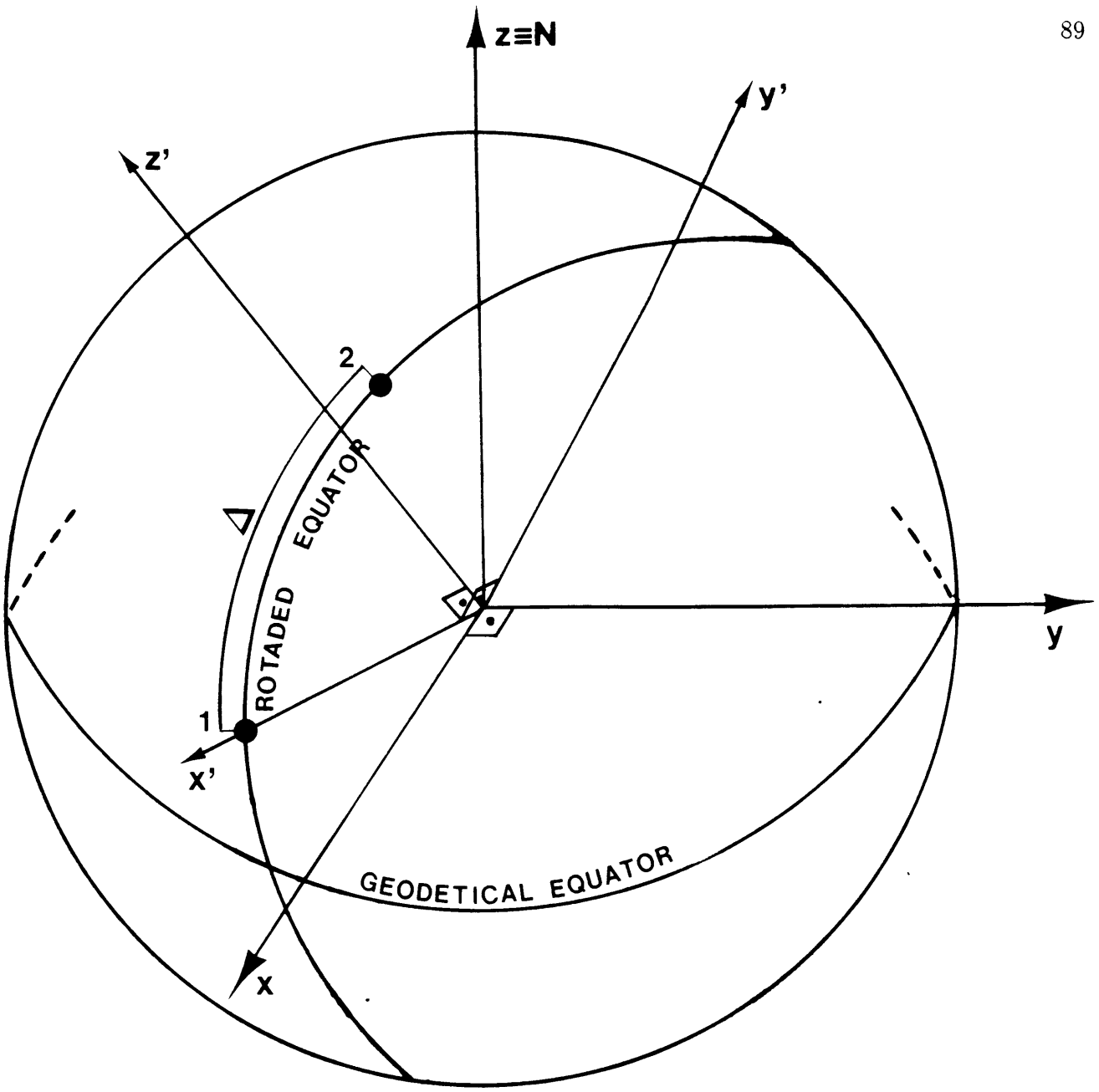
z≡N
y'
z'
2
ROTADED EQUATOR
Δ
y
1
x'
GEODETICAL EQUATOR
x

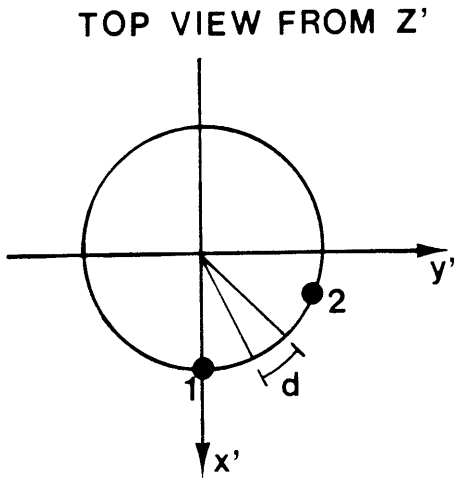
TOP VIEW FROM Z'
y'
2
d
1
x'

FIGURE 5.4

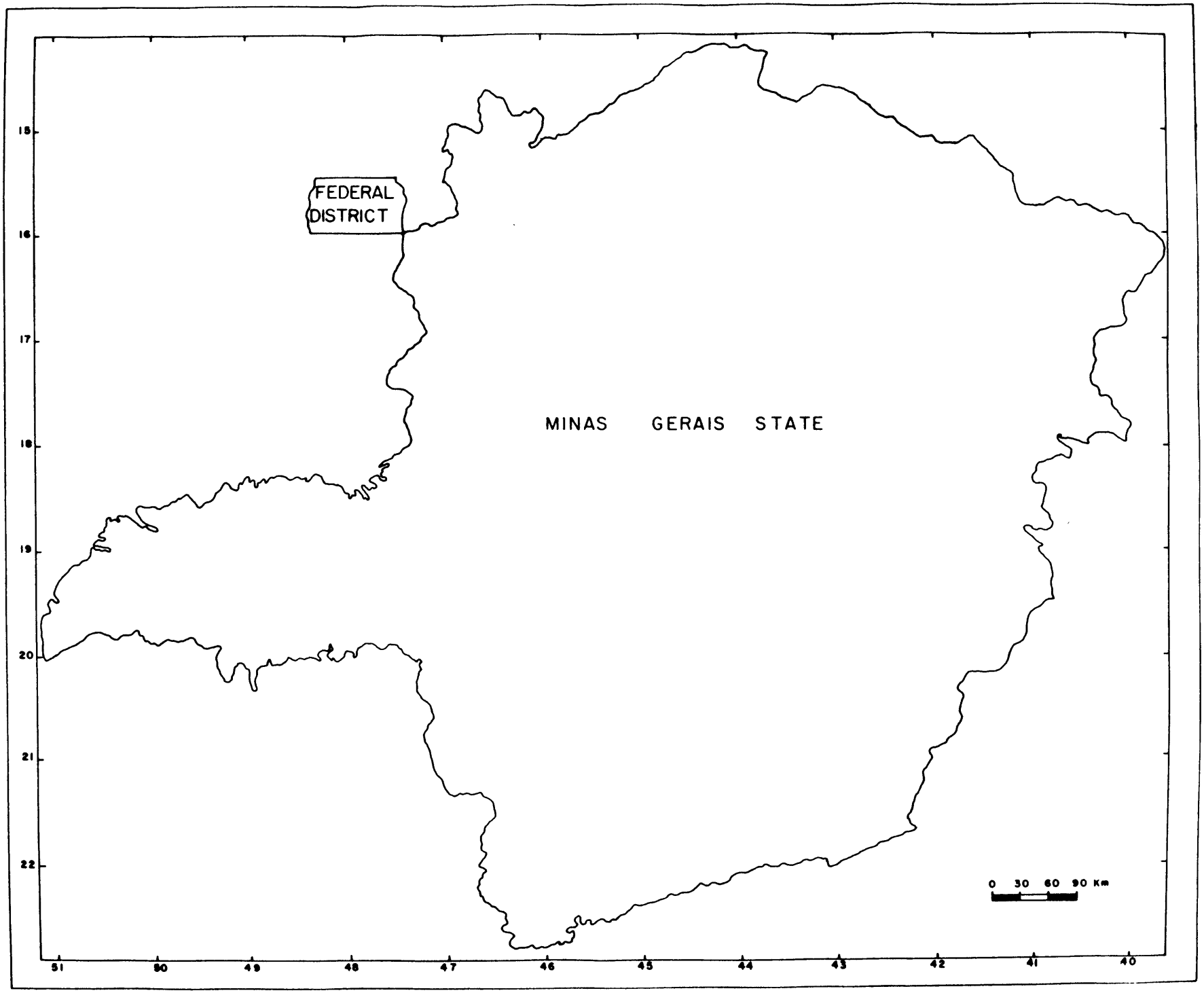
FEDERAL
DISTRICT
MINAS GERAIS STATE
0 30 60 90 Km
15
16
17
18
19
20
21
22
51
50
49
48
47
46
45
44
43
42
41
40

FIGURE 5.5

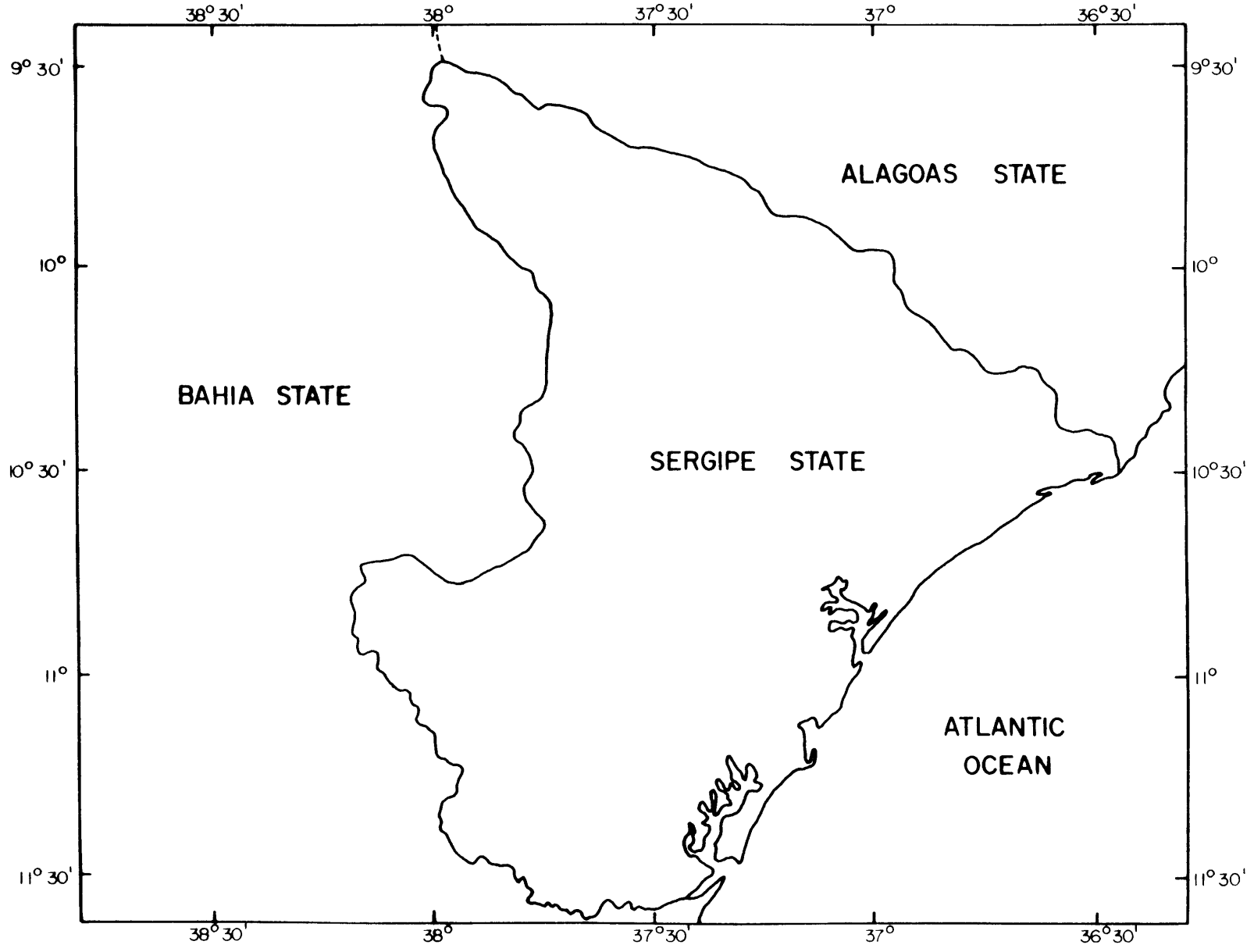
38° 30'
38°
37° 30'
37°
36° 30'
9° 30'
10°
10° 30'
11°
11° 30'
ALAGOAS STATE
BAHIA STATE
SERGIPE STATE
ATLANTIC
OCEAN

FIGURE 5.6

Chapter 6

The Area-Age Relationship and Global Sea-Level Changes

6.1 Introduction

In this chapter we will define the area-age distributions for the present time and for the times of anomalies 13 and 25 (35.58 and 58.94 Ma, respectively). Then, as the ultimate goal of the thesis, we will use the changes in the area-age distributions for the three particular times to derive changes in the sea level, together with the uncertainties in these changes. We will test the hypothesis that past sea-level changes were mainly controlled by the distribution of area and age of the oceanic crust.

6.2 The Theoretical Area-Age Relationship

Sclater *et al.* [1980] determined the distribution of area as a function of the age of the ocean floor at the present time, using areas measured from an equal-area map of the oceans on which isochrons had been plotted. They found that the

area per unit age decreases with age in an approximately linear fashion. Parsons [1982] used these results and proposed an equation for the derivative of area, A, with respect to age, t, of the form

$$\frac{dA}{dt} = C_o\left(1 - \frac{t}{t_m}\right) \qquad (6.1)$$

where C_o is the rate of generation of new ocean floor and t_m is the maximum age. This linear relation between the area per unit age and age is empirical. There is no theory that justifies that this relation must be linear. In order to reduce the effect of errors in isochron locations, ages, and area measurements, Parsons [1982] combined adjacent age intervals from the area calculations of Sclater *et al.* [1980]. By integrating Equation (6.1), Parsons [1982] gave the cumulative area (the area of the ocean floor that is younger than a given age),

$$A(t) = C_o t\left(1 - \frac{t}{2t_m}\right) \qquad (6.2)$$

Parsons [1982] explained why the empirical relations (6.1) and (6.2) describe so well the area-age distribution and the cumulative area versus age distribution, built on the area-age data given by Sclater *et al.* [1980], by considering the balance between plate generation and plate consumption. According to Parsons [1982], this is due to the fact that at any given time, new area of the ocean floor is generated at a rate equal to C_o at that time. He also postulated that the total amount of consumption must be equal to C_o so that the total area preserved at anytime is constant. As the ocean gets older, the initial area per unit age, C_o, experiences a constant rate of consumption, C_o/t_m, and hence decreases with time.

Parsons [1982] also calculated a theoretical hypsometric curve for the oceans by combining this relationship between area and age, with the relationship between age and depth. Parsons and Sclater [1977] showed that the variation of the mean depth, $\delta(t)$, with age can be described by

$$\delta(t) = d_o + at^{1/2} \qquad 0 \leq t < 70Ma$$

$$\delta(t) = d_r - be^{-\frac{t}{\tau}} \qquad t > 20Ma \tag{6.3}$$

where the values of the constants involved above, when t is measured in millions of years, are

$$a = 350\frac{m}{(Ma)^{\frac{1}{2}}}, \quad d_o = 2500m, \quad b = 3200m, \quad d_r = 6400m, \quad \tau = 62.8Ma$$

The two expressions differ by less than 20 m between 20 and 50 Ma. Their derivatives, which we used later, amplify the differences but agree within 1% at 35 Ma, which is where Parsons [1982] matched the different expressions.

Parsons [1982] calculated the derivative of area with respect to depth (area per unit depth interval), which can be expressed as:

$$\frac{dA}{d\delta} = \frac{dA}{dt}\frac{dt}{d\delta} \tag{6.4}$$

By substituting (6.1) and (6.3) into (6.4), Parsons [1982] got

$$\frac{dA}{d\delta} = \frac{2C_o t^{\frac{1}{2}}}{a}\left(1 - \frac{t}{t_m}\right) \qquad 0 \leq t \leq 35Ma$$

$$\frac{dA}{d\delta} = \frac{C_o \tau e^{\frac{t}{\tau}}}{b}\left(1 - \frac{t}{t_m}\right) \qquad 35 < t \leq 180Ma \tag{6.5}$$

Equations (6.3) and (6.5) represent a parameterized hypsometric curve with the age of the ocean floor as the parameter with the assumption that the derivative of area with respect to age, t, is linear dependent on age.

Changes in the area-age distribution, leading to changes in the hypsometric curve, result in global changes in sea level.

The volume of water, V_o, above the ocean floor is given by

$$V_o = \int_0^{t_m} \delta(t) \frac{dA}{dt} dt = \int_0^{t_m} [d_r - e(t)] \frac{dA}{dt} dt \qquad (6.6)$$

where e(t) is the elevation of the ocean floor above the reference depth, d_r (*Parsons, 1982*). In his derivation, Parsons [1982] neglected the volume of water that floods the continental margins since this represents only 15% of the volume change associated with the increased water depth, even when 50% of the continents are flooded [Hays and Pitman, 1973; Turcotte and Burke, 1978]. Parsons [1982] calculated a value of $1.51 \times 10^9 km^3$ for V_o by substituting (6.1) and (6.3) in (6.6). He compared his value with that of Menard and Smith [1966], who estimated a value of $1.35 \times 10^9 km^3$ by using the actual hypsometric distribution.

According to Parsons [1982], the thermal structure of the plates determines the elevation $e(t)$. The total volume of water above the ocean floor, V_o, and the total area of the oceans, $A(t_m)$, are considered to be constant. Thus, any changes in dA/dt must be balanced in equation (6.6) by changes in the reference depth, d_r. As Parsons [1982] noted, with allowance for the isostatic response, any variation in the water depth everywhere will cause a sea-level change. Accordingly, we are interested in changes in the area-age distribution.

Parsons [1982] also discussed how the area-age distribution, dA/dt, can be modified. Changes in the rate of plate generation, in the distribution of consumption with age, or in the total oceanic area as the area occupied by continents changes, will modify the area-age distribution. Following Parsons [1982], we consider the total oceanic area to be constant. This way, the area-age distribution and consequently, calculated sea-level changes, will result only from changes in the rate of plate generation over geologic time and in the distribution of consumption with age.

6.3 Area Measurements

We measured the areas for particular age intervals for the present time, for the anomaly 13 time (35.58 Ma), and for anomaly 25 time (58.94 Ma). These two particular times were chosen because the magnetic anomalies are well defined for these ages and mainly because they represent times of different area-age distributions than the present configuration. The area calculations were made using the method described in Chapter 5. Tables 6.1 to 6.15 list the area measurements and the uncertainties associated with these measurements for the present time. Tables 6.16 to 6.28 give these values for the reconstruction at anomaly 13 time (35.58 Ma) and Tables 6.29 to 6.38 give those for the reconstruction at anomaly 25 time (58.94 Ma).

The areas were measured between the isochrons of a specific magnetic anomaly age and between the boundaries formed by the limits of younger magnetic anomaly isochrons. The uncertainties in these areas were calculated by rotating one of the boundaries formed by one of the magnetic anomaly isochrons using the partial uncertainty poles and angles for the specific magnetic anomaly listed in the tables in Chapter 4. By this procedure, the individual measurements of area are for the cumulative areas (i.e. the area younger than the time of a specific magnetic anomaly). This was done to avoid combining uncertainties in younger reconstructions.

The calculated areas were separated into age groups and the values were used to calculate the dA/dt versus age graphs for each particular time (Figures 6.1 to 6.3). We also calculated the cumulative area versus age graphs for each particular time (Figures 6.4 to 6.6).

If we look at the dA/dt versus age graph for the present time, we notice a large difference between our results and those of Parsons [1982]. Our area versus age data do not agree with the linear relation given by Sclater *et al.*

[1980] (Equation 6.1). The difference results from differences in the isochrons of certain areas, where we used more recent magnetic anomaly and rotation parameters and obtained a different pattern from that inferred by Sclater *et al.*[1980]. Major differences occur for the Nazca-Pacific isochrons and for the Indian Ocean. There is no theory that justifies the linear relation between $\frac{dA}{dt}$ and t determined empirically by Sclater *et al.*[1980] and Parsons [1982].

6.4 Variations in the Volume of the Oceans

The total volume of the ocean basins is given by,

$$V = \int_0^{t_m} \delta(t) \frac{dA(t)}{dt} dt \qquad (6.7)$$

where $\delta(t)$ is the mean depth of the ocean at age t and $\frac{dA(t)}{dt}$ is the area per unit age of the ocean between age t and $t + dt$. Solving this integral by parts, we obtain

$$V = A(t_m)\delta(t_m) - \int_0^{t_m} A(t) \frac{d\delta(t)}{dt} dt \qquad (6.8)$$

The variation of the mean depth with age, $\delta(t)$, can be described by Equations (6.3) (Parsons and Sclater, 1977). We match the two equations at 40 Ma, when they differ by less than 10 m. So, the integral in Equation (6.8) becomes

$$\int_0^{t_m} A(t) \frac{d\delta(t)}{dt} dt = \int_0^{40Ma} A(t) \frac{d\delta(t)}{dt} dt + \int_{40Ma}^{180Ma} A(t) \frac{d\delta(t)}{dt} dt \qquad (6.9)$$

where $t_m (= 180Ma)$, the maximum age of the ocean floor.

We have evaluated $A(t)$ at discrete times, t_i, of selected magnetic anomalies. Let us assume that the area, $A(t)$ between two different magnetic anomalies, t_{i-1} and t_i, can be described by the linear equation,

$$A(t) = A(t_{i-1}) + \frac{A(t_i) - A(t_{i-1})}{t_i - t_{i-1}} (t - t_{i-1}) \qquad t_{i-1} < t < t_i \qquad (6.10)$$

Now, we solve the integral between 0 and $40Ma$ in Equation (6.9). From the depth equations given by Parsons and Sclater [1977] (Equation 6.3), we know that,

$$\frac{d\delta(t)}{dt} = \frac{1}{2}at^{-\frac{1}{2}} \tag{6.11}$$

So, we have

$$A(t)\frac{d\delta(t)}{dt} = \frac{a}{2}\{[A(t_{i-1})-(\frac{A(t_i)-A(t_{i-1})}{t_i-t_{i-1}})t_{i-1}]\frac{1}{\sqrt{t}}+[\frac{A(t_i)-A(t_{i-1})}{t_i-t_{i-1}}]\sqrt{t}\} \tag{6.12}$$

Evaluating one term in the first integral of Equation (6.9) leads to the integral

$$\int_{t_{i-1}}^{t_i} A(t)\frac{d\delta(t)}{dt}dt = a\sqrt{t}[A(t_{i-1})-\frac{A(t_i)-A(t_{i-1})}{t_i-t_{i-1}}t_{i-1}]+a\frac{t^{\frac{3}{2}}}{3}[\frac{A(t_i)-A(t_{i-1})}{t_i-t_{i-1}}]\Big|_{t_{i-1}}^{t_i}$$

$$= at_i^{\frac{1}{2}}[A(t_{i-1})-(\frac{A(t_i)-A(t_{i-1})}{t_i-t_{i-1}})t_{i-1}]+\frac{a}{3}t_i^{\frac{3}{2}}[\frac{A(t_i)-A(t_{i-1})}{t_i-t_{i-1}}]$$

$$-at_{i-1}^{\frac{1}{2}}[A(t_{i-1})-\frac{A(t_i)-(A(t_{i-1})}{t_i-t_{i-1}})t_{i-1}]-\frac{a}{3}t_{i-1}^{\frac{3}{2}}[\frac{A(t_i)-A(t_{i-1})}{t_i-t_{i-1}}]$$

$$= (at_i^{\frac{1}{2}}-at_{i-1}^{\frac{1}{2}})A(t_{i-1})+(-at_i^{\frac{1}{2}}t_{i-1}+\frac{a}{3}t_i^{\frac{3}{2}}+at_{i-1}^{\frac{3}{2}}-\frac{a}{3}t_{i-1}^{\frac{3}{2}})[\frac{A(t_i)-A(t_{i-1})}{t_i-t_{i-1}}]$$

$$= a\{A(t_{i-1})t_i^{\frac{1}{2}}-A(t_{i-1})t_{i-1}^{\frac{1}{2}}+[-\frac{t_i^{\frac{1}{2}}t_{i-1}}{t_i-t_{i-1}}A(t_i)+\frac{t_i^{\frac{1}{2}}t_{i-1}}{t_i-t_{i-1}}A(t_{i-1})$$

$$+\frac{1}{3}\frac{t_i^{\frac{3}{2}}}{t_i-t_{i-1}}A(t_i)-\frac{1}{3}\frac{t_i^{\frac{3}{2}}}{t_i-t_{i-1}}A(t_{i-1})+\frac{2}{3}\frac{t_{i-1}^{\frac{3}{2}}}{t_i-t_{i-1}}A(t_i)-\frac{2}{3}\frac{t_{i-1}^{\frac{3}{2}}}{t_i-t_{i-1}}A(t_{i-1})]\}$$

$$= a\{[t_i^{\frac{1}{2}}-t_{i-1}^{\frac{1}{2}}+\frac{t_i^{\frac{1}{2}}t_{i-1}}{t_i-t_{i-1}}-\frac{1}{3}\frac{t_i^{\frac{3}{2}}}{t_i-t_{i-1}}-\frac{2}{3}\frac{t_{i-1}^{\frac{3}{2}}}{t_i-t_{i-1}}]A(t_{i-1})$$

$$+[-\frac{t_i^{\frac{1}{2}}t_{i-1}}{t_i - t_{i-1}} + \frac{1}{3}\frac{t_i^{\frac{3}{2}}}{t_i - t_{i-1}} + \frac{2}{3}\frac{t_{i-1}^{\frac{3}{2}}}{t_i - t_{i-1}}]A(t_i)\}$$

$$= a\{[\frac{2t_i^{\frac{3}{2}} - 3t_i t_{i-1}^{\frac{1}{2}} + t_{i-1}^{\frac{3}{2}}}{3(t_i - t_{i-1})}]A(t_{i-1}) + [\frac{t_i^{\frac{3}{2}} - 3t_i^{\frac{1}{2}}t_{i-1} + 2t_{i-1}^{\frac{3}{2}}}{3(t_i - t_{i-1})}]A(t_i)\}$$

So, letting $t_0 = 0Ma$, for which $A(t_0) = 0$, we can write

$$V_{0_1} = \int_{0Ma}^{40Ma} A(t)d\delta(t) = \frac{a}{3}\sum_{i=1}^{N}\{\Theta_i A(t_{i-1}) + \Phi_i A(t_i)\} \tag{6.13}$$

where $t_N = 40Ma$, and

$$\Theta_i = [\frac{2t_i^{\frac{3}{2}} - 3t_i t_{i-1}^{\frac{1}{2}} + t_{i-1}^{\frac{3}{2}}}{t_i - t_{i-1}}]$$

and

$$\Phi_i = [\frac{t_i^{\frac{3}{2}} - 3t_i^{\frac{1}{2}}t_{i-1} + 2t_{i-1}^{\frac{3}{2}}}{t_i - t_{i-1}}]$$

Now, we solve the integral between 40 and $180Ma$ in Equation (6.9). From the depth equations given by Parsons and Sclater [1977] (Equation 6.3), we know that,

$$\frac{d\delta(t)}{dt} = \frac{b}{\tau}e^{-\frac{t}{\tau}} \tag{6.14}$$

For an interval of age between t_{i-1} and t_i, we have

$$A(t)\frac{d\delta(t)}{dt} = \frac{b}{\tau}\{[A(t_{i-1}) - (\frac{A(t_i) - A(t_{i-1})}{t_i - t_{i-1}})t_{i-1}]e^{-\frac{t}{\tau}} + [\frac{A(t_i) - A(t_{i-1})}{t_i - t_{i-1}}]te^{-\frac{t}{\tau}}\} \tag{6.15}$$

This leads us to the integral

$$\int_{t_{i-1}}^{t_i} A(t)d\delta(t) = \{\frac{b}{\tau}(-\tau)e^{-\frac{t}{\tau}}\Big|_{t_{i-1}}^{t_i}[A(t_{i-1}) - (\frac{A(t_i) - A(t_{i-1})}{t_i - t_{i-1}})t_{i-1}]\}$$

$$+\{\frac{b}{\tau}(\frac{A(t_i) - A(t_{i-1})}{t_i - t_{i-1}})[-\tau t e_{t_{i-1}}^{-\frac{t}{\tau}t_i} - \tau^2 e_{t_{i-1}}^{-\frac{t}{\tau}t_i}]\}$$

$$= b\{-e^{-\frac{t_i}{\tau}} + (\frac{t_{i-1}e^{-\frac{t_i}{\tau}}}{t_i - t_{i-1}})A(t_i) - (\frac{t_{i-1}e^{-\frac{t_i}{\tau}}}{t_i - t_{i-1}})A(t_{i-1}) + e^{-\frac{t_{i-1}}{\tau}}A(t_{i-1})$$

$$-(\frac{t_{i-1}e^{-\frac{t_{i-1}}{\tau}}}{t_i - t_{i-1}})A(t_i) + (\frac{t_{i-1}e^{-\frac{t_{i-1}}{\tau}}}{t_i - t_{i-1}})A(t_{i-1}) - (\frac{t_ie^{-\frac{t_i}{\tau}}}{t_i - t_{i-1}})A(t_i)$$

$$+(\frac{t_ie^{-\frac{t_i}{\tau}}}{t_i - t_{i-1}})A(t_{i-1}) + (\frac{t_{i-1}e^{-\frac{t_{i-1}}{\tau}}}{t_i - t_{i-1}})A(t_i) - (\frac{t_{i-1}e^{-\frac{t_{i-1}}{\tau}}}{t_i - t_{i-1}})A(t_{i-1})$$

$$-(\frac{\tau e^{-\frac{t_i}{\tau}}}{t_i - t_{i-1}})A(t_i) + (\frac{\tau e^{-\frac{t_i}{\tau}}}{t_i - t_{i-1}})A(t_{i-1}) + (\frac{\tau e^{-\frac{t_{i-1}}{\tau}}}{t_i - t_{i-1}})A(t_i) - (\frac{\tau e^{-\frac{t_{i-1}}{\tau}}}{t_i - t_{i-1}})A(t_{i-1})\}$$

$$= b\{[e^{-\frac{t_{i-1}}{\tau}} + \frac{\tau(e^{-\frac{t_i}{\tau}} - e^{-\frac{t_{i-1}}{\tau}})}{t_i - t_{i-1}}]A(t_{i-1}) + [-e^{-\frac{t_i}{\tau}} - \frac{\tau(e^{-\frac{t_i}{\tau}} - e^{-\frac{t_{i-1}}{\tau}})}{t_i - t_{i-1}}]A(t_i)\}$$

So, we can write

$$V_{0_2} = \int_{40Ma}^{180Ma} A(t)d\delta(t) = b\sum_{i=N+1}^{M}\{\Omega_i A(t_{i-1}) + \Psi_i A(t_i)\} \tag{6.16}$$

where $t_M = 180Ma$, and

$$\Omega_i = [e^{-\frac{t_{i-1}}{\tau}} + \frac{\tau(e^{-\frac{t_i}{\tau}} - e^{-\frac{t_{i-1}}{\tau}})}{t_i - t_{i-1}}]$$

and

$$\Psi_i = [-e^{-\frac{t_i}{\tau}} - \frac{\tau(e^{-\frac{t_i}{\tau}} - e^{-\frac{t_{i-1}}{\tau}})}{t_i - t_{i-1}}]$$

The total volume of the oceans at a particular time is given by

$$V_0 = A(t_m)\delta(t_m) - (V_{0_1} + V_{0_2}) \tag{6.17}$$

We checked the numerical scheme by comparing results with the analytic solution for $\frac{dA}{dt}$ linear in t, and found the disagreement to be less than 0.01%.

Since all estimates of $A(t_i)$ are independent of one another, we assume that the uncertainties in each can be treated as random. Thus, the uncertainties involved in the calculation of V_{0_1} are given by:

$$\Delta V_{0_1} = \{(\frac{a}{3})^2[\Theta_1^2\Delta A_1^2 + \sum_{i=1}^{N-1}(\Phi_i+\Theta_{i+1})^2\Delta A_i^2 + \Phi_N^2\Delta A_N^2]\}^{\frac{1}{2}} \tag{6.18}$$

and the uncertainties associated with V_{0_2} are given by:

$$\Delta V_{0_2} = \{b^2[\Omega_{N+1}^2\Delta A_{N+1}^2 + \sum_{i=N+1}^{M-1}(\Psi_i+\Omega_{i+1})^2\Delta A_i^2 + \Psi_M^2\Delta A_M^2]\}^{\frac{1}{2}} \tag{6.19}$$

The total uncertainty involved in the calculation of the volume of the oceans at a particular time, due to the area-age distribution, is given by

$$\Delta V_0 = \sqrt{\Delta V_{0_1}^2 + \Delta V_{0_2}^2} \tag{6.20}$$

We seek an estimate of the difference in the volume of the oceans at different times:

$$\epsilon V = V_{particular\ time} - V_{present\ time}$$

Again, because the estimates of the volumes are independent of one another, the uncertainty in their difference is simply

$$\Delta\epsilon V = \sqrt{\Delta V_{0_{present\ time}}^2 + \Delta V_{0_{particular\ time}}^2} \tag{6.21}$$

The values in Tables (6.16) to (6.38) and the above equations were used to compute the change in the volume of the ocean basins with respect to the present time and the respective uncertainties associated with the volume changes. We take the total area of the oceans $A(t_m)$ to be $2.967 \times 10^8 km^2$. The maximum depth $\delta(t_m)$ is $6.218 km$. Below, we consider changes of this area with time.

For the present time, Equations (6.13), (6.16), (6.18), and (6.19) yield:

$$V_{0_1} = 0.7547 \times 10^8 km^3 \pm 0.70 \times 10^6 km^3$$

$$V_{0_2} = 2.8446 \times 10^8 km^3 \pm 2.51 \times 10^6 km^3$$

The above values in Equations (6.17) and (6.20) yield:

$$V_{0_{present\ time}} = 1.48509 \times 10^9 km^3 \pm 2.61 \times 10^6 km^3$$

For anomaly 13 time (35.58 Ma), using Equations (6.13), (6.16), (6.18), and (6.19), we got the following values:

$$V_{0_1} = 0.7846 \times 10^8 km^3 \pm 0.98 \times 10^6 km^3$$

$$V_{0_2} = 2.9439 \times 10^8 km^3 \pm 3.53 \times 10^6 km^3$$

Using the above values in Equations (6.17), (6.20) and (6.21), we obtain

$$V_{0_{anomaly\ 13\ time}} = 1.47217 \times 10^9 km^3 \pm 3.66 \times 10^6 km^3$$

The difference in the volume of the ocean basins at the time of anomaly 13 from that for the present time is

$$\epsilon V_{an13-pres} = 12.92 \times 10^6 km^3 \pm 4.50 \times 10^6 km^3$$

For anomaly 25 time (58.94 Ma), Equations (6.13), (6.16), (6.18), and (6.19), yield the following values:

$$V_{0_1} = 0.8918 \times 10^8 km^3 \pm 1.01 \times 10^6 km^3$$

$$V_{0_2} = 3.1174 \times 10^8 km^3 \pm 3.27 \times 10^6 km^3$$

Using the above values in Equations (6.17), (6.20) and (6.21), we obtain

$$V_{0_{anomaly\ 25\ time}} = 1.44410 \times 10^9 km^3 \pm 3.43 \times 10^6 km^3$$

The difference in the volume of the ocean basins between the time of anomaly 25 and the present time is given by

$$\epsilon V_{an25-pres} = 40.98 \times 10^6 km^3 \pm 4.30 \times 10^6 km^3$$

6.5 Sea-Level Changes

Pitman [1978] showed that transgressions and regressions result from changes in the rates of sea-level rise or fall. He derived a quantitative relationship between the position of the shoreline and the rates of subsidence, sea-level changes, and sedimentation at Atlantic-type passive margins.

Pitman [1978] argued that to translate changes in the total ridge volume into sea-level changes, two corrections are needed. If the change in the water depth is h, a subsidence of the floor of ocean basin relative to the continent, d, must occur, but because of isostasy, $h \neq d$. If the density of the upper mantle is $3.4 g/cm^3$, the change in the sea-level is $(h - d) = 0.7h$. Second, a correction must be made for the hypsometric distribution (i.e. for the shape of the ocean basin). Pitman [1978] assumed that with the increase in the sea level there is a linear increase in the area covered by the sea ($0.17 \times 10^6 km^2$ for each meter rise in sea level). Based on these two corrections he showed that the change in continental freeboard (change in the sea level) $(h - d)$ caused by a change in the volume of the oceans, (ϵV), may be computed from

$$\epsilon V = A_0 h + (0.7h)^2 \frac{170}{2} \qquad (6.22)$$

where ϵV (in Km^3) is the difference between the present volume of the oceans and the volume at time t, A_0 is the present total area of the oceans (calculated here to be $296,723,115\ \mathrm{Km}^2$) and h is measured in Km.

This equation can be rewritten as

$$\epsilon V = \frac{A_0(h - d)}{0.7} + (h - d)^2 \frac{170}{2} \qquad (6.23)$$

Solving Equation (6.23) for $(h - d)$, we get

$$(h - d) = \frac{\sqrt{(\frac{A_0}{0.7})^2 + 340\epsilon V} - \frac{A_0}{0.7}}{170} \qquad (6.24)$$

Substituting the values of differences in the volume of the oceans calculated in the previous section, together with Equation (6.24), we obtain a fall in the sea-level of 30 ± 10 meters from anomaly 13 time (35.58 Ma) to the present time. From anomaly 25 time (58.94 Ma) to the present time, we obtain a sea-level fall of 97 ± 10 meters.

To check what would be the change in the sea level if in the past the distribution of the mean depth of the oceans would not be described by equations (6.3), we made a simple test. Assuming that the variation of the mean depth with age could be described just by the $t^{\frac{1}{2}}$ relation of equation (6.3), we calculated a decrease in the sea level of 32 meters since anomaly 13 time (35.58 Ma) and a decrease in sea level of 98 meters. Comparing these values with the results above, we conclude that if the distribution of mean depth with age in the past 60 million years was different from the present distribution, we would still have practically the same changes in sea level.

6.6 The Northward Motion of India

The calculated changes in sea level given above are based on the assumption that the area of the ocean basins has remained constant. This is very unlikely, but to estimate the change in area with time from reconstructions is virtually impossible. The uncertainties are enormous and they dominate any calculation of uncertainties in calculations of sea level. To examine how a change in area affects sea level, we consider what is probably the largest change in area, the penetration of India into Eurasia.

Since about 50 Ma, the total area of the oceans probably has being decreasing due to India moving northward with respect to Eurasia, with that penetration absorbed largely by crustal thickening apparently with almost no extrusion (England and Houseman, 1986). Let us estimate the contribution of

this change in the area of the oceans to the variation in the sea level.

For the calculation at anomaly 13 time (35.58 Ma), we assume an average northward motion since that time of $50\frac{km}{Ma}$ (with a 20% uncertainty), of a section of $2000km$ in width (with an uncertainty of 10%) of continental crust migrating northward, and with a $5km$ mean depth of the ocean basin created by the diminution of continental area (but with an uncertainty of 30%). This yields

$$\epsilon V^{35.58Ma}_{India\ motion} = 35.58Ma \times 50\frac{km}{Ma} \times 2000km \times 5km = 17.8 \times 10^6 km^3$$

The percentage uncertainty associated with this value is given by

$$\sqrt{(0.20)^2 + (0.10)^2 + (0.30)^2} = 37\%$$

which corresponds to an uncertainty of $6.7 \times 10^6 km^3$ in volume.

For the compression of Eurasia between the time of collision and the time of anomaly 13, let us assume the collision occurred at about $50Ma$ with an uncertainty of 5 Ma, and a northward motion of $100\frac{km}{Ma}$ with a 20 % uncertainty. We obtain

$$\epsilon V^{50-35.58Ma}_{India\ motion} = (50 - 35.58)Ma \times 100\frac{km}{Ma} \times 2000km \times 5km = 14.42 \times 10^6 km^3$$

The per cent uncertainty associated with this value is roughly

$$\sqrt{(0.30)^2 + (0.20)^2 + (0.10)^2 + (0.30)^2} = 48.0\%$$

So, for the reconstruction at anomaly 25 time (58.94 Ma), the penetration of India into Eurasia has created a volume of ocean given by

$$\epsilon V^{58.94Ma}_{India\ motion} = (17.8 + 14.4) \times 10^6 km^3 = 32.2 \times 10^6 km^3$$

The per cent uncertainty associated with this value is given by

$$\sqrt{(0.37)^2 + (0.48)^2} = 61\%$$

which is an uncertainty of $19.6 \times 10^6 km^3$.

Using Equation (6.24) to translate these values into differences in the sea-level, we get a difference of 42 meters $\pm$ 16 meters for the reconstruction at anomaly 13 time (35.58 Ma) and a difference of 76 meters $\pm$ 46 meters at anomaly 25 time (58.94 Ma).

The contribution to the variations in the sea level of the change in the volume of the oceans due to the northward motion of India is very large, comparable with that due to the difference in the mean age of the ocean floor. For the reconstruction at anomaly 13 time (35.58 Ma) the change in the sea level due to differences in the area-age distribution of the oceans is smaller than the estimated sea-level change due to the compression of the northern part of India against Eurasia. For the reconstruction at anomaly 25 time (58.94 Ma), the change in sea-level caused by the northward motion of India is smaller than the change in sea-level calculated from variations in the area-age distribution of the oceans, but they are comparable.

6.7 Conclusions

The area-age distributions of the ocean floor at the present time and at the times of anomalies 13 and 25 (35.58 and 58.94 Ma, respectively) were computed here. The area-age distribution at the present time disagrees with the conclusion originally made by Sclater *et al.*[1980] and used later by Parsons [1982], that the area per unit age decreases following an approximately linear dependence on age.

The differences in the area-age distributions were used to calculate differences in the total volume of the oceans. These differences in the total volume of the oceans were translated into changes in the sea-level following the analysis of Pitman [1978]. The uncertainties involved in the calculations were also com-

puted. The differences in the total volume of the oceans should have caused a change in the sea level of 30 ± 10 meters since anomaly 13 time (35.58 Ma) and a change of 97 ± 10 meters since anomaly 25 time (58.94 Ma), assuming that the area of the ocean basins has been constant. These results agree with the predictions of some sedimentary studies. The uncertainties in the final numbers indicate that it is important to continue this research with the calculations of changes of sea level during other periods of time, to see if it is possible to define sharper sea-level changes.

Following the analysis of Turcotte and Burke [1978], these changes in the sea level would represent a change in the ridge heat flow of 3.351×10^{11} cal/sec since anomaly 13 time (35.58 Ma) and a change in the ridge heat flow of 6.664×10^{11} cal/sec since the time of anomaly 25 (58.94 Ma). This suggests that the convection process is not a steady state process.

We also notice, however, that the change in area of the ocean basins due to the northward movement of India since its collision with Eurasia could be very important and a major factor in sea-level changes since the collision time (about 50 Ma). For the anomaly 13 reconstruction, the change in the volume of the oceans due to the northward motion of India could be responsible for larger variations in the sea level than is the change in the area-age distribution of the oceans. For the anomaly 25 time (58.94 Ma) reconstruction, the collision of India with Eurasia results in smaller changes in sea level than the variation in the area-age distribution of the oceans but, nonetheless, the changes due to this collision are very significant.

The combination of the changes in the sea level due to differences in the area-age distribution with the sea-level changes caused by the penetration of India into Eurasia give us a change in the sea level of 72 ± 19 meters since the time of anomaly 13 (35.58 Ma) and a change in the sea level of 173 ± 47 meters since anomaly 25 time (58.94 Ma).

There are $30.11 \times 10^6 Km^3 \pm 2.5 \times 10^6 Km^3$ of ice present today in Antarctica which is about 90% of the world's ice (Drewey, 1983). This would represent a difference in sea level of 71 meters $\pm$ 6 meters. So, the combination of the changes in sea level due to the previous factors and the assumption that most of the ice was formed in the past 30 m.y., give us a change in sea level of 143 ± 25 meters since the time of anomaly 13 (35.58 Ma) and a change in the sea level of 244 ± 53 meters.

The changes in the total area of the ocean basins due to other collision boundaries is considered here to be small and are ignored. The changes in the volume of the ocean basins due to seamounts and plateaus are also ignored. There is no reliable way to estimate their values in the past. The volume of ocean water is assumed to be constant. Ninety percent of the water is believed to have been formed during the first billion years of earth's history and, during the Phanerozoic the production of juvenile water was insignificant (Holland, 1984). There is an error associated with the study of sea-level changes due to these factors.

We also could have additional errors due to the subduction of young sea floor in the past with no record of its age preserved at the present time. If all the subducted ocean floor that we considered to be older than anomaly M25 in the reconstruction for anomaly 13 time, with age between 144.42 Ma and 180 Ma, were very young sea floor, with age between 0 Ma and 6.43 Ma, we would have a change of 144 meters due to change in the area-age distribution. In a similar way, if all the subducted ocean floor that we considered to be older than anomaly M25 at the reconstruction at anomaly 25 time, with age between 121.06 Ma and 180 Ma, were very young sea floor, with age between 0 Ma and 9.53 Ma, we would have a change of 307 meters due to changes in the area-age distribution. These two examples show the extreme error that could arise from our lack of knowledge about the age of the portion of ocean floor that was

subducted in the past and is no longer present today.

Figure Captions

Figure 6.1 Graph showing the variation of the ratio between area and time, $\frac{dA}{dt}$, as a function of time, t, for the present time.

Figure 6.2 Graph showing the variation of the ratio between area and time, $\frac{dA}{dt}$, as a function of time, t, for the time of anomaly 13 (35.58 Ma).

Figure 6.3 Graph showing the variation of the ratio between area and time, $\frac{dA}{dt}$, as a function of time, t, for the time of anomaly 25 (58.94 Ma).

Figure 6.4 Graph of the variations of cumulative area, A, versus time, t. The red represents the variation for the present time. The blue shows the variation for the time of anomaly 13 (35.58 Ma). The green shows the variation for the time of anomaly 25 (58.94 Ma).

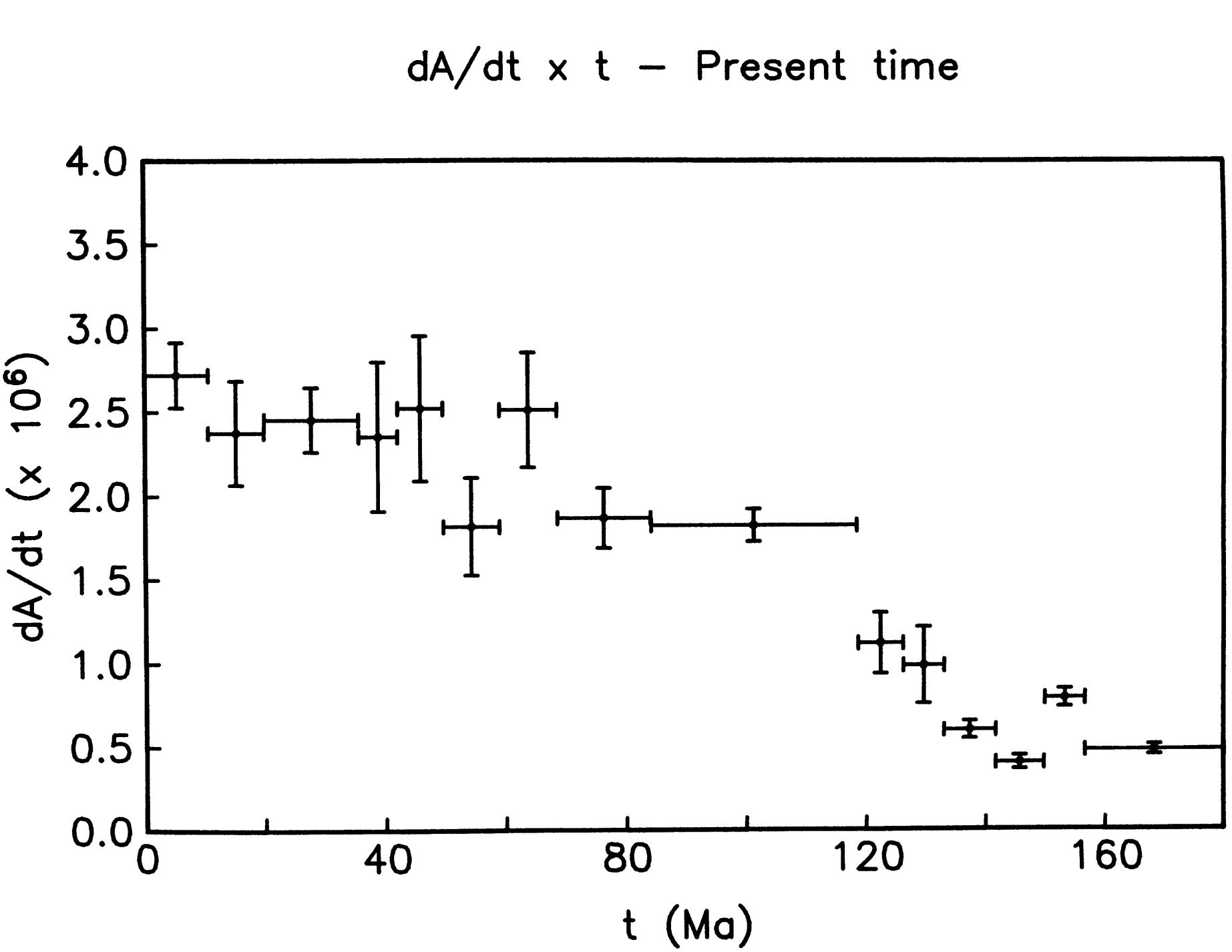
dA/dt x t – Present time
dA/dt (x 10⁶)
4.0
3.5
3.0
2.5
2.0
1.5
1.0
0.5
0.0
0
40
80
120
160
t (Ma)

FIGURE 6.1

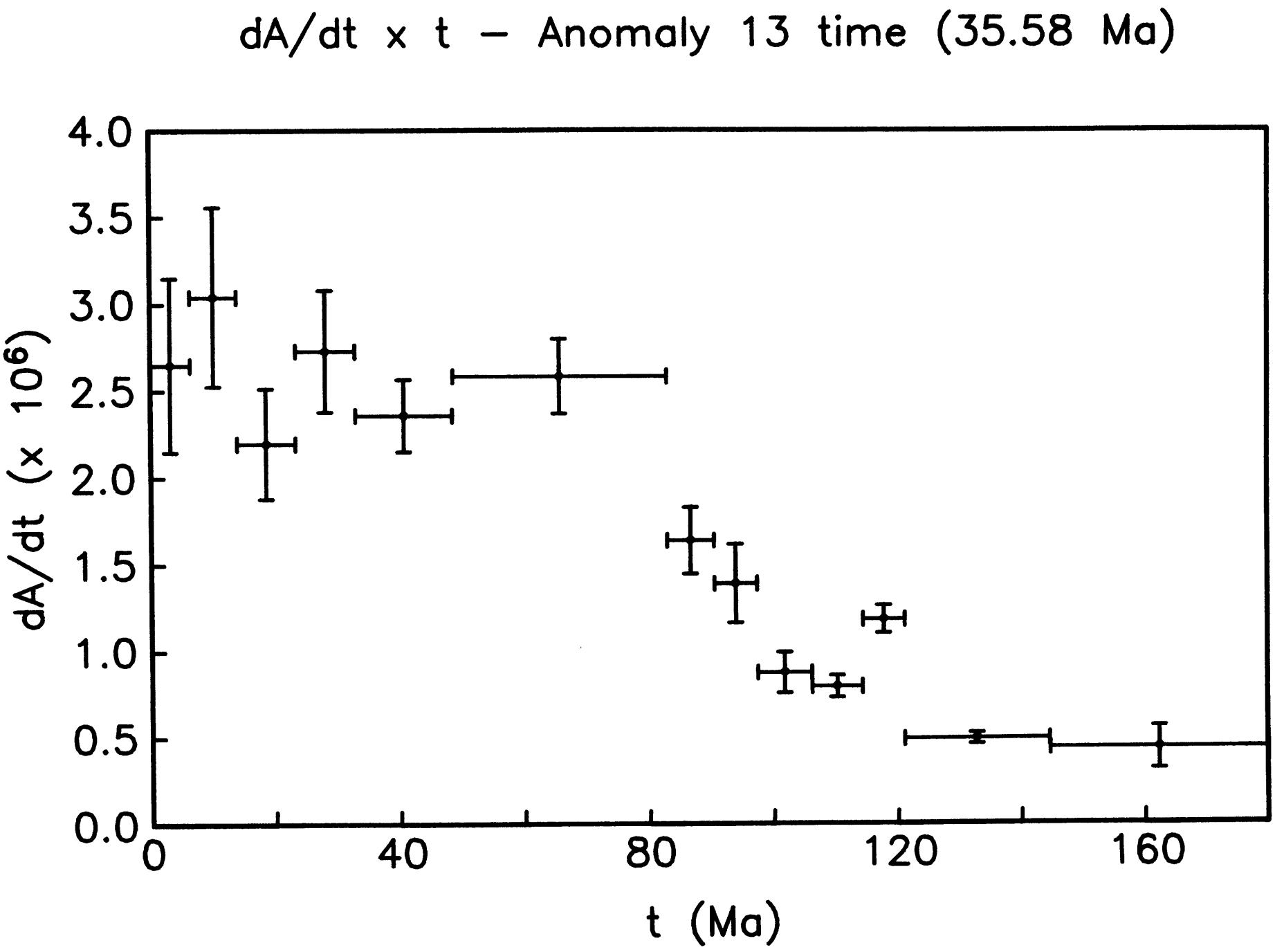
dA/dt x t – Anomaly 13 time (35.58 Ma)
dA/dt (x 10⁶)
4.0
3.5
3.0
2.5
2.0
1.5
1.0
0.5
0.0
0
40
80
120
160
t (Ma)

FIGURE 6.2

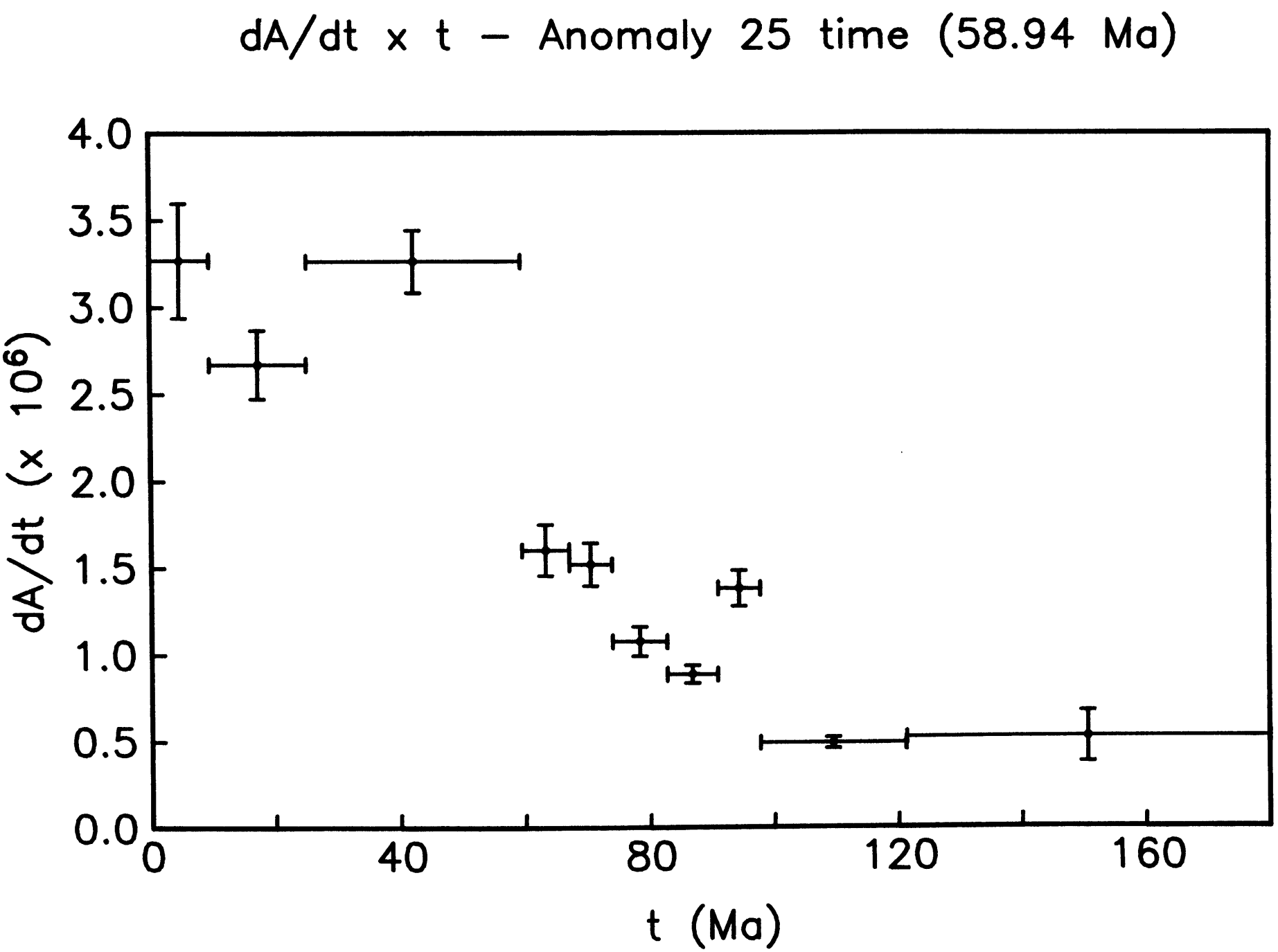
dA/dt x t – Anomaly 25 time (58.94 Ma)
dA/dt (x 10⁶)
4.0
3.5
3.0
2.5
2.0
1.5
1.0
0.5
0.0
0
40
80
120
160
t (Ma)

FIGURE 6.3

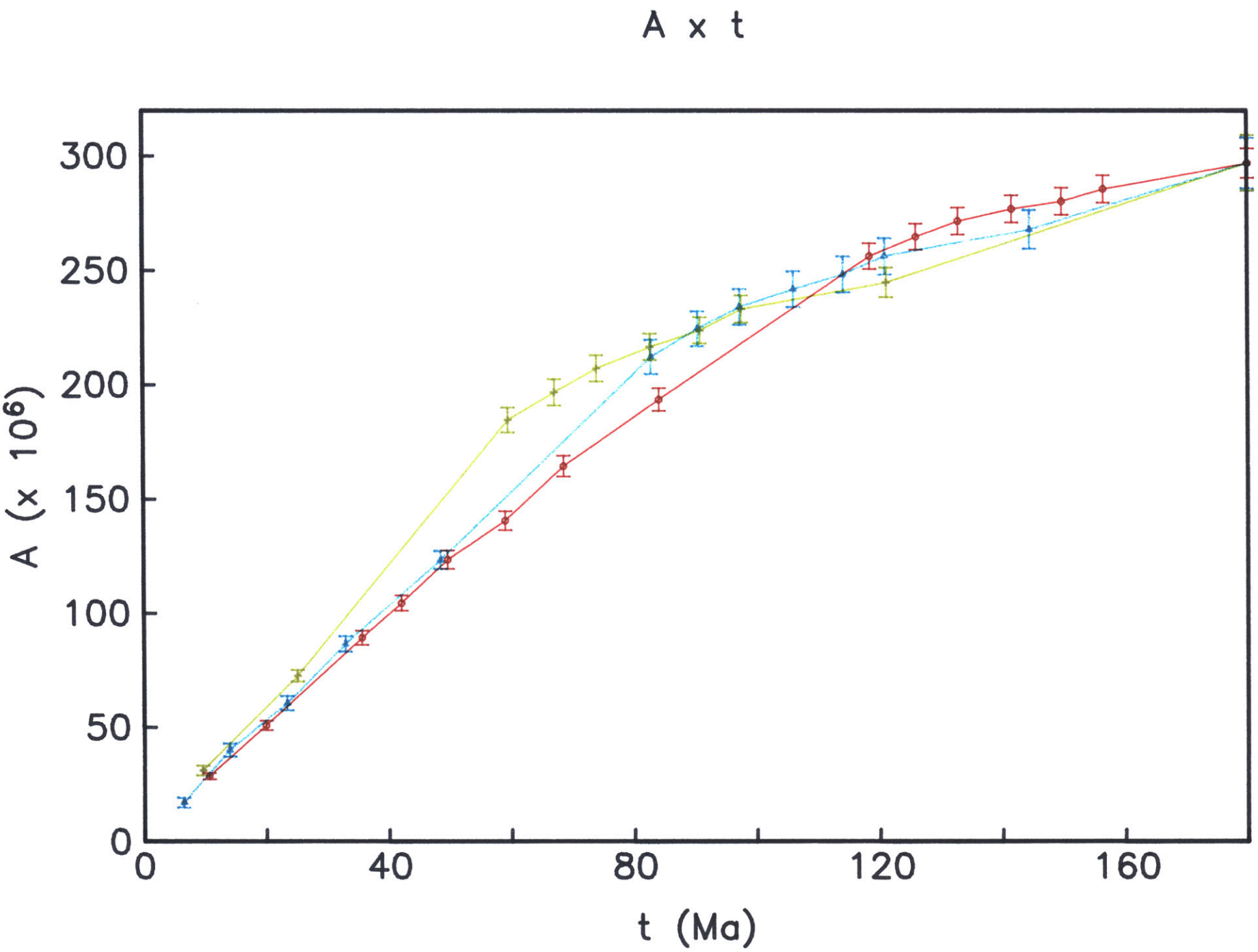

FIGURE 6.4

Chapter 7

Summary and Conclusions

The first task of the work presented here was to organize a set of magnetic anomalies, fracture zones and plate boundaries that included all the data collected and presented until now in the geophysical literature. We also collected published sets of rotation parameters. These first two steps involved a detailed search in the literature followed by the digitization of all the data that were not included in an earlier database. We compiled isochrons for the times of magnetic anomalies 5 (10.59 Ma), 6 (19.90 Ma), 13 (35.58 Ma), 18 (42.01 Ma), 21 (49.55 Ma), 25 (58.94 Ma), 30-31 (68.47 Ma), 34 (84.00 Ma), M0 (118.35 Ma), M4 (125.91 Ma), M11 (132.78 Ma), M16 (141.52 Ma), M21 (149.65 Ma), and M25 (156.42 Ma).

The second task of this thesis was the analysis of the magnetic and bathymetric data in order to test the rotation parameters. This resulted in the calculation of some new rotation parameters and of the uncertainties associated with them to build a consistent set of parameters with calculated uncertainties that would work with all the plate boundaries.

These first two objectives were performed in Chapters 2, 3, and 4. Chapter 2 describes our study on the rigidity of the Pacific plate during late Cre-

taceous and Tertiary time. We analyzed magnetic anomaly and fracture zone crossings resulting in the set of consistent rotation parameters with associated uncertainties for the Pacific-Farallon, Pacific-Vancouver, and Pacific-Kula plates between the times of anomalies 13 and 32. The Pacific and Farallon plates between the Pioneer and Agassiz fracture zones appear to have been rigid, with neither broken into two plates during that interval of time. Therefore, the additional Tertiary plate boundary inferred by *Gordon and Cox* [1980] and *Suárez and Molnar* [1980] must have been south of the area studied within the Pacific plate south of the latitude 43°S, or within the Antarctic plate. Based on the reanalysis of early Tertiary magnetic anomalies on the Pacific plate south of the Campbell Plateau, *Stock and Molnar* [1987] concluded that this boundary existed until a little before anomaly 18 time (42.01 Ma) and is now beneath the Bellingshausen sea. They named this plate which had boundaries with the Pacific and the Antarctic plates, the Bellingshausen plate.

We also concluded that the spacings of magnetic anomalies 13, 18, and 21 north of the Pioneer fracture zone and the orientations of the Pioneer, Mendocino, and Surveyor fracture zones differ from those south of the Pioneer fracture zone and suggest that between the formation of anomalies 25 and 21, the northern part of the Farallon plate split from the rest of it to form the Vancouver plate, as *Menard* [1978] had inferred. This showed that it has been the Vancouver plate, not the Farallon plate, that was subducted beneath most of the western North America from about 55 Ma until the spreading center was destroyed at the subduction zone.

In Chapter 3, we studied the Tertiary plate motions in the southeastern Pacific. We analyzed the data of Cande *et al.* [1982] with the calculation of rotation parameters and associated uncertainties. Although we are not able to constrain very well some of the rotation parameters, it was the first time that rotation parameters were calculated for this dataset. The southeastern

Pacific has had a complex tectonic history with spreading between several pairs of plates. Our analysis agrees with the model for the evolution of this region originally proposed by Weissel *et al.* [1977] and supported by Cande *et al.* [1982], involving a major reorganization of plate boundaries between anomaly 26 time and anomaly 18 time. Although the lengths of the spreading centers in this region are not large, a reanalysis of the original magnetic and bathymetric data, together with future collection of new data may reduce the uncertainties and further improve the details of the tectonic history of the region.

A global analysis of magnetic anomaly and fracture zone data, and of published rotation parameters, described in Chapter 4, was used to build a consistent set of global rotation parameters with calculated uncertainties. These were used together with digitized plate boundaries to define isochron maps for the present time and for reconstructions at anomaly 13 time (35.58 Ma) and at anomaly 25 time (58.94 Ma). It is the first time that a global analysis of rotation parameters and their uncertainties has been made, resulting in a consistent world map of the age of the oceans.

In Chapter 5 we present the method used to calculate areas on the surface of the earth. The errors associated with the method were discussed. It is a reliable and innovative method used in Chapter 6 to determine the distribution of area with age of the ocean floor for the present time and for the reconstructions at the times of anomalies 13 and 25 (35.58 Ma and 58.94 Ma, respectively). The area-age distribution at the present time disagree with the conclusion originally made by Sclater *et al.*[1980] and used by Parsons [1982], that the area per unit age decreases following an approximately linear dependence on age.

The ultimate goal was to analyze the area-age distribution for the present time and for the reconstructions at anomalies 13 and 25 times (35.58 Ma and 58.94 Ma respectively), and to associate the changes in these area-age distributions with sea-level changes. We used the differences in the area-age distribu-

tions to calculate differences in the total volume of the oceans. The differences in the total volume of the oceans should have caused a change in the sea level of 30 ± 10 meters since anomaly 13 time (35.58 Ma) and a change of 97 ± 10 meters since anomaly 25 time (58.94 Ma). The uncertainties involved in these values indicate that it is important to continue this research with the calculations of changes of sea level during other periods of time to see if we can define sharper changes in the sea level.

We also notice that the northwards movement of India since its collision with Eurasia is a major factor in changes in the sea level since about 50 Ma, the time of the collision. For the anomaly 13 reconstruction, the change in the volume of the oceans due to the northern motion of India yields a difference in sea level of about 42 meters $\pm$ 16 meters and for the anomaly 25 reconstruction, we have a difference of about 76 meters $\pm$ 46 meters.

The combination of the changes in the sea level due to differences in the area-age distribution with the sea-level changes caused by the penetration of India into Eurasia give us a change in the sea level of 72 ± 19 meters since the time of anomaly 13 (35.58 Ma) and a change in the sea level of 173 ± 47 meters since anomaly 25 time (58.94 Ma).

The present volume of ice in Antarctica would represent a difference in sea level of 71 meters $\pm$ 6 meters. The combination of the changes in sea level due to the previous factors and the assumption that most of the ice was formed in the past 30 m.y., give us a change in sea level of 143 ± 25 meters since the time of anomaly 13 (35.58 Ma) and a change in the sea level of 244 ± 53 meters.

This is the first time a study of changes in sea level due to changes in the distribution of area with age of the oceans is done with the calculation of the associated uncertainties.

Figure Captions

Figure 7.1. Late Cretaceous to present sea-level curves (adapted from Kominz, 1984). For comparison, our results are plotted over the curves presented in Figure 1.1.

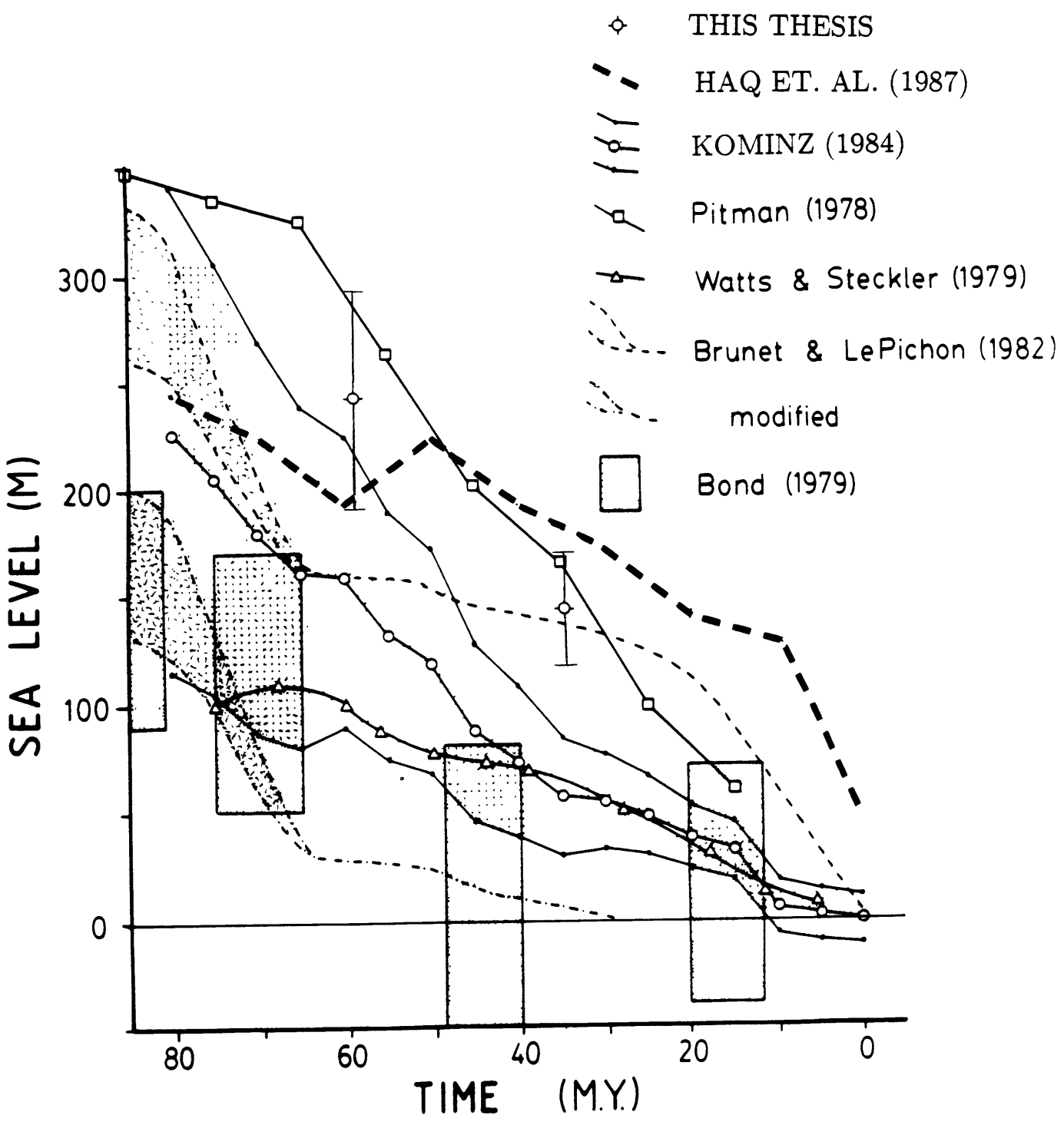
THIS THESIS
HAQ ET. AL. (1987)
KOMINZ (1984)
Pitman (1978)
Watts & Steckler (1979)
Brunet & LePichon (1982)
modified
Bond (1979)
SEA LEVEL (M)
300
200
100
0
80
60
40
20
0
TIME (M.Y.)

FIGURE 7.1

References

Adamek, S., F. Tajima, and D. A. Wiens, Seismic rupture associated with subduction of the Cocos Ridge, *Tectonics*, em 6, 757-774, 1987.

Ager, D., V., Major marine cycles in the Mesozoic, *J. geol. Soc. London, 138*, 159-166, 1981.

Anderson, R., N., D. W. Forsyth, P. Molnar, and J. Mammerickx, Fault plane solutions of earthquakes on the Nazca Plate boundaries and the Easter Plate, *Earth Planet Sci Lett, 24*, 188- 202, 1974.

Anderson, R., N., M. G. Langseth, and J. G. Sclater, The mechanisms of heat transfer through the floor of the Indian Ocean, *J Geophys Res, 82*, 3391-3409, 1977.

Angevine, C., L., and P. L. Heller, Global sea-level changes and supercontinent breakup, *Eos Trans AGU, 67*, 1210, 1986.

Atwater, T., Implications of plate tectonics for the Cenozoic tectonic evolution of Western North America, *Geol Soc Am Bull, 81*, 3513-3536, 1970.

Atwater, T., and H. W. Menard, Magnetic lineations in the northeast Pacific, *Earth Planet Sci Lett, 7*, 445-450, 1970.

Atwater, T., and P. Molnar, Relative motion of the Pacific and North American plates deduced from sea-floor spreading in the Atlantic, Indian, and South Pacific Oceans, *in Proceedings of the conference on tectonic problems of the San Andreas Fault System*, edited by R. L. Kovach, and A. Nur, pp. 136-148, Stanford University, 1973.

Bardos, A., Geomagnetism, sea level and tectonics, *Physics Today, 41*, 120-122, 1988.

Barron E., J., C. G. A. Harrison, J. L. Sloan II, and W. W. Hay, Paleogeography, 180 million years ago to the present, em Eclogae geol. Helv., em 74, 443-470, 1981.

Barron, E., J., and W. M. Washington, The role of geographical variables in explaining paleoclimates: results from cretaceous climate model sensitivity studies, em J Geophys Res, em 89, 1267-1279, 1984.

Bassinger, B., G., O. E. DeWald, and G. Peter, Interpretation of the magnetic anomalies off Central California, *J Geophys Res, 74*, 1484-1487, 1969.

Berger, W., H., and E. L. Winterer, Plate stratigraphy and the fluctuating carbonate line, *Spec. Publs int. Ass. Sediment.*, *1*, 11-48, 1974.

Berggren, W., A., D. V. Kent, J. J. Flynn, and J. A. Van Couvering, Cenozoic geochronology, *Geol Soc Am Bull*, *96*, 1407- 1418, 1985.

Bergh, H., W., Mesozoic sea floor off Dronning Maud Land, Antarctica, *Nature*, *269*, 686-687, 1977.

Bergh, H., W., and D. M. Barrett, Agulhas Basin magnetic bight, *Nature*, *287*, 591-595, 1980.

Bergh, H., W., and I. O. Norton, Prince Edward Fracture Zone and the evolution of the Mozambique Basin, *J Geophys Res*, *81*, 5221- 5239, 1976.

Berner, R., A., A. C. Lasaga, and R. M. Garrels, The carbonate-silicate geochemical cycle and its effect on atmospheric carbon dioxide over the past 100 million years, *Am Jour of Sci*, *283*, 641-683,1983.

Besse, J., and V. Courtillot, Paleogeographic maps of the continents bordering the Indian Ocean since the early Jurassic, *J Geophys Res*, *93*, 11791-11808, 1988.

Bullard, E., J. E. Everett, and A. G. Smith, The fit of the continents around the Atlantic, *Phil. Trans. R. Soc.*, *A258*, 41- 51, 1965.

Bunce, E., T., and P. Molnar, Seismic reflection profiling and basement topography in the Somali Basin: possible fracture zones between Madagascar and Africa, *J Geophys Res*, *82*, 5305- 5311, 1977.

Byrne, T., Late Paleocene demise of the Kula-Pacific spreading center, *Geology*, *7*, 341-344, 1979.

Cande, S., C., E. M. Herron, and B. R. Hall, The early Cenozoic tectonic history of the southeast Pacific, *Earth Planet Sci Lett*, *57*, 63-74, 1982.

Cande, S., C., and Y. Kristoffersen, Late Cretaceous magnetic anomalies in the North Atlantic, *Earth Planet Sci Lett*, *35*, 215- 224, 1977.

Cande, S., C., J. L. LaBrecque, and W. F. Haxby, Plate kinematics of the South Atlantic: chron C34 to present, *J Geophys Res*, *93*, 13479-13492, 1988.

Cande, S., C., R. B. Leslie, J. C. Parra, and M. Hobart, Interaction between the Chile Ridge and Chile Trench: geophysical and geothermal evidence, *J Geophys Res*, *92*, 495-520, 1987.

Cande, S., C., and J. C. Mutter, A revised identification of the oldest sea-floor spreading anomalies between Australia and Antarctica, *Earth Planet Sci Lett*, *58*, 151-160, 1982.

Caress, D., W., H. W. Menard, and R. N. Hey, Eocene reorganization of the Pacific-Farallon spreading center north of the Mendocino fracture zone, *J Geophys Res*, *93*, 2813-2838, 1988.

Chang, T., Spherical regression, *The Annals of Statistics*, *14*, 907-924, 1986.

Chang, T., On the statistical properties of estimated rotations, *J Geophys Res*, *92*, 6319-6329, 1987.

Chase, C., G., Plate kinematics: The Americas, East Africa, and the rest of the world, *Earth Planet Sci Lett*, *37*, 355-368, 1978.

Chase, T., E., H. W. Menard, and Mammerickx, Topography of the North Pacific, Charts 1-10, Inst. of Mar. Resour., Scripps Inst. of Oceanogr., San Diego, La Jolla, 1970.

Christoffel, D., A., and R. K. H. Falconer, Marine magnetic measurements in the southwest Pacific Ocean and the identification of new tectonic features, *in Antarctic Oceanology II: The Australian-New Zealand sector*, *Antarctic Res. Ser.*, *Vol. 19*, edited by D. E. Hayes, pp. 197-209, American Geophys. Union, Washington, 1972.

Clague, D., A., and R. D. Jarrard, Tertiary Pacific plate motion deduced from the Hawaiian-Emperor chain, *Geol Soc Am Bull*, *84*, 1135-1154, 1973.

Cochran, J., R., Somali Basin, Chain Ridge, and origin of the northern Somali Basin gravity and geoid low, *J Geophys Res*, *93*, 11985-12008, 1988.

Coffin, M., F., and P. D. Rabinowitz, Reconstruction of Madagascar and Africa: Evidence from the Davie Fracture Zone and Western Somali Basin, *J Geophys Res*, *92*, 9385-9406, 1987.

Davis, D., M., and S. C. Solomon, Variations in the velocities of the major plates since the late Cretaceous, *Tectonophysics*, *74*, 189-208, 1981.

Davis, E., E., and C. R. B. Lister, Fundamentals of ridge crest topography, *Earth Planet Sci Lett*, *21*, 405-413, 1974.

DeMets, C., R. G. Gordon, and D. F. Argus, Intraplate deformation and closure of the Australia-Antarctica plate circuit, *J Geophys Res*, *93*, 11877-11897, 1988.

Detrick, R., S., and S. T. Crough, Island subsidence, hot spots, and lithospheric thinning, *J Geophys Res*, *83*, 1236-1244, 1978.

Detrick, R., S., J. G. Sclater, and J. Thiede, The subsidence of aseismic ridges, *Earth Planet Sci Lett*, *34*, 185-196, 1977.

Detrick Jr, R., S., An analysis of geoid anomalies across the Mendocino Fracture Zone: implications for thermal models of the lithosphere, *J Geophys Res*, *86*, 11751-11762, 1981.

Dunbar, J., A., and D. S. Sawyer, Implications of continental crust extension for plate reconstruction: an example from the Gulf of Mexico, *Tectonics*, *6*, 739-755, 1987.

Eldholm, O., and M. Talwani, Sediment distribution and structural framework of the Barents Sea, *Geol Soc Am Bull*, *88*, 1015-1029, 1977.

Elvers, D., K. Potter, D. Seidel, and J. Morley, IDOE 1971 survey, NOS seamap profiles plate BGM-1-71, Natl. Oceanic and Atmos. Admin., U. S. Dep. of Commer., Washington, D. C., 1972.

Elvers, D., S. P. Srivastava, K. Potter, J. Morley, and D. Sdidel, Asymetric spreading across the Juan de Fuca and Gorda Rises as obtained from a detailed magnetic survey, *Earth Planet Sci Lett*, *20*, 211-219, 1973.

Embleton, B., J., J., and M. W. McElhinny, The paleoposition of Madagascar: paleomagnetic evidence from the Isalo group, *Earth Planet Sci Lett*, *27*, 329-341, 1975.

Engebretson, D., C., A. Cox, and R. G. Gordon, Relative motions between oceanic plates of the Pacific Basin, *J Geophys Res*, *89*, 10291-10310, 1984.

Engebretson, D., C., A. Cox, and R. G. Gordon, Relative motions between oceanic and continental plates in the Pacific Basin, *Geol. Soc. Am. Spec. Pap.*, p. 59, 1985.

England, P., and G. Houseman, Finite strain calculations of continental deformation 2. Comparison with the India-Asia collission zone, em J Geophys Res, em 91, 3664-3676, 1986.

England, P., and R. Wortel, Some consequences of the subduction of young slabs, *Earth Planet Sci Lett*, *47*, 403-415, 1980.

Fisher, R., L., and J. G. Sclater, Tectonic evolution of the Southwest Indian Ocean since the Mid-cretaceous: plate motions and stability of the pole of Antarctica/Africa for at least 80 Myr, *Geophys J R Astron Soc*, *73*, 553-576, 1983.

Forsyth, D., and S. Uyeda, On the relative importance of the driving forces of plate motion, *Geophys J R Astron Soc*, *43*, 163- 200, 1975.

Geller, C., A., J. K. Weissel, and R. N. Anderson, Heat transfer and intraplate deformation in the central Indian Ocean, *J Geophys Res*, *88*, 1018-1032, 1983.

Glen, W., and H. Frankel, The jubilee of plate tectonics, *Eos Trans AGU, 69*, 583-585, 1988.

Gordon, R., G., and A. Cox, Paleomagnetic test of the early Tertiary plate circuit between the Pacific Basin plates and the Indian plate, *J Geophys Res, 85*, 6534-6546, 1980.

Gordon, R., G., A. Cox, and C. E. Harter, Absolute motion of an individual plate estimated from its ridge and trench boundaries, *Nature, 274*, 752-755, 1978.

Gordon, R., G., M. O. McWilliams, and A. Cox, Pre-Tertiary velocities of the continents: A lower bound from paleomagnetic data, *J Geophys Res, 84*, 5480-5486, 1979.

Grim, P., J., and B. H. Erickson, Fracture zones and magnetic anomalies south of the Aleutian Trench, *J Geophys Res, 74*, 1488- 1494, 1969.

Hamburger, M., W., and B. L. Isacks, Deep earthquakes in the Southwest Pacific: a tectonic interpretation, *J Geophys Res, 92*, 13841-13854, 1987.

Handschumacher, D., W., Post-Eocene plate tectonics of the Eastern Pacific, *in The geophysics of the Pacific Ocean Basin and its margin, Geophysical Monograph 19*, edited by G. H. Sutton, M. H. Manghnani, and R. Moberly, pp. 177-202, American Geophys. Union, Washington, D.C., 1976.

Handschumacher, D., W., S. T. Okamura, and P. K. Wong, Magnetic and bathymetric profiles from the central and southeastern Pacific: 10 N-45 S, 70 W-150 W, *Int. Decade of Ocean Explor. and Office of Nav. Res.*, p. 175, Honolulu, Hawaii, 1975.

Hanks, T., C., The Kuril trench - Hokkaido rise system: large shallow earthquakes and simple models of deformation, *Geophys J R Astron Soc, 23*, 173-189, 1971.

Haq, B., U., J. Hardenbol, and P. R. Vail, Chronology of fluctuating sea levels since the Triassic, *Science, 235*, 1156- 1167, 1987.

Harland, W., B., A. V. Cox, P. G. Llewellyn, C. A. Pickton, A. G. Smith, and R. Walters, *A geologic time scale*, Cambridge University Press, p. 128, New York, 1982.

Harrison, C., G., A., and J. G. Sclater, Origin of the disturbed magnetic zone between the Murray and Molokai fracture zones, *Earth Planet Sci Lett, 14*, 419-427, 1972.

Hay, W., W., C. A. Shaw, and C. N. Wold, Mass balanced paleogeographic reconstructions, em Geologische Rundschau, em 78, 207-242, 1989.

Hay, W., W., J. L. Sloan II, and C. N. Wold, Mass/age distribution and composition of sediments on the ocean floor and the global rate of sediment subduction, *Physical Research*, *93*, 14933-14940, 1988.

Hayes, D., E., Age-depth relationships and depth anomalies in the Southeast Indian Ocean and South Atlantic Ocean, *J Geophys Res*, *93*, 2937-2954, 1988.

Hayes, D., E., and J. R. Heirtzler, Magnetic anomalies and their relation to the Aleutian Island Arc, *J Geophys Res*, *73*, 4637- 4646, 1968.

Hayes, D., E., and W. C. Pitman III, Magnetic lineations in the North Pacific, *in Geological investigations of the North Pacific - Memoir 126*, edited by J. D. Hays, pp. 291-314, The Geological Society of America, Boulder, 1970.

Hayes, D., E., and J. Ringis, Seafloor spreading in the Tasman Sea, *Nature*, *243*, 454-458, 1973.

Hayes, D., E., and M. Talwani, Geophysical investigation of the Macquarie Ridge Complex, *in Antarctic Oceanology II: The Australian-New Zealand Sector, Antarctic Res. Ser.*, edited by D. E. Hayes, pp. 211-234, American Geophys. Union, Washington, 1972.

Hayes, J., D., and W. C. Pitman, III, Lithospheric plate motion, sea level changes and climatic and ecological consequences, *Nature*, *246*, 18-22, 1973.

Hellinger, S., J., The statistics of finite rotations in plate tectonics, Ph D thesis,, Mass. Inst. of Technol., p. 172, Cambridge, 1979.

Hellinger, S., J., The uncertainties of finite rotations in plate tectonics, *J Geophys Res*, *86*, 9312-9318, 1981.

Hempton, M., R., Constraints on Arabian plate motion and extensional history of the Red Sea, *Tectonics*, *6*, 687-705, 1987.

Herron, E., M., Crustal plates and sea floor spreading in the Southeastern Pacific, *in Biology of the Antarctic Seas IV, Antarctic Research Series*, edited by J. L. Reid, pp. 229-238, American Geophysical Union, Washington, 1971.

Herron, E., M., Sea-floor spreading and the Cenozoic history of the East-Central Pacific, *Geol Soc Am Bull*, *83*, 1671-1692, 1972.

Herron, E., M., and J. R. Heirtzler, Sea-floor spreading near the Galapagos, *Science*, *158*, 775-780, 1967.

Herron, E., M., and B. E. Tucholke, Sea-floor magnetic patterns and basement structure in the southeastern Pacific, *in Initial reports of the Deep Sea Drilling Project*, edited by C. D. Hollister, and C. Craddock, pp. 263-278, U.S. Government Printing Office, Washington, 1976.

Hey, R., Tectonic evolution of the Cocos-Nazca spreading center, *Geol Soc Am Bull, 88*, 1404-1420, 1977a.

Hey, R., A new class of "pseudofaults" and their bearing on plate tectonics: a propagating rift model, *Earth Planet Sci Lett, 37*, 321-325, 1977b.

Hey, R., N., H. W. Menard, T. M. Atwater, and D. W. Caress, Changes in direction of seafloor spreading revisited, *J Geophys Res, 93*, 2803-2811, 1988.

Hilde, T., W., C., N. Isezaki, and J. M. Wageman, The Mesozoic sea-floor spreading in the North Pacific, *in The geophysics of the Pacific Ocean Basin and its margin, Geophysical Monograph 19*, edited by G. H. Sutton, M. H. Manghnani, and R. Moberly, pp. 205-226, American Geophys. Union, Washington, D.C., 1976.

Johnson, B., D., C. M. Powell, and J. J. Veevers, Spreading history of the eastern Indian Ocean and Greater India's northward flight from Antarctica and Australia, *Geol Soc Am Bull, 87*, 1560-1566, 1976.

Johnson, B., D., C. M. Powell, and J. J. Veevers, Early spreading history of the Indian Ocean between India and Australia, *Earth Planet Sci Lett, 47*, 131-143, 1980.

Jordan, T., H., Composition and development of the continental tectosphere, *Nature, 274*, 544-548, 1978.

Jordan, T., H., The deep structure of the continents, *Scientific American, 240*, 92-107, 1979.

Jordan, T., H., Continents as a chemical boundary layer, *Phil. Trans. R. Soc. Lond., A 301*, 359-373, 1981.

Jurdy, D., M., The subduction of the Farallon Plate beneath North America as derived from relative plate motions, *Tectonics, 3*, 107-113, 1984.

Jurdy, D., M., and M. Stefanick, Errors in plate rotations as described by covariance matrices and their combination in reconstructions, *J Geophys Res, 92*, 6310-6318, 1987.

Jurdy, D., M., and M. Stefanick, Plate-driving forces over the Cenozoic Era, *J Geophys Res, 93*, 11833-11844, 1988.

Kastens, K., A., A compedium of causes and effects of processes at transform faults and fracture zones, *Reviews of Geophysics*, *25*, 1554-1562, 1987.

Kent, D., V., and F. M. Gradstein, A Cretaceous and Jurassic geochronology, *Geol Soc Am Bull*, *96*, 1419-1427, 1985.

Kent, D., V., and F. M. Gradstein, A Jurassic to recent chronology, *in The geology of North America - The Western North Atlantic region*, edited by P. R. Vogt, and B. E. Tucholke, pp. 45-50, Geological Soc. of America, 1986.

Kerr, R., A., Refining and defending the Vail sea level curve, *Science*, *235*, 1141-1142, 1987.

Klitgord, K., D., and H. Schouten, Plate kinematics of the central Atlantic, *in The Geology of North America - The Western Atlantic region*, edited by P. R. Vogt, and B. E. Tucholke, pp. 351-378, Geological Soc. of America, 1986.

Kominz, M., A., Oceanic ridge volumes and sea-level change - An error analysis, *in Interregional unconformities and hydrocarbon accumulation*, edited by J. S. Schlee, p. 184, AAPG, Tulsa, 1984.

Kristoffersen, Y., The Nansen Ridge, Arctic Ocean: some geophysical observations of the rift valley at slow spreading rate, *Tectonophysics*, *89*, 161-172, 1982.

Kristoffersen, Y., and M. Talwani, Extinct triple junction south of Greenland and the Tertiary motion of Greenland relative to North America, *Geol Soc Am Bull*, *88*, 1037-1049, 1977.

LaBrecque, J., L., and D. E. Hayes, Seafloor spreading history of the Agulhas Basin, *Earth Planet Sci Lett*, *45*, 411-428, 1979.

LaBrecque, J., L., D. V. Kent, and S. C. Cande, Revised magnetic polarity time scale for Late Cretaceous and Cenozoic time, *Geology*, *5*, 330-335, 1977.

LaBrecque, J., L., and C. A. Raymond, Seafloor spreading anomalies in the Magsat field of the North Atlantic, *J Geophys Res*, *90*, 2565-2575, 1985.

Larson, R., L., Late Jurassic sea-floor spreading in the Eastern Indian Ocean, *Geology*, *3*, 69-71, 1975.

Larson, R., L., The early Cretaceous - late Jurassic magnetic reversal time scale, and the Phoenix magnetic lineations revisited, *in The geophysics of the Pacific Ocean Basin and its margin, Geophysical Monograph 19*, edited by, p. 203, American Geophys. Union, Washington, D.C., 1976a.

Larson, R., L., Late Jurassic and Early Cretaceous evolution of the Western Central Pacific Ocean, *J. Geomag. Geoelectr.*, *28*, 219-236, 1976b.

Larson, R., L., Early Cretaceous breakup of Gondwanaland off western Australia, *Geology*, *5*, 57-60, 1977.

Larson, R., L., and C. G. Chase, Relative velocities of the Pacific, North America and Cocos plates in the Middle America region, *Earth Planet Sci Lett*, *7*, 425-428, 1970.

Larson, R., L., and C. G. Chase, Late Mesozoic evolution of the western Pacific ocean, *Geol Soc Am Bull*, *83*, 3627-3644, 1972.

Larson, R., L., and T. W. C. Hilde, A revised time scale of magnetic reversals for the early Cretaceous and late Jurassic, *J Geophys Res*, *80*, 2586-2594, 1975.

Larson, R., L., and W. C. Pitman III, World-wide correlation of Mesozoic magnetic anomalies, and its implications, *Geol Soc Am Bull*, *83*, 3645-3662, 1972.

Larson, R., L., S. M. Smith, and C. G. Chase, Magnetic lineations of early Cretaceous age in the western equatorial Pacific Ocean, *Earth Planet Sci Lett*, *15*, 315-319, 1972.

Larson, R., L., and F. N. Spiess, East Pacific Crest: a near- botton geophysical failure, *Science*, *163*, 68-71, 1969.

Lawver, L., A., and H. J. B. Dick, The American-Antarctic Ridge, *J Geophys Res*, *88*, 8193-8202, 1983.

Lawver, L., A., and D. T. Sandwell, SEABEAM and magnetics survey of the Bullard Fracture Zone: a young product of major plate reorganizations, Research proposal to the National Science Foundation, , 1986.

Lawver, L., A., J. G. Sclater, and L. Meinke, Mesozoic and Cenozoic reconstructions of the South Atlantic, *Tectonophysics*, *114*, 233-254, 1985.

LePichon, X., and D. E. Hayes, Marginal offsets, fracture zones, and the early opening of the South Atlantic, *J Geophys Res*, *76*, 6283-6292, 1971.

Liu, C., S., J. R. Curray, and J. M. McDonald, New constraints on the tectonic evolution of the eastern Indian Ocean, *Earth Planet Sci Lett*, *65*, 331-342, 1983.

Lonsdale, P., and K. D. Klitgord, Structure and tectonic history of the eastern Panama basin, *Geol Soc Am Bull*, *89*, 981-999, 1978.

Lourden, K., E., Magnetic anomalies in the West Philippine Basin, *in The Geophysics of the Pacific Ocean Basin and its margin - geophysical monograph 19*, edited by G. H. Sutton, M. H. Manghnani, R. Moberly, and E. U. McAfee, pp. 253-267, American Geophys. Union, Washington, 1976.

Malahoff, A., and D. W. Handschumacher, Magnetic anomalies south of the Murray Fracture Zone: new evidence for a secondary sea- floor spreading center and strike-slip movement, *J Geophys Res*, *76*, 6265-6275, 1971.

Mammerickx, J., R. N. Anderson, H. W. Menard, and S. M. Smith, Morphology and tectonic evolution of the East-Central Pacific, *Geol Soc Am Bull*, *86*, 111-118, 1975.

Mammerickx, J., and G. F. Sharman, Tectonic evolution of the North Pacific during the Cretaceous quiet period, *J Geophys Res*, *93*, 3009-3024, 1988.

Markl, R., G., Evidence for the breakup of eastern Gondwanaland by the early Cretaceous, *Nature*, *251*, 196-200, 1974.

Martin, A., K., S. W. Goodlad, C. J. H. Hartnady, and A. duPlessis, Cretaceous palaeopositions of the Falkland Plateau relative to southern Africa using Mesozoic seafloor spreading anomalies, *Geophys J R Astron Soc*, *71*, 567-579, 1982.

Martin, A., K., and C. J. H. Hartnady, Plate tectonic development of the South West Indian Ocean: a revised reconstruction of East Antarctica and Africa, *J Geophys Res*, *91*, 4767-4786, 1986.

Martin, A., K., C. J. H. Hartnady, and S. W. Goodlad, A revised fit of South America and South Central Africa, *Earth Planet Sci Lett*, *54*, 293-305, 1981.

Mason, R., G., and A. D. Raff, Magnetic survey off the west coast of North America, 32 N latitude to 42 N latitude, *Geol Soc Am Bull*, *72*, 1259-1265, 1961.

Masson, D., G., Evolution of the Mascarene Basin, western Indian Ocean, and the significance of the Amirante Arc, *Marine Geophys. Researches*, *6*, 365-382, 1984.

McKenzie, D., Some remarks on the development of sedimentary basins, *Earth Planet Sci Lett*, *40*, 25-32, 1978.

McKenzie, D., The evolution of propagating rifts, *Nature*, *300*, 740-741, 1982.

McKenzie, D., and W. J. Morgan, Evolution of triple junctions, *Nature*, *224*, 125-133, 1969.

McKenzie, D., and R. L. Parker, Plate tectonics in w space, *Earth Planet Sci Lett*, *22*, 285-293, 1974.

McKenzie, D., and J. G. Sclater, The evolution of the Indian Ocean since the Late Cretaceous, *Geophys J R Astron Soc*, *24*, 437-528, 1971.

McKenzie, D., P., Some remarks on heat flow and gravity anomalies, *J Geophys Res*, *72*, 6261-6273, 1967.

McKenzie, D., P., D. Davies, and P. Molnar, Plate tectonics of the Red Sea and East Africa, *Nature*, *226*, 243-248, 1970.

McNutt, M., K., Nonuniform magnetization of seamounts: a least squares approach, *J Geophys Res*, *91*, 3686-3700, 1986.

McNutt, M., K., and R. Batiza, Paleomagnetism of northern Cocos seamounts: constraints on absolute plate motions, *Geology*, *9*, 148-154, 1981.

McNutt, M., K., and H. W. Menard, Constraints on yield strength in the oceanic lithosphere derived from observations of flexure, *Geophys J R Astron Soc*, *71*, 363-394, 1982.

Menard, H., W., Elevation and subsidence of oceanic crust, *Earth Planet Sci Lett*, *6*, 275-284, 1969.

Menard, H., W., Fragmentation of the Farallon plate by pivoting subduction, *Journal of Geology*, *86*, 99-110, 1978.

Menard, H., W., and T. Atwater, Changes in direction of sea floor spreading, *Nature*, *219*, 463-467, 1968.

Menard, H., W., and T. Atwater, Origin of fracture zone topography, *Nature*, *222*, 1037-1040, 1969.

Meybeck, M., Global chemical weathering of surfical rocks estimated from river dissolved loads, em Am Jour of Sci, em 287, 401-426, 1987.

Miller, K., G., R. G. Fairbanks, and G. S. Mountain, Tertiary oxygen isotope synthesis, sea level history, and continental margin erosion, *Paleoceanography*, *2*, 1-19, 1987.

Minster, J., B., and T. H. Jordan, Present-day plate motions, *J Geophys Res*, *83*, 5331-5354, 1978.

Minster, J., B., T. H. Jordan, P. Molnar, and E. Haines, Numerical modelling of instantaneous plate tectonics, *Geophys J R Astron Soc*, *36*, 541-576, 1974.

Molnar, P., Fault plane solutions of earthquakes and direction of motion in the Gulf of California and on the Rivera Fracture Zone, *Geol Soc Am Bull*, *84*, 1651-1658, 1973.

Molnar, P., Continental tectonics in the aftermath of plate tectonics, *Nature*, *335*, 131-137, 1988.

Molnar, P., and T. Atwater, Relative motion of hot spots in the mantle, *Nature*, *246*, 288-291, 1973.

Molnar, P., and T. Atwater, Interarc spreading and cordilleran tectonics as alternates related to the age of subducted oceanic lithosphere, *Earth Planet Sci Lett*, *41*, 330-340, 1978.

Molnar, P., T. Atwater, J. Mammerickx, and S. M. Smith, Magnetic anomalies, bathymetry and the tectonic evolution of the South Pacific since the Late Cretaceous, *Geophys J R Astron Soc*, *40*, 383-420, 1975.

Molnar, P., and W. Chen, Evidence of large Cainozoic crustal shortening of Asia, *Nature*, *273*, 218-220, 1978.

Molnar, P., W. P. Chen, and P. Tapponier, Constraints of the amount of north-south shortening in Tibet during the Cenozoic, *in Symposium on Qinghai-Zizang (Tibet) Plateau*, edited by, pp. 757-761, Acad. Sinica, Peking, 1980.

Molnar, P., and D. Gray, Subduction of continental lithosphere: some constraints and uncertainties, *Geology*, *7*, 58-62, 1979.

Molnar, P., and H. Lyon-Caen, Some simple physical aspects of the support, structure, and evolution of mountain belts, *in Processes in continental lithospheric deformation - Special paper 218*, edited by S. P. Clark Jr, C. Burchfiel, and J. Suppe, pp. 179-207, Geological Soc. of America, 1988.

Molnar, P., F. Pardo-Casas, and J. Stock, The Cenozoic and Late Cretaceous evolution of the Indian Ocean Basin: uncertainties in the reconstructed positions of the Indian, African and Antarctic plates, *Basin Research*, *1*, 23-40, 1988.

Molnar, P., and J. M. Stock, A method for bounding uncertainties in combined plate reconstructions, *J Geophys Res*, *90*, 12537- 12544, 1985.

Molnar, P., and L. R. Sykes, Plate tectonics in the Hispaniola area: discussion, *Geol Soc Am Bull*, *82*, 1123-1126, 1971.

Molnar, P., and P. Tapponnier, A possible dependence of tectonic strength on the age of the crust in Asia, *Earth Planet Sci Lett*, *52*, 107-114, 1981.

Moore Jr, T., C., T. S. Loutit, and S. M. Greenlee, Estimating short-term changes in eustatic sea level, *Paleoceanography*, *2*, 625-637, 1987.

Norton, I., O., and J. G. Sclater, A model for the evolution of the Indian Ocean and the breakup of Gondwanaland, *J Geophys Res*, *84*, 6803-6830, 1979.

Oldenburg, D., W., and J. N. Brune, An explanation for the orthogonality of ocean ridges and transform faults, *J Geophys Res*, *80*, 2575-2585, 1975.

Oliver, P., J., Report on workshop on plate reconstructions of the New Zealand region - report G122, Department of Sci. and Indust. Res, p. New Zeal. Geol. Survey, Lower Hutt, 1987.

Orcutt, J., A., Introduction and tribute to H. W. Menard 1920- 1986, *J Geophys Res*, *93*, 2771-2774, 1988.

Pardo-Casas, F., and P. Molnar, Relative motion of the Nazca (Farallon) and South American plates since late Cretaceous time, *Tectonics*, *6*, 233-248, 1987.

Parker, R., L., and D. W. Oldenburg, Thermal model of ocean ridges, *Nature*, *242*, 137-139, 1973.

Parsons, B., The rates of plate creation and consumption, *Geophys J R Astron Soc*, *67*, 437-448, 1981.

Parsons, B., Causes and consequences of the relation between area and age of the ocean floor, *J Geophys Res*, *87*, 289-302, 1982.

Parsons, B., and D. McKenzie, Mantle convection and the thermal structure of the plates, *J Geophys Res*, *83*, 4485-4496, 1978.

Parsons, B., and P. Molnar, The origin of outer topographic rises associated with trenches, *Geophys J R Astron Soc*, *45*, 707-712, 1976.

Parsons, B., and F. M. Richter, A relation between the driving force and geoid anomaly associated with mid-ocean ridges, *Earth Planet Sci Lett*, *51*, 445-450, 1980.

Parsons, B., and J. G. Sclater, An analysis of the variation of ocean floor bathymetry and heat flow with age, *J Geophys Res*, *82*, 803-827, 1977.

Patriat, P., J. Segoufin, J. Goslin, and P. Beuzart, Relative positions of Africa and Antarctica in the Upper Cretaceous: evidence for non-stationary behaviour of fracture zones, *Earth Planet Sci Lett*, *75*, 204-214, 1985.

Peter, G., Magnetic anomalies and fracture pattern in the northeast Pacific Ocean, *J Geophys Res*, *71*, 5365-5374, 1966.

Peter, G., B. H. Erickson, and P. J. Grim, Magnetic structure of the Aleutian Trench and northeast Pacific Basin, in *The Sea*, edited by A. E. Maxwell, pp. 191-222, Wiley-Interscience, New York, 1970.

Pitman III, W., C., Relationship between eustacy and stratigraphic sequences of passive margins, *Geol Soc Am Bull*, *89*, 1389-1403, 1978.

Pitman III, W., C., and D. E. Hayes, Sea-floor spreading in the Gulf of Alaska, *J Geophys Res*, *73*, 6571-6580, 1968.

Pitman III, W., C., E. M. Herron, and J. R. Heirtzler, Magnetic anomalies in the Pacific and seafloor spreading, *J Geophys Res*, *73*, 2069-2085, 1968.

Pitman III, W., C., and M. A. Kominz, New eustatic sea level curve from oceanographic data, *AAPG Bulletin*, *65*, 973, 1981.

Pitman III, W., C., and M. Talwani, Sea-floor spreading in the North Atlantic, *Geol Soc Am Bull*, *83*, 619-646, 1972.

Rabinowitz, P., D., M. F. Coffin, and D. Falvey, The separation of Madagascar and Africa, *Science*, *220*, 67-69, 1983.

Rabinowitz, P., D., and J. LaBrecque, The Mesozoic South Atlantic Ocean and evolution of its continental margins, *J Geophys Res*, *84*, 5973-6002, 1979.

Raff, A., D., Boundaries of an area of very long magnetic anomalies in the northeast Pacific, *J Geophys Res*, *71*, 2631- 2636, 1966.

Raff, A., D., and R. G. Mason, Magnetic survey off the west coast of North America, 40N latitude to 52N latitude, *Geol Soc Am Bull*, *72*, 1267-1270, 1961.

Rampino, M., R., Geomagnetism, sea level and tectonics, *Physics Today*, *41*, 120-122, 1988.

Reches, Z., and G. Schubert, Models of post-Miocene deformation of the Arabian Plate, *Tectonics*, *6*, 707-725, 1987.

Renkin, M., L., and J. G. Sclater, Depth and age in the North Pacific, *J Geophys Res*, *93*, 2919-2935, 1988.

Rosa, J., W., C., Uncertainties in reconstructions of the Pacific, Farallon, Vancouver and Kula plates and constraints on the rigidity of the Pacific and Farallon (and Vancouver) plates between 73 and 35 m.y. ago, *Eos Trans AGU*, *67*, 1108, 1986.

Rosa, J., W., C., and P. Molnar, Uncertainties in reconstructions of the Pacific, Farallon, Vancouver, and Kula plates and constraints on the rigidity of

the Pacific and Farallon (and Vancouver) plates between 72 and 35 Ma, *Eos Trans AGU, 68*, 175, 1987.

Rosa, J., W., C., and P. Molnar, Uncertainties in reconstructions of the Pacific, Farallon, Vancouver, and Kula plates and constraints on the rigidity of the Pacific and Farallon (and Vancouver) plates between 72 and 35 Ma, *J Geophys Res, 93*, 2997- 3008, 1988.

Rosencrantz, E., M. I. Ross, and J. G. Sclater, Age and spreading history of the Cayman Trough as determined from depth, heat flow, and magnetic anomalies, *J Geophys Res, 93*, 2141-2157, 1988.

Royer, J., and D. T. Sandwell, Evolution of the Eastern Indian Ocean since the Late Cretaceous: constraints from GEOSAT altimetry, submitted to *J. Geophys. Res.*, 1988.

Royer, J., and R. Schlich, Southeast Indian Ridge between the Rodriguez Triple Junction and the Amsterdam and Saint-Paul Islands: Detailed kinematics for the past 20 m.y., *J Geophys Res, 93*, 13524-13550, 1988.

Rubey, W., W., Geologic history of sea water, *Bull. Geol. Soc. Am., 62*, 1111-1148, 1961.

Sahagian, D., Epeirogenic motions of Africa as inferred from Cretaceous shoreline deposits, *Tectonics, 7*, 125-138, 1988.

Sandwell, D., T., and D. C. McAdoo, Marine gravity of the Southern Ocean and Antarctic margin from Geosat, *J Geophys Res, 93*, 10389-10396, 1988.

Sandwell, D., T., and G. Schubert, Geoid height-age relation from SEASAT altimeter profiles across the Mendocino Fracture Zone, *J Geophys Res, 87*, 3949-3958, 1982.

Schlanger, S., O., H. C. Jenkyns, and I. Premoli-Silva, Volcanism and vertical tectonics in the Pacific basin related to global cretaceous transgressions, *Earth Planet Sci Lett, 52*, 435-449, 1981.

Schlich, R., Sea floor spreading history and deep-sea drilling results in the Madagascar and Mascarene Basins, western Indian Ocean, in *Initial reports of the deep sea drilling project - Volume XXV*, edited by T. L. Vallier, and S. M. White, pp. 663- 678, National Science Foundation, Washington, 1974.

Schneider, J., F., and I. S. Sacks, Stress in the contorted Nazca plate beneath southern Peru from local earthquakes, *J Geophys Res, 92*, 13887-13902, 1987.

Schouten, H., and S. C. Cande, Paleomagnetic poles from marine magnetic anomalies, *Geophys J R Astron Soc, 44*, 567-575, 1976.

Schubert, G., and A. P. S. Reymer, Continental volume and freeboard through geological time, *Nature*, em 316, 336-339, 1985.

Schubert, G., C. Froidevaux, and D. A. Yuen, Oceanic lithosphere and asthenosphere: thermal and mechanical structure, *J Geophys Res*, *81*, 3525-3540, 1976.

Sclater, J., G., R. N. Anderson, and M. L. Bell, Elevation of ridges and evolution of the central eastern Pacific, *J Geophys Res*, *76*, 7888-7915, 1971.

Sclater, J., G., C. Bowin, R. Hey, H. Hoskins, J. Peirce, J. Phillips, and C. Tapscott, The Bouvet triple junction, *J Geophys Res*, *81*, 1857-1869, 1976.

Sclater, J., G., E. Boyle, and J. M. Edmond, A quantitative analysis of some factors affecting carbonate sedimentation in the oceans, in *Deep drilling results in the Atlantic Ocean; continental margins and paleoenvironment - Proc. Symp. n.3*, edited by M. Talwani, W. Hay, and W. B. F. Ryan, pp. 235-248, American Geophys. Union, 1979.

Sclater, J., G., and R. L. Fisher, Evolution of the East Central Indian Ocean with emphasis on the tectonic setting of the Ninetyeast Ridge, *Geol Soc Am Bull*, *85*, 683-702, 1974.

Sclater, J., G., R. L. Fisher, P. Patriat, C. Tapscott, and B. Parsons, Eocene to recent development of the South-west Indian Ridge, a consequence of the evolution of the Indian Ocean Triple Junction, *Geophys J R Astron Soc*, *64*, 587-604, 1981.

Sclater, J., G., and Francheteau, The implications of terrestrial heat flow observations on current tectonic and geochemical models of the crust and upper mantle of the Earth, *Geophys J R Astron Soc*, *20*, 509-542, 1970.

Sclater, J., G., S. Hellinger, and C. Tapscott, The paleobathymetry of the Atlantic Ocean from the Jurassic to the present, *Journal of Geology*, *85*, 509-552, 1977.

Sclater, J., G., C. Jaupart, and D. Galson, The heat flow through oceanic and continental crust and the heat loss of the Earth, *Rev Geophys Space Phys*, *18*, 269-311, 1980.

Sclater, J., G., B. P. Luyendyk, and L. Meinke, Magnetic lineations in the southern part of the Central Indian Basin, *Geol Soc Am Bull*, *87*, 371-378, 1976.

Sclater, J., G., B. Parsons, and C. Jaupart, Oceans and continents: Similarities and differences in the mechanisms of heat loss, *J Geophys Res*, *86*, 11535-11552, 1981.

Sclater, J., G., and C. Tapscott, The history of the Atlantic, *Sci. American, 240*, 156-174, 1979.

Scrutton, R., A., Davie Fracture Zone and the movement of Madagascar, *Earth Planet Sci Lett, 39*, 84-88, 1978.

Scrutton, R., A., W. B. Heptonstall, and J. H. Peacock, Constraints on the motion of Madagascar with respect to Africa, *Marine geology, 43*, 1-20, 1981.

Segoufin, J., Anomalies magnetiques mesozoiques dans le bassin de Mozambique, *C. R. Acad. Sc. Paris, t.287*, 109-112, 1978.

Segoufin, J., and P. Patriat, Existence d'anomalies mesozoiques dans le bassin de Somalie. Implications pour les relations Afrique-Antarctique-Madagascar, *C. R. Acad. Sc. Paris, t.291*, 85-88 Serie B, 1980.

Segoufin, J., and P. Patriat, Reconstructions de l'ocean Indien occidental pour les epoques des anomalies M21, M2 et 34. Paleoposition de Madagascar, *Bull. Soc. geol. France, 23*, 603- 607, 1981.

Shaw, P., R., Investigations of relative plate motions in the South Atlantic using Seasat altimeter data, *J Geophys Res, 92*, 9363-9375, 1987.

Sheridan, R., E., Pulsation tectonics as the control of continental breakup, *Tectonophysics, 143*, 59-73, 1987.

Shih, J., and P. Molnar, Analysis and implications of the sequence of ridge jumps that eliminated the Surveyor transform fault, *J Geophys Res, 80*, 4815-4822, 1975.

Simpson, E., S., W., Mesozoic magnetic lineations in the Mozambique Basin, *Earth Planet Sci Lett, 43*, 260-264, 1979.

Smith, A., G., and A. Hallam, The fit of the southern continents, *Nature, 225*, 139-144, 1970.

Solomon, S., C., and R. G. Butler, Prospecting for dead slabs, *Earth Planet Sci Lett, 21*, 421-430, 1974.

Solomon, S., C., N. H. Sleep, and R. M. Richardson, On the forces driving plate tectonics: inferences from absolute plate velocities and intraplate stress, *Geophys J R Astron Soc, 42*, 769-801, 1975.

Sproll, W., P., and R. S. Dietz, Morphological continental drift fit of Australia and Antarctica, *Nature, 222*, 345-348, 1969.

Srivastava, S., P., and C. R. Tapscott, Plate kinematics of the North Atlantic, in *The Geology of North America - The Western North Atlantic region*,

edited by P. R. Vogt, and B. E. Tucholke, pp. 379-404, Geological Soc. of America, 1986.

Stein, C., A., and J. R. Cochran, The transition between the Sheba Ridge and Owen Basin: rifting of old oceanic lithosphere, *Geophys J R Astron Soc*, *81*, 47-74, 1985.

Stein, R., S., A model for the relation between spreading rate and oblique spreading, *Earth Planet Sci Lett*, *39*, 313-318, 1978.

Stein, R., S., Plate tectonic prediction fulfilled, *Physics Today*, *41*, 42-44, 1988.

Stock, J., and P. Molnar, Uncertainties in the relative positions of the Australia, Antarctica, Lord Howe, and Pacific plates since the Late Cretaceous, *J Geophys Res*, *87*, 4697-4714, 1982.

Stock, J., and P. Molnar, Some geometrical aspects of uncertainties in combined plate reconstructions, *Geology*, *11*, 697-701, 1983.

Stock, J., and P. Molnar, Revised history of early Tertiary plate motion in the south-west Pacific, *Nature*, *325*, 495-499, 1987.

Stock, J., and P. Molnar, Uncertainties and implications of the late Cretaceous and Tertiary position of North America relative to the Farallon, Kula, and Pacific Plates, *Tectonics*, *7*, 1339- 1384, 1988.

Suarez, G., and P. Molnar, Paleomagnetic data and pelagic sediment facies and the motion of the Pacific plate relative to the spin axis since the Late Cretaceous, *J Geophys Res*, *85*, 5257-5280, 1980.

Suarez, G., P. Molnar, and B. C. Burchfiel, Seismicity, fault plane solutions, depth of faulting, and active tectonics of the Andes of Peru, Ecuador, and southern Colombia, *J Geophys Res*, *88*, 10403-10428, 1983.

Talwani, M., and O. Eldholm, Evolution of the Norwegian-Greenland Sea, *Geol Soc Am Bull*, *88*, 969-999, 1977.

Tamaki, K., and R. Larson, The mesozoic tectonic history of the Magellan Microplate in the western central Pacific, *J Geophys Res*, *93*, 2857-2874, 1988.

Tapponnier, P., and P. Molnar, Slip-line field theory and large- scale continental tectonics, *Nature*, *264*, 319-324, 1976.

Tapscott, C., R., P. Patriat, R. L. Fisher, J. G. Sclater, H. Hoskins, and B. Parsons, The Indian Ocean Triple Junction, *J Geophys Res*, *85*, 4723-4739, 1980.

Tardy Y., R. N'kounkou, and J. L. Probst, The global water cycle and continental erosion during Phanerozoic time (570 my), em Am Jour of Sci., em 289, 455-483, 1989.

Thorne, J., and A. B. Watts, Seismic reflectors and unconformities at passive continental margins, *Nature*, *311*, 365- 370, 1984.

Trehu, A., J. G. Sclater, and J. Nabelek, The depth and thickness of the ocean crust and its dependence upon age, *Bull. Soc. geol. France*, *18*, 917-930, 1976.

Turcotte, D., L., Flexure, *Advances in Geophysics*, *21*, 51-86, 1979.

Turcotte, D., L., and K. Burke, Global sea-level changes and the thermal structure of the Earth, *Earth Planet Sci Lett*, *41*, 341- 346, 1978.

Turcotte, D., L., and E. R. Oxburgh, Finite amplitude convective cells and continental drift, *J. Fluid Mech.*, *28*, 29-42, 1967.

Uruski, C., I., and L. M. Parson, A compilation of geophysical data on the East Greenland continental margin and its use in gravity modelling across the continent-ocean transition, *Institute of Oceanographic Sciences, Report, 214*, 1-53, 1985

Vacquier, V., Transcurrent faulting in the ocean floor, *Phil. Trans. R. Soc., A258*, 77-81, 1965.

Vacquier, V., A. D. Raff, and R. E. Warren, Horizontal displacements in the floor of the northeastern Pacific Ocean, *Geol Soc Am Bull*, *72*, 1251-1258, 1961.

Vail, P., R., Sequence stratigraphy - Yes; global sealevel link - No, *Lamont newsletter*, *17*, 5, 1988.

Vail, P., R., J. Hardenbol, and R. G. Todd, Jurassic unconformities, chronostratigraphy, and sea-level changes from seismic stratigraphy and biostratigraphy, in *Interregional unconformities and hydrocarbon accumulation*, edited by J. S. Schlee, AAPG, 1984.

Vink, G., E., Continental rifting and the implications for plate tectonic reconstructions, *J Geophys Res*, *87*, 10677-10688, 1982.

Vogt, P., R., The present plate boundary configuration, in *The geology of North America - The Western North Atlantic region*, edited by P. R. Vogt, and B. E. Tucholke, pp. 189-204, Geological Soc. of America, 1986a.

Vogt, P., R., Plate kinematics during the last 20 m.y. and the problem of "present" motions, in *The geology of North America - The Western North*

Atlantic region, edited by P. R. Vogt, and B. E. Tucholke, pp. 405-425, Geological Soc. of America, 1986b.

Vogt, P., R., C. N. Anderson, and D. R. Bracey, Mesozoic magnetic anomalies, sea-floor spreading, and geomagnetic reversals in the Southwestern North Atlantic, *J Geophys Res*, *76*, 4796-4823, 1971.

Vogt, P., R., and O. E. Avery, Detailed magnetic surveys in the Northeast Atlantic and Labrador Sea, *J Geophys Res*, *79*, 363-389, 1974.

Vogt, P., R., G. L. Johnson, and L. Kristjansson, Morphology and magnetic anomalies north of Iceland, *J Geophys*, *47*, 67-80, 1980.

Vogt, P., R., L. C. Kovacs, C. Bernero, and S. P. Srivastava, Asymmetric geophysical signatures in the Greenland-Norwegian and Sothern Labrador seas and the Eurasia basin, *Tectonophysics*, *89*, 95-160, 1982.

Vogt, P., R., and R. K. Perry, North Atlantic Ocean: bathymetry and plate tectonic evolution, *Geological Soc. of America Map and Chart Ser.*, MC, 21 p., 1982.

Vogt, P., R., R. K. Perry, R. H. Feden, H. S. Fleming, and N. Z. Cherkis, The Greenland-Norwegian Sea and Iceland environment: geology and geophysics, in *The Arctic Ocean, from the collection: The ocean basins and margins*, edited by A. E. M. Nairn, M. Churkin Jr, and F. G. Stehli, pp. 493-598, Prenum Press, New York, 1981.

Vogt, P., R., P. T. Taylor, L. C. Kovacs, and G. L. Johnson, The Canada basin: aeromagnetic constraints on structure and evolution, *Tectonophysics*, *89*, 295-336, 1982.

Von Herzen, R., P., R. S. Detrick, S. T. Crough, D. Epp, and U. Fehn, Thermal origin of the Hawaiian Swell: heat flow evidence and thermal models, *J Geophys Res*, *87*, 6711-6723, 1982.

Watts, A., B., Tectonic subsidence, flexure and global changes of sea level, *Nature*, *297*, 1-6, 1982.

Watts, A., B., J. H. Bodine, and N. M. Ribe, Observations of flexure and the geological evolution of the Pacific Ocean basin, *Nature*, *283*, 532-537, 1980.

Watts, A., B., J. R. Cochran, P. Patriat, and M. Doucoure, A bathymetry and altimetry profile across the Southwest Indian Ridge crest at 31S latitude, *Earth Planet Sci Lett*, *73*, 129-139, 1985.

Watts, A., B., J. R. Cochran, and G. Selzer, Gravity anomalies and flexure of the lithosphere: a three-dimensional study of the Great Meteor Seamount, northeast Atlantic, *J Geophys Res*, *80*, 1391-1398, 1975.

Watts, A., B., and M. S. Steckler, Subsidence and eustasy at the continental margin of eastern North America, in *Deep drilling results in the Atlantic Ocean; continental margins and paleoenvironment - Maurice Ewing Ser.*, Proc. Symp., n.3, edited by M. Talwani, W. Hay, and W. B. F. Ryan, pp. 218-234, American Geophys. Union, 1979.

Weissel, J., K., and R. N. Anderson, Is there a Caroline Plate?, *Earth Planet Sci Lett*, *41*, 143-158, 1978.

Weissel, J., K., and D. E. Hayes, Magnetic anomalies in the southeast Indian Ocean, in *Antarctic Oceanology II: The Australian-New Zealand Sector, Antarctic Res. Ser.*, edited by D. E. Hayes, pp. 165-196, American Geophys. Union, Washington, 1972.

Weissel, J., K., D. E. Hayes, and E. M. Herron, Plate tectonics synthesis: the displacements between Australia, New Zealand, and Antarctica since the late Cretaceous, *Marine Geology*, *25*, 231-277, 1977.

Weissel, J., K., and A. B. Watts, Tectonic evolution of the Coral Sea Basin, *J Geophys Res*, *84*, 4572-4582, 1979.

Wilson, D., S., A kinematic model for the Gorda Deformation Zone as a diffuse southern boundary of the Juan de Fuca Plate, *J Geophys Res*, *91*, 10259-10269, 1986.

Wilson, D., S., Tectonic history of the Juan de Fuca Ridge over the last 40 million years, *J Geophys Res*, *93*, 11863-11876, 1988.

Wilson, D., S., R. N. Hey, and C. Nishimura, Propagation as a mechanism of reorientation of the Juan de Fuca Ridge, *J Geophys Res*, *89*, 9215-9225, 1984.

Wise, D., u., Continental margins, freeboard and the volumes of continents and oceans through time, in em The Geology of Continental Margins., edited by C. A. Burke and C. L. Drake, pp. 45-58, Springer-Verlag, New York, 1974.

Woods, M., T., and G. F. Davies, Late Cretaceous genesis of the Kula plate, *Earth Planet Sci Lett*, *58*, 161-166, 1982.

Worsley, T., R., D. Nance, and J. B. Moody, Global tectonics and eustasy for the past 2 billion years, em Marine Geo., em 58, 378-400, 1984.

Appendix A
Chapter 2 Tables

TABLE 2.1. Ages for the Magnetic Anomalies

Magnetic Anomaly	Age, Ma: Used in This Study*	Age, Ma: Used in *Engebretson et al.* [1984]‡
13	35.58	37.06
18	42.26	42.49
21	49.54	48.08
25	58.94	55.97
30–31	68.47	66.93
32	71.51†	69.60

*Source of ages is *Berggren et al.* [1985] unless otherwise indicated.

†Source of age is *Kent and Gradstein* [1985].

‡Source of ages is *Harland et al.* [1982].

TABLE 2.2. Poles of Rotations for Pacific-Farallon Magnetic Anomalies South of the Pioneer Fracture Zone and for Pacific-Farallon Magnetic Anomalies Older than Anomaly 25 North of the Pioneer Fracture Zone

		Pole		
Rotated Anomaly	Fixed Anomaly	Lat*	Long*	Angle, deg
13	18	80.71	101.84	-4.10
13	21	82.06	119.39	-8.39
13	25	75.91	81.36	-12.43
13	30–31	74.52	81.28	-16.10
13	32	74.32	80.77	-17.30
18	21	82.26	140.00	-4.30
18	25	73.36	74.85	-8.37
18	30–31	72.34	76.60	-12.05
18	32	72.29	76.35	-13.25
21	25	59.77	59.09	-4.36
21	30–31	64.86	66.00	-8.00
21	32	65.81	66.61	-9.19
25	30–31	69.87	79.17	-3.69
25	32	70.37	77.89	-4.89
30–31	32	71.89	73.76	-1.20

* North and east are positive. Rotation angles are positive counterclockwise. Lat, latitude; Long, longitude.

TABLE 2.3. Poles of Rotations for Pacific-Vancouver Magnetic Anomalies Younger than Anomaly 21 North of the Pioneer Fracture Zone

Rotated Anomaly	Fixed Anomaly	Pole Lat*	Pole Long*	Angle, deg
13	18	78.00	140.00	-5.55
13	21	76.70	139.40	-11.12
18	21	75.40	139.40	-5.57

* North and east are positive. Rotation angles are positive counterclockwise. Lat, latitude; Long, longitude.

TABLE 2.4. Poles of Rotations for Pacific-Kula Magnetic Anomalies

Rotated Anomaly	Fixed Anomaly	Pole Lat*	Pole Long*	Angle, deg
25	30–31	27.50	126.25	-3.10
25	32	27.50	126.25	-4.60
30–31	32	27.50	126.25	-1.50

* North and east are positive. Rotation angles are positive counterclockwise. Lat, latitude; Long, longitude.

TABLE 2.5. Partial Uncertainty Rotations for Reconstructions in Table 2.2

Rotation	Northern Center (or Skewed Misfits)	Southern Center (or Offset Magnetic Anomalies)	Mismatched Fracture Zones
13–18	33.46°N	55.24°S	8.33°N
	131.55°W	113.81°W	36.00°W
	±0.360°	±0.180°	±0.180°
18–21	33.50°N	55.08°S	8.74°N
	135.62°W	117.06°W	39.78°W
	±0.360°	±0.180°	±0.180°
21–25	33.75°N	53.78°S	11.60°N
	141.00°W	116.83°W	43.11°W
	±0.360°	±0.180°	±0.180°
25–30	33.78°N	53.75°S	11.60°N
	145.23°W	121.08°W	47.34°W
	±0.360°	±0.180°	±0.180°
30–32*	41.42°N	45.15°S	14.13°N
	154.01°W	126.52°W	51.18°W
	±1.21°	±0.180°	±0.180°

Method used to calculate uncertainties is that developed by *Stock and Molnar* [1983] and modified slightly by *Molnar and Stock* [1985] (Figure 2.2a).

*Variation of the method outlined by *Stock and Molnar* [1983] (Figure 2.2b).

TABLE 2.6. Partial Uncertainty Rotations for Reconstructions in Table 2.3

Rotation	Skewed Misfit	Mismatched Magnetic Anomalies	Mismatched Fracture Zones
13–18	48.99°N	40.99°S	0.98°N
	148.31°W	146.32°W	57.17°W
	±1.31°	±0.180°	±0.180°
18–21	48.13°N	41.86°S	1.00°N
	143.93°W	141.92°W	52.81°W
	±1.60°	±0.180°	±0.180°

Method used to calculate uncertainties is that developed by *Stock and Molnar* [1983] and modified slightly by *Molnar and Stock* [1985] (Figure 2.2a).

TABLE 2.7. Partial Uncertainty Rotations for Reconstructions in Table 2.4

Rotation	Skewed Misfit	Mismatched Magnetic Anomalies	Mismatched Fracture Zones
25–30	48.66°N	00.00°	41.34°N
	171.25°W	81.25°W	8.75°E
	±1.750°	±0.180°	±0.180°
30–32	47.26°N	00.00°	42.74°N
	169.50°W	79.50°W	10.49°E
	±2.73°	±0.360°	±0.250°

Method used to calculate uncertainties is that developed by *Stock and Molnar* [1983] and modified slightly by *Molnar and Stock* [1985] (Figure 2.2a).

Appendix B

Chapter 3 Tables

TABLE 3.1. Poles of Rotation for Aluk-West Antarctic (/Bellingshausen) and for reconstructions of anomalies on the West Antarctica (/Bellingshausen) plate formed by Aluk-West Antarctica (/Bellingshausen) spreading

Rotation	Pole			Comments
	Lat*	Long*	Angle, deg	
04†	-31.00	-43.50	-2.20	total angle
05†	-31.00	-41.50	-4.90	total angle
05–06†	-31.00	-48.50	-6.30	
06–07†	-29.00	-44.00	-2.00	
07–10†	-25.00	-44.00	-1.10	
10–13†	-25.00	-44.00	-1.00	
13–18†	-25.00	-44.00	-1.60	
13–18‡	-25.00	-50.00	-1.10	
18–20†	-25.00	-44.00	-1.70	
18–20‡	-25.00	-50.00	-0.60	
22–23‡	-25.00	-50.00	-0.60	
23–24‡	-62.45	-77.17	-10.55	
24–25‡	-58.38	-73.50	-11.15	
25–26‡	-62.13	-81.07	-10.02	
26–27‡	-64.81	-93.24	31.74	
27–28‡	-25.00	-60.00	-1.10	
28–29‡	-25.00	-55.00	-1.10	

* North and east are positive. Rotation angles are positive counterclockwise. Lat, latitude; Long, longitude.

† Parameters calculated using data north of fracture zone 'G'.

‡ Parameters calculated using data south of fracture zone 'G'.

TABLE 3.3. Poles of Rotations for anomalies originally on the Antarctic (/Bellingshausen) plate formed by Antarctic (/Bellingshausen)-Farallon spreading

Rotation	Pole		
	Lat*	Long*	Angle, deg
10–13	-50.00	-20.00	1.90
13–18	-50.00	-20.00	2.20
12–18	-50.00	-20.00	2.40
18–19	-50.00	-20.00	1.10
19–20	-50.00	-20.00	0.80

* North and east are positive. Rotation angles are positive counterclockwise. Lat, latitude; Long, longitude.

TABLE 3.4. Poles of Rotation for reconstructions of anomalies originally on the Pacific plate formed by Pacific-Aluk spreading for the area northwest of the Palmer Peninsula (See Figure 3.2, Figure 1 of *Cande et al.* [1982]).

Rotation	Pole		
	Lat*	Long*	Angle, deg
21–22	70.00	112.00	3.00
22–23	70.00	112.00	2.70
23–24	70.00	112.00	3.40
24–25	70.00	112.00	8.60
25–26	70.00	112.00	6.40
26–27	70.00	112.00	9.30

* North and east are positive. Rotation angles are positive counterclockwise. Lat, latitude; Long, longitude.

TABLE 3.5. Poles of Rotation for reconstructions of anomalies originally on the Pacific plate formed by Pacific-Aluk spreading for the area northeast of New Zealand (See Figure 3 of *Cande et al.* [1982]).

Rotation	Pole		
	Lat*	Long*	Angle, deg
29–30†	-70.00	-112.00	9.50
30–31†	-70.00	-112.00	6.20
31–32†	-55.00	100.00	3.40
32–33†	-55.00	100.00	4.60
33–34†	-45.00	80.00	3.60

* North and east are positive. Rotation angles are positive counterclockwise. Lat, latitude; Long, longitude.

†All these rotations follow two other rotations in the following order: $-76.00, 151.00, -39.70$ and $-54.90, -95.10, 30.00$.

TABLE 3.6. Poles of Rotation for Nazca-Antarctica

Rotation	Pole		
	Lat*	Long*	Angle, deg
05	-34.62	87.20	7.54
06	-51.06	81.43	15.40
13	-52.64	61.73	23.61

* North and east are positive. Rotation angles are positive counterclockwise. Lat, latitude; Long, longitude.

TABLE 3.7. Partial Uncertainty Rotations for Aluk-West Antarctic (/Bellingshausen) and for reconstructions of anomalies on the West Antarctic (/Bellingshausen) plate formed by Aluk-West Antarctic (/Bellingshausen) spreading

	End Points of Plate Boundaries and Azimuth of Transform Faults					Skewed Fit				Mismatched Fracture Zones				Mismatched Magnetic Anomalies			
Rotation	Lat*	Long*	Lat*	Long*	Azimuth	Lat*	Long*	Angle, deg	Angle,† km	Lat*	Long*	Angle, deg	Angle, km	Lat*	Long*	Angle, deg	Angle, km
04**	-58.44	-64.46	-60.61	-64.53	126	-59.52	-64.49	9.48	1056 (20)	-17.34	57.56	0.18	20	-24.22	155.64	0.18	20
05**	-60.10	-63.79	-61.57	-64.03	130	-60.83	-63.91	14.00	1559 (20)	-18.25	62.32	0.18	20	-21.92	159.95	0.18	20
05-06**																	
06-07**	-62.37	-69.42	-64.93	-74.39	129	-63.67	-71.79	6.09	678 (20)	-16.21	54.18	0.18	20	-20.16	150.30	0.18	20
07-10**	-62.35	-71.53	-64.59	-76.01	129	-63.49	-73.68	6.86	764 (20)	-16.31	52.25	0.18	20	-20.30	148.46	0.18	20
10-13**	-61.85	-72.30	-63.71	-76.67	129	-62.80	-74.42	7.54	840 (20)	-16.72	51.35	0.18	20	-20.81	147.90	0.18	20
13-18**																	
13-18***																	
18-20**																	
18-20***																	
22-23***	-64.63	-80.57	-64.83	-80.92	133	-64.73	-80.74	82.29	9167 (20)	-16.93	49.40	0.18	20	-18.19	145.13	0.18	20
23-24***	-64.44	-81.76	-64.60	-82.20	133	-64.52	-81.98	82.29	9167 (20)	-17.06	48.11	0.18	20	-18.34	143.95	0.18	20
24-25***	-63.69	-85.45	-63.83	-86.13	133	-63.76	-85.79	62.34	6945 (20)	-17.55	44.12	0.18	20	-18.87	140.32	0.18	20
25-26***	-63.35	-86.73	-63.53	-88.43	133	-63.44	-87.58	26.38	2938 (20)	-17.75	42.25	0.18	20	-19.09	138.61	0.18	20
26-27***	-62.06	-89.38	-62.76	-90.97	130	-62.41	-90.17	20.17	2247 (20)	-17.32	36.47	0.18	20	-20.78	133.27	0.18	20
27-28***	-61.92	-91.32	-64.58	-95.23	134	-63.26	-93.18	6.45	718 (20)	-18.21	37.59	0.18	20	-18.88	134.05	0.18	20
28-29***	-63.30	-94.30	-63.57	-95.10	131	-63.44	-94.70	45.72	5093 (20)	-17.06	33.17	0.18	20	-19.72	129.48	0.18	20

* North and east are positive. Rotation angles are positive counterclockwise. Lat, latitude; Long, longitude.

** Parameters calculated using data north of fracture zone 'G'.

*** Parameters calculated using data south of fracture zone 'G'.

† Values in parentheses give overlap or underlap in kilometers of endpoints of the plate boundary.

TABLE 3.8. Partial Uncertainty Rotations for reconstructions of anomalies originally on the Antarctic (/Bellingshausen) plate formed by Antarctic (/Bellingshausen)-Farallon spreading

	End Points of Plate Boundaries and Azimuth of Transform Faults					Skewed Fit				Mismatched Fracture Zones				Mismatched Magnetic Anomalies			
Rotation	Lat*	Long*	Lat*	Long*	Azimuth	Lat*	Long*	Angle, deg	Angle,† km	Lat*	Long*	Angle, deg	Angle, km	Lat*	Long*	Angle, deg	Angle, km
10–13	-51.73	-86.18	-57.26	-76.56	22	-54.59	-81.70	2.62	292 (20)	32.49	-55.33	0.18	20	-12.54	26.53	0.18	20
13–18	-50.54	-91.87	-58.82	-74.89	22	-54.97	-84.25	1.61	180 (20)	32.15	-57.99	0.18	20	-12.42	24.05	0.18	20
12–18	-50.54	-91.87	-55.88	-82.81	22	-53.30	-87.62	2.71	302 (20)	33.65	-60.88	0.18	20	-12.94	20.32	0.18	20
18–19	-52.72	-91.33	-59.15	-76.37	22	-56.16	-84.47	1.96	218 (20)	31.09	-58.53	0.18	20	-12.04	24.08	0.18	20
19–20	-54.06	-88.00	-59.19	-79.08	22	-56.70	-83.84	2.90	323 (20)	30.60	-58.05	0.18	20	-11.87	24.82	0.18	20

* North and east are positive. Rotation angles are positive counterclockwise. Lat, latitude; Long, longitude.

TABLE 3.9. Partial Uncertainty Rotations for reconstructions of anomalies originally on the Pacific plate formed by Pacific-Aluk spreading for the area northwest of the Palmer Peninsula (See Figure 3.2, Figure 1 of Cande et al. [1982]).

	End Points of Plate Boundaries and Azimuth of Transform Faults					Skewed Fit				Mismatched Fracture Zones				Mismatched Magnetic Anomalies			
Rotation	Lat*	Long*	Lat*	Long*	Azimuth	Lat*	Long*	Angle, deg	Angle,† km	Lat*	Long*	Angle, deg	Angle, km	Lat*	Long*	Angle, deg	Angle, km
21–22	-59.96	-80.58	-60.98	-81.52	132	-60.47	-81.04	18.37	2046 (20)	-19.26	47.03	0.18	20	-21.49	144.94	0.18	20
22–23	-59.39	-81.93	-60.72	-82.75	132	-60.06	-82.33	14.80	1649 (20)	-19.51	45.63	0.18	20	-21.77	143.77	0.18	20
23–24	-58.87	-83.49	-59.24	-83.61	132	-59.05	-83.55	55.60	6194 (20)	-20.12	44.13	0.18	20	-22.47	142.84	0.18	20
24–25	-57.22	-87.02	-57.95	-87.31	128	-57.58	-87.16	27.43	3056 (20)	-19.27	36.24	0.18	20	-24.99	135.62	0.18	20
25–26	-56.25	-89.78	-56.91	-90.14	124	-56.58	-89.96	29.82	3321 (20)	-17.94	29.42	0.18	20	-27.17	128.98	0.18	20
26–27	-55.26	-94.22	-56.16	-94.36	124	-55.71	-94.29	22.86	2546 (20)	-18.36	24.84	0.18	20	-27.84	124.94	0.18	20

* North and east are positive. Rotation angles are positive counterclockwise. Lat, latitude; Long, longitude.

TABLE 3.10. Partial Uncertainty Rotations for reconstructions of anomalies originally on the Pacific plate formed by Pacific-Aluk spreading for the area northeast of New Zealand (See Figure 3 of Cande et al. [1982]).

	End Points of Plate Boundaries and Azimuth of Transform Faults					Skewed Fit				Mismatched Fracture Zones				Mismatched Magnetic Anomalies			
Rotation	Lat*	Long*	Lat*	Long*	Azimuth	Lat*	Long*	Angle, deg	Angle,† km	Lat*	Long*	Angle, deg	Angle, km	Lat*	Long*	Angle, deg	Angle, km
29–30	-45.44	-144.98	-46.07	-146.76	129	-45.76	-145.86	14.80	1649 (20)	-26.04	-25.74	0.18	20	-32.83	82.64	0.18	20
30–31	-44.48	-145.00	-45.40	-148.04	133	-44.95	-146.51	8.79	979 (20)	-28.86	-23.13	0.18	20	-31.17	86.34	0.18	20
31–32	-41.66	-144.88	-43.58	-151.92	129	-42.67	-148.34	3.73	415 (20)	-27.56	-29.58	0.18	20	-34.85	81.72	0.18	20
32–33	-38.93	-150.01	-40.64	-156.24	127	-39.83	-153.09	4.05	451 (20)	-27.53	-37.32	0.18	20	-37.83	76.55	0.18	20
33–34	-36.11	-150.08	-38.23	-159.56	134	-37.26	-154.75	2.63	292 (20)	-33.56	-34.44	0.18	20	-34.92	83.16	0.18	20

* North and east are positive. Rotation angles are positive counterclockwise. Lat, latitude; Long, longitude.

TABLE 3.11. Partial Uncertainty Poles for Nazca-Antarctica

	End Points of Plate Boundaries and Azimuth of Transform Faults					Skewed Fit				Mismatched Fracture Zones				Mismatched Magnetic Anomalies			
Rotation	Lat*	Long*	Lat*	Long*	Azimuth	Lat*	Long*	Angle, deg	Angle,† km	Lat*	Long*	Angle, deg	Angle, km	Lat*	Long*	Angle, deg	Angle, km
05**	-38.08	-96.96	-47.65	-76.21	76	-43.33	-87.40	2.31	257 (20)	-46.33	83.89	0.18	20	-4.36	178.48	0.18	20
06	-49.29	-78.55	-54.01	-75.31	79	-51.66	-77.01	4.01	447 (20)	6.80	4.32	0.18	20	-37.51	89.07	0.18	20

* North and east are positive. Rotation angles are positive counterclockwise. Lat, latitude; Long, longitude.

** Partial uncertainty rotations calculated using end points of isochrons.

Appendix C
Chapter 4 Tables

TABLE 4.1. Ages of magnetic anomalies

Magnetic Anomaly	Position	Age (Ma)
05	old edge	10.59†
06	center	19.90†
13	center	35.58†
18	center of broad normal epoch	42.01†
21	center	49.55†
25	center	58.94†
30-31	center of reversed pol. bet. 30 and 31	68.47†
34	young edge	84.00‡
M0	center	118.35‡
M4	center	125.91‡
M11	center of first reversal	132.78‡
M16	center	141.52‡
M21	center	149.65‡
M25	center	156.42‡

† *Berggren et al.*[1985]

‡ *Kent and Gradstein*[1985]

TABLE 4.2. Poles of Rotation for Aluk-West Antarctic (/Bellingshausen) and for reconstructions of anomalies on the West Antarctica (/Bellingshausen) plate formed by Aluk-West Antarctica (/Bellingshausen) spreading

Rotation	Pole			Comments
	Lat*	Long*	Angle, deg	
04†	-31.00	-43.50	-2.20	total angle
05†	-31.00	-41.50	-4.90	total angle
05–06†	-31.00	-48.50	-6.30	
06–07†	-29.00	-44.00	-2.00	
07–10†	-25.00	-44.00	-1.10	
10–13†	-25.00	-44.00	-1.00	
13–18†	-25.00	-44.00	-1.60	
13–18‡	-25.00	-50.00	-1.10	
18–20†	-25.00	-44.00	-1.70	
18–20‡	-25.00	-50.00	-0.60	
22–23‡	-25.00	-50.00	-0.60	
23–24‡	-62.45	-77.17	-10.55	
24–25‡	-58.38	-73.50	-11.15	
25–26‡	-62.13	-81.07	-10.02	
26–27‡	-64.81	-93.24	31.74	
27–28‡	-25.00	-60.00	-1.10	
28–29‡	-25.00	-55.00	-1.10	

* North and east are positive. Rotation angles are positive counterclockwise. Lat, latitude; Long, longitude.

† Parameters calculated using data north of fracture zone 'G'.

‡ Parameters calculated using data south of fracture zone 'G'.

TABLE 4.3. Poles of Rotation for anomalies originally on the Pacific plate formed by Pacific-Farallon spreading

Rotation	Pole		
	Lat*	Long*	Angle, deg
21–22	82.28	138.57	-0.90
22–23	82.28	138.57	-0.80
23–24	82.28	138.57	-0.80

* North and east are positive. Rotation angles are positive counterclockwise. Lat, latitude; Long, longitude.

TABLE 4.4. Poles of Rotations for anomalies originally on the Antarctic (/Bellingshausen) plate formed by Antarctic (/Bellingshausen)-Farallon spreading

Rotation	Pole		
	Lat*	Long*	Angle, deg
10–13	-50.00	-20.00	1.90
13–18	-50.00	-20.00	2.20
12–18	-50.00	-20.00	2.40
18–19	-50.00	-20.00	1.10
19–20	-50.00	-20.00	0.80

* North and east are positive. Rotation angles are positive counterclockwise. Lat, latitude; Long, longitude.

TABLE 4.5. Poles of Rotation for reconstructions of anomalies originally on the Pacific plate formed by Pacific-Aluk spreading for the area northwest of the Palmer Peninsula (See Figure 3.2, Figure 1 of *Cande et al.* [1982]).

Rotation	Pole		
	Lat*	Long*	Angle, deg
21–22	70.00	112.00	3.00
22–23	70.00	112.00	2.70
23–24	70.00	112.00	3.40
24–25	70.00	112.00	8.60
25–26	70.00	112.00	6.40
26–27	70.00	112.00	9.30

* North and east are positive. Rotation angles are positive counterclockwise. Lat, latitude; Long, longitude.

TABLE 4.6. Poles of Rotation for reconstructions of anomalies originally on the Pacific plate formed by Pacific-Aluk spreading for the area northeast of New Zealand (See Figure 3 of *Cande et al.* [1982]).

Rotation	Pole		
	Lat*	Long*	Angle, deg
29–30†	-70.00	-112.00	9.50
30–31†	-70.00	-112.00	6.20
31–32†	-55.00	100.00	3.40
32–33†	-55.00	100.00	4.60
33–34†	-45.00	80.00	3.60

* North and east are positive. Rotation angles are positive counterclockwise. Lat, latitude; Long, longitude.

†All these rotations follow two other rotations in the following order: $-76.00, 151.00, -39.70$ and $-54.90, -95.10, 30.00$.

TABLE 4.7. Poles of Rotation for Nazca-Antarctica

Rotation	Pole		
	Lat*	Long*	Angle, deg
05	-34.62	87.20	7.54
06	-51.06	81.43	15.40
13	-52.64	61.73	23.61

* North and east are positive. Rotation angles are positive counterclockwise. Lat, latitude; Long, longitude.

TABLE 4.8. Poles of Rotation for East Antarctica-Africa

Magnetic Anomaly	Age (Ma)	Pole Lat*	Pole Long*	Pole Angle, deg	Reference and Comments
05	10.59†	11.72	-43.84	1.55	*Molnar et al.*[1988]
06	19.90†	11.72	-43.84	2.79	*Molnar et al.*[1988]
13	35.58†	8.57	-39.59	5.58	*Molnar et al.*[1988]
18	42.01†	8.79	-40.72	6.95	*Molnar et al.*[1988]
21	49.55†	8.09	-39.28	8.65	*Molnar et al.*[1988]
25	58.94†	6.43	-39.15	10.94	*Molnar et al.*[1988]
30-31	68.47†	2.22	-40.74	12.50	*Molnar et al.*[1988]
34	84.00‡	-5.03	-36.12	18.24	*Molnar et al.*[1988]
M0	118.35‡	-3.95	-28.15	42.84	*1
M4	125.91‡	-13.29	-24.01	46.40	*2
M11	132.78‡	-11.63	-26.04	47.90	*2
M16	141.52‡	-8.68	-28.76	50.36	*3
M21	149.65‡	-3.77	-31.85	54.16	*3
Closure (M22)	152.11‡	-2.4	-32.7	55.4	*Norton and Sclater*[1979], *Lawver et al.*[1985]

† *Berggren et al.*[1985]

‡ *Kent and Gradstein*[1985]

* North and east are positive. Rotation angles are positive counterclockwise. Lat, latitude; Long, longitude.

*1 – Interpolated using *Molnar et al.*'s [1988] anomaly 34 pole and *Norton and Sclater*'s [1979] anomaly M1 pole.

*2 – Interpolated using *Ségoufin and Patriat*'s [1980] anomalies M2 and M15 poles.

*3 – Interpolated using *Ségoufin and Patriat*'s [1980] anomaly M15 pole and *Norton and Sclater*'s [1979] anomaly M22 pole.

TABLE 4.9. Poles of Rotation for East Antarctica-India

Magnetic Anomaly	Age (Ma)	Pole Lat*	Pole Long*	Angle, deg	Reference and Comments
05	10.59†	26.09	20.48	5.60	*Molnar et al.*[1988]
06	19.90†	18.47	29.56	11.37	*Molnar et al.*[1988]
13	35.58†	13.42	30.52	20.51	*Molnar et al.*[1988]
18	42.01†	15.61	29.26	23.94	*Molnar et al.*[1988]
21	49.55†	16.36	23.96	27.99	*Molnar et al.*[1988]
25	58.94†	16.95	12.60	35.51	*Molnar et al.*[1988]
30-31	68.47†	11.76	11.53	50.66	*Molnar et al.*[1988]
34	84.00‡	11.79	8.57	62.25	*Molnar et al.*[1988]
M0	118.35‡	-1.39	10.38	89.44	***
M4	125.91‡	-5.83	15.37	91.27	***
M11	132.78‡	-5.80	15.61	91.18	***
M16	141.65‡	-5.85	13.43	92.46	***
M21	149.65‡	0.10	8.91	86.56	***
Closure	Jurassic	1.0	-7.7	88.9	*Smith and Hallam*[1970]**

† *Berggren et al.*[1985]

‡ *Kent and Gradstein*[1985]

* North and east are positive. Rotation angles are positive counterclockwise. Lat, latitude; Long, longitude.

**Referenced in *Norton and Sclater*[1979]

*** Calculated through the plate circuit.

TABLE 4.10. Poles of Rotation for India-Africa

Magnetic Anomaly	Age (Ma)	Pole Lat*	Pole Long*	Angle, deg	Reference and Comments
05	10.59†	25.88	37.94	-5.06	*Molnar et al.*[1988]
06	19.90†	17.73	44.44	-10.78	*Molnar et al.*[1988]
13	35.58†	14.57	46.75	-19.20	*Molnar et al.*[1988]
18	42.01†	17.46	46.85	-22.23	*Molnar et al.*[1988]
21	49.55†	19.67	42.41	-25.11	*Molnar et al.*[1988]
25	58.94†	22.79	29.38	-29.93	*Molnar et al.*[1988]
30-31	68.47†	18.45	23.47	-44.14	*Molnar et al.*[1988]
34	84.00‡	23.36	19.57	-51.54	*Molnar et al.*[1988]
M0	118.35‡	18.62	28.40	-60.83	**
M4	125.91‡	19.41	30.70	-61.37	**
M11	132.78‡	20.31	33.44	-62.13	**
M16	141.65‡	20.36	34.15	-62.57	**
M21	149.65‡	23.32	41.33	-64.01	**
Closure	Jurassic	29.6	36.1	-56.8	*Norton and Sclater*[1979]

† *Berggren et al.*[1985]

‡ *Kent and Gradstein*[1985]

* North and east are positive. Rotation angles are positive counterclockwise. Lat, latitude; Long, longitude.

** Rotation parameters calculated from the plate circuit, using the India-Madagascar closure pole calculated from the India-Africa and Africa-Madagascar closure poles from *Norton and Sclater*[1979].

TABLE 4.11. Poles of Rotation for East Antarctica-Australia

Magnetic Anomaly	Age (Ma)	Pole Lat*	Pole Long*	Angle, deg	Reference and Comments
05	10.59†	8.70	35.56	6.65	*Stock and Molnar*[1982,1988]
06	19.90†	8.95	32.07	11.90	*Stock and Molnar*[1982,1988]
13	35.58†	11.68	31.81	20.46	*Stock and Molnar*[1982,1988]
18	42.01†	8.68	34.52	22.80	*Stock and Molnar*[1988]
21	49.55†	5.15	35.75	25.04	Extrapolated from A25 and A30-31 poles
25	58.94†	4.45	35.99	25.55	*Stock and Molnar*[1988]
30-31	68.47†	3.76	36.23	26.08	*Stock and Molnar*[1988]
34	84.00‡	4.9	35.8	26.81	*Royer and Sandwell, 1989*
Closure	96.‡	1.0	38.0	28.30	**

† *Berggren et al.*[1985]

‡ *Kent and Gradstein*[1985]

* North and east are positive. Rotation angles are positive counterclockwise. Lat, latitude; Long, longitude.

** Closure of continent-ocean boundary,*Royer and Sandwell, 1989*

TABLE 4.12. Poles of Rotation for Pacific-West Antarctica

Magnetic Anomaly	Age (Ma)	Pole Lat*	Pole Long*	Pole Angle, deg	Reference and Comments
05	10.59†	72.00	-70.00	9.75	*Stock and Molnar*[1982,1987,1988]
06	19.90†	71.25	-73.19	15.41	*Stock and Molnar*[1982,1987,1988]
13	35.58†	74.83	-56.86	28.01	*Stock and Molnar*[1982,1987,1988]
18	42.01†	75.08	-51.25	32.56	*Stock and Molnar*[1982,1987,1988]
21	49.55†	72.85	-53.21	35.11	Interpolated by Stock (personal communication)
25	58.94†	70.40	-54.85	38.46	*Stock and Molnar*[1988]**
30-31	68.47†	66.09	-56.94	46.27	*Stock and Molnar*[1988]**
34 (Closure)	84.00‡	62.97	-58.05	54.25	***

† *Berggren et al.*[1985]

‡ *Kent and Gradstein*[1985]

* North and east are positive. Rotation angles are positive counterclockwise. Lat, latitude; Long, longitude.

** Calculated here from parameters given by *Stock and Molnar*[1987,1988].

*** Time when the Campbell Plateau broke away from Antarctica *Christoffel and Falconer*[1972]. Rotation parameters extrapolated by distance here using the data from *Stock and Molnar*[1988].

TABLE 4.13. Poles of Rotation for Pacific-Bellingshausen

Magnetic Anomaly	Age (Ma)	Pole Lat*	Pole Long*	Angle, deg	Reference and Comments
05	10.59†	72.00	-70.00	9.75	***Stock and Molnar*[1988]
06	19.90†	71.25	-73.19	15.41	***Stock and Molnar*[1988]
13	35.58†	74.83	-56.86	28.01	***Stock and Molnar*[1988]
18	42.01†	75.08	-51.25	32.56	***Stock and Molnar*[1988]
21	49.55†	73.38	-54.65	35.90	Interpolated here
25	58.94†	71.61	-57.47	40.11	*Stock and Molnar*[1982,1988]
30-31	68.47†	71.65	-49.00	53.75	*Stock and Molnar*[1982,1988]
34	84.00‡	68.0	-50.0	66.0	*Molnar et al.*[1975]

† *Berggren et al.*[1985]

‡ *Kent and Gradstein*[1985]

* North and east are positive. Rotation angles are positive counterclockwise. Lat, latitude; Long, longitude.

**Same as Pacific-West Antarctica for these times (see Table 4.12).

TABLE 4.14. Poles of Rotation for Greenland-Europe

Magnetic Anomaly	Age (Ma)	Pole Lat*	Pole Long*	Angle, deg	Reference and Comments
05	10.59†	65.29	131.14	2.41	*Klitgord and Schouten* (1986, pers. comm.)
06	19.90†	66.82	137.95	4.86	*Klitgord and Schouten* (1986, pers. comm.)
13	35.58†	63.55	137.05	7.38	*Klitgord and Schouten* (1986, pers. comm.)
18	42.01†	55.40	141.05	8.33	*Klitgord and Schouten*[1986]
21	49.55†	51.88	133.58	9.16	**
Closure	56.(?)	9.70	-45.08	13.57	*** *Klitgord and Schouten* (1986, pers. comm.)

†*Berggren et al.*[1985]

‡*Kent and Gradstein*[1985]

*North and east are positive. Rotation angles are positive counterclockwise.

Lat, latitude; Long, longitude.

**Calculated here.

***Closure occurred a little before A24 time.

TABLE 4.15. Poles of Rotation for Greenland-North America

Magnetic Anomaly	Age (Ma)	Pole Lat*	Pole Long*	Angle, deg	Reference and Comments
05	10.59†				Since about 45 Ma, no motion *Laughton* [1972]
06	19.90†				Since about 45 Ma, no motion *Laughton* [1972]
13	35.58†				Since about 45 Ma, no motion *Laughton* [1972]
18	42.01†				Since about 45 Ma, no motion *Laughton* [1972]
21	49.55†	30.85	-153.02	-1.11	***
25	58.94†	12.93	-144.32	-2.93	*Klitgord and Schouten* (1986, pers. comm.)
30-31	68.47†	53.30	-128.63	-5.65	Calculated here
34	84.00‡	66.63	-113.59	-11.27	Calculated here
Closure	95.(?)	73.97	-107.20	-13.62	**

* North and east are positive. Rotation angles are positive counterclockwise. Lat, latitude; Long, longitude.

**Closing of Labrador Sea to initial opening at 95(?)Ma (*Srivastava and Tapscott* [1986]).

*** Calculated through the plate circuit GRE-EUR-NAM.

TABLE 4.16. Poles of Rotation for [North America + Greenland]-Europe

Magnetic Anomaly	Age (Ma)	Pole Lat*	Pole Long*	Angle, deg	Reference and Comments
05	10.59†	64.57	133.84	2.39	*Klitgord and Schouten* (1988, pers. comm.
06	19.90†	66.82	137.05	4.86	*Klitgord and Schouten* [1986]
13	35.58†	63.55	137.05	7.38	*Klitgord and Schouten* [1986]
18	42.01†	55.40	141.05	8.33	*Klitgord and Schouten* [1986]
21	49.55†	52.79	142.31	9.82	*Klitgord and Schouten* [1986]
25	58.94†	46.57	145.45	12.83	*Klitgord and Schouten* [1986]
30-31	68.47†	58.92	148.00	15.43	Calculated here
34	84.00‡	70.62	153.05	20.20	Calculated here
Closure	91.(?)	79.83	143.02	25.90	*Srivastava and Tapscott* [1986]

† *Berggren et al.*[1985]

‡ *Kent and Gradstein*[1985]

* North and east are positive. Rotation angles are positive counterclockwise. Lat, latitude; Long, longitude.

TABLE 4.17. Poles of Rotation for Iberia-North America

Magnetic Anomaly	Age (Ma)	Pole Lat*	Pole Long*	Pole Angle, deg	Reference and Comments
30-31	68.47†	71.16	136.68	-16.32	Calculated here
34	84.00‡	77.33	129.23	-21.32	Calculated here
M0	118.35‡	74.13	-2.80	-43.10	Calculated here**
M4	125.91‡	73.35	-2.24	-45.18	Calculated here**

† *Berggren et al.*[1985]

‡ *Kent and Gradstein*[1985]

* North and east are positive. Rotation angles are positive counterclockwise. Lat, latitude; Long, longitude.

** Calculated by adding the respective stage poles for the stage rotations between Africa and North America and the anomaly 34 rotation pole for Iberia-North America spreading.

TABLE 4.18. Poles of Rotation for Africa-North America

Magnetic Anomaly	Age (Ma)	Pole Lat*	Pole Long*	Pole Angle, deg	Reference and Comments
05	10.59†	79.53	71.47	-2.66	**
06	19.90†	79.57	37.84	-5.29	**
13	35.58†	76.41	7.12	-9.81	**
18	42.01†	75.36	-0.28	-12.44	**
21	49.55†	74.51	-4.83	-15.32	**
25	58.94†	80.60	-0.50	-18.07	**
30-31	68.47†	82.28	-2.61	-21.33	**
34	84.00‡	76.55	-20.73	-29.60	**
M0	118.35‡	66.30	-19.90	-54.25	*Klitgord and Schouten*[1986]
M4	125.91‡	66.13	-19.00	-56.39	*Klitgord and Schouten*[1986]
M11	132.78‡	65.97	-18.49	-57.50	***
M16	141.52‡	66.10	-18.40	-59.79	*Klitgord and Schouten*[1986]
M21	149.65‡	66.50	-18.10	-61.92	*Klitgord and Schouten*[1986]
M25	156.42‡	67.15	-16.00	-64.70	*Klitgord and Schouten*[1986]
Closure(min)	175.0‡	66.97	-12.34	-74.57	*Klitgord and Schouten*[1986]
Closure(max)	175.0‡	66.95	-12.02	-75.55	*Klitgord and Schouten*[1986]

† *Berggren et al.*[1985]

‡ *Kent and Gradstein*[1985]

* North and east are positive. Rotation angles are positive counterclockwise. Lat, latitude; Long, longitude.

** *Klitgord and Schouten*[1986], *Stock and Molnar*[1988]

*** Interpolated here using *Klitgord and Schouten*'s [1986] M10N and M16 poles.

TABLE 4.19. Poles of Rotation for Africa-South America

Magnetic Anomaly	Age (Ma)	Pole Lat*	Pole Long*	Angle, deg	Reference and Comments
05	10.59†	59.66	-38.31	-3.72	*Cande et al.*[1988]
06	19.90†	59.50	-37.44	-7.25	*Cande et al.*[1988]
13	35.58†	57.42	-33.92	-13.49	*Cande et al.*[1988]
18	42.01†	57.66	-32.34	-16.18	*Cande et al.*[1988]
21	49.55†	58.10	-33.95	-20.13	*Pardo-Casas and Molnar*[1987]
25	58.94†	60.53	-34.57	-22.31	*Pardo-Casas and Molnar*[1987]
30-31	68.47†	62.96	-35.30	-25.05	*Pardo-Casas and Molnar*[1987]
34	84.00‡	63.06	-36.63	-33.58	*Pardo-Casas and Molnar*[1987]
M0	118.35‡	51.78	-34.74	-52.51	*Martin et al.*[1982]
M4	125.91‡	49.33	-33.67	-54.30	*Martin et al.*[1982]
Closure (M11)**	132.78‡	46.75	-32.65	-56.40	*Martin et al.*[1982]

† *Berggren et al.*[1985]

‡ *Kent and Gradstein*[1985]

* North and east are positive. Rotation angles are positive counterclockwise. Lat, latitude; Long, longitude.

** Closure pole time given by *Martin et al.*[1982] was at anomaly M10N time (131.50 Ma).

TABLE 4.20. Poles of Rotation for South America- East Antarctica

Magnetic Anomaly	Age (Ma)	Pole Lat*	Pole Long*	Pole Angle, deg	Reference and Comments
05	10.59†	81.82	-12.13	2.92	**
06	19.90†	79.26	-13.65	5.77	**
13	35.58†	78.60	-4.67	10.69	**
18	42.01†	78.04	8.23	12.78	**
21	49.55†	79.20	6.32	16.02	**
25	58.94†	81.79	46.81	18.19	**
30-31	68.47†	80.55	65.30	21.84	**
34	84.00‡	80.09	81.83	31.54	**
M0	118.35‡	70.42	96.81	44.60	**
M4	125.91‡	72.49	96.63	51.97	**
M11	132.78‡	70.81	86.44	50.32	**

† *Berggren et al.*[1985]

‡ *Kent and Gradstein*[1985]

* North and east are positive. Rotation angles are positive counterclockwise. Lat, latitude; Long, longitude.

**Calculated by rotating SAM to AFR to East ANT.

TABLE 4.21. Poles of Rotation for Nazca-Pacific

Magnetic Anomaly	Age (Ma)	Pole Lat*	Pole Long*	Pole Angle, deg	Reference and Comments
05	10.59†	56.64	-87.88	-16.30	*Pardo-Casas and Molnar*[1987]
06	19.90†	62.38	-93.02	-30.18	*Pardo-Casas and Molnar*[1987]
13	35.58†	69.85	-106.13	-49.54	*Pardo-Casas and Molnar*[1987]
18	42.01†	73.03	-113.78	-56.59	*Rosa and Molnar*[1988]
21	49.55†	74.76	-122.26	-64.99	*Rosa and Molnar*[1988]
25	58.94†	78.82	-137.59	-71.35	*Rosa and Molnar*[1988]
30-31	68.47†	79.95	-152.26	-77.83	*Rosa and Molnar*[1988]
34	84.00‡	81.20	174.25	-89.03	**

† *Berggren et al.*[1985]

‡ *Kent and Gradstein*[1985]

* North and east are positive. Rotation angles are positive counterclockwise. Lat, latitude; Long, longitude.

**Calculated here from Nazca-Pacific A30-31 pole and Pacific-Farallon stage pole A30-31–A34.

TABLE 4.22. Poles of Rotation for Australia-Lord Howe Rise

Magnetic Anomaly	Age (Ma)	Pole Lat*	Pole Long*	Angle, deg	Reference and Comments
05					No motion
06					No motion
13					No motion
18					No motion
21					No motion
25	58.94†	-4.49	139.36	1.71	*Stock and Molnar*[1982,1988]
30-31	68.47†	-8.70	139.34	8.97	*Stock and Molnar*[1982,1988]
34	84.00‡	-12.81	139.32	21.16	Extrapolated using *Stock and Molnar*[1982,1988]
Closure	90.(?)	-14.0	142.0	23.0	*Weissel et al.*[1977]

† *Berggren et al.*[1985]

‡ *Kent and Gradstein*[1985]

* North and east are positive. Rotation angles are positive counterclockwise. Lat, latitude; Long, longitude.

TABLE 4.23. Poles of Rotation for anomalies on the Pacific plate formed by Pacific-Farallon spreading

Rotation	Age (Ma)	Pole Lat*	Pole Long*	Angle, deg	Reference and Comments
05–06					
06–13					
13–18	**	80.71	101.84	-4.10	*Rosa and Molnar* [1988]
13–18	42.01***	80.71	101.84	-3.95	***
18–21	**	82.26	140.00	-4.30	*Rosa and Molnar* [1988]
18–21	***	82.28	138.57	-4.45	***
21–25		59.77	59.09	-4.36	*Rosa and Molnar* [1988]
25–30-31		69.87	79.17	-3.69	*Rosa and Molnar* [1988]
30-31–34		63.62	57.11	-6.70	Interpolated by Rosa
25–34		66.0	64.0	-10.35	*Engebretson et al.*[1984]
34–M0		65.0	56.0	-14.6	*Engebretson et al.*[1984]
M0–M4		9.0	16.0	-3.88	Interpolated from *Engebretson et al.*[1984]
M4–M11		9.0	16.0	-3.52	Interpolated from *Engebretson et al.*[1984]
M11–M16		25.0	47.0	-2.99	Interpolated from *Engebretson et al.*[1984]
M16–M21		25.0	47.0	-2.78	Interpolated from *Engebretson et al.*[1984]
M21–M25		25.0	47.0	-2.31	Interpolated from *Engebretson et al.*[1984]
M25–PM26		25.0	47.0	-0.52	Interpolated from *Engebretson et al.*[1984]

* North and east are positive. Rotation angles are positive counterclockwise. Lat, latitude; Long, longitude.

**Calculated by *Rosa and Molnar* [1988] using the age of 42.26 Ma for the center of the earliest minor reversal within anomaly 18 on the DNAG timescale (*Berggren et al.*[1985]).

***Interpolated by *Stock and Molnar* [1988] using the parameters and data from *Rosa and Molnar* [1988] but using the age of 42.01 Ma for the center of the broad normal epoch of anomaly 18 on the DNAG timescale (*Berggren et al.*[1985]).

Note 1: All the ages used here are those of the DNAG timescale used on the previous tables, except when noted.

Note 2: Younger anomaly rotated over the fixed older anomaly.

TABLE 4.24. Poles of Rotation for anomalies on the Pacific plate formed by Pacific-Vancouver spreading

Rotation	Age (Ma)	Pole Lat*	Pole Long*	Angle, deg	Reference and Comments
00–05		73.43	6.14	-3.77	(See Note 3)
05–06		86.01	27.56	-3.64	(See Note 3)
06–13		79.62	61.91	-7.49	(See Note 3)
13–18	**	78.00	-140.00	-5.55	*Rosa and Molnar* [1988]
13–18	42.01***	78.00	-140.00	-5.33	***
18–21	**	75.40	-139.40	-5.57	*Rosa and Molnar* [1988]
18–21	***	75.50	-139.40	-5.79	***
21–25					Same as Pacific-Farallon (see Table 4.22)
25–30-31					Same as Pacific-Farallon (see Table 4.22)
30-31–34					Same as Pacific-Farallon (see Table 4.22)

* North and east are positive. Rotation angles are positive counterclockwise. Lat, latitude; Long, longitude.

**Calculated by *Rosa and Molnar* [1988] using the age of 42.26 Ma for the center of the earliest minor reversal within anomaly 18 on the DNAG timescale (*Berggren et al.*[1985]).

***Interpolated by *Stock and Molnar* [1988] using the parameters and data from *Rosa and Molnar* [1988] but using the age of 42.01 Ma for the center of the broad normal epoch of anomaly 18 on the DNAG timescale (*Berggren et al.*[1985]).

Note 1: All the ages used here are those of the DNAG timescale used on the previous tables, except when noted.

Note 2: Younger anomaly rotated over the fixed older anomaly.

Note 3: Calculated using stage poles of *Wilson*[1988].

TABLE 4.25. Poles of Rotation for anomalies on the Pacific plate formed by Pacific-Kula spreading

Rotation	Age (Ma)	Pole Lat*	Pole Long*	Pole Angle, deg	Reference and Comments
05–06					No spreading
06–13					No spreading
13–18					No spreading
18–22					No spreading
22–25		27.50	126.25	-2.17	Extrapolated from *Rosa and Molnar*[1988]
25–30-31		27.50	126.25	-3.10	*Rosa and Molnar*[1988]
30-31–34		18.0	111.0	-8.61	Extrapolated from *Engebretson et al.*[1984]
34–M0		-48.0	3.0	-25.3	From Pacific-Izanagi-1 poles of *Engebretson et al.*[1984]
M0–M4		-48.0	3.0	-6.15	From Pacific-Izanagi-1 poles of *Engebretson et al.*[1984]
M4–M11		-48.0	3.0	-9.55	From Pacific-Izanagi-1 poles of *Engebretson et al.*[1984]
M11–M16		-15.0	88.0	-4.1	From Pacific-Izanagi-1 poles of *Engebretson et al.*[1984]

* North and east are positive. Rotation angles are positive counterclockwise. Lat, latitude; Long, longitude.

Note 1: All the ages used here are those of the DNAG timescale used on the previous tables, except when noted.

Note 2: Younger anomaly rotated over the fixed older anomaly.

TABLE 4.26. Poles of Rotation for India-Australia

Magnetic Anomaly	Age (Ma)	Pole Lat*	Pole Long*	Pole Angle, deg	Reference and Comments
05					Since 42.7 Ma, no motion *Royer and Sandwell*[1989]
06					Since 42.7 Ma, no motion *Royer and Sandwell*[1989]
13					Since 42.7 Ma, no motion *Royer and Sandwell*[1989]
18					Since 42.7 Ma, no motion *Royer and Sandwell*[1989]
21	49.55†	6.61	-7.86	-4.38	*Royer and Sandwell*[1989]
25	58.94†	2.57	-0.2	-14.25	*Royer and Sandwell*[1989]
30-31	68.47†	1.7	-2.1	-28.43	*Royer and Sandwell*[1989]
34	84.00‡	0.4	-3.1	-42.16	*Royer and Sandwell*[1989]

† *Berggren et al.*[1985]

‡ *Kent and Gradstein*[1985]

* North and east are positive. Rotation angles are positive counterclockwise. Lat, latitude; Long, longitude.

TABLE 4.27. Poles of Rotation for Madagascar-Africa

Magnetic Anomaly	Age (Ma)	Pole Lat*	Pole Long*	Angle, deg	Reference and Comments
05					Fixed to Africa since 112.5 Ma *Cochran*[1988]
06					Fixed to Africa since 112.5 Ma *Cochran*[1988]
13					Fixed to Africa since 112.5 Ma *Cochran*[1988]
18					Fixed to Africa since 112.5 Ma *Cochran*[1988]
21					Fixed to Africa since 112.5 Ma *Cochran*[1988]
25					Fixed to Africa since 112.5 Ma *Cochran*[1988]
30-31					Fixed to Africa since 112.5 Ma *Cochran*[1988]
34					Fixed to Africa since 112.5 Ma *Cochran*[1988]
M0	118.35‡	5.42	-76.18	0.65	*Ségoufin and Patriat*[1980], *Cochran*[1988]**
M4	125.91‡	5.42	-76.18	3.06	*Ségoufin and Patriat*[1980], *Cochran*[1988]**
M11	132.78‡	5.43	-76.19	5.96	*Ségoufin and Patriat*[1980], *Cochran*[1988]**
M16	141.52‡	6.10	-78.54	6.74	*Ségoufin and Patriat*[1980], *Cochran*[1988]**
M21	149.65‡	4.04	-71.40	14.41	*Ségoufin and Patriat*[1980], *Cochran*[1988]**
Closure		-10.0	-30.0	14.2	*Coffin and Rabinowitz*[1987]

† *Berggren et al.*[1985]

‡ *Kent and Gradstein*[1985]

* North and east are positive. Rotation angles are positive counterclockwise. Lat, latitude; Long, longitude.

** Calculated from *Ségoufin and Patriat*'s [1980] pole based on measured distances between anomalies.

TABLE 4.28. Partial Uncertainty Rotations for Aluk-West Antarctic (/Bellingshausen) and for reconstructions of anomalies on the West Antarctic (/Bellingshausen) plate formed by Aluk-West Antarctic (/Bellingshausen) spreading

	End Points of Plate Boundaries and Azimuth of Transform Faults					Skewed Fit				Mismatched Fracture Zones				Mismatched Magnetic Anomalies			
Rotation	Lat*	Long*	Lat*	Long*	Azimuth	Lat*	Long*	Angle, deg	Angle,† km	Lat*	Long*	Angle, deg	Angle, km	Lat*	Long*	Angle, deg	Angle, km
04**	-58.44	-64.46	-60.61	-64.53	126	-59.52	-64.49	9.48	1056 (20)	-17.34	57.56	0.18	20	-24.22	155.64	0.18	20
05**	-60.10	-63.79	-61.57	-64.03	130	-60.83	-63.91	14.00	1559 (20)	-18.25	62.32	0.18	20	-21.92	159.95	0.18	20
05-06**																	
06-07**	-62.37	-69.42	-64.93	-74.39	129	-63.67	-71.79	6.09	678 (20)	-16.21	54.18	0.18	20	-20.16	150.30	0.18	20
07-10**	-62.35	-71.53	-64.59	-76.01	129	-63.49	-73.68	6.86	764 (20)	-16.31	52.25	0.18	20	-20.30	148.46	0.18	20
10-13**	-61.85	-72.30	-63.71	-76.67	129	-62.80	-74.42	7.54	840 (20)	-16.72	51.35	0.18	20	-20.81	147.90	0.18	20
13-18**																	
13-18***																	
18-20**																	
18-20***																	
22-23***	-64.63	-80.57	-64.83	-80.92	133	-64.73	-80.74	82.29	9167 (20)	-16.93	49.40	0.18	20	-18.19	145.13	0.18	20
23-24***	-64.44	-81.76	-64.60	-82.20	133	-64.52	-81.98	82.29	9167 (20)	-17.06	48.11	0.18	20	-18.34	143.95	0.18	20
24-25***	-63.69	-85.45	-63.83	-86.13	133	-63.76	-85.79	62.34	6945 (20)	-17.55	44.12	0.18	20	-18.87	140.32	0.18	20
25-26***	-63.35	-86.73	-63.53	-88.43	133	-63.44	-87.58	26.38	2938 (20)	-17.75	42.25	0.18	20	-19.09	138.61	0.18	20
26-27***	-62.06	-89.38	-62.76	-90.97	130	-62.41	-90.17	20.17	2247 (20)	-17.32	36.47	0.18	20	-20.78	133.27	0.18	20
27-28***	-61.92	-91.32	-64.58	-95.23	134	-63.26	-93.18	6.45	718 (20)	-18.21	37.59	0.18	20	-18.88	134.05	0.18	20
28-29***	-63.30	-94.30	-63.57	-95.10	131	-63.44	-94.70	45.72	5093 (20)	-17.06	33.17	0.18	20	-19.72	129.48	0.18	20

* North and east are positive. Rotation angles are positive counterclockwise. Lat, latitude; Long, longitude.

** Parameters calculated using data north of fracture zone 'G'.

*** Parameters calculated using data south of fracture zone 'G'.

† Values in parentheses give overlap or underlap in kilometers of endpoints of the plate boundary

TABLE 4.29. Partial Uncertainty Rotations for reconstructions of anomalies originally on the Antarctic (/Bellingshausen) plate formed by Antarctic (/Bellingshausen)-Farallon spreading

	End Points of Plate Boundaries and Azimuth of Transform Faults					Skewed Fit				Mismatched Fracture Zones				Mismatched Magnetic Anomalies			
Rotation	Lat*	Long*	Lat*	Long*	Azimuth	Lat*	Long*	Angle, deg	Angle,† km	Lat*	Long*	Angle, deg	Angle, km	Lat*	Long*	Angle, deg	Angle, km
10–13	-51.73	-86.18	-57.26	-76.56	22	-54.59	-81.70	2.62	292 (20)	32.49	-55.33	0.18	20	-12.54	26.53	0.18	20
13–18	-50.54	-91.87	-58.82	-74.89	22	-54.97	-84.25	1.61	180 (20)	32.15	-57.99	0.18	20	-12.42	24.05	0.18	20
12–18	-50.54	-91.87	-55.88	-82.81	22	-53.30	-87.62	2.71	302 (20)	33.65	-60.88	0.18	20	-12.94	20.32	0.18	20
18–19	-52.72	-91.33	-59.15	-76.37	22	-56.16	-84.47	1.96	218 (20)	31.09	-58.53	0.18	20	-12.04	24.08	0.18	20
19–20	-54.06	-88.00	-59.19	-79.08	22	-56.70	-83.84	2.90	323 (20)	30.60	-58.05	0.18	20	-11.87	24.82	0.18	20

* North and east are positive. Rotation angles are positive counterclockwise. Lat, latitude; Long, longitude.

TABLE 4.30. Partial Uncertainty Rotations for reconstructions of anomalies originally on the Pacific plate formed by Pacific-Aluk spreading for the area northwest of the Palmer Peninsula (See Figure 3.2, Figure 1 of Cande et al. [1982]).

	End Points of Plate Boundaries and Azimuth of Transform Faults					Skewed Fit				Mismatched Fracture Zones				Mismatched Magnetic Anomalies			
Rotation	Lat*	Long*	Lat*	Long*	Azimuth	Lat*	Long*	Angle, deg	Angle,† km	Lat*	Long*	Angle, deg	Angle, km	Lat*	Long*	Angle, deg	Angle, km
21–22	-59.96	-80.58	-60.98	-81.52	132	-60.47	-81.04	18.37	2046 (20)	-19.26	47.03	0.18	20	-21.49	144.94	0.18	20
22–23	-59.39	-81.93	-60.72	-82.75	132	-60.06	-82.33	14.80	1649 (20)	-19.51	45.63	0.18	20	-21.77	143.77	0.18	20
23–24	-58.87	-83.49	-59.24	-83.61	132	-59.05	-83.55	55.60	6194 (20)	-20.12	44.13	0.18	20	-22.47	142.84	0.18	20
24–25	-57.22	-87.02	-57.95	-87.31	128	-57.58	-87.16	27.43	3056 (20)	-19.27	36.24	0.18	20	-24.99	135.62	0.18	20
25–26	-56.25	-89.78	-56.91	-90.14	124	-56.58	-89.96	29.82	3321 (20)	-17.94	29.42	0.18	20	-27.17	128.98	0.18	20
26–27	-55.26	-94.22	-56.16	-94.36	124	-55.71	-94.29	22.86	2546 (20)	-18.36	24.84	0.18	20	-27.84	124.94	0.18	20

* North and east are positive. Rotation angles are positive counterclockwise. Lat, latitude; Long, longitude.

TABLE 4.31. Partial Uncertainty Rotations for reconstructions of anomalies originally on the Pacific plate formed by Pacific-Aluk spreading for the area northeast of New Zealand (See Figure 3 of Cande et al. [1982]).

	End Points of Plate Boundaries and Azimuth of Transform Faults					Skewed Fit				Mismatched Fracture Zones				Mismatched Magnetic Anomalies			
Rotation	Lat*	Long*	Lat*	Long*	Azimuth	Lat*	Long*	Angle, deg	Angle,† km	Lat*	Long*	Angle, deg	Angle, km	Lat*	Long*	Angle, deg	Angle, km
29–30	-45.44	-144.98	-46.07	-146.76	129	-45.76	-145.86	14.80	1649 (20)	-26.04	-25.74	0.18	20	-32.83	82.64	0.18	20
30–31	-44.48	-145.00	-45.40	-148.04	133	-44.95	-146.51	8.79	979 (20)	-28.86	-23.13	0.18	20	-31.17	86.34	0.18	20
31–32	-41.66	-144.88	-43.58	-151.92	129	-42.67	-148.34	3.73	415 (20)	-27.56	-29.58	0.18	20	-34.85	81.72	0.18	20
32–33	-38.93	-150.01	-40.64	-156.24	127	-39.83	-153.09	4.05	451 (20)	-27.53	-37.32	0.18	20	-37.83	76.55	0.18	20
33–34	-36.11	-150.08	-38.23	-159.56	134	-37.26	-154.75	2.63	292 (20)	-33.56	-34.44	0.18	20	-34.92	83.16	0.18	20

* North and east are positive. Rotation angles are positive counterclockwise. Lat, latitude; Long, longitude.

TABLE 4.32. Partial Uncertainty Poles for Nazca-Antarctica

	End Points of Plate Boundaries and Azimuth of Transform Faults					Skewed Fit				Mismatched Fracture Zones				Mismatched Magnetic Anomalies			
Rotation	Lat*	Long*	Lat*	Long*	Azimuth	Lat*	Long*	Angle, deg	Angle,† km	Lat*	Long*	Angle, deg	Angle, km	Lat*	Long*	Angle, deg	Angle, km
05**	-38.08	-96.96	-47.65	-76.21	76	-43.33	-87.40	2.31	257 (20)	-46.33	83.89	0.18	20	-4.36	178.48	0.18	20
06	-49.29	-78.55	-54.01	-75.31	79	-51.66	-77.01	4.01	447 (20)	6.80	4.32	0.18	20	-37.51	89.07	0.18	20

* North and east are positive. Rotation angles are positive counterclockwise. Lat, latitude; Long, longitude.

** Partial uncertainty rotations calculated using end points of isochrons.

TABLE 4.33. Partial Uncertainty Rotations for East Antarctica-Africa

	End Points of Plate Boundaries and Azimuths of Transform Faults					Skewed Fit				Mismatched Fracture Zones				Mismatched Magnetic Anomalies			
Magnetic Anomaly	Lat*	Long*	Lat*	Long*	Azimuth	Lat*	Long*	Angle, deg	Angle,† km	Lat*	Long*	Angle, deg	Angle, km	Lat*	Long*	Angle, deg	Angle, km
05	-44.00	36.59	-26.58	66.60	N5E	-36.22	53.25	0.52	58 (15)	53.48	61.67	0.18	20	4.03	-33.79	0.09	10
06	-43.48	36.76	-29.11	59.60	N8E	-36.84	49.25	0.67	75 (15)	52.42	62.44	0.18	20	6.39	-35.93	0.11	12
13	-42.17	37.54	-34.90	51.00	N10E	-38.72	44.62	1.61	180 (20)	50.21	60.36	0.18	20	7.79	-39.09	0.18	20
18**						-35.69	48.66	1.61	180	53.72	60.21	0.34	38	5.65	-37.25	0.22	25
21**						-34.85	48.83	1.53	170	54.57	60.67	0.40	45	5.59	-37.25	0.27	30
25‡						-41.19	38.88	0.53		46.63	61.02	0.18		-11.23	138.89	0.18	
30-31**						-42.59	32.06	2.32	258	47.35	35.66	0.72	80	1.79	-56.30	0.27	30
34	-44.46	23.01	-34.76	41.19	N5E	-39.96	32.75	1.22	135 (20)	49.78	40.51	0.36	40	3.83	-54.03	0.13	15
M0‡						-16.33	43.28	0.71		73.63	46.83	0.18		-0.96	133.56	0.18	
M4‡						-15.96	43.31	0.69		74.01	46.94	0.18		-0.96	133.58	0.18	
M11‡						-15.33	43.37	0.66		74.64	47.15	0.18		-0.96	133.63	0.18	
M16‡						-14.79	43.45	0.64		75.18	47.36	0.18		-0.97	133.70	0.18	
M21‡						-14.32	43.49	0.63		75.64	47.53	0.18		-0.97	133.74	0.18	
Closure																	

Source for the partial uncertainty rotations for anomalies 05, 06, 13, 18, 21, 30-31 and 34 is Stock and Molnar [1988].

* North and east are positive. Rotation angles are positive counterclockwise. Lat, latitude; Long, longitude.

** Pole positions, angles, and partial uncertainty rotations interpolated between those for neighboring anomalies.

† Values in parentheses give overlap or underlap in kilometers of endpoints of the plate boundary.

‡ End points of plate boundaries were taken as the end points of the respective isochrons.

TABLE 4.34. Partial Uncertainty Rotations for East Antarctica-India

	End Points of Plate Boundaries and Azimuth of Transform Faults					Skewed Fit				Mismatched Fracture Zones				Mismatched Magnetic Anomalies			
Magnetic Anomaly	Lat*	Long*	Lat*	Long*	Azimuth	Lat*	Long*	Angle, deg	Angle,† km	Lat*	Long*	Angle, deg	Angle, km	Lat*	Long*	Angle, deg	Angle, km
05‡						-19.42	61.14	0.80		57.86	117.00	0.31		24.53	-19.60	0.16	
06‡						-22.30	70.78	2.09		40.70	140.12	0.44		41.02	1.68	0.31	
13‡						-35.21	41.80	1.73		15.34	120.63	0.55		50.62	11.10	0.23	
18	....	....	....	....	....	-20.45	80.46	7.13	794	69.42	87.23	0.36	40	2.22	-8.71	0.90	100
21	....	....	....	....	....	-18.17	81.00	7.13	794	71.70	87.83	0.36	40	2.03	-8.33	0.90	100
25	-11.10	78.10	-12.30	80.00	N2E	-11.70	78.95	7.01	781 (15)	78.13	88.72	0.36	40	1.96	-10.64	0.27	30
30-31	-4.15	77.30	-8.55	83.25	N2E	-6.35	80.26	2.10	234 (15)	83.34	97.78	0.36	40	1.99	-9.52	0.11	12
34	0.00	80.33	....	....	N2E	0.00	80.33	10.30	1147**	88.00	170.33	0.36	40	2.00	-9.67	0.36	40
M0‡						-21.19	34.57	6.12		49.59	97.49	1.76		32.56	-41.10	0.40	
M04‡						-27.29	30.24	13.86		46.44	87.38	2.09		30.96	-41.73	0.40	
M11‡						-26.38	31.82	21.22		49.62	86.15	1.96		28.13	-42.80	0.40	
M16‡						-25.12	32.99	27.25		51.69	86.59	1.90		26.86	-43.27	0.40	
M21‡						-20.30	40.12	23.25		64.34	79.77	1.42		15.02	-44.18	0.39	
Closure																	

Source for the partial uncertainty rotations for anomalies 18, 21, 25, 30-31 and 34 is Stock and Molnar [1988].

* North and east are positive. Rotation angles are positive counterclockwise. Lat, latitude; Long, longitude.

** Mismatch of 100 km at 5 degrees from pole.

† Values in parentheses give overlap or underlap in kilometers of endpoints of the plate boundary.

‡ Rotation parameters and partial uncertainty parameters calculated from other boundaries in the Indian Ocean.

TABLE 4.35. Partial Uncertainty Rotations for India-Africa

	End Points of Plate Boundaries and Azimuth of Transform Faults					Skewed Fit				Mismatched Fracture Zones				Mismatched Magnetic Anomalies			
Magnetic Anomaly	Lat*	Long*	Lat*	Long*	Azimuth	Lat*	Long*	Angle, deg	Angle,† km	Lat*	Long*	Angle, deg	Angle, km	Lat*	Long*	Angle, deg	Angle, km
05	0.75	59.60	-22.40	67.00	N57E	-10.84	63.16	0.64	71 (15)	32.34	146.20	0.18	20	55.46	-10.69	0.09	10
06	-25.05	65.65	....	....	N58E	-25.05	65.65	2.00**	223**	28.69	140.83	0.27	30	50.20	9.77	0.27	30
13	-17.95	61.80	-37.10	69.35	N61E	-27.57	65.24	0.77	85 (15)	25.45	140.85	0.27	30	50.83	15.10	0.13	15
18	....	....	....	....	....	-8.92	58.97	2.76	308	56.61	135.72	0.36	40	32.90	-25.20	0.90	100
21	....	....	....	....	....	-9.91	57.79	2.76	308	54.50	133.60	0.36	40	33.69	-25.53	0.90	100
25	1.35	55.85	-27.57	55.50	N34E	-13.11	55.69	1.08	120 (30)	53.85	127.10	0.27	30	33.00	-25.61	0.18	20
30-31‡	....	....	....	....	....	-33.77	57.26	2.85		31.24	123.33	1.36		40.51	2.11	0.73	
34‡	....	....	....	....	....	-16.57	79.55	10.33		39.87	155.17	0.97		45.45	7.14	0.49	
M0***						-8.34	16.80	4.10		30.92	101.77	0.36		57.73	-59.76	0.36	
M04***						-5.54	17.67	4.36		31.06	104.32	0.36		58.34	-63.27	0.36	
M11***						-2.02	19.00	4.29		31.04	107.78	0.36		58.88	-67.64	0.36	
M16***						-0.76	20.09	4.23		30.72	109.63	0.36		59.26	-68.62	0.36	
M21***						7.34	21.09	4.10		31.00	115.53	0.36		57.95	-80.78	0.36	
Closure																	

Source for the partial uncertainty rotations for anomalies 05, 06, 13, 18, 21, 25, 30-31 and 34 is Stock and Molnar [1988].

* North and east are positive. Rotation angles are positive counterclockwise. Lat, latitude; Long, longitude.

** Mismatch of 1 degree (111.4 km) at 30 degrees from pole.

*** Partial uncertainty parameters were calculated from the plate circuit IND-MAD-AFR.

† Value in parentheses give overlap or underlap in kilometers of endpoints of the plate boundary.

‡ Rotation parameters and partial uncertainty poles calculated from other boundaries in the Indian Ocean

TABLE 4.36. Partial Uncertainty Rotations for East Antarctica-Australia

	End Points of Plate Boundaries and Azimuth of Transform Faults					Skewed Fit				Mismatched Fracture Zones				Mismatched Magnetic Anomalies			
Magnetic Anomaly	Lat*	Long*	Lat*	Long*	Azimuth	Lat*	Long*	Angle, deg	Angle,† km	Lat*	Long*	Angle, deg	Angle, km	Lat*	Long*	Angle, deg	Angle, km
05	-39.16	90.99	-59.28	155.63	0E	-53.68	115.90	0.47	20	36.32	115.90	0.18	20	0.00	-154.10	0.18	20
06	-37.90	95.13	-56.69	157.22	N2W	-51.50	120.02	0.48	20	38.47	117.46	0.18	20	1.24	-151.55	0.18	20
13	-25.70	82.37	-51.50	157.55	0E	-44.93	111.95	0.35	20	45.07	111.95	0.18	20	0.00	-158.05	0.18	20
18	-38.35	130.60	-50.25	156.15	0E	-45.01	142.05	0.96	20	44.99	142.05	0.18	20	0.00	-127.95	0.18	20
21‡						-42.50	141.09	1.92	40	47.50	140.90	0.36	40	0.09	-128.99	0.36	40
25	†	†	†	†		-43.47	141.46	1.92	40	46.53	141.36	0.36	40	0.05	-128.59	0.36	40
30-31	†	†	†	†		-43.18	141.35	1.92	40	46.82	141.22	0.36	40	0.06	-128.71	0.36	40
34‡						-40.77	140.77	1.92	40	49.22	141.43	0.36	40	-0.33	-128.95	0.36	40
Closure‡						-38.91	140.17	1.92	40	51.08	138.68	0.36	40	0.73	-130.42	0.36	40

Source for the partial uncertainty rotations for anomalies 05, 06, 13, 18, 25 and 30-31 is Stock and Molnar [1988].

* North and east are positive. Rotation angles are positive counterclockwise. Lat, latitude; Long, longitude.

† These best fit poles were calculated by interpolation between the anomaly 18 pole [Stock and Molnar, 1982] and the magnetic quite zone fit [Konig, 1980], using distances given by Cande and Mutter [1982]. Partial uncertainty rotation axes were rotated from anomaly 18, with angle value doubled to reflect additional uncertainty in these interpolated poles.

‡ Partial uncertainty rotation axes were rotated from anomaly 18, with angle value doubled to reflect additional uncertainty in these interpolated poles.

TABLE 4.37. Partial Uncertainty Rotations for Pacific-West Antarctica

	End Points of Plate Boundaries and Azimuth of Transform Faults					Skewed Fit				Mismatched Fracture Zones				Mismatched Magnetic Anomalies			
Magnetic Anomaly	Lat*	Long*	Lat*	Long*	Azimuth	Lat*	Long*	Angle, deg	Angle,† km	Lat*	Long*	Angle, deg	Angle, km	Lat*	Long*	Angle, deg	Angle, km
05	-35.83	-103.85	-63.01	-147.25	N70W	-51.31	-119.14	0.55	20	12.34	166.72	0.18	20	35.97	-94.14	0.18	20
06	-61.05	-140.26	-44.74	-101.13	N70W	-54.46	-116.84	0.37	20	11.47	169.65	0.18	20	33.11	-92.74	0.18	20
13	-55.59	-100.38	-61.63	-133.62	N60W	-59.68	-115.52	1.14	20	14.62	-179.03	0.18	20	25.93	-81.75	0.18	25
18	-53.97†	-97.41	-66.82†	-149.29	N62W	-62.83	-117.84	0.38	20	12.38	177.47	0.18	20	23.78	-86.98	0.18	20
21‡						-64.64	-114.11	0.76	40	10.89	179.82	0.36	40	22.60	-85.58	0.36	40
25‡						-66.88	-108.71	0.76	40	8.89	-177.22	0.36	40	21.16	-83.74	0.36	40
30-31‡						-71.40	-92.96	0.76	40	4.08	-170.75	0.36	40	18.12	-79.41	0.36	40
34 (Closure)‡						-74.48	-70.71	0.76	40	-1.07	-164.57	0.36	40	15.48	-74.86	0.36	40

Source for the partial uncertainty rotations for anomalies 05, 06, 13 and 18 is Stock and Molnar [1988].

* North and east are positive. Rotation angles are positive counterclockwise. Lat, latitude; Long, longitude.

† Endpoint rotated from the Pacific plate.

‡ Partial uncertainty rotation axes were rotated from anomaly 18, with angle value doubled to reflect additional uncertainty in these interpolated poles.

TABLE 4.38. Partial Uncertainty Rotations for Pacific-Bellingshausen

	End Points of Plate Boundaries and Azimuth of Transform Faults					Skewed Fit				Mismatched Fracture Zones				Mismatched Magnetic Anomalies			
Magnetic Anomaly	Lat*	Long*	Lat*	Long*	Azimuth	Lat*	Long*	Angle, deg	Angle,† km	Lat*	Long*	Angle, deg	Angle, km	Lat*	Long*	Angle, deg	Angle, km
05	-35.83	-103.85	-63.01	-147.25	N70W	-51.31	-119.14	0.55	20	12.34	166.72	0.18	20	35.97	-94.14	0.18	20
06	-61.05	-140.26	-44.74	-101.13	N70W	-54.46	-116.84	0.37	20	11.47	169.65	0.18	20	33.11	-92.74	0.18	20
13	-55.59	-100.38	-61.63	-133.62	N60W	-59.68	-115.52	1.14	20	14.62	-179.03	0.18	20	25.93	-81.75	0.18	25
18	-53.97†	-97.41	-66.82†	-149.29	N62W	-62.83	-117.84	0.38	20	12.38	177.47	0.18	20	23.78	-86.98	0.18	20
21‡						-60.71	-125.67	1.14	20	18.47	-179.12	0.18	20	21.89	-81.41	0.18	20
25	-60.02	-112.67	-65.38	-128.7	N52W	-62.93	-119.95	1.14	20	16.27	-175.13	0.18	20	21.02	-78.69	0.18	20
30-31	-62.23	-106.08	-67.42	-125.88	N54W	-65.15	-115.02	2.10	20	14.30	-171.62	0.18	20	19.87	-76.33	0.18	20
34**						-74.48	-70.71	0.76	40	-1.07	-164.57	0.36	40	15.48	-74.86	0.36	40

Source for the partial uncertainty rotations for anomalies 05, 06, 13, 18, 25 and 30-31 is Stock and Molnar [1988].

* North and east are positive. Rotation angles are positive counterclockwise. Lat, latitude; Long, longitude.

** Partial uncertainty rotations are the same as those for Pacific-Antarctica spreading.

† Endpoint rotated from the Pacific plate.

‡ Partial uncertainty rotations were rotated from anomaly 25.

TABLE 4.39. Partial Uncertainty Rotations for Greenland-Europe

	End Points of Plate Boundaries and Azimuth of Transform Faults					Skewed Fit				Mismatched Fracture Zones				Mismatched Magnetic Anomalies			
Magnetic Anomaly	Lat*	Long*	Lat*	Long*	Azimuth	Lat*	Long*	Angle, deg	Angle,† km	Lat*	Long*	Angle, deg	Angle, km	Lat*	Long*	Angle, deg	Angle, km
05	72.74	8.89	56.81	-31.87	115	66.04	-17.79	0.91	101 (20)	-9.88	49.13	0.18	20	-21.59	-44.82	0.18	20
06	72.42	11.07	56.78	-30.03	120	65.90	-15.67	0.91	101 (20)	-11.78	46.54	0.18	20	-20.70	-47.98	0.18	20
13	71.85	13.33	56.70	-28.20	120	65.63	-13.41	0.91	101 (20)	-11.91	48.85	0.18	20	-20.94	-45.78	0.18	20
18	71.35	15.08	56.68	-26.96	120	65.42	-11.73	0.91	101 (20)	-12.00	50.56	0.18	20	-21.11	-44.14	0.18	20
21	70.78	15.17	56.20	-26.94	122	64.93	-11.52	0.90	100 (20)	-12.97	48.97	0.18	20	-21.06	-46.12	0.18	20
Closure																	

* North and east are positive. Rotation angles are positive counterclockwise. Lat, latitude; Long, longitude.

† Values in parentheses give overlap or underlap in kilometers of end points of the plate boundary.

TABLE 4.40. Partial Uncertainty Rotations for Greenland-North America

	End Points of Plate Boundaries and Azimuth of Transform Faults					Skewed Fit				Mismatched Fracture Zones				Mismatched Magnetic Anomalies			
Magnetic Anomaly	Lat*	Long*	Lat*	Long*	Azimuth	Lat*	Long*	Angle, deg	Angle,† km	Lat*	Long*	Angle, deg	Angle, km	Lat*	Long*	Angle, deg	Angle, km
21‡						55.89	-27.01	1.26		17.03	89.87	0.34		-28.57	9.47	0.23	
25	61.62	-60.27	55.59	-47.84	65	58.75	-53.52	2.33	260 (20)	12.66	58.22	0.18	20	-28.04	-24.91	0.18	20
30-31	61.47	-61.28	55.11	-49.97	65	58.41	-55.11	2.37	264 (20)	12.79	56.55	0.18	20	-28.34	-26.42	0.18	20
34	61.27	-62.80	54.79	-51.88	65	58.15	-56.84	2.38	265 (20)	12.89	54.76	0.18	20	-28.57	-28.08	0.18	20
Closure																	

* North and east are positive. Rotation angles are positive counterclockwise. Lat, latitude; Long, longitude.

† Values in parentheses give overlap or underlap in kilometers of end points of the plate boundary.

‡ Partial uncertainty rotations calculated through the plate circuit.

TABLE 4.41. Partial Uncertainty Rotations for [North America + Greenland]-Europe

	End Points of Plate Boundaries and Azimuth of Transform Faults					Skewed Fit				Mismatched Fracture Zones				Mismatched Magnetic Anomalies			
Magnetic Anomaly	Lat*	Long*	Lat*	Long*	Azimuth	Lat*	Long*	Angle, deg	Angle,† km	Lat*	Long*	Angle, deg	Angle, km	Lat*	Long*	Angle, deg	Angle, km
05	72.71	8.45	39.00	-17.50	103	56.42	-10.58	0.29	32	-7.23	68.40	0.13	15	32.59	153.74	0.07	8
06	72.12	9.05	45.00	-31.36	105	64.58	-12.63	0.47	52	-6.57	63.35	0.13	15	24.59	150.63	0.09	10
13	71.60	11.15	39.00	-25.39	93	56.55	-14.91	0.42	47	-2.05	71.98	0.13	15	33.37	160.63	0.09	10
18**						50.84	-21.87	0.64		-2.04	66.31	0.16		37.03	157.08	0.10	
21	55.86	-27.10	39.00	-23.55	93	47.56	-24.99	0.91	101	-2.02	62.81	0.18	20	42.37	150.97	0.11	12
25***						47.41	-22.25	0.47		-7.58	58.77	0.24		41.39	140.88	0.08	
30-31****						48.63	-16.67	2.36		5.95	79.76	0.22		41.18	173.26	0.09	
34	52.11	-17.42	46.48	-13.96	80	49.35	-15.88	2.55	283	4.11	78.93	0.22	25	40.35	172.43	0.09	10
M0‡						49.35	-15.88	5.00		4.11	78.93	0.44		40.35	172.43	0.18	
M4‡						49.35	-15.88	5.00		4.11	78.93	0.44		40.35	172.43	0.18	
Closure																	

* North and east are positive. Rotation angles are positive counterclockwise. Lat, latitude; Long, longitude.

** Partial uncertainty rotations interpolated between those for anomalies 13 and 21.

*** Partial uncertainty rotations extrapolated from those for anomalies 21 and 24.

**** Partial uncertainty rotations interpolated between those for anomalies 24 and 31.

‡ Partial uncertainty rotations for North America-Iberia spreading. Partial uncertainty poles are the same as those for anomaly34 rotation, with twice the angle.

TABLE 4.42. Partial Uncertainty Rotations for Africa-North America

	End Points of Plate Boundaries and Azimuth of Transform Faults					Skewed Fit				Mismatched Fracture Zones				Mismatched Magnetic Anomalies			
Magnetic Anomaly	Lat*	Long*	Lat*	Long*	Azimuth	Lat*	Long*	Angle, deg	Angle, km	Lat*	Long*	Angle, deg	Angle, km	Lat*	Long*	Angle, deg	Angle, km
05**						30.42	-40.23	0.32	36	-8.63	44.66	0.09	10	58.12	120.54	0.036	4
06	23.66	-47.89	37.48	-35.52	104	30.72	-42.15	0.41	46	-12.00	40.59	0.09	10	56.53	111.83	0.036	4
13	24.44	-49.93	37.53	-37.16	105	31.13	-43.99	0.42	47	-12.80	38.12	0.09	10	55.77	108.61	0.036	4
18‡						31.30	-45.00	0.63	70	-13.18	36.81	0.13	15	55.43	106.95	0.072	8
21	21.80	-52.70	33.52	-46.30	098	27.70	-49.67	0.63	71	-7.08	36.59	0.13	15	61.26	113.51	0.045	5
25	21.90	-54.65	33.77	-48.23	085	27.87	-51.62	0.71	79	4.42	40.72	0.09	10	61.72	138.98	0.045	5
30-31‡						27.46	-51.18	0.48	53	2.58	40.16	0.13	15	62.40	135.12	0.09	10
34	18.05	-60.92	37.60	-46.28	115	28.02	-54.27	0.35	39	-21.91	23.37	0.13	15	53.14	80.94	0.045	5
M0	29.00	-66.53	40.04	-51.42	125	34.75	-59.48	0.93	104 (15)	-28.12	8.76	0.13	15	42.30	69.67	0.13	15
M04	29.02	-67.55	40.03	-52.60	125	34.75	-60.57	0.94	105 (15)	-28.12	7.67	0.13	15	42.30	68.58	0.13	15
M11	29.02	-68.03	40.04	-53.67	112	34.74	-61.33	0.96	107 (15)	-17.93	15.70	0.13	15	49.63	83.33	0.13	15
M16	29.00	-69.27	40.42	-54.43	112	34.93	-62.37	0.93	103 (15)	-17.88	14.61	0.13	15	49.47	82.43	0.13	15
M21	29.00	-70.60	41.70	-52.60	112	35.68	-62.32	0.80	89 (15)	-17.71	14.42	0.13	15	48.86	97.02	0.13	15
M25	29.31	-72.03	41.90	-56.00	122	35.87	-64.65	0.86	96 (15)	-25.43	5.24	0.13	15	43.41	68.51	0.13	15
Closure																	

Source for the partial uncertainty rotations for anomalies 05, 06, 13, 18, 21, 25, 30-31 and 34 is Stock and Molnar [1988].

* North and east are positive. Rotation angles are positive counterclockwise. Lat, latitude; Long, longitude.

** Best pole and angle interpolated (by time scale) between values for anomaly 05 (center) and anomaly 06; partial uncertainty rotations rotated from anomaly 05 (center) [Stock and Molnar, 1988].

‡ Partial uncertainty rotations interpolated between those of neighboring anomalies.

TABLE 4.43. Partial Uncertainty Rotations for Africa-South America

Magnetic Anomaly	End Points of Plate Boundaries and Azimuth of Transform Faults					Skewed Fit				Mismatched Fracture Zones				Mismatched Magnetic Anomalies			
	Lat*	Long*	Lat*	Long*	Azimuth	Lat*	Long*	Angle, deg	Angle, km	Lat*	Long*	Angle, deg	Angle, km	Lat*	Long*	Angle, deg	Angle, km
05	-17.80	-14.90	-50.80	-9.50	078	-34.33	-12.76	0.63	70	9.89	70.40	0.22	25	53.88	-33.41	0.13	15
06	-19.20	-17.25	-49.85	-14.90	080	-34.53	-16.29	1.02	113	8.22	68.00	0.22	25	54.22	-33.57	0.22	25
13	-29.60	-20.05	-50.85	-18.20	082	-40.23	-19.28	1.46	162	6.10	65.53	0.22	25	49.12	-31.56	0.16	18
18						-35.61	-20.46	1.38	154	4.17	66.54	0.33	37	54.07	-29.24	0.20	22
21						-35.64	-22.80	1.15	128	3.88	64.40	0.28	31	54.08	-30.97	0.16	18
25						-35.65	-24.09	1.38	154	3.71	63.23	0.33	37	54.10	-31.91	0.20	22
30-31						-31.05	-29.46	1.16	130	3.47	58.45	0.28	31	58.71	-37.27	0.19	21
34	-16.28	-31.45	-47.70	-39.15	090	-32.05	-34.63	0.65	72	0.00	55.37	0.22	25	57.95	-34.63	0.09	10
M0	-49.97	-36.18	-51.78	-36.96	087	-50.88	-36.56	10.97	1222 (20)	1.89	51.11	0.18	20	39.06	-40.43	0.18	20
M04	-49.96	-37.99	-51.38	-38.86	087	-50.67	-38.42	13.51	1505 (20)	1.90	49.26	0.18	20	39.26	-42.29	0.18	20
Closure (M11)†						-50.52	-39.58	15.82		1.90	49.51	0.18		39.17	-41.38	0.18	

Source for the partial uncertainty rotations for anomalies 05, 06, 13, 18, 21, 25, 30-31 and 34 is Pardo-Casas and Molnar [1987].

* North and east are positive. Rotation angles are positive counterclockwise. Lat, latitude; Long, longitude.

† Partial uncertainty rotations extrapolated from those for anomalies M0 and M04.

TABLE 4.44. Partial Uncertainty Rotations for South America–Antarctica

	End Points of Plate Boundaries and Azimuth of Transform Faults					Skewed Fit				Mismatched Fracture Zones				Mismatched Magnetic Anomalies			
Magnetic Anomaly	Lat*	Long*	Lat*	Long*	Azimuth	Lat*	Long*	Angle, deg	Angle, km	Lat*	Long*	Angle, deg	Angle, km	Lat*	Long*	Angle, deg	Angle, km
05						38.28	-165.27	0.75		-1.20	-76.22	0.39		51.69	12.25	0.23	
06						36.12	-173.86	1.15		14.18	-73.24	0.49		50.33	34.50	0.28	
13						41.69	-157.62	2.08		10.99	-57.67	0.69		46.23	44.02	0.27	
18						38.81	-153.48	2.00		11.71	-53.88	0.79		48.79	49.82	0.44	
21						39.22	-149.70	1.81		15.15	-46.93	0.70		46.82	59.84	0.47	
25						26.82	-172.96	1.45		27.99	-172.96	0.39		49.38	60.91	0.37	
30-31						48.51	-159.29	2.50		41.09	11.22	0.92		4.72	105.35	0.52	
34						48.96	-158.80	1.32		41.03	21.99	0.54		-0.39	111.65	0.29	
M0						5.12	-140.85	10.98		83.55	-178.38	0.65		-3.91	128.80	0.26	
M04						-8.42	-132.65	13.51		80.71	-157.75	0.66		-3.88	136.77	0.23	
M11						-12.30	-133.24	15.77		62.03	-67.48	0.85		24.70	142.51	1.19	

All partial uncertainty rotations were calculated from other boundaries in the South Atlantic Ocean.

* North and east are positive. Rotation angles are positive counterclockwise. Lat, latitude; Long, longitude.

TABLE 4.45. Partial Uncertainty Rotations for Nazca-Pacific

	End Points of Plate Boundaries and Azimuth of Transform Faults					Skewed Fit				Mismatched Fracture Zones				Mismatched Magnetic Anomalies			
Magnetic Anomaly	Lat*	Long*	Lat*	Long*	Azimuth	Lat*	Long*	Angle, deg	Angle, km	Lat*	Long*	Angle, deg	Angle, km	Lat*	Long*	Angle, deg	Angle, km
05	2.94	-108.64	-32.27	-122.37	N105E	-14.77	-114.93	2.79	311	-14.49	-21.02	0.90	100	69.07	-68.50	0.90	100
06	3.47	-115.09	-31.15	-130.34	N99E	-13.96	-122.13	5.58	622	-8.73	-29.94	1.80	200	73.44	-88.84	1.80	200
13	-13.94	-134.45	-31.36	-136.70	N80E	-23.65	-135.63	0.79	88	9.15	-49.68	0.90	100	64.44	-159.36	0.13	15
18**						-24.81	-143.44	1.58	176	9.69	-57.97	1.80	200	63.12	-167.67	0.26	30
21**						-25.95	-152.12	1.58	176	9.25	-66.67	1.80	200	62.22	-174.69	0.26	30
25**						-28.12	-157.82	1.58	176	12.72	-74.75	1.80	200	58.65	173.50	0.26	30
30-31**						-30.26	-164.00	1.58	176	13.75	-82.22	1.80	200	56.14	166.39	0.26	30
34**						-34.52	-173.45	1.58	176	17.02	-95.61	1.80	200	50.37	152.70	0.26	30

Source for the partial uncertainty rotations for anomalies 05, 06, and 13 is Pardo-Casas and Molnar [1987].

* North and east are positive. Rotation angles are positive counterclockwise. Lat, latitude; Long, longitude.

** Partial uncertainty rotation axes were rotated from anomaly 13, with angle value doubled to reflect additional uncertainty in these interpolated poles.

TABLE 4.46. Partial Uncertainty Rotations for Australia-Lord Howe Rise

	End Points of Plate Boundaries and Azimuth of Transform Faults					Skewed Fit				Mismatched Fracture Zones				Mismatched Magnetic Anomalies			
Magnetic Anomaly	Lat*	Long*	Lat*	Long*	Azimuth	Lat*	Long*	Angle, deg	Angle, km	Lat*	Long*	Angle, deg	Angle, km	Lat*	Long*	Angle, deg	Angle, km
25	†	†	†	†		-40.30	157.06	1.73	20	18.19	-129.12	0.18	20	-44.09	-57.69	0.18	20
30-31	‡	‡	‡	‡		-39.20	157.96	2.36	20	27.16	-136.78	0.18	20	-38.76	-71.11	0.18	20
34	**	**	**	**		-38.28	158.69	3.39		20.67	-131.11	0.18		-42.79	-61.58	0.18	
Closure																	

Source for the partial uncertainty rotations for anomalies 25 and 30-31 is Stock and Molnar [1988].

* North and east are positive. Rotation angles are positive counterclockwise. Lat, latitude; Long, longitude.

† Partial uncertainty rotation axes have been rotated from anomaly 28 [Stock and Molnar, 1988].

‡ Partial uncertainty rotation axes have been rotated from anomaly 32 [Stock and Molnar, 1988].

** Partial uncertainty rotations were extrapolated from those for anomalies 25 and 30-31.

TABLE 4.47. Partial Uncertainty Rotations for reconstructions of anomalies on the Pacific plate formed by Pacific-Farallon spreading

	End Points of Plate Boundaries and Azimuth of Transform Faults					Skewed Fit				Mismatched Fracture Zones				Mismatched Magnetic Anomalies			
Rotation	Lat*	Long*	Lat*	Long*	Azimuth	Lat*	Long*	Angle, deg	Angle, km	Lat*	Long*	Angle, deg	Angle, km	Lat*	Long*	Angle, deg	Angle, km
00-05***						18.39	-118.02	1.32		8.54	-25.16	0.36		-69.59	-91.37	0.36	
05-06**	34.02	-121.22	2.72	-115.37	81	18.39	-118.02	0.66	73 (20)	8.54	-25.16	0.18	20	-69.59	-91.37	0.18	20
06-13**	40.15	-131.59	-9.52	-127.53	80	15.32	-129.30	0.43	47 (20)	9.64	-36.63	0.18	20	-71.77	-95.59	0.18	20
13-18†						33.46	-131.55	0.36		8.33	-36.00	0.18		-55.24	-113.81	0.18	
18-21†						33.50	-135.62	0.36		8.74	-39.78	0.18		-55.08	-117.06	0.18	
21-25†						33.75	-141.00	0.36		11.60	-43.11	0.18		-53.78	-116.83	0.18	
25-30-31†						33.78	-145.23	0.36		11.60	-47.34	0.18		-53.75	-121.08	0.18	
30-31-34‡						41.42	-154.01	1.21		14.13	-51.18	0.18		-45.15	-126.52	0.18	
34-M0**	44.15	164.18	5.10	191.26	68	25.22	179.96	0.46	51 (20)	19.81	-80.27	0.18	20	-57.01	-136.57	0.18	20
M0-M04**	42.94	162.14	5.23	189.61	70	24.69	178.01	0.47	52 (20)	18.10	-83.34	0.18	20	-58.62	-140.93	0.18	20
M04-M11**	39.78	160.67	5.12	187.67	50	23.01	175.94	0.50	55 (20)	36.27	-75.90	0.18	20	-44.84	-119.04	0.18	20
M11-M16**	34.87	156.85	14.86	183.71	43	25.47	171.40	0.66	74 (20)	41.32	-73.84	0.18	20	-38.00	-120.45	0.18	20
M16-M21**	30.76	158.14	13.30	181.12	40	22.43	170.35	0.76	84 (20)	45.08	-75.19	0.18	20	-36.45	-117.40	0.18	20
M21-M25**	28.78	156.76	14.64	173.74	38	21.93	165.67	0.98	109 (20)	46.97	-78.78	0.18	20	-34.83	-120.59	0.18	20

* North and east are positive. Rotation angles are positive counterclockwise. Lat, latitude; Long, longitude.

**End points of plate boundaries were taken as the end points of the respective isochrons.

*** Partial uncertainty poles are the same as those for the 05-06 rotation with twice the angle.

†Source is Rosa and Molnar [1988] (Chapter 2, Table 2.5). Method used to calculate uncertainties is that developed by Stock and Molnar [1983] and modified slightly by Molnar and Stock [1985] (Figure 2.2a).

‡Partial uncertainty rotations are the same as those for the rotation 30-31-32, as calculated by Rosa and Molnar [1988]. Variation of the method outlined by Stock and Molnar [1983] (Figure 2.2b).

TABLE 4.48. Partial Uncertainty Rotations for reconstructions of anomalies on the Pacific plate formed by Pacific-Vancouver spreading

	End Points of Plate Boundaries and Azimuth of Transform Faults					Skewed Fit				Mismatched Fracture Zones				Mismatched Magnetic Anomalies			
Rotation	Lat*	Long*	Lat*	Long*	Azimuth	Lat*	Long*	Angle, deg	Angle, km	Lat*	Long*	Angle, deg	Angle, km	Lat*	Long*	Angle, deg	Angle, km
00-05**	53.11	-133.08	40.14	-131.05	88	46.63	-131.94	1.58	176 (20)	1.37	-40.49	0.18	20	-43.34	-129.19	0.18	20
05-06**	55.86	-135.54	39.93	-135.88	88	47.89	-135.74	1.29	144 (20)	1.34	-44.25	0.18	20	-42.07	-133.04	0.18	20
06-13**	59.38	-142.80	38.53	-131.57	89	49.08	-135.99	0.94	105 (20)	0.65	-45.24	0.18	20	-40.91	-134.67	0.18	20
13-18						48.99	-148.31	1.31		0.98	-57.17	0.18		-40.99	-146.32	0.18	
18-21						48.13	-143.93	1.60		1.00	-52.81	0.18		-41.86	-141.92	0.18	
21-25**	51.01	-157.43	38.24	-141.34	73	44.90	-148.49	1.21	135 (20)	11.95	-46.31	0.18	20	-42.63	-125.07	0.18	20

Partial source for this table is Rosa and Molnar [1988] (Chapter 2, Table 2.6).

* North and east are positive. Rotation angles are positive counterclockwise. Lat, latitude; Long, longitude.

**End points of plate boundaries were taken as the end points of the respective isochrons.

Method used to calculate uncertainties is that developed by Stock and Molnar [1983] and modified slightly by Molnar and Stock [1985] (Figure 2.2a).

TABLE 4.49. Partial Uncertainty Rotations for reconstructions of anomalies on the Pacific plate formed by Pacific-Kula spreading

	End Points of Plate Boundaries and Azimuth of Transform Faults					Skewed Fit				Mismatched Fracture Zones				Mismatched Magnetic Anomalies			
Rotation	Lat*	Long*	Lat*	Long*	Azimuth	Lat*	Long*	Angle, deg	Angle, km	Lat*	Long*	Angle, deg	Angle, km	Lat*	Long*	Angle, deg	Angle, km
22-25**	51.01	-157.43	48.38	-185.36	179	50.54	-171.78	1.14	127 (20)	39.45	9.52	0.18	20	0.63	-81.01	0.18	20
25–30-31						48.66	-171.25	1.75		41.34	8.75	0.18		0.00	-81.25	0.18	20
30-31–34***						47.26	-169.50	2.73		42.74	10.49	0.25		0.00	-79.50	0.36	
34-M0**	44.15	164.18	42.84	147.83	157	43.79	155.92	1.73	193 (20)	41.65	7.44	0.18	20	16.38	-97.72	0.18	20
M0-M4**	42.94	162.14	42.39	147.42	157	42.90	154.75	1.90	212 (20)	42.40	6.69	0.18	20	16.63	-99.14	0.18	20
M4-M11**	39.78	160.67	38.34	144.15	142	39.35	152.32	1.60	178 (20)	37.54	23.26	0.18	20	28.43	-91.32	0.18	20
M11-M16**	34.87	156.85	33.69	142.05	166	34.50	149.40	1.68	187 (20)	53.09	6.85	0.18	20	11.50	-112.56	0.18	20
M16-M21**	30.76	158.14	28.80	143.06	155	29.99	150.53	1.56	174 (20)	51.71	13.53	0.18	20	21.47	-106.35	0.18	20
M21-M25**	28.78	156.76	24.00	143.92	155	26.53	150.21	1.66	184 (20)	54.18	16.44	0.18	20	22.22	-108.03	0.18	20

Partial source for this table is Rosa and Molnar [1988] (Chapter 2, Table 2.7).

*North and east are positive. Rotation angles are positive counterclockwise. Lat, latitude; Long, longitude.

**End points of plate boundaries were taken as the end points of the respective isochrons.

***Partial uncertainty rotations are the same as those for the rotation 30-31–32, as calculated by Rosa and Molnar [1988].

Method used to calculate uncertainties is that developed by Stock and Molnar [1983] and modified slightly by Molnar and Stock [1985] (Figure 2.2a).

TABLE 4.50. Partial Uncertainty Rotations for India-Australia

	End Points of Plate Boundaries and Azimuth of Transform Faults					Skewed Fit				Mismatched Fracture Zones				Mismatched Magnetic Anomalies			
Magnetic Anomaly	Lat*	Long*	Lat*	Long*	Azimuth	Lat*	Long*	Angle, deg	Angle,† km	Lat*	Long*	Angle, deg	Angle, km	Lat*	Long*	Angle, deg	Angle, km
21	-11.99	90.19	-2.26	98.46	0	-7.14	94.37	1.62	180 (20)	82.86	94.37	0.18	20	0.00	-175.63	0.18	20
25	-17.54	89.79	-7.96	98.36	0	-12.78	94.16	1.62	181 (20)	77.21	94.16	0.18	20	0.00	-175.84	0.18	20
30-31	-25.26	89.08	-6.20	101.41	0	-15.82	95.54	0.92	103 (20)	74.18	95.54	0.18	20	0.00	-174.46	0.18	20
34	-23.63	90.76	-12.08	104.05	0	-17.97	97.62	1.21	134 (20)	72.03	97.62	0.18	20	0.00	-172.38	0.18	20

* North and east are positive. Rotation angles are positive counterclockwise. Lat, latitude; Long, longitude.

† Values in parentheses give overlap or underlap in kilometers of end points of the plate boundary.

TABLE 4.51. Partial Uncertainty Rotations for Madagascar-Africa

	End Points of Plate Boundaries and Azimuth of Transform Faults					Skewed Fit				Mismatched Fracture Zones				Mismatched Magnetic Anomalies			
Magnetic Anomaly	Lat*	Long*	Lat*	Long*	Azimuth	Lat*	Long*	Angle, deg	Angle, km	Lat*	Long*	Angle, deg	Angle, km	Lat*	Long*	Angle, deg	Angle, km
M0**	-2.98	49.61	-7.61	41.43	1.	-5.31	45.53	4.40	490 (40)	84.60	56.22	0.36	40	-1.00	135.63	0.36	40
M4**	-2.22	49.65	-6.86	41.40	1.	-4.55	45.54	4.36	486 (40)	85.34	57.94	0.36	40	-1.00	135.62	0.36	40
M11**	-0.97	49.77	-5.61	41.36	1.	-3.30	45.57	4.29	478 (40)	86.55	62.45	0.36	40	-1.00	135.63	0.36	40
M16**	-0.10	49.91	-4.51	41.32	1.	-2.21	45.62	4.23	471 (40)	87.57	69.96	0.36	40	-1.00	135.66	0.36	40
M21**	1.03	50.00	-4.00	41.29	1.	-1.49	45.65	4.10	457 (40)	88.21	79.53	0.36	40	-1.00	135.68	0.36	40
Closure																	

* North and east are positive. Rotation angles are positive counterclockwise. Lat, latitude; Long, longitude.

** End points of plate boundaries taken from the respective isochrons used in this study. The isochrons were taken or interpolated from Cochran [1988].

Appendix D
Chapter 6 Tables

TABLE 6.1. Area measurements for the present time.

Areas for the age interval from the present to anomaly 5 time (0 to 10.59 Ma).

	Calculated Area	Positive Uncertainty	Negative Uncertainty	Nature of Area
	746604	10843	-10821	Africa-North America spreading
	3049831	192519	-192639	Africa-South America spreading
	755783	86671	-86672	Antarctica-Africa spreading
	3966869	99587	-99570	Antarctica-Australia spreading
	1206664	56166	-56169	Antarctica-India spreading
	755885	90026	-90095	Greenland-Europe spreading
	776391	38900	-38880	India-Africa spreading
	799766	27062	-26892	Nazca-Antarctica spreading
	450335	14276	-14261	North America-Europe spreading
	711381	76099	-76136	Pacific-Antarctica spreading
	2990109	70595	-70646	Pacific-Bellingshausen spreading
	576768	27636	-27823	Pacific-Vancouver spreading
	1493605	57709	-62355	Pacific-Farallon spreading
	5200005	291002	-289356	Nazca-Pacific spreading
	163777	58608	-58392	South America-Antarctica spreading
	1054062			Galapagos Region (Nazca-Cocos)
	3400000			Marginal Basins
	425475			Red Sea
	156242			South part of Red Sea
	116132	12280	-12280	Antarctica-Aluk †
TOTAL	28795684	1468580	-1468580	
dA/dt	2719139			

† Estimated uncertainties.

TABLE 6.2. Area measurements for the present time.

Areas for the age interval from anomaly 5 time to anomaly 6 time (10.59 Ma to 19.90 Ma).

	Calculated Area	Positive Uncertainty	Negative Uncertainty	Location of Area
	679260	11309	-11306	Africa-North America spreading
	2915827	297155	-297277	Africa-South America spreading
	568440	84204	-84195	Antarctica-Africa spreading
	3051875	101079	-101292	Antarctica-Australia spreading
	1110528	90080	-90431	Antarctica-India spreading
	675768	84748	-84609	Greenland-Europe spreading
	577351	31244	-377393	India-Africa spreading
	837071	213511	-203545	Nazca-Antarctica spreading
	497381	31230	-31178	North America-Europe spreading
	654304	43421	-43481	Pacific-Antarctica spreading
	1784089	66072	-65771	Pacific-Bellingshausen spreading
	455346	33565	-33585	Pacific-Vancouver spreading
	1905196	88795	-106207	Pacific-Farallon spreading
	3870664	544021	-277287	Nazca-Pacific spreading
	134794	69425	-69551	South America-Antarctica spreading
	2100000			Marginal Basins
	278763	17530	-17530	Antarctica-Aluk †
TOTAL	22096657	1988699	-2099182	
dA/dt	2373432			

† Estimated uncertainties.

TABLE 6.3. Area measurements for the present time.

Areas for the age interval from anomaly 6 time to anomaly 13 time (19.90 Ma to 35.58 Ma).

	Calculated Area	Positive Uncertainty	Negative Uncertainty	Location of Area
	1020389	11193	-11191	Africa-North America spreading
	4963792	525199	-525977	Africa-South America spreading
	1138158	79931	-79888	Antarctica-Africa spreading
	5184735	99096	-98448	Antarctica-Australia spreading
	1332697	118225	-25820	Antarctica-India spreading
	618392	125428	-124827	Greenland-Europe spreading
	43532	207511	-154426	India-Africa spreading
	547884	20439	-20428	North America-Europe spreading
	635814	101217	-101113	Pacific-Antarctica spreading
	2396783	60574	-60324	Pacific-Bellingshausen spreading
	1297182	43595	-43625	Pacific-Vancouver spreading
	5131220	96883	-96987	Pacific-Farallon spreading
	5336500	95985	-95780	Nazca-Pacific spreading
	272470	134771	-135104	South America-Antarctica spreading
	7500000			Marginal Basins
	277886	23650	-23650	Antarctica-Aluk †
	392594	23480	-23480	Antarctica-Farallon †
	334085	18060	-18060	Nazca-Antarctica †
TOTAL	38424113	2228598	-2036478	
dA/dt	2450517			

† Estimated uncertainties.

TABLE 6.4. Area measurements for the present time.

Areas for the age interval from anomaly 13 time to anomaly 18 time (35.58 Ma to 42.01 Ma).

	Calculated Area	Positive Uncertainty	Negative Uncertainty	Location of Area
	558452	22148	-22137	Africa-North America spreading
	2103914	429708	-422670	Africa-South America spreading
	551016	143105	-143087	Antarctica-Africa spreading
	1473112	163793	-163771	Antarctica-Australia spreading
	533787	112289	-85093	Antarctica-India spreading
	711417	123410	-123063	Greenland-Europe spreading
	518109	286105	-309960	India-Africa spreading
	288386	22942	-22943	North America-Europe spreading
	201057	39076	-39100	Pacific-Antarctica spreading
	731855	49498	-48866	Pacific-Bellingshausen spreading
	678133	40308	-40205	Pacific-Vancouver spreading
	2520884	99503	-99453	Pacific-Farallon spreading
	2330873	93297	-91319	Nazca-Pacific spreading
	128826	167940	-167715	South America-Antarctica spreading
	1480000			Marginal Basins
	115350	18070	-18070	Antarctica-Aluk †
	196185	20940	-20940	Antarctica-Farallon †
TOTAL	15121356	2026262	-2011140	
dA/dt	2351688			

† Estimated uncertainties.

TABLE 6.5. Area measurements for the present time.

Areas for the age interval from anomaly 18 time to anomaly 21 time (42.01 Ma to 49.55 Ma).

	Calculated Area	Positive Uncertainty	Negative Uncertainty	Location of Area
	607234	16784	-16757	Africa-North America spreading
	3317116	349268	-349084	Africa-South America spreading
	572440	159119	-159223	Antarctica-Africa spreading
	1357693	328885	-330471	Antarctica-Australia spreading
	723067	220619	-214236	Antarctica-India spreading
	442260	123960	-123400	Greenland-Europe spreading
	196886	70541	-69212	Greenland-North America spreading
	2122460	214261	-209859	India-Africa spreading
	350776	25044	-24975	North America-Europe spreading
	552914	81872	-81987	Pacific-Antarctica spreading
	827109	40168	-40606	Pacific-Bellingshausen spreading
	598625	38036	-37996	Pacific-Vancouver spreading
	2740674	98255	-98186	Pacific-Farallon spreading
	2077696	91290	-89175	Nazca-Pacific spreading
	136601	9727	-39768	India-Australia spreading
	78660	154917	-155036	South America-Antarctica spreading
	1700000			Marginal Basins
	176578	19870	-19870	Antarctica-Aluk †
	241765	21680	-21680	Antarctica-Farallon †
	14331	7220	-7220	Pacific-Aluk †
	163959	14460	-14460	Pacific-Antarctica †
TOTAL	18998844	2298860	-2317859	
dA/dt	2519741			

† Estimated uncertainties.

TABLE 6.6. Area measurements for the present time.

Areas for the age interval from anomaly 21 time to anomaly 25 time (49.55 Ma to 58.94 Ma).

	Calculated Area	Positive Uncertainty	Negative Uncertainty	Location of Area
	781483	16966	-16963	Africa-North America spreading
	1915020	435746	-428272	Africa-South America spreading
	822631	68608	-68901	Antarctica-Africa spreading
	318278	341037	-340107	Antarctica-Australia spreading
	204345	34472	-34478	Australia-Lord Howe Rise spreading
	197368	55749	-55855	Greenland-North America spreading
	1052401	41692	-42136	India-Africa spreading
	722271	17390	-17378	North America-Europe spreading
	516411	69719	-69566	Pacific-Antarctica spreading
	885557	31762	-31666	Pacific-Bellingshausen spreading
	159677	18055	-18208	Pacific-Kula spreading
	3205335	133541	-133570	Pacific-Farallon spreading
	684335	13849	-14044	India-Australia spreading
	154875	85817	-86756	South America-Antarctica spreading
	1870000			Marginal Basins
	596081	122437	-119605	Nazca-Pacific
	1020545	123960	-123400	Greenland-Europe ‡
	255684	21680	-21680	Antarctica-Aluk †
	230559	20780	-20780	Pacific-Aluk †
	79789	9030	-9030	Pacific-Antarctica †
	89286	11750	-11750	Pacific-Farallon †
	955358	38520	-38520	Antarctica-India †
	340182	16970	-16970	Antarctica-India †
TOTAL	17057471	1944552	-1927494	
dA/dt	1816557			

TABLE 6.7. Area measurements for the present time.

Areas for the age interval from anomaly 25 time anomaly 30-31 time (58.94 Ma to 68.47 Ma)

	Calculated Area	Positive Uncertainty	Negative Uncertainty	Location of Area
	799560	23801	-23827	Africa-North America spreading
	2297438	310291	-306299	Africa-South America spreading
	695612	162528	-162266	Antarctica-Africa spreading
	291084	321589	-322467	Antarctica-Australia spreading
	741626	32256	-32293	Australia-Lord Howe Rise spreading
	198230	55990	-54509	Greenland-North America spreading
	476784	19470	-19502	North America-Iberia, Iberia-Europe, and North America
	1142287	68376	-67974	Pacific-Antarctica spreading
	1288226	26628	-26462	Pacific-Bellingshausen spreading
	484678	37522	-37603	Pacific-Kula spreading
	2941000	134687	-134542	Pacific-Farallon spreading
	608978	143127	-139439	Nazca-Pacific spreading
	224986	27908	-27980	India-Australia spreading
	1303292	407568	-409217	South America-Antarctica spreading
	2420000			Marginal Basins
	1010506	32180	-32180	South America-Antarctica (Weddell Sea)
	255363	11790	-11790	Africa-South America
	293689	25110	-25110	Antarctica-Aluk †
	241341	20420	-20420	Pacific-Aluk †
	154108	16270	-16270	Pacific-Antarctica †
	231631	14720	-14720	Antarctica-India †
	2349250	90760	-90760	Antarctica-India †
	2330359	70070	-70070	India-Africa †
	1152944	27680	-27680	India-Africa †
TOTAL	23932972	2321498	-2297565	
dA/dt	2511330			

† Estimated uncertainties.

TABLE 6.8. Area measurements for the present time.

Areas for the age interval from anomaly 30-31 time to anomaly 34 time (68.47 Ma to 84.00 Ma

	Calculated Area	Positive Uncertainty	Negative Uncertainty	Location of Area
	1367430	14015	-14012	Africa-North America spreading
	6190112	174521	-173049	Africa-South America spreading
	1300549	63673	-63458	Antarctica-Africa spreading
	454122	315260	-316260	Antarctica-Australia spreading
	1001567	33277	-33298	Australia-Lord Howe Rise spreading
	298094	56351	-54696	Greenland-North America spreading
	752383	20260	-20150	North America-Iberia, Iberia-Europe, and North America
	1105011	68155	-68118	Pacific-Antarctica spreading
	2501455	34284	-33835	Pacific-Bellingshausen spreading
	705466	54398	-54286	Pacific-Kula spreading
	4659261	346460	-346736	Pacific-Farallon spreading
	297841	183949	-180028	Nazca-Pacific spreading
	569118	203199	-203277	South America-Antarctica spreading
	3830000			Marginal Basins
	560975	28940	-28940	Africa-South America
	298768	17700	-17700	Antarctica-India †
	1752973	53890	-53890	Antarctica-India †
	1383941	44600	-44600	India-Africa †
TOTAL	29029066	1973976	-1973976	
dA/dt	1869225			

† Estimated uncertainties.

TABLE 6.9. Area measurements for the present time.

Areas for the age interval from anomaly 34 time to anomaly M0 time (84.00 Ma to 118.35 Ma).

	Calculated Area	Positive Uncertainty	Negative Uncertainty	Location of Area
	4273181	41870	-41818	Africa-North America spreading
	5148197	94064	-94061	Africa-South America spreading
	2333685	56356	-68408	Antarctica-Africa spreading
	636297	70292	-72039	North America-Iberia spreading
	1337215	35593	-35920	Pacific-Kula spreading
	10971625	119393	-119118	Pacific-Farallon spreading
	1363552	477514	-476777	South America-Antarctica spreading
	14235547	711777	-711777	Pac-Phoe-Naz-Bell-Ant spreading **
	720000			Marginal Basins
	56600	8050	-8050	Greenland-North America spreading †
	842059	46960	-46960	North America-Europe spreading †
	6626430	174521	-174521	Africa-South America spreading ‡
	138384	12500	-12500	Africa-South America spreading †
	3418472	58980	-58980	Antarctica-India spreading †
	3712548	91150	-91150	Antarctica-Australia spreading †
	82041	22290	-22290	Pacific-Antarctica spreading †
	441515	22280	-22280	Pacific-Bellingshausen spreading †
	1466227	146623	-146623	Indian Ocean **
	372181	37218	-37218	Antarctica-Australia spreading **
	1699886	26180	-26180	Antarctica-India spreading ‡
	384559	16638	-16638	Australia-Lord Howe Rise spreading ‡
	270681	19650	-19650	India-Africa spreading ‡
	982789	32420	-32420	India-Australia spreading (NW Australia) †
	1190618	35910	-35910	India-Australia spreading (NW Australia) †
TOTAL	62704289	2382763	-2382763	
dA/dt	1825452			

† Estimated uncertainties.

‡ Same as 30-31–34 uncertainties.

** Uncertainties arbitrarily assigned.

TABLE 6.10. Area measurements for the present time.

Areas for the age interval from anomaly M0 time to anomaly M4 time (118.35 Ma to 125.91 Ma).

	Calculated Area	Positive Uncertainty	Negative Uncertainty	Location of Area
	499886	42934	-42920	Africa-North America spreading
	1920065	99656	-99338	Africa-South America spreading
	608804	59620	-60642	Antarctica-Africa spreading
	58983	17340	-17340	North America-Iberia spreading †
	1982607	45350	-45350	Pacific-Phoenix spreading †
	237552	24581	-24635	Pacific-Kula spreading
	1438030	97950	-97906	Pacific-Farallon spreading
	335247	459360	-459654	South America-Antarctica spreading
	660000			Marginal Basins
	751816	43880	-43880	India-Australia (NW Australia) †
TOTAL	8492990	968201	-968201	
dA/dt	1123411			

† Estimated uncertainties.

TABLE 6.11. Area measurements for the present time.

Areas for the age interval from anomaly M4 time to anomaly M11 time (125.91 Ma to 132.78 Ma).

	Calculated Area	Positive Uncertainty	Negative Uncertainty	Location of Area
	245689	40744	-40722	Africa-North America spreading
	486201	82250	-82268	Africa-South America spreading
	406402	63084	-64269	Antarctica-Africa spreading
	1576704	44390	-44390	Pacific-Phoenix spreading †
	464718	27338	-27300	Pacific-Kula spreading
	1382629	96892	-96733	Pacific-Farallon spreading
	301291	601637	-601151	South America-Antarctica spreading
	610000			Marginal Basins
	239185	18400	-18400	North America-Iberia spreading
	320309	13720	-13720	India-Australia (NW Australia) †
	778955	22440	-22440	India-Australia (NW Australia) †
TOTAL	6812083	1110369	-1110369	
dA/dt	991570			

† Estimated uncertainties.

TABLE 6.12. Area measurements for the present time.

Areas for the age interval from anomaly M11 time to anomaly M16 time (132.78 Ma to 141.52 Ma

	Calculated Area	Positive Uncertainty	Negative Uncertainty	Location of Area
	528502	40899	-40904	Africa-North America spreading
	431529	65362	-66471	Antarctica-Africa spreading
	1389700	41530	-41530	Pacific-Phoenix spreading †
	546569	31147	-31166	Pacific-Kula spreading
	1205968	85124	-85005	Pacific-Farallon spreading
	610000			Marginal Basins
	546816	27240	-27240	South America-Antarctica spreading (Weddell Sea)
	15983	3250	-3250	India-Australia (NW Australia) †
TOTAL	5275067	332329	-332329	
dA/dt	603555			

† Estimated uncertainties.

TABLE 6.13. Area measurements for the present time.
Areas for the age interval from anomaly M16 time to anomaly M21 time (141.52 Ma to 149.65 Ma).

	Calculated Area	Positive Uncertainty	Negative Uncertainty	Location of Area
	547731	15774	-37809	Africa-North America spreading
	450012	67384	-68486	Antarctica-Africa spreading
	1266588	41530	-41530	Pacific-Phoenix spreading †
	594973	28769	-28785	Pacific-Kula spreading
	332990	64439	-64749	Pacific-Farallon spreading
	100459	8740	-8740	India-Australia spreading (NW Australia) †
TOTAL	3292753	226636	-250099	
dA/dt	405013			

† Estimated uncertainties.

TABLE 6.14. Area measurements for the present time.
Areas for the age interval from anomaly M21 time to anomaly M25 time (149.65 Ma to 156.42 Ma).

	Calculated Area	Positive Uncertainty	Negative Uncertainty	Location of Area
	883465	43031	-43033	Africa-North America spreading
	2204727	36750	-36750	Pacific-Phoenix spreading †
	568584	29718	-29618	Pacific-Kula spreading
	682163	55870	-55747	Pacific-Farallon spreading
	848721	84872	-84872	Indian Ocean **
	194535	11980	-11980	India-Australia (NW Australia) †
TOTAL	5382195	262221	-262000	
dA/dt	795007			

† Estimated uncertainties.

** Uncertainties arbitrarily assigned.

TABLE 6.15. Area measurements for the present time.
Areas with age older than anomaly M25 time (156.42 Ma to 180.0 Ma).

	Calculated Area	Positive Uncertainty	Negative Uncertainty	Location of Area
	9025140	451257	-451257	Pac-Far-Kul-Pho spreading **
	2216272	63040	-63040	Africa-North America spreading †
	66163	7740	-7740	India-Australia (NW Australia) †
TOTAL	11307575	522037	-522037	
dA/dt	479541			

† Estimated uncertainties.

** Uncertainties arbitrarily assigned.

TABLE 6.16. Area measurements for the anomaly 13 time (35.58 Ma).
Areas for the age interval from anomaly 13 time to anomaly 18 time (0.00 to 6.43 Ma).

	Calculated Area	Positive Uncertainty	Negative Uncertainty	Location of Area
	558452	22148	-22137	Africa-North America spreading
	2103914	429708	-422670	Africa-South America spreading
	551016	143105	-143087	Antarctica-Africa spreading
	1473112	163793	-163771	Antarctica-Australia spreading
	533787	112289	-85093	Antarctica-India spreading
	711417	123410	-123063	Greenland-Europe spreading
	518109	286105	-309960	India-Africa spreading
	288386	22942	-22943	North America-Europe spreading
	201057	39076	-39100	Pacific-Antarctica spreading
	731855	49498	-48866	Pacific-Bellingshausen spreading
	1480000			Marginal Basins
	1895781	80267	-80308	Pacific-Farallon spreading (Pacific Plate)
	1408478	22362	-33459	Pacific-Farallon spreading (Farallon Plate)
	2633371	147705	-154267	Nazca-Pacific spreading
	617732	13637	-13604	Pacific-Vancouver spreading (Vancouver Plate)
	745084	14982	-15208	Pacific-Vancouver spreading (Pacific Plate)
	566642	407056	-406772	South America-Antarctica spreading
TOTAL	17018193	2280438	-2280438	
dA/dt	2646686			

TABLE 6.17. Area measurements for the anomaly 13 time (35.58 Ma).
Areas for the age interval from anomaly 18 time to anomaly 21 time (6.43 Ma to 13.97 Ma).

	Calculated Area	Positive Uncertainty	Negative Uncertainty	Location of Area
	607234	16784	-16757	Africa-North America spreading
	3317116	349268	-349084	Africa-South America spreading
	572440	159119	-159223	Antarctica-Africa spreading
	1357693	328885	-330471	Antarctica-Australia spreading
	723067	220619	-214236	Antarctica-India spreading
	442260	123960	-123400	Greenland-Europe spreading
	196886	70541	-69212	Greenland-North America spreading
	2122460	214261	-209859	India-Africa spreading
	350776	25044	-24975	North America-Europe spreading
	552914	81872	-81987	Pacific-Antarctica spreading
	827109	40168	-40606	Pacific-Bellingshausen spreading
	1700000			Marginal Basins
	2740674	98255	-98186	Pacific-Farallon spreading (Pacific plate)
	1613871	77228	-82731	Pacific-Farallon spreading (Farallon plate)
	3204153	143916	-144029	Nazca-Pacific spreading
	570693	168222	-168053	Pacific-Vancouver spreading (Vancouver plate)
	756493	26391	-26591	Pacific-Vancouver spreading (Pacific plate)
	985766	21720	-21720	Australia-India spreading
	275746	375636	-375618	South America-Antarctica spreading
TOTAL	22917351	2750082	-2750082	
dA/dt	3039436			

† Estimated uncertainties.

TABLE 6.18. Area measurements for the anomaly 13 time (35.58 Ma).
Areas for the age interval from anomaly 21 time to anomaly 25 time (13.97 Ma to 23.36 Ma).

	Calculated Area	Positive Uncertainty	Negative Uncertainty	Location of Area
	781483	16966	-16963	Africa-North America spreading
	1915020	435746	-428272	Africa-South America spreading
	822631	68608	-68901	Antarctica-Africa spreading
	318278	341037	-340107	Antarctica-Australia spreading
	204345	34472	-34478	Australia-Lord Howe Rise spreading
	197368	55749	-55855	Greenland-North America spreading
	1052401	41692	-42136	India-Africa spreading
	722271	17390	-17378	North America-Europe spreading
	516411	69719	-69566	Pacific-Antarctica spreading
	885557	31762	-31666	Pacific-Bellingshausen spreading
	1870000			Marginal Basins
	1020545	123960	-123400	Greenland-Europe spreading ‡
	955358	38520	-38520	Antarctica-India spreading †
	340182	16970	-16970	Antarctica-India spreading †
	3205335	133541	-133570	Pacific-Farallon spreading (Pacific plate)
	1038199	34377	-47039	Pacific-Farallon spreading (Farallon plate)
	1970953	204786	-205175	Nazca-Pacific spreading
	40707	46133	-47301	Pacific-Vancouver spreading (Vancouver plate)
	95687	45220	-45107	Pacific-Vancouver spreading (Vancouver plate)
	827366	41084	-41154	Pacific-Kula spreading
	1789160	45110	-45110	Australia-India spreading †
	47008	64871	-64871	South America-Antarctica spreading
TOTAL	20616265	2102859	-2102859	
dA/dt	2195555			

† Estimated uncertainties.

‡ Same as 18-21 uncertainties.

TABLE 6.19. Area measurements for the anomaly 13 time (35.58 Ma).

Areas for the age interval from anomaly 25 time anomaly 30-31 time (23.36 Ma to 32.89 Ma)

	Calculated Area	Positive Uncertainty	Negative Uncertainty	Location of Area
	799560	23801	-23827	Africa-North America spreading
	2297438	310291	-306299	Africa-South America spreading
	695612	162528	-162266	Antarctica-Africa spreading
	291084	321589	-322467	Antarctica-Australia spreading
	741626	32256	-32293	Australia-Lord Howe Rise spreading
	198230	55990	-54509	Greenland-North America spreading
	476784	19470	-19502	North America-Iberia, Iberia-Europe, and North America
	1142287	68376	-67974	Pacific-Antarctica spreading
	1288226	26628	-26462	Pacific-Bellingshausen spreading
	2420000			Marginal Basins
	255363	11790	-11790	Africa-South America spreading
	154108	16270	-16270	Pacific-Antarctica spreading †
	231631	14720	-14720	Antarctica-India spreading †
	2349250	90760	-90760	Antarctica-India spreading †
	2330359	70070	-70070	India-Africa spreading †
	1152944	27680	-27680	India-Africa spreading
	2941000	134687	-134542	Pacific-Farallon spreading (Pacific plate)
	928223	28632	-41868	Pacific-Farallon spreading (Farallon plate)
	2135982	239767	-240468	Nazca-Pacific spreading
	470647	31460	-31460	Pacific-Kula spreading (Kula plate)
	1949686	46550	-46550	Australia-India spreading
	264439	377039	-377038	South America-Antarctica spreading
	484678	37522	-37603	Pacific-Kula spreading (Pacific plate)
TOTAL	25999157	2365923	-2365923	
dA/dt	2728138			

† Estimated uncertainties.

TABLE 6.20. Area measurements for the anomaly 13 time (35.58 Ma).

Areas for the age interval from anomaly 30-31 time to anomaly 34 time (32.89 Ma to 48.42 Ma

	Calculated Area	Positive Uncertainty	Negative Uncertainty	Location of Area
	1367430	14015	-14012	Africa-North America spreading
	6190112	174521	-173049	Africa-South America spreading
	1300549	63673	-63458	Antarctica-Africa spreading
	454122	315260	-316260	Antarctica-Australia spreading
	1001567	33277	-33298	Australia-Lord Howe Rise spreading
	298094	56351	-54696	Greenland-North America spreading
	752383	20260	-20150	North America-Iberia, Iberia-Europe, and North America
	1105011	68155	-68118	Pacific-Antarctica spreading
	2501455	34284	-33835	Pacific-Bellingshausen spreading
	3830000			Marginal Basins
	560975	28940	-28940	Africa-South America spreading
	298768	17700	-17700	Antarctica-India spreading †
	1752973	53890	-53890	Antarctica-India spreading †
	1383941	44600	-44600	India-Africa spreading †
	4659261	346460	-346736	Pacific-Farallon spreading (Pacific plate)
	1400500	27129	-41176	Pacific-Farallon spreading (Farallon plate)
	2974926	319192	-321053	Nazca-Pacific spreading
	2371726	131576	-102955	Pacific-Kula spreading (Kula plate)
	883116	45590	-45590	Australia-India spreading
	816613	203182	-203068	South America-Antarctica spreading
	705466	54398	-54286	Pacific-Kula spreading (Pacific plate)
TOTAL	36608988	2306366	-2269757	
dA/dt	2357308			

† Estimated uncertainties.

TABLE 6.21. Area measurements for the anomaly 13 time (35.58 Ma).
Areas for the age interval from anomaly 34 time to anomaly M0 time (48.42 Ma to 82.77 Ma).

	Calculated Area	Positive Uncertainty	Negative Uncertainty	Location of Area
	4273181	41870	-41818	Africa-North America spreading
	5148197	94064	-94061	Africa-South America spreading
	2333685	56356	-68408	Antarctica-Africa spreading
	636297	70292	-72039	North America-Iberia spreading
	56600	8050	-8050	Greenland-North America spreading †
	842059	46960	-46960	North America-Europe spreading †
	6626430	174521	-174521	Africa-South America spreading ‡
	138384	12500	-12500	Africa-South America spreading †
	3418472	58980	-58980	Antarctica-India spreading †
	3712548	91150	-91150	Antarctica-Australia spreading †
	82041	22290	-22290	Pacific-Antarctica spreading †
	441515	22280	-22280	Pacific-Bellingshausen spreading †
	1466227	146623	-146623	Indian Ocean **
	372181	37218	-37218	Antarctica-Australia spreading **
	1699886	26180	-26180	Antarctica-India spreading ‡
	384559	16638	-16638	Australia-Lord Howe Rise spreading ‡
	270681	19650	-19650	India-Africa spreading ‡
	6309473	878333	-856316	Nazca-Pacific spreading
	9988487	456058	-457073	Pacific-Kula spreading (Pacific plate)
	10971625	119393	-119118	Pacific-Farallon spreading (Pacific plate)
	19964270	1996427	-1996427	Pac-Far-Ant-Bel-Pho spreading **
	446850	26270	-26270	Australia-India spreading †
	5666850	283342	-283342	Australia-India spreading **
	1781459	472412	-471392	South America-Antarctica spreading
	982789	32420	-32420	Australia-India spreading †
	720000			Marginal Basins
TOTAL	88734746	5235350	-5235350	
dA/dt	2583253			

† Estimated uncertainties.

‡ Same as 30-31–34 uncertainties.

TABLE 6.22. Area measurements for the anomaly 13 time (35.58 Ma).
Areas for the age interval from anomaly M0 time to anomaly M4 time (82.77 Ma to 90.33 Ma).

	Calculated Area	Positive Uncertainty	Negative Uncertainty	Location of Area
	499886	42934	-42920	Africa-North America spreading
	1920065	99656	-99338	Africa-South America spreading
	608804	59620	-60642	Antarctica-Africa spreading
	58983	17340	-17340	North America-Iberia spreading †
	660000			Marginal Basins
	986644	54940	-54940	Pacific-Kula spreading (Pacific plate) †
	4758996	78280	-78280	Pacific-Phoenix spreading (Pacific plate) †
	1438030	97950	-97906	Pacific-Farallon spreading (Pacific plate)
	936320	65542	-65542	Australia-India spreading †
	520778	458308	-462597	South America-Antarctica spreading
TOTAL	12388506	1028246	-1028246	
dA/dt	1638691			

† Estimated uncertainties.

TABLE 6.23. Area measurements for the anomaly 13 time (35.58 Ma).
Areas for the age interval from anomaly M4 time to anomaly M11 time (90.33 Ma to 97.20 Ma).

	Calculated Area	Positive Uncertainty	Negative Uncertainty	Location of Area
	245689	40744	-40722	Africa-North America spreading
	486201	82250	-82268	Africa-South America spreading
	406402	63084	-64269	Antarctica-Africa spreading
	610000			Marginal Basins
	239185	18400	-18400	North America-Iberia spreading
	1098402	28357	-30200	Pacific-Kula spreading (Pacific plate)
	3410940	56196	-76184	Pacific-Phoenix spreading (Pacific plate)
	1382629	96892	-96733	Pacific-Farallon spreading (Pacific plate)
	577007	602359	-601764	South America-Antarctica spreading
	320309	13720	-13720	India-Australia (NW Australia) †
	778955	22440	-22440	India-Australia (NW Australia) †
TOTAL	9555719	1089352	-1118019	
dA/dt	1390934			

† Estimated uncertainties.

TABLE 6.24. Area measurements for the anomaly 13 time (35.58 Ma).

Areas for the age interval from anomaly M11 time to anomaly M16 time (97.20 Ma to 105.94 Ma)

	Calculated Area	Positive Uncertainty	Negative Uncertainty	Location of Area
	528502	40899	-40904	Africa-North America spreading
	431529	65362	-66471	Antarctica-Africa spreading
	610000			Marginal Basins
	1664895	334177	-331478	Pacific-Kula spreading (Pacific plate)
	2684612	27537	-36525	Pacific-Phoenix spreading (Pacific plate)
	1205968	85124	-85005	Pacific-Farallon spreading (Pacific plate)
	546816	27240	-27240	South America-Antarctica spreading (Weddell Se
	15983	3250	-3250	India-Australia (NW Australia) †
TOTAL	7688305	722701	-730389	
dA/dt	879669			

† Estimated uncertainties.

TABLE 6.25. Area measurements for the anomaly 13 time (35.58 Ma).

Areas for the age interval from anomaly M16 time to anomaly M21 time (105.94 Ma to 114.07 Ma).

	Calculated Area	Positive Uncertainty	Negative Uncertainty	Location of Area
	547731	15774	-37809	Africa-North America spreading
	450012	67384	-68486	Antarctica-Africa spreading
	2876898	121158	-118959	Pacific-Kula spreading (Pacific plate)
	2153762	74610	-74610	Pacific-Phoenix spreading (Pacific plate) †
	332990	64439	-64749	Pacific-Farallon spreading (Pacific plate)
	138572	11450	-11450	Australia-India spreading †
TOTAL	6499965	354815	-376063	
dA/dt	799504			

† Estimated uncertainties.

TABLE 6.26. Area measurements for the anomaly 13 time (35.58 Ma).
Areas for the age interval from anomaly M21 time to anomaly M25 time (114.07 Ma to 120.84 Ma).

	Calculated Area	Positive Uncertainty	Negative Uncertainty	Location of Area
	883465	43031	-43033	Africa-North America spreading
	848721	84872	-84872	Indian Ocean **
	3170640	94565	-93601	Pacific-Kula spreading (Pacific plate)
	1888961	75540	-75540	Pacific-Phoenix spreading (Pacific plate) †
	682163	55870	-55747	Pacific-Farallon spreading (Pacific plate)
	538903	31980	-31980	Australia-India spreading †
TOTAL	8012853	385858	-384773	
dA/dt	1183582			

† Estimated uncertainties.

** Uncertainties arbitrarily assigned.

TABLE 6.27. Area measurements for the anomaly 13 time (35.58 Ma).
Areas with age older than anomaly M25 time and younger than 144.42 Ma (120.84 Ma to 144.42 Ma).

	Calculated Area	Positive Uncertainty	Negative Uncertainty	Location of Area
	2216272	63040	-63040	Africa-North America spreading †
	9025140	451257	-451257	Pac-Far-Kul-Pho spreading **
	411418	32690	-32690	Australia-India spreading †
TOTAL	11652830	546987	-546987	
dA/dt	494183			

† Estimated uncertainties.

** Uncertainties arbitrarily assigned.

TABLE 6.28. Area measurements for the anomaly 13 time (35.58 Ma).
Areas with age older than 144.42 and younger than 180.0 Ma (144.42 Ma to 180.0 Ma).

	Calculated Area	Positive Uncertainty	Negative Uncertainty	Location of Area
	15661270	3132254	-3132254	Pac-Far-Kul-Pho spreading **
TOTAL	15661270	3132254	-3132254	
dA/dt	440171			

† Estimated uncertainties.

** Uncertainties arbitrarily assigned.

TABLE 6.29. Area measurements for the anomaly 25 time (58.94 Ma).
Areas for the age interval from anomaly 25 time anomaly 30-31 time (0.0 Ma to 9.

	Calculated Area	Positive Uncertainty	Negative Uncertainty	Location of Area
	799560	23801	-23827	Africa-North America spreading
	2297438	310291	-306299	Africa-South America spreading
	695612	162528	-162266	Antarctica-Africa spreading
	291084	321589	-322467	Antarctica-Australia spreading
	741626	32256	-32293	Australia-Lord Howe Rise spreading
	198230	55990	-54509	Greenland-North America spreading
	476784	19470	-19502	North America-Iberia, Iberia-Europe, and North
	1142287	68376	-67974	Pacific-Antarctica spreading
	1288226	26628	-26462	Pacific-Bellingshausen spreading
	2420000			Marginal Basins
	255363	11790	-11790	Africa-South America spreading
	154108	16270	-16270	Pacific-Antarctica spreading
	231631	14720	-14720	Antarctica-India spreading
	2349250	90760	-90760	Antarctica-India spreading
	2330359	70070	-70070	India-Africa spreading
	1152944	27680	-27680	India-Africa spreading
	2208612	238735	-238887	Nazca-Pacific spreading
	2941000	134687	-134542	Pacific-Farallon spreading (Pacific plate)
	4086467	304510	-301618	Pacific-Farallon spreading (Fara plate)
	4100022	60860	-60860	Australia-India spreading
	470647	31460	-31460	Pacific-Kula spreading (Kula plate)
	484678	37522	-37603	Pacific-Kula spreading (Pacific plate)
TOTAL	31115928	2240347	-2209231	
dA/dt	3265050			

† Estimated uncertainties.

TABLE 6.30. Area measurements for the anomaly 25 time (58.94 Ma).
Areas for the age interval from anomaly 30-31 time to anomaly 34 time (9.53 Ma to

	Calculated Area	Positive Uncertainty	Negative Uncertainty	Location of Area
	1367430	14015	-14012	Africa-North America spreading
	6190112	174521	-173049	Africa-South America spreading
	1300549	63673	-63458	Antarctica-Africa spreading
	454122	315260	-316260	Antarctica-Australia spreading
	1001567	33277	-33298	Australia-Lord Howe Rise spreading
	298094	56351	-54696	Greenland-North America spreading
	752383	20260	-20150	North America-Iberia, Iberia-Europe, and North
	1105011	68155	-68118	Pacific-Antarctica spreading
	2501455	34284	-33835	Pacific-Bellingshausen spreading
	3830000			Marginal Basins
	560975	28940	-28940	Africa-South America spreading
	298768	17700	-17700	Antarctica-India spreading
	1752973	53890	-53890	Antarctica-India spreading
	1383941	44600	-44600	India-Africa spreading
	2627165	295521	-296219	Nazca-Pacific spreading
	4659261	346460	-346736	Pacific-Farallon spreading (Pacific Plate)
	5900342	232600	-286501	Pacific-Farallon spreading (Fara Plate)
	1879094	38750	-38750	Pacific-Kula spreading (Kula Plate)
	2850244	59670	-59670	Australia-India spreading
	705466	54398	-54286	Pacific-Kula spreading (Pacific Plate)
TOTAL	41418952	2153785	-2195204	
dA/dt	2667028			

† Estimated uncertainties.

TABLE 6.31. Area measurements for the anomaly 25 time (58.94 Ma).
Areas for the age interval from anomaly 34 time to anomaly M0 time (25.06 Ma to 59.41 Ma).

	Calculated Area	Positive Uncertainty	Negative Uncertainty	Location of Area
	4273181	41870	-41818	Africa-North America spreading
	5148197	94064	-94061	Africa-South America spreading
	2333685	56356	-68408	Antarctica-Africa spreading
	636297	70292	-72039	North America-Iberia spreading
	720000			Marginal Basins
	56600	8050	-8050	Greenland-North America spreading †
	842059	46960	-46960	North America-Europe spreading †
	6626430	174521	-174521	Africa-South America spreading ‡
	138384	12500	-12500	Africa-South America spreading †
	3418472	58980	-58980	Antarctica-India spreading †
	3712548	91150	-91150	Antarctica-Australia spreading †
	82041	22290	-22290	Pacific-Antarctica spreading †
	441515	22280	-22280	Pacific-Bellingshausen spreading †
	1466227	146623	-146623	Indian Ocean **
	372181	37218	-37218	Antarctica-Australia spreading **
	1699886	26180	-26180	Antarctica-India spreading ‡
	384559	16638	-16638	Australia-Lord Howe Rise spreading ‡
	270681	19650	-19650	India-Africa spreading ‡
	6866470	501640	-500639	Nazca-Pacific spreading
	10971625	119393	-119118	Pacific-Farallon spreading (Pacific plate)
	25918938	1295947	-1295947	Pacific-Farallon spreading (Farallon plate) **
	2101436	127753	-132201	Pacific-Kula spreading (Kula plate)
	16953824	560139	-529409	Pacific-Kula spreading (Pacific plate)
	3199269	159963	-159963	Australia-India spreading **
	5745195	287260	-287260	Australia-India spreading **
	982789	32420	-32420	Australia-India spreading †
TOTAL	111910361	4364504	-4364504	
dA/dt	3257943			

† Estimated uncertainties.

‡ Same as 30-31-34 uncertainties.

TABLE 6.32. Area measurements for the anomaly 25 time (58.94 Ma).
Areas for the age interval from anomaly M0 time to anomaly M4 time (59.41 Ma to 66.97 Ma).

	Calculated Area	Positive Uncertainty	Negative Uncertainty	Location of Area
	499886	42934	-42920	Africa-North America spreading
	1920065	99656	-99338	Africa-South America spreading
	608804	59620	-60642	Antarctica-Africa spreading
	58983	17340	-17340	North America-Iberia spreading †
	660000			Marginal Basins
	821510	164302	-164302	Farallon-Phoenix spreading **
	1438030	97950	-97906	Pacific-Farallon spreading (Pacific plate)
	65183	15924	-16879	Pacific-Farallon spreading (Farallon plate)
	1549344	26369	-23691	Pacific-Kula spreading (Pacific plate)
	3403398	93014	-92027	Pacific-Phoenix spreading (Pacific plate)
	1068752	101690	-101690	Australia-India spreading (Australia plate)
TOTAL	12093955	798201	-786107	
dA/dt	1599729			

† Estimated uncertainties.

TABLE 6.33. Area measurements for the anomaly 25 time (58.94 Ma).
Areas for the age interval from anomaly M4 time to anomaly M11 time (66.97 Ma to 73.84 Ma).

	Calculated Area	Positive Uncertainty	Negative Uncertainty	Location of Area
	245689	40744	-40722	Africa-North America spreading
	486201	82250	-82268	Africa-South America spreading
	406402	63084	-64269	Antarctica-Africa spreading
	610000			Marginal Basins
	239185	18400	-18400	North America-Iberia spreading
	574369	114874	-114874	Farallon-Phoenix spreading **
	1382629	96892	-96733	Pacific-Farallon spreading (Pacific plate)
	73832	18131	-18728	Pacific-Farallon spreading (Farallon plate)
	1622161	20516	-18829	Pacific-Kula spreading (Pacific plate)
	3690194	82957	-75580	Pacific-Phoenix spreading (Pacific plate)
	320309	13720	-13720	India-Australia (NW Australia) †
	778955	22440	-22440	India-Australia (NW Australia) †
TOTAL	10429926	604936	-604936	
dA/dt	1518184			

† Estimated uncertainties.

TABLE 6.34. Area measurements for the anomaly 25 time (58.94 Ma).
Areas for the age interval from anomaly M11 time to anomaly M16 time (73.84 Ma to 82.58 Ma).

	Calculated Area	Positive Uncertainty	Negative Uncertainty	Location of Area
	528502	40899	-40904	Africa-North America spreading
	431529	65362	-66471	Antarctica-Africa spreading
	610000			Marginal Basins
	1205968	85124	-85005	Pacific-Farallon spreading (Pacific plate)
	1588533	216241	-208045	Pacific-Farallon spreading (Farallon plate)
	2128236	25113	-22306	Pacific-Kula spreading (Pacific plate)
	2901347	64439	-51770	Pacific-Phoenix spreading (Pacific plate)
	15983	3250	-3250	India-Australia (NW Australia) †
TOTAL	9410098	536376	-508145	
dA/dt	1076670			

† Estimated uncertainties.

TABLE 6.35. Area measurements for the anomaly 25 time (58.94 Ma).

Areas for the age interval from anomaly M16 time to anomaly M21 time (82.58 Ma to 90.71 Ma).

	Calculated Area	Positive Uncertainty	Negative Uncertainty	Location of Area
	547731	15774	-37809	Africa-North America spreading
	450012	67384	-68486	Antarctica-Africa spreading
	332990	64439	-64749	Pacific-Farallon spreading (Pacific plate)
	3602482	83828	-86821	Pacific-Kula spreading (Pacific plate)
	2302945	40083	-61357	Pacific-Phoenix spreading (Pacific plate)
TOTAL	7236160	271508	-319222	
dA/dt	890057			

† Estimated uncertainties.

Page 247

TABLE 6.37. Area measurements for the anomaly 25 time (58.94 Ma).

Areas with age older than anomaly M25 time and younger than 121.06 Ma (97.48 Ma to 121.06 Ma).

	Calculated Area	Positive Uncertainty	Negative Uncertainty	Location of Area
	2216272	63040	-63040	Africa-North America spreading †
	9025140	451257	-451257	Pac-Far-Kul-Pho spreading **
	411418	32690	-32690	Australia-India spreading †
TOTAL	11652830	546987	-546987	
dA/dt	494183			

† Estimated uncertainties.

** Uncertainties arbitrarily assigned.

TABLE 6.38. Area measurements for the anomaly 25 time (58.94 Ma).
Areas with age older than 121.06 and younger than 180.0 Ma (121.06 Ma to 180.0 Ma).

	Calculated Area	Positive Uncertainty	Negative Uncertainty	Location of Area
	15167638	3033528	-3033528	Pac-Far-Kul-Pho spreading **
	15797439	3159488	-3159488	Area North of India **
TOTAL	30965077	.6193016	-6193016	
dA/dt	525366			

† Estimated uncertainties.

** Uncertainties arbitrarily assigned.

ANOMALY 13 RECONSTRUCTION (35.58 Ma)

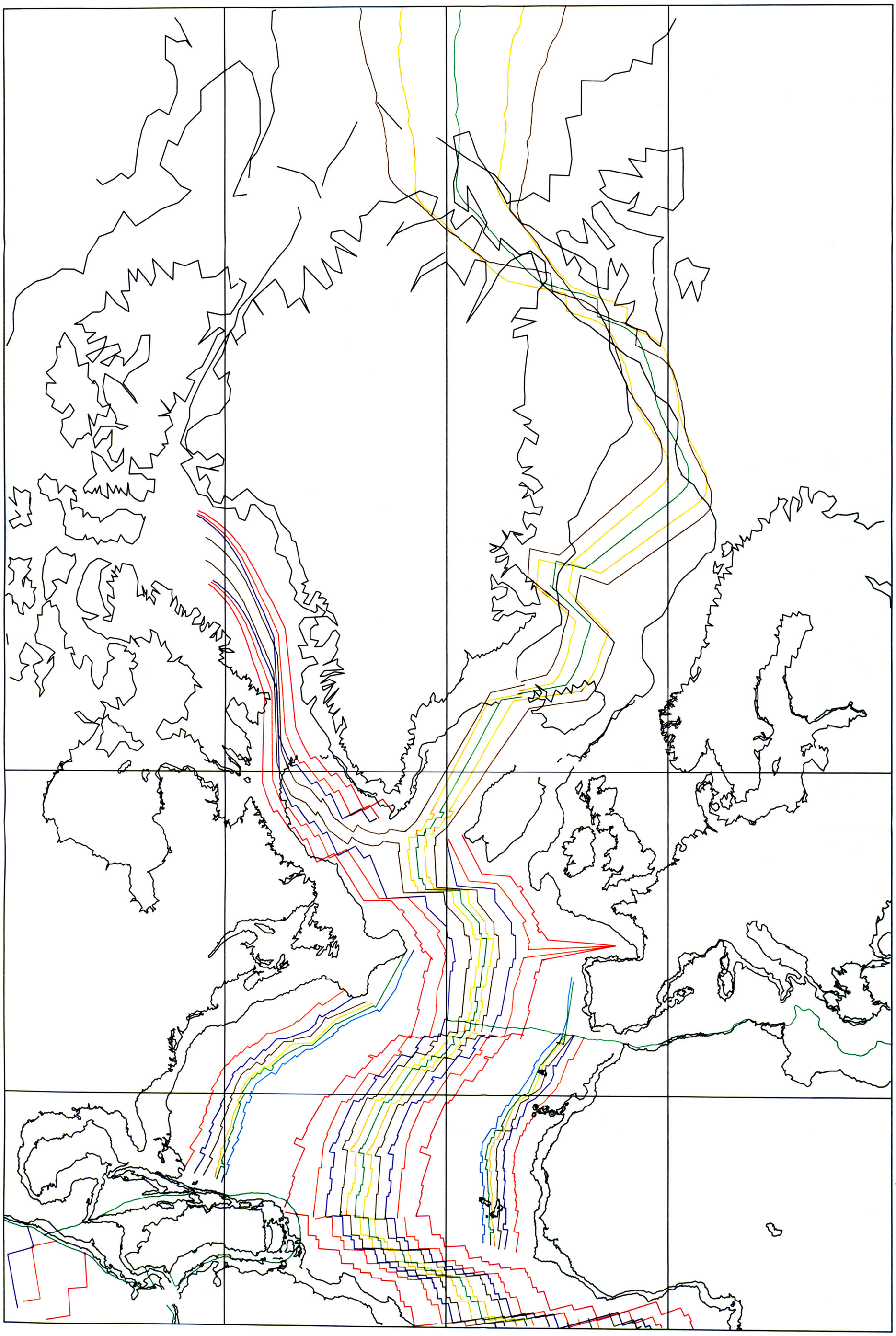

ANOMALY 13 RECONSTRUCTION (35.58 Ma)

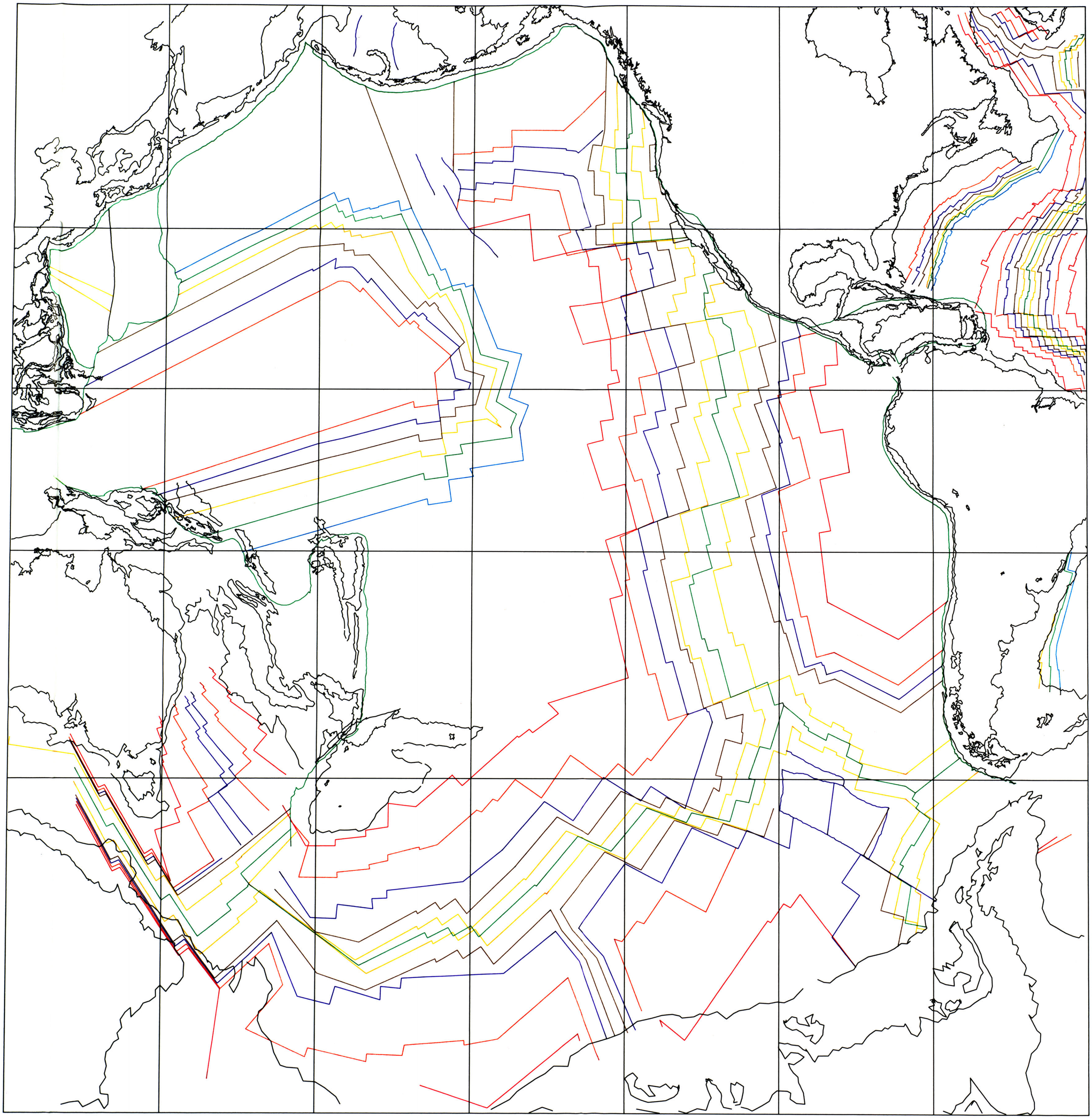

ANOMALY 13 RECONSTRUCTION (35.58 Ma)

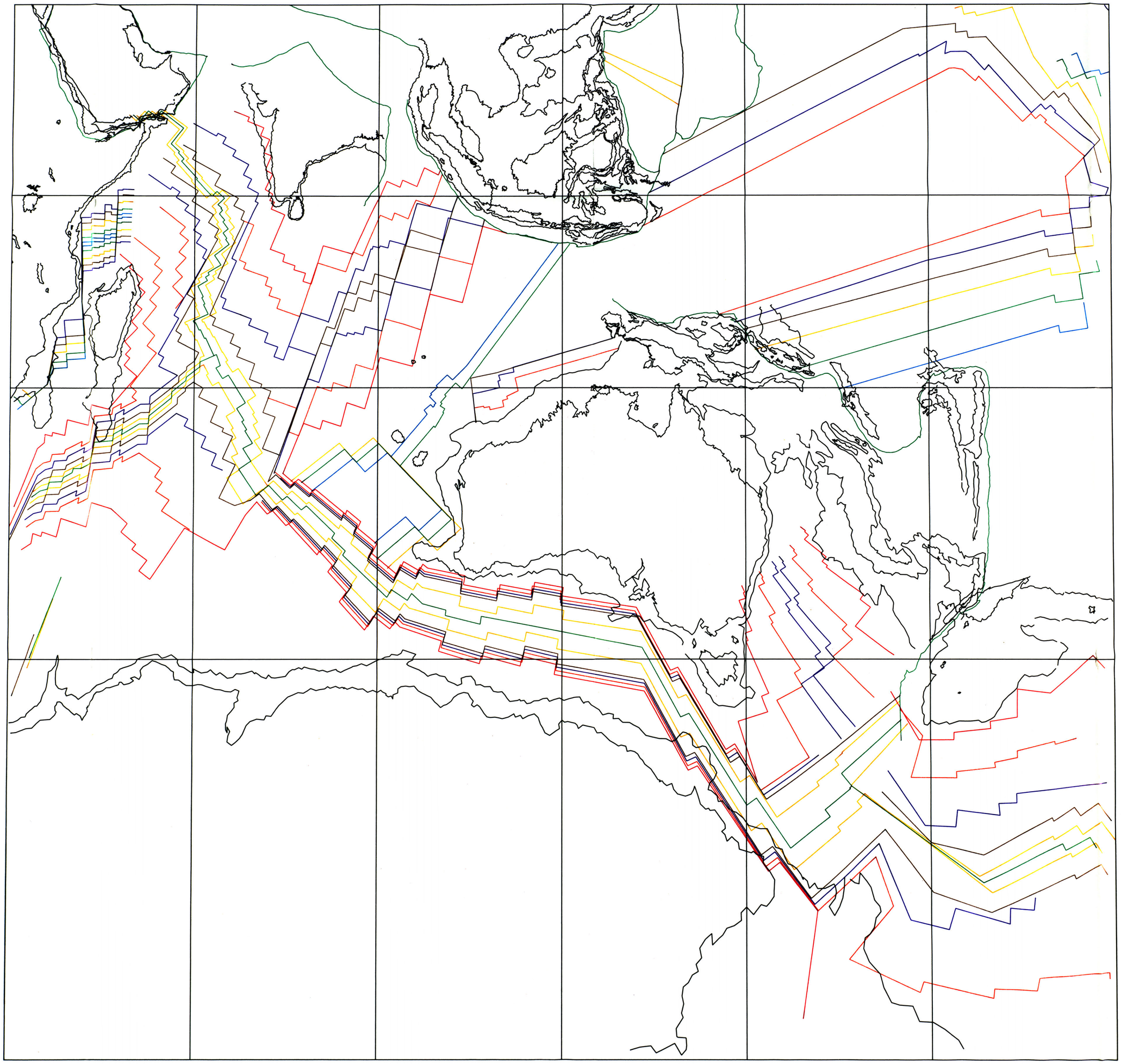

ANOMALY 13 RECONSTRUCTION (35.58 Ma)

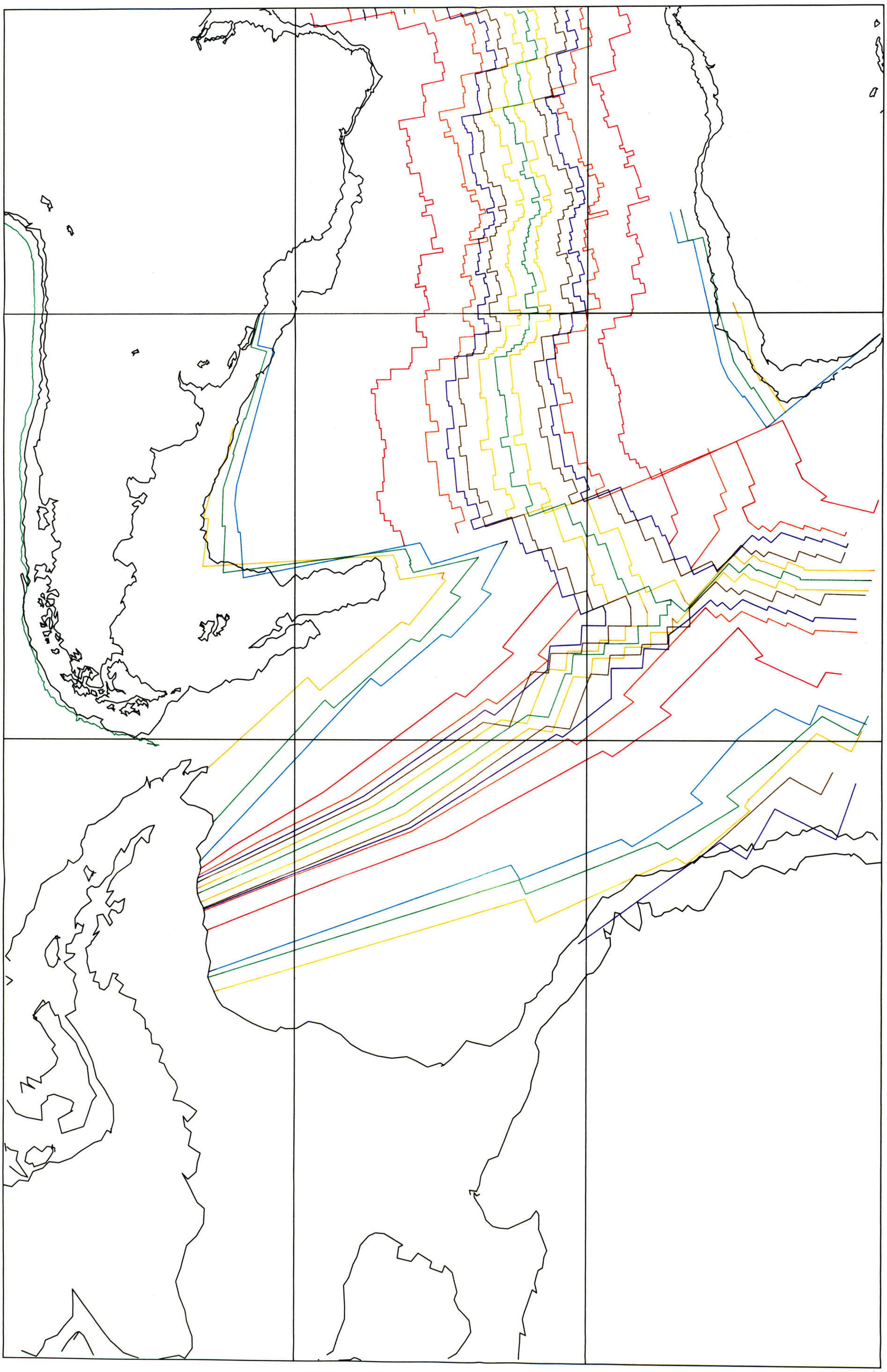

ANOMALY 13 RECONSTRUCTION (35.58 Ma) – AGE OF THE OCEANS

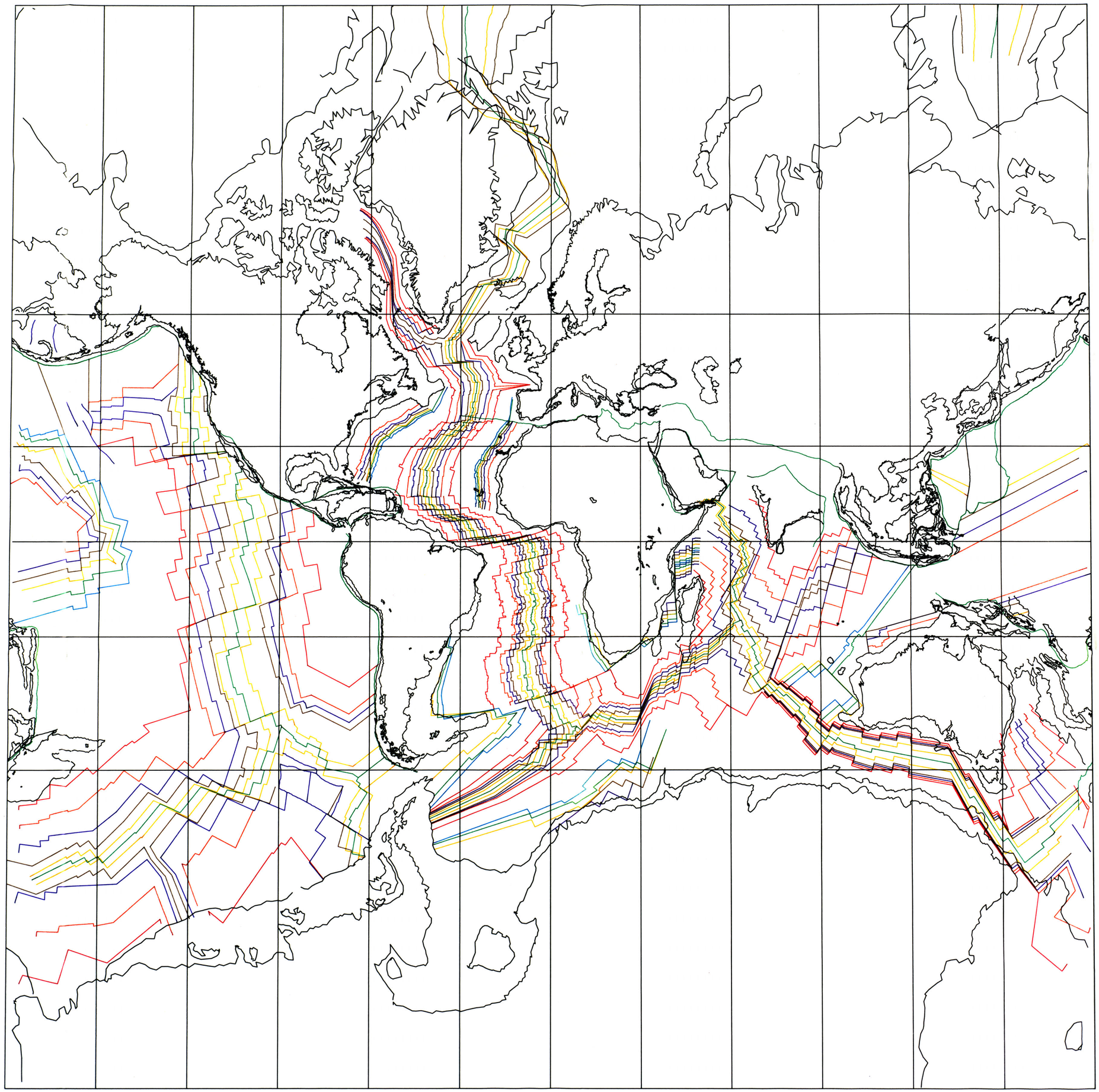

ANOMALY 25 RECONSTRUCTION (58 94 Ma) – AGE OF THE OCEANS

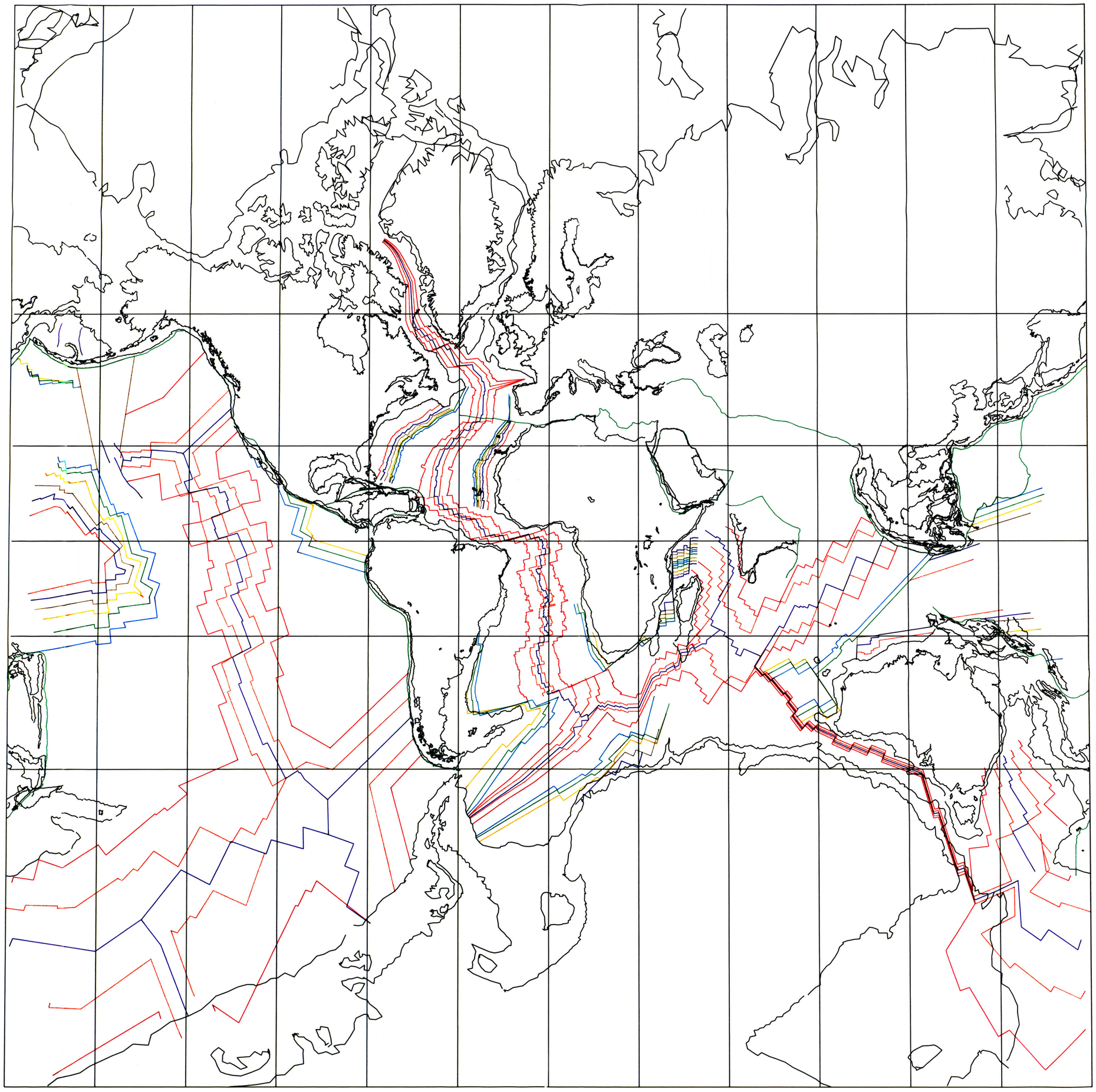

ANOMALY 25 RECONSTRUCTION (58.94 Ma)

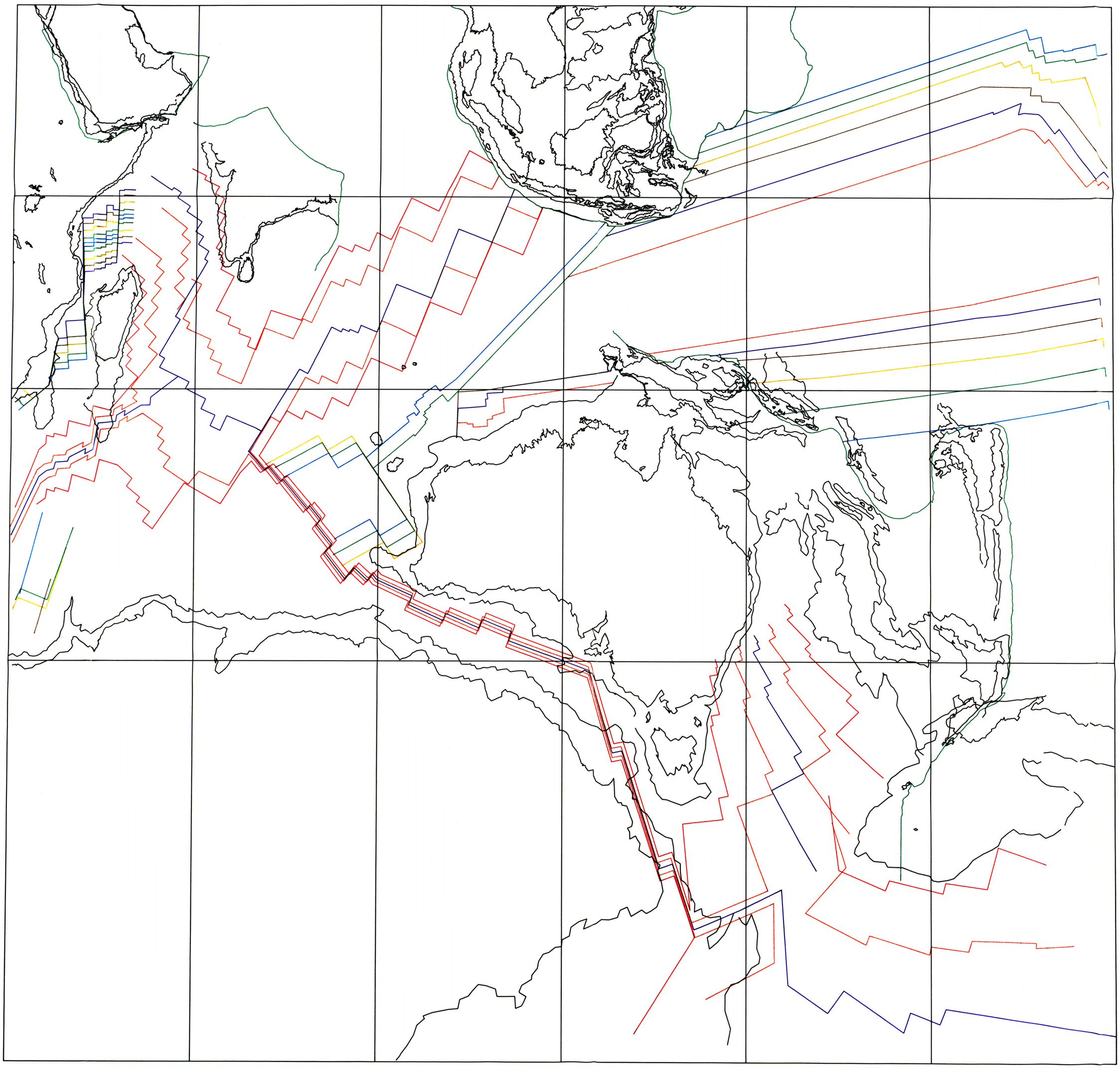

ANOMALY 25 RECONSTRUCTION (58.94 Ma)

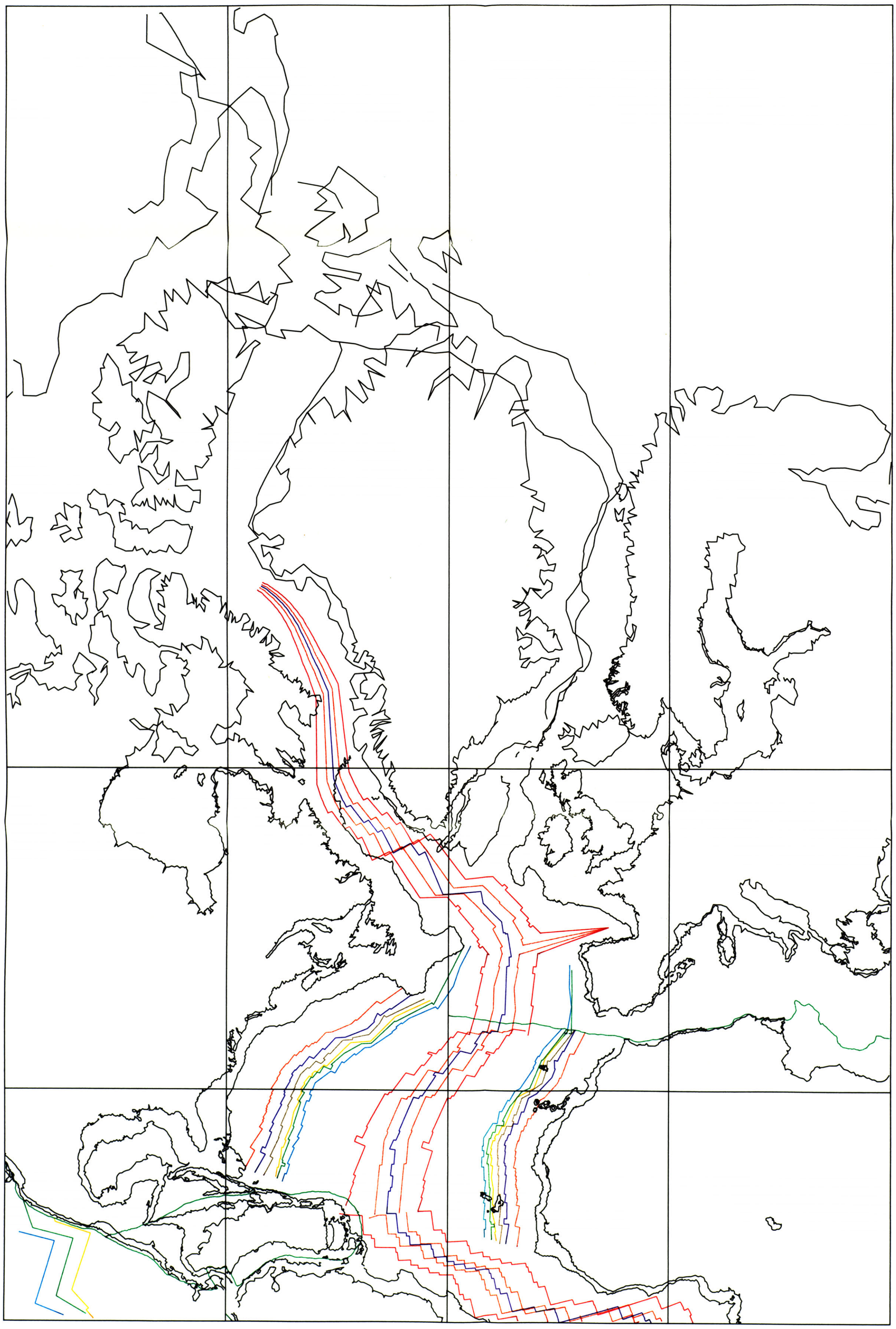

ANOMALY 25 RECONSTRUCTION (58.94 Ma)

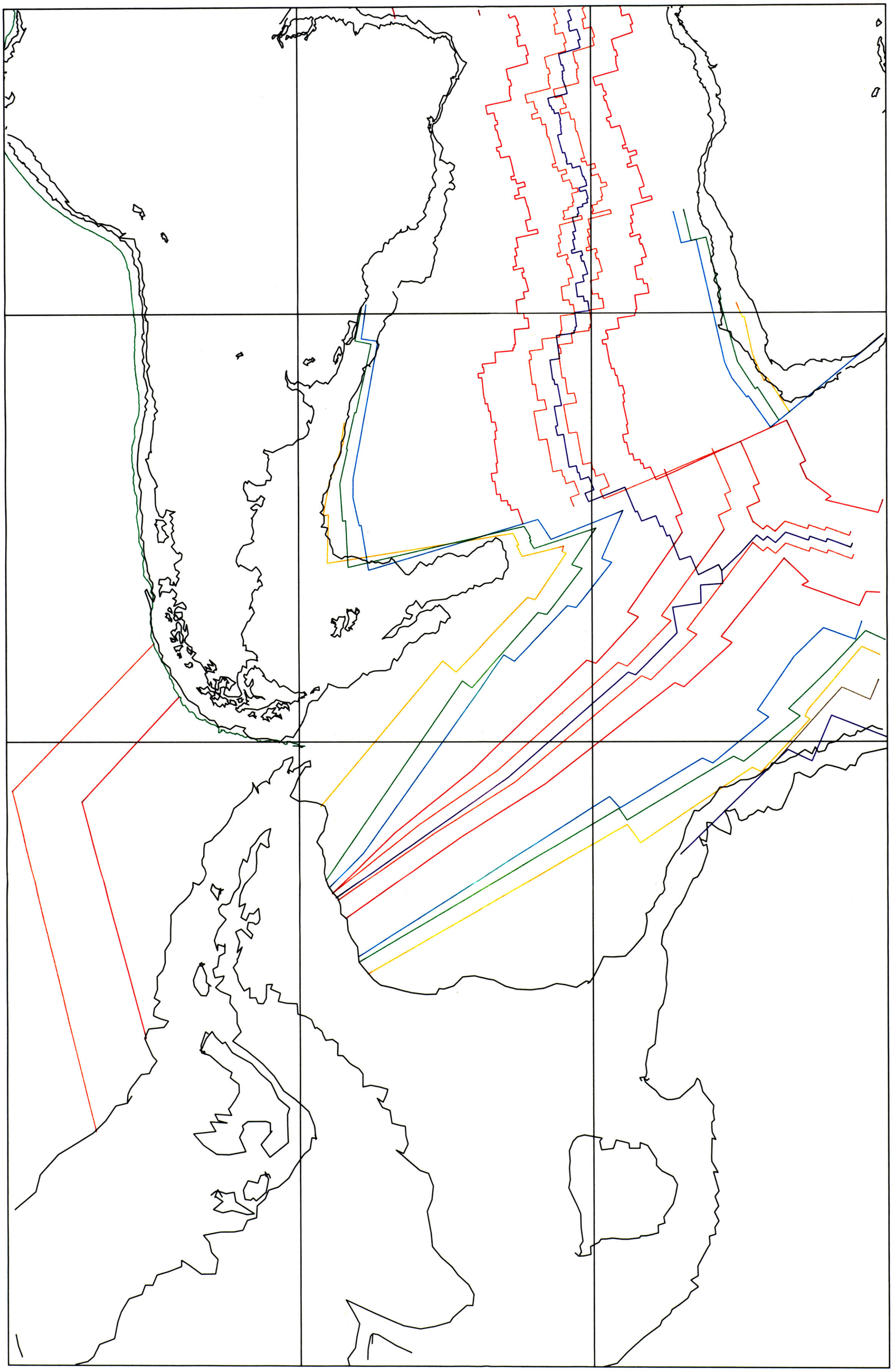

ANOMALY 25 RECONSTRUCTION (58.94 Ma)

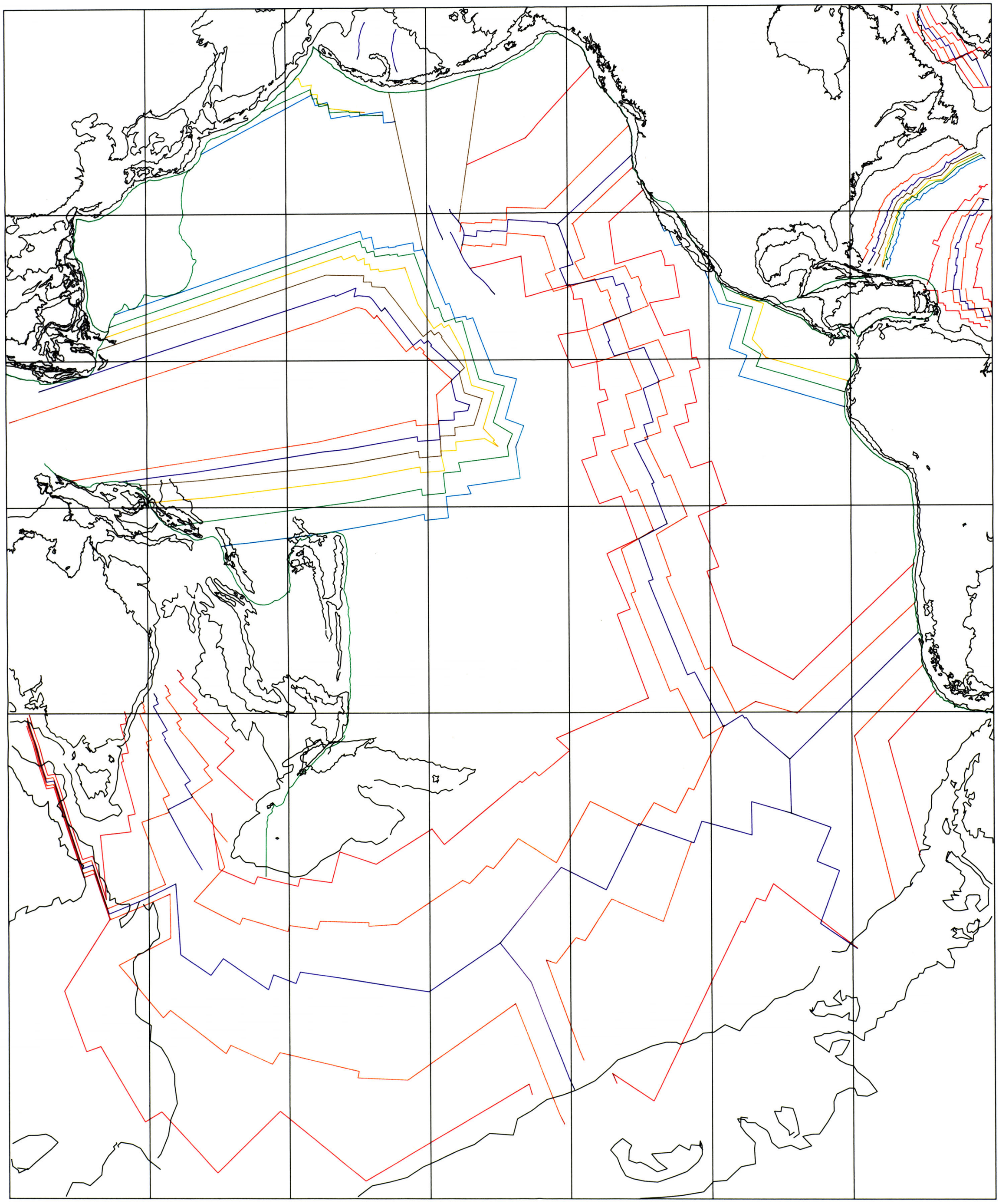

PRESENT TIME -- AGE OF THE OCEANS

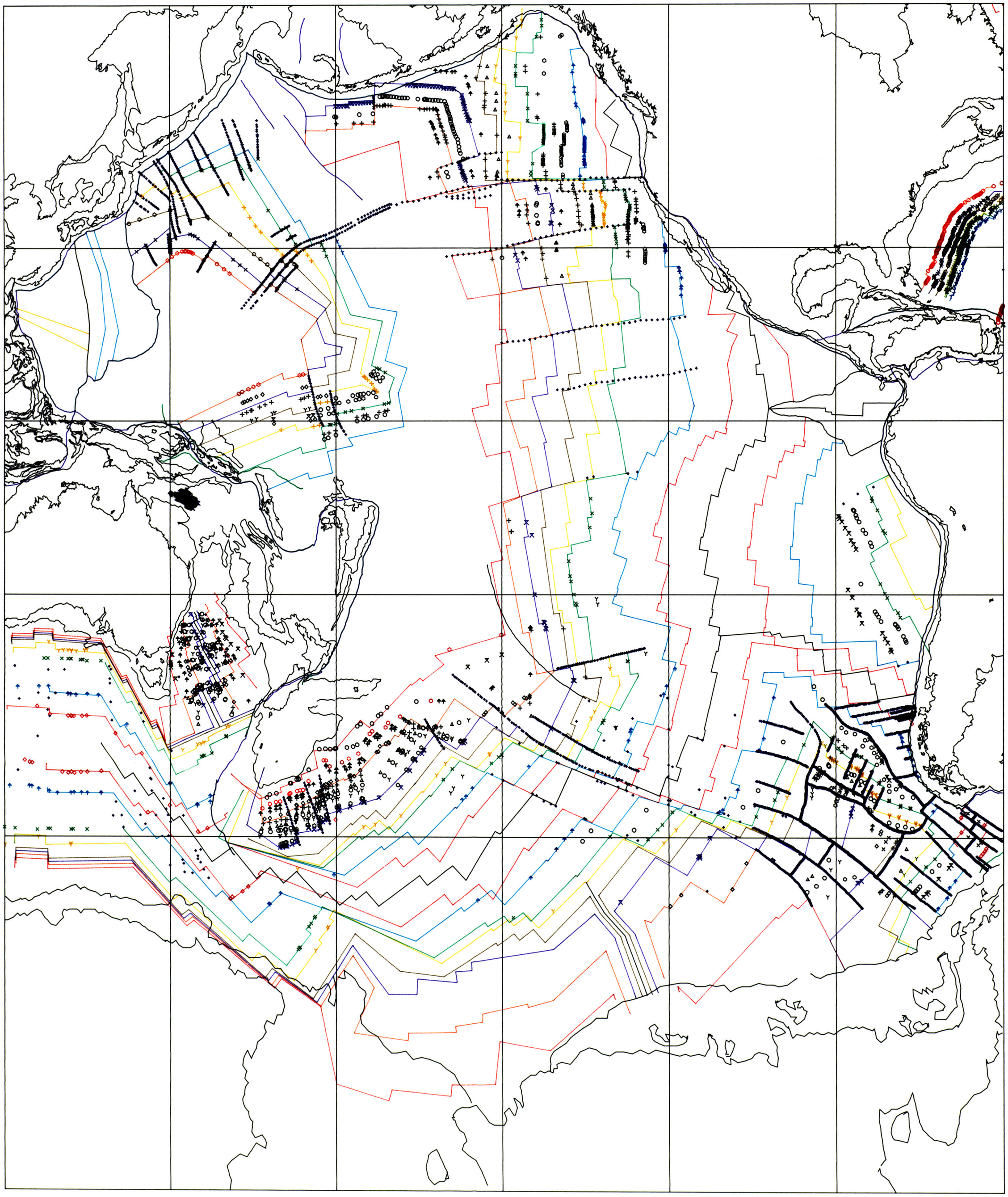

PRESENT TIME -- AGE OF THE OCEANS

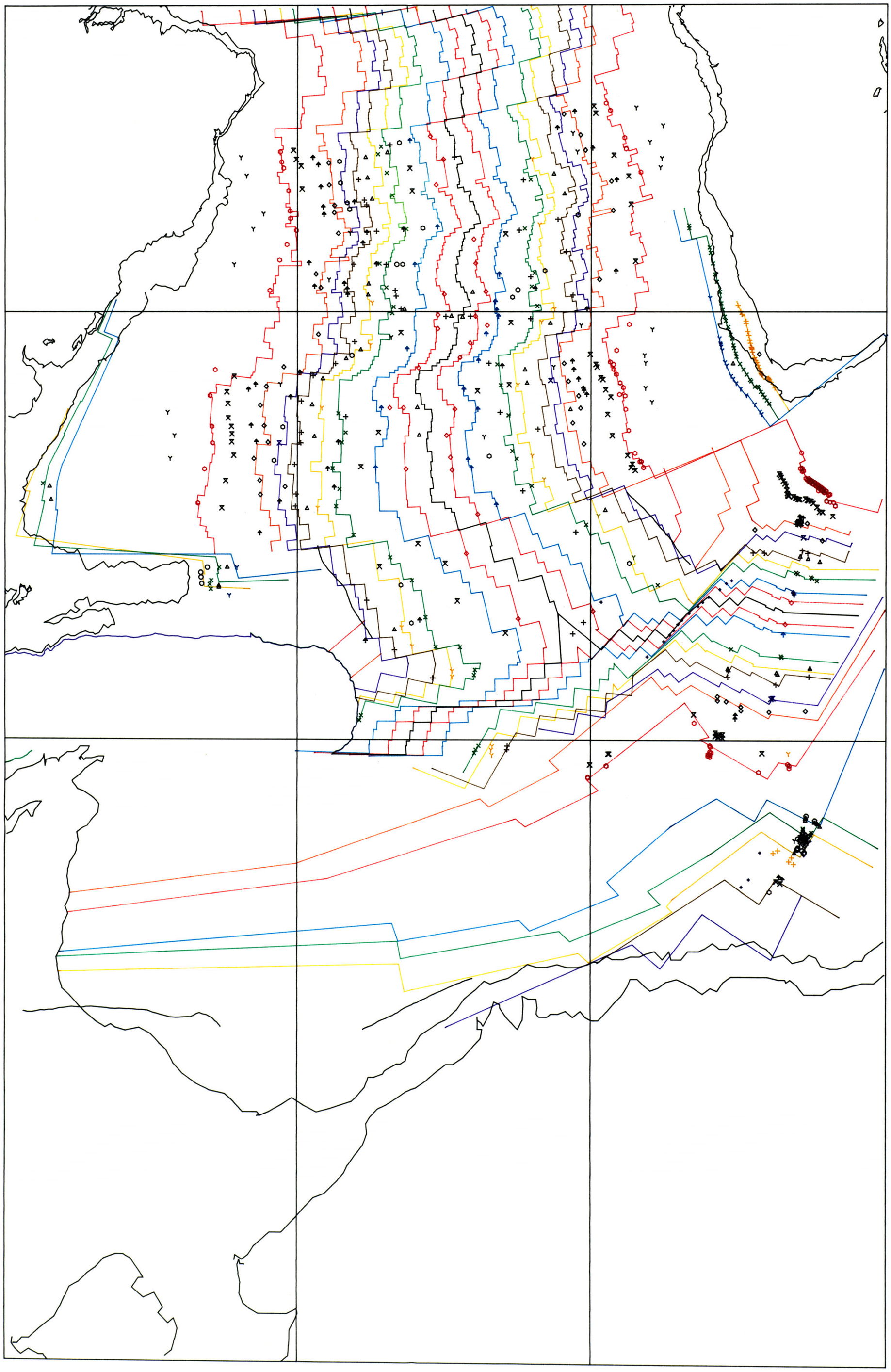

PRESENT TIME -- AGE OF THE OCEANS

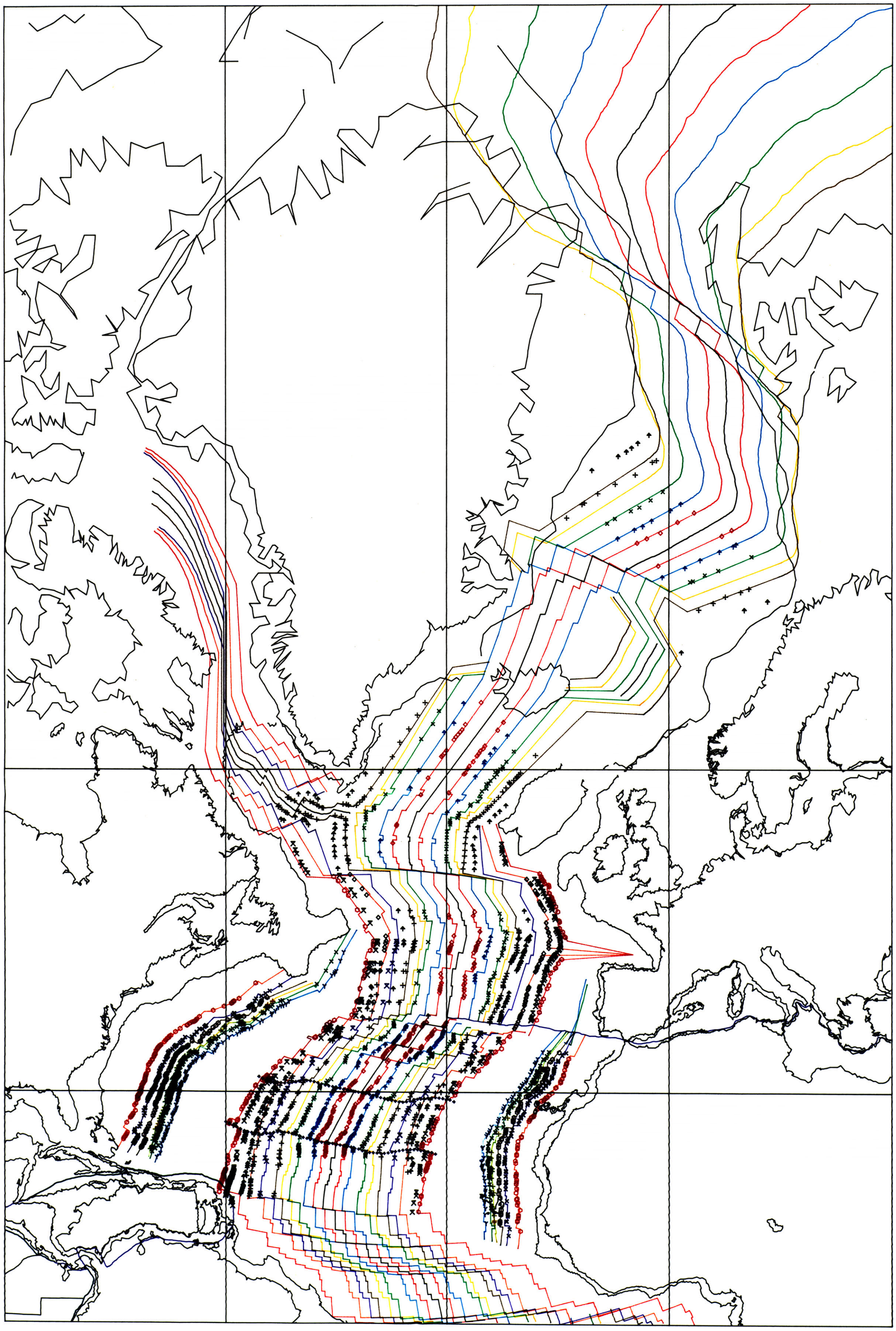

PRESENT TIME -- AGE OF THE OCEANS

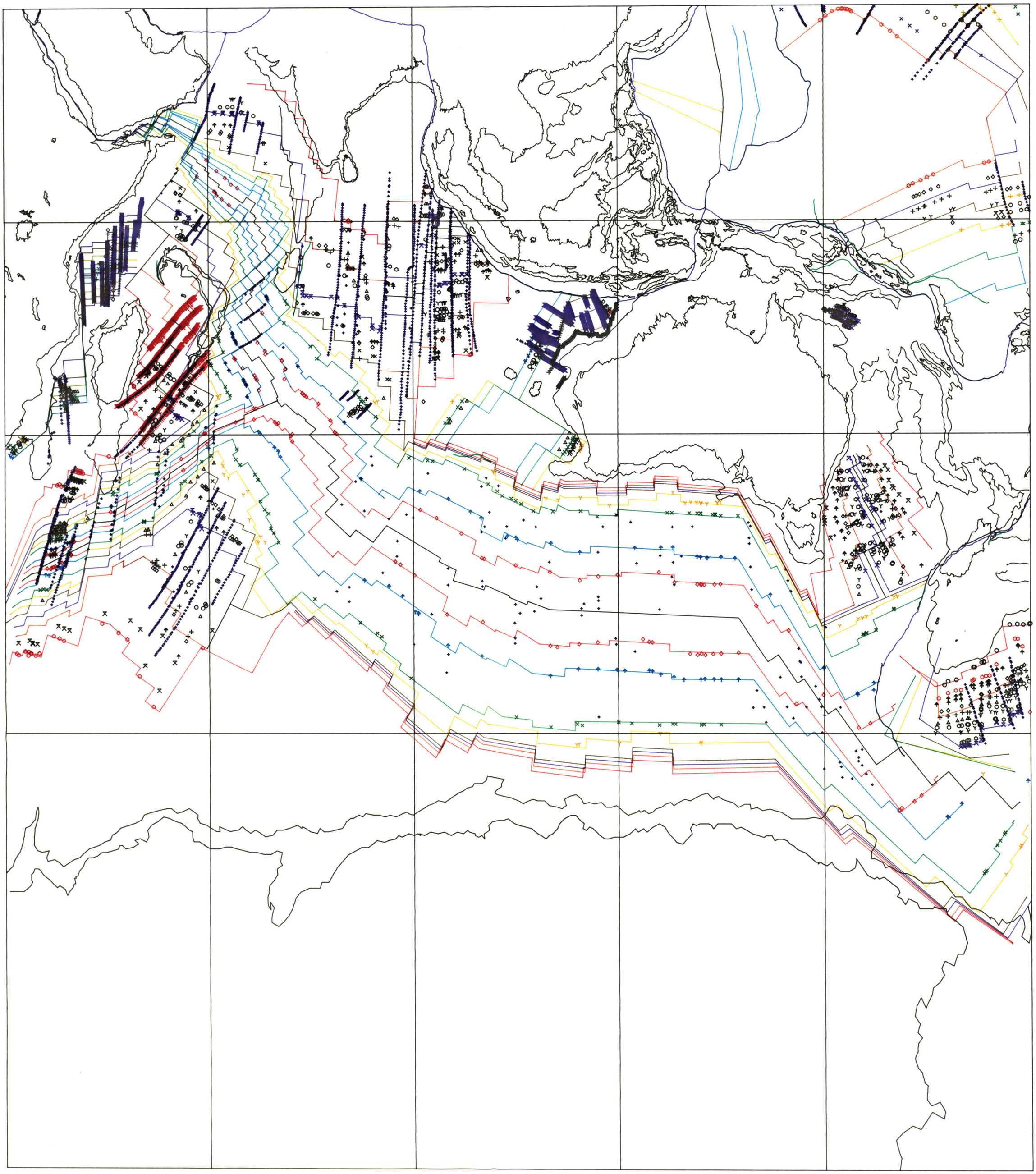

PRESENT TIME -- AGE OF THE OCEANS